PHD

Experimental investigation of the hygrothermal performance of single and multi-layer wall systems in the context of Iran's construction techniques

Mohammad, Shaghayegh

Award date:
2020

Awarding institution:
University of Bath

Experimental investigation of the hygrothermal performance of single and multi-layer wall systems in the context of Iran's construction techniques

Submitted by
Shaghayegh Mohammad
For the degree of Doctor of Philosophy

University of Bath
Department of Architecture & Civil Engineering
August 2020

To my parents, Nahid and Ghasem

and my brother, Kaveh

For their unconditional love.

Acknowledgement

First, I would like to thank my supervisor, Dr. Steve.Lo, for his understanding, support and willingness to help.

I cannot thank enough all the technicians in the ACE department laboratory who made this work possible with their expertise. Thanks to William Bazeley, Martin Nadu, Neil Price, Ian Benford, David Surgenor and Robert Dyer for all their invaluable help.

I also owe a debt of gratitude to Dr. Andrew Shea, without whom this adventure would not have started.

Lastly, I would like to thank all my friends who have been part of my life and have supported me during these difficult years. I carry a bit of you all with me.

Shima Ghasemi, Safoura Valizadeh, Asieh Kazemi, Fatemeh Jahedpari, Vasantha Ramasamy, Loredana Saccone, Manuel Herrera, Niloufar Nikghadam, Maryam Nouralizadeh, Nooshin Kayyal, Mehdi Shafikhani, Mina Mohammad, Rosemary Cunningham, Kamran Cheraghchi, Francis Moran, Neal Holcroft, Daniel Fosas, Yahya Alshamsi, Dima Albadra, Vesna Raicic, Mahan Amani, Yazan Osaily, Anna Chaliasou, Olivia Cook, Berrak Balci, Kaveh Heshmati, Ameneh & Saeed Mazinani, Diana Mouska, Abhishek Upadhyay, And Sara, Andrew & Colin.

Abstract

The general awareness about anthropogenic climate change and destruction of the planet earth ecosystem has resulted in worldwide efforts to reduce GHG emissions (the main cause of global warming phenomenon) and a more sustainable approach towards the use of natural resources. Building sector as one of the largest consumers of energy and natural resources has great potential in reducing \co2 emissions and contributing to a more sustainable environment. The main focus of almost all building regulations aiming to reduce energy consumption, is on the reduction of the building fabric heat loss/gain by mandating the use of thermal insulation materials and/or thermal mass effect. This highlights the importance of building fabric in controlling indoor environment and hence energy consumption; therefore implying the importance of appropriate choice of materials for building fabric design as well as accurate investigation of its performance. The former cannot be done without considerations of embodied carbon of construction materials in an era when strict sustainability criteria are required by credential systems. And the latter requires a holistic approach devising a dynamic hygrothermal (as opposed to steady-state and only-thermal) study considering simultaneous heat and moisture transfer and interactions of adjacent layers in a multi-layer system. In a mutual order, the motive to abide by sustainability criteria in building design has resulted in an increased interest in use of natural materials increasing the need to adapt a dynamic approach to study the varying behaviour of natural materials.

Iran is amongst the 10 major contributors to CO2 emissions. Despite requirements of the national building regulation, Code 19, most buildings lack a robust fabric design in modern structures. They are mainly built of slender single layer blockwork made of hollow fired clay, LECA or AAC, plastered internally with gypsum plaster and externally with sand-cement render. In rare cases where use of thermal insulation is not ignored, PIR boards are used to minimise heat flow through the envelope. Poor wall design alongside the harsh nature of the climate prevalent in most parts of the country makes it difficult to provide thermal comfort without excessive use of air-conditioning systems. To improve wall construction design, an investigation was firstly done on the hygrothermal performance of construction blocks in single-layer constructions. This was done in an experimental set-up built in the laboratory, combining the hot-box and in-situ methods of measuring thermal transmittance. In the next stage, application of non-conventional materials having lower embodied carbon was proposed replacing PIR insulation with expanded cork board insulation, gypsum plaster with earth, and cement with lime render. The hygrothermal performance of these alternative multi-layer assemblies was

investigated under dynamic periodic boundary conditions representing hot dry and hot humid weather condition using the experimental set-up. The result was compared against the conventional multi-layer wall system.

The result indicated different performance of single-layer blockworks in steady-state and dynamic condition from theoretical assumptions with lower thermal transmittance values being reported under dynamic conditions than in steady-state. PIR insulated specimens under hot dry condition resulted in the least discrepancy from the steady-state assumptions. While hygroscopic wall systems and the presence of moisture resulted in more discrepancy. LECA-Cork wall system resulted in significantly lower thermal transmittance values than calculated, under both hot dry and hot humid conditions making it the best candidate for wall design next to AAC-PIR. Plotting the temperature and humidity profiles of the layers of the wall systems, showed the difference in humidity profiles of different wall systems despite having similar temperature profiles indicating the importance of considering the moisture element in building fabric's thermal performance evaluations.

Earth is known for its high moisture absorption capacity. Earth plaster in Iran was traditionally mixed with plant-based aggregates such as straw to improve its mechanical strength. The role of these plant-based aggregates in improving moisture buffering capacity of earth plasters has not been thoroughly studied. In this study, earth was separately mixed with three plant-based aggregates (wheat straw, wood shaving, rice husk) and a mineral aggregate (diatomaceous earth) known for its high moisture absorbent properties. An investigation was carried out using 4 different moisture buffering protocols on the improvement of moisture buffering capacity of earth plaster after the addition of the aggregates. The result indicated that wood shaving and diatomaceous earth result in the highest improvement in moisture buffering capacity under a dynamic test protocol known as NordTest Moisture Buffer Value which is widely accepted as the most realistic protocol representing a real-life scenario. On the other hand, unlike other mixes, addition of wheat straw reduced the MBV which can be justified by simultaneous reduction of water vapour permeability of earth-straw mix as the lowest permeability values were recorded for straw mixes.

Table of contents

Chapter 3. Methodology

Chapter 4. Results and discussion

Chapter 5. Conclusion and future work

List of figures

List of tables

Nomenclature

Symbol	*Definition*	*Unit*
a	Thermal diffusivity	m^2/s
b	Thermal effusivity	$W.s^{1/2}/m^2.K$
b_m	Moisture effusivity	$kg/(m^2Pa.s^{0.5})$
C	Heat capacity	J/ (kg. K)
C_e	Specific heat capacity of ice	J/ (kg. K)
C_w	Specific heat capacity of water	J/ (kg. K)
D_ϕ	Liquid conduction coefficient	kg/ms
g_v	Vapour diffusion flux density	kg/m^2s
g_w	Liquid transport flux density	kg/m^2s
G	Vapour flow rate	Kg/s
h_e	Specific melting enthalpy	J/kg
h_v	Latent heat of phase change	J/kg
H	Total enthalpy	J/m^3
H_w	Enthalpy of moisture	J/m^3
MBV	Moisture Buffer Value	$kg/(m^2{\cdot}\%RH)$
P	Water vapour partial pressure	Pa
P_s	Saturation vapour pressure	Pa
q	Heat flux density	W/m^2
S_h	Heat source/heat sink	W/m^3
S_w	Moisture source/ Moisture sink	kg/m^3s
t_p	Period	s
U-value	Thermal transmittance	W/m^2K
w	Moisture content	kg/kg
Y-value	Thermal admittance	W/m^2K
δ_a	Water vapour permeability of still air	kg/(m.s.Pa)
δ_p	Water vapour permeability	kg/(m.s.Pa)
λ	Thermal conductivity	W/mK
μ	Water vapour resistance factor	-
ξ	Moisture sorption capacity	kg/kg
ρ_0	Dry density	kg/m^3
ρ_s	Bulk density	kg/m^3
ϑ	Temperature	^oC
φ	Relative humidity	%

Abbreviations

Abbreviation	*Definition*
AAC	Autoclaved Aerated Concrete
BS	British Standard
CBI	Cork Board Insulation
CHB	Calibrated Hot Box
DE	Diatomaceous Earth
EN	European Standard
HD	Hot Dry
HFM	Heat Flow Meter
HH	Hot Humid
GHB	Guarded Hot Box
GHP	Guarded Hot Plate
IAQ	Indoor Air Quality
ISO	International Standards Organisation
LECA	Lightweight Expanded Clay Aggregate
MBC	Moisture Buffering Capacity
MBV	Moisture Buffer Value
PIR	Polyisocyanurate
RH	Relative Humidity
SLS	Sum of Least Square

Chapter 1.

Introduction

1.1. Global context

1.1.1. Building industry and environmental impact

Global awareness towards anthropogenic climate change resulting from increasing concentrations of Green House Gases (GHG) in the atmosphere, has led to a world-wide cooperation to reduce fossil fuel consumption and to find less polluting energy resources. Fossil fuels are acknowledged as the main source of carbon dioxide emissions and account for approximately three-quarters of GHG emissions. This awareness has led to international conventions such as the United Nations Framework Convention on Climate Change (UNFCCC)(1994) when climate change was considered as a problem, followed by the Kyoto Protocol (1997) that established international emissions reduction targets, and finally the Paris Agreement that came to force on November 2016 to strengthen the global response to the threat of climate change by keeping the global temperature rise of this century well below 2°C (unfccc.int). The building sector is responsible for one third of global GHG emissions, both in developed and developing countries (Allouhi et al., 2015). The sector consumes a vast amount of energy to maintain thermal comfort in buildings (Aditya et al., 2017). According to the United Nations Environment Program, buildings and construction sector consume 36% of the world global energy and account for 39% of world emissions (Figure 1-1). Similar values have been reported by the U.S. Department of Energy and European Commission (Asdrubali et al., 2015 and Schiavoni et al., 2016). Being one of the major energy consuming sectors, there is enormous potential for energy saving by taking appropriate measures in the design and construction of buildings (Schiavoni et al., 2016). The construction industry is a major contributor to CO_2 emissions, yet the Intergovernmental Panel on Climate Change lists buildings as having the largest estimated economic mitigation potential amongst the sectors investigated (Ruuska, 2015).

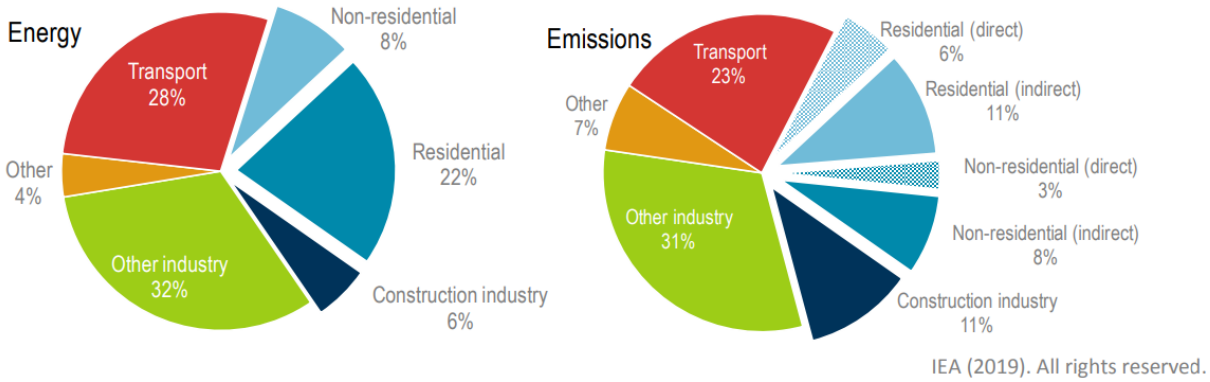

Figure 1-1: Global share of buildings and construction final energy (36%) and emissions (39%), 2018 (IEA & UNEP, 2019)

The energy consumption of a building is strongly dependent on the characteristics of its envelope as it is the border between the internal and external environment and directly influences the

thermal comfort of the building occupants (Schiavoni et al., 2016). According to CIBSE (2000), building envelope has the largest influence on heating/cooling loads of a building and subsequently the resulting methods of environmental room control. Cao et al. (2016) state that the advanced designs of building envelopes have the potential to reduce heating and cooling loads by 40%. This emphasises the importance of designing the building fabric to a high standard to moderate harsh outdoor climate without much use of mechanical systems (CIBSE, 2000). Walls occupy the largest surface area of a building fabric. Amongst elements of heat loss in building fabric i.e. windows, doors, thermal bridges and opaque walls, the latter is responsible for the most significant thermal losses in a building (Asdrubali et al., 2013). The general awareness about the potential of reducing building energy consumption by improving building fabric has been incorporated into building codes and regulations by recommending or mandating the use of thermally insulating materials to reduce heat flow paths through the building fabric elements.

On the other hand, along with the energy efficiency, there are other aspects that need to be taken into account when decisions are made on the choice of materials for building fabric design. The energy embodied in materials and their effect on Indoor Air Quality (IAQ) are elements of sustainable design that needs consideration in early design stage if fabric design is to comply with sustainability targets and credentials.

1.1.2. Embodied energy of construction materials

The building industry is, after food production, the largest consumer of raw materials in the world (Berge, 2009). It is therefore important for the construction industry as one of the major consumers of energy and natural resources to focus on sustainability as a major principle to abide by. In line with this comes the importance of construction materials and their contribution to the life cycle environmental impact of buildings (Pargana et al., 2014). For many years, energy conservation research was focused on the operating energy of a building due to its large share in the total life cycle energy of a building. However, with stricter building energy codes, widespread use of more effective insulation materials and efficient appliances, the energy performance of buildings has improved resulting in lower operating energy used during the lifetime of buildings. More emphasis has, therefore, been directed towards the energy embodied in the buildings' construction materials (Cabeza et al., 2013 (a)). Modern building materials are associated with greater use of energy and natural resources in their manufacture compared to traditional materials; as we have moved from earth, timber and plant-based fibres and products to concrete, metal, inorganic binders and plastic (Cabeza et al., 2013). The importance of choice of materials with regards to the total embodied

energy and environmental impact of buildings has resulted in increased interest in more natural (less heavily manufactured) and less energy-intensive alternatives (Ashour et al., 2011).

1.1.3. Indoor air quality, health and comfort

Building envelope can contribute to a healthier indoor environment by improving IAQ. The topic has gained interest as the recent introduction of stricter building codes has encouraged the construction of more air-tight buildings, resulting in poor indoor air quality and increased number of health-related issues (Laborel et al., 2016). Building fabric through hygroscopic properties of its constituting layers can act as moisture buffer and regulate indoor humidity levels. On the other hand, as natural materials have higher moisture buffering capacity, increased interest in the use of these materials due to their lower embodied carbon has also introduced the concept of breathable constructions; hygroscopic structures that allow water vapour to permeate through, get absorbed/ desorbed to and out of material and let the building "breathe". The hygroscopicity of building materials and their contribution to an improved IAQ is another factor to be considered when decisions are made on choice of materials for building envelope design.

1.1.4. Hygrothermal performance of building envelope

As it is discussed more in detail in chapter 2, the performance of the building envelope is the result of both heat and moisture transfer/interactions through/with materials. Absorption/ desorption of moisture by building materials (due to their hygroscopic properties), changes their basic thermo-physical properties and adds more complexity to heat transfer. This requires a holistic hygrothermal analysis of the building envelope. It should be noted that in this study "hygrothermal performance" is used as opposed to the more common phrase "thermal performance"; as the performance of the building fabric depends on both its thermal and hygric performance. The study of hygrothermal performance of the wall systems is more important in the time when use of natural building materials is becoming more favourable to reduce environmental impacts and meet sustainability criteria. Natural materials are more hygroscopic with more significant changes in their behaviour when exposed to moisture (See section 2.4.3).

On the other hand, the interactions of the layers of the envelope in a multi-layer system result in a dynamic behaviour which differs from expectations dictated by steady-state calculations. In this way the overall performance of the wall is not simply the summation of the steady-state properties of every single layer. It is, therefore, important for an optimum wall design that the characteristics of its components are investigated holistically in a realistic condition and the compatibility of the layers in terms of response to moisture transfer is taken into account (see section 2.9) (Kočí et al., 2012). This also ensures the durability of construction as well as the health and comfort of its

occupants.

1.2. Regional context;

1.2.1. energy consumption in Iran

In the last few decades, the energy consumption in Iran has increased dramatically due to rapid population growth, industrialisation and urbanisation. In 2018, Iran was one of the 10 major carbon dioxide emitting countries of the world, Figure 1-2 (Enerdata,2020). In November 2016, Iran signed the Paris Agreement, along with 194 other countries, as one of the non-Annex I parties in a global response to the threat of climate change. Previously, in 1992, by signing the UNFCCC and ratifying the Kyoto Protocol in November 2005, Iran formed a national movement to incorporate energy saving principles in different sectors in the country. Iran's national climate change office (NCCO) was established in 1996 and the Iranian Fuel Conservation Organisation in 2000.

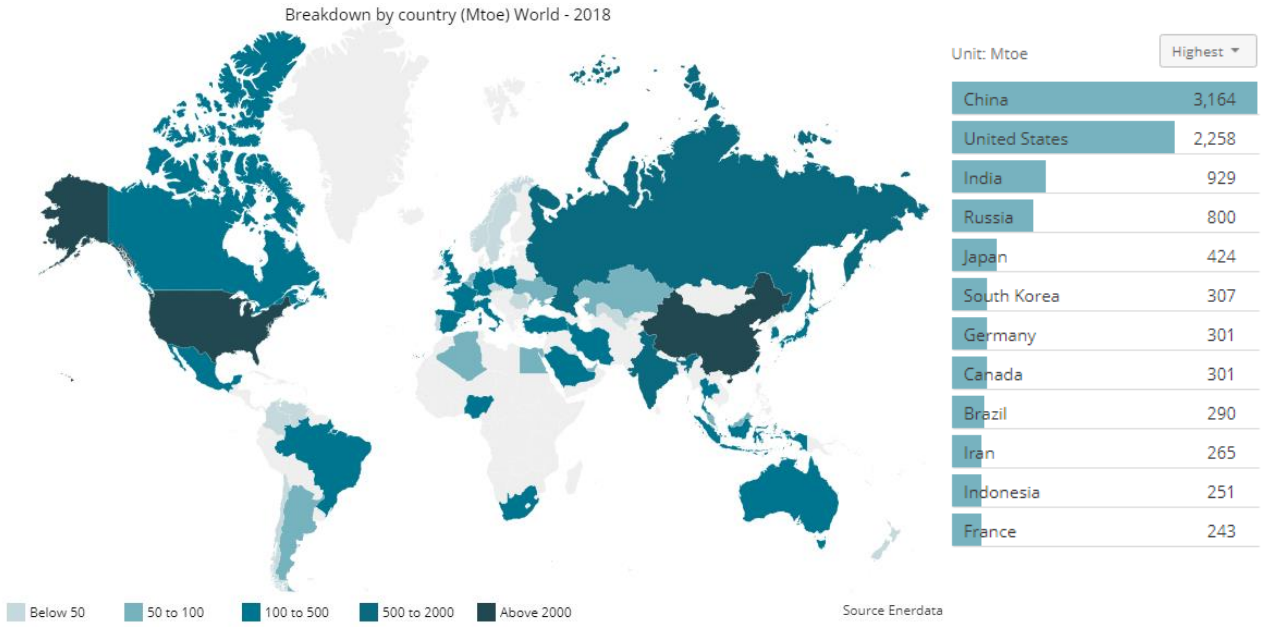

Figure 1-2: Energy consumption of countries for the year 2018 (Enerdata,2020)

Amongst the top 10 CO_2 emitting countries, Iran has had the greatest increase in CO_2 emissions over the last 40 years (Nejat et al., 2015). The same trend is observed for energy consumption in the residential sector being 315% higher in 2018 than it was in 1990 (Figure 1-3). In 2018, the residential sector accounted for 27% of the total energy consumption making it the largest energy consuming sector in the country (Figure 1-4). This led to the government intervention to control this trend in the last decade. In 2009, the government decided to gradually reduce energy subsidies and to increase energy prices resulting in a short-time slump in energy demand (Nejat et al., 2015). In the building sector, the first mitigating policy was to introduce the first building energy code, Code 19 of the national buildings regulations in 1992, which was revised once in 2002, and again in

2010. This code covers all building types and focuses mostly on heat loss through the building fabric and introduces measures to reduce the heat transmittance value. Initially its application was voluntary, however, the government made it compulsory, firstly in the capital in 2004, then in large cities in 2007 and then later for all cities in 2011.

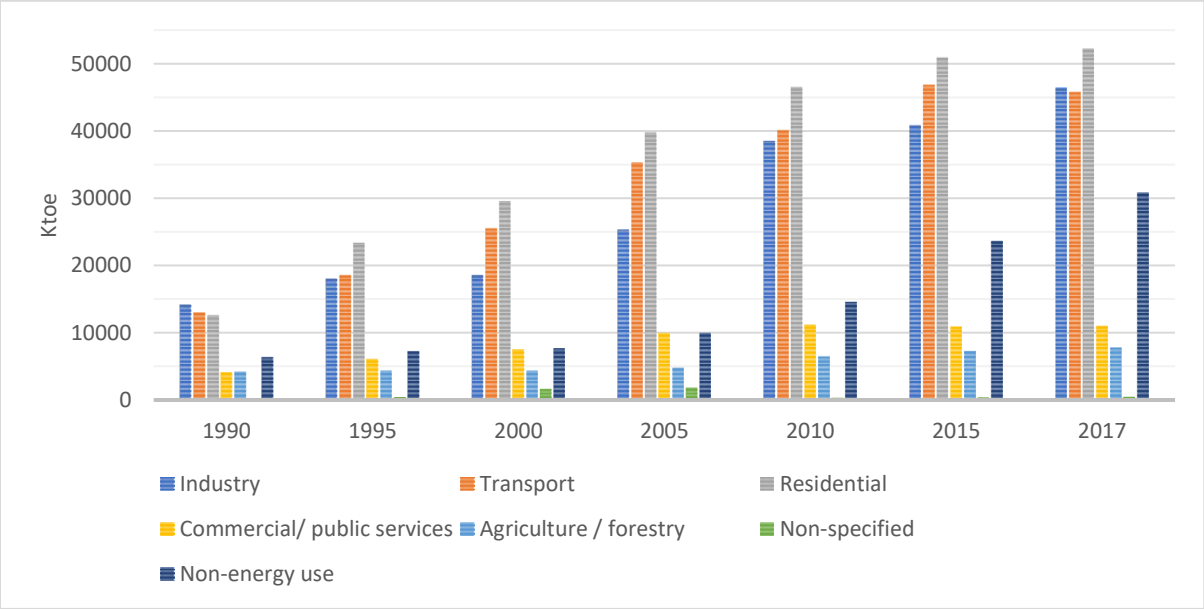

Figure 1-3: Total final energy consumptions by sectors in Iran from 1990 to 2017 (IEA, 2020)

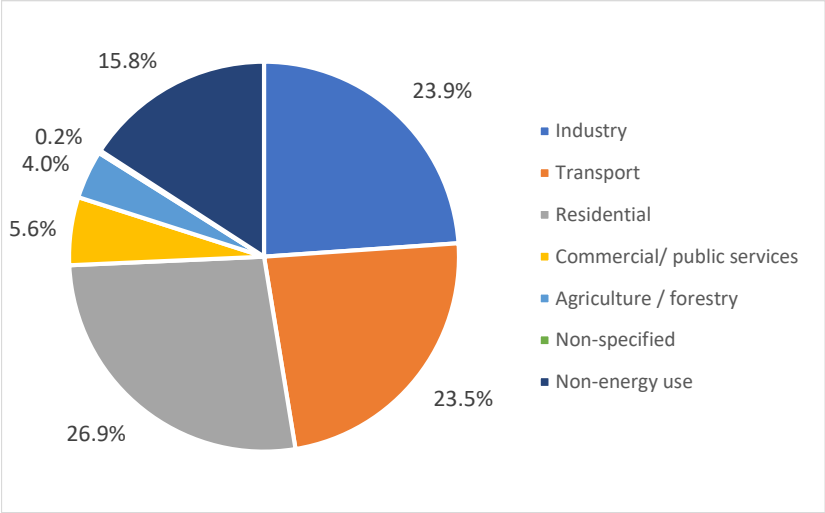

Figure 1-4: Total final energy consumptions by sectors in Iran in 2017 (IEA, 2020)

1.2.2. Shortcomings of the current wall construction practice in Iran

During 60s and 70s, the Iranian government's economic development plans resulted in rapid economic growth and industrial development of the country. Between 1964 and 1978, the oil, gas and construction industries expanded by almost 500 percent. This sped up the process of modernisation of the country which had started far before this date in 20s and resulted in rapid urbanisation and migration of populations from villages to large cities (Curtis & Hooglund, 2008).

More houses were then needed to accommodate the incoming population. In this situation, the newly introduced “beam and column” structural system was welcomed by construction industry as it would make the rapid construction of multi-storey buildings possible. This modern architecture not only introduced a new lifestyle to Iranian people’s lives but also replaced the traditional vernacular construction techniques used by generations to moderate the harsh climate. One of these techniques was the use of thermal mass in buildings’ thick envelopes to act as heat storage. In summer, this helps delaying the dissipation of heat to indoor space to later time in the evening when outdoor cooler temperatures could be used to cool indoor space and the structure of the building by ventilation and radiation. Modern architecture replaced these thick wall systems with slender alternatives; the trend which was encouraged by the increase in land price which forced the designers to make most of the space by reducing the thickness of the building envelope as much as possible. This occurred throughout the country without considering the requirements of, sometimes harsh, local climates in different parts of the country, as the use of mechanical air-conditioning units became widespread, encouraged by low energy prices in the country. These slender wall alternatives struggle to provide thermal comfort for occupants without constant use of mechanical building services.

Figure 1-5: Traditional (left) vs. modern (right) wall construction in Iran

Current wall constructions consist of either a single layer of blockwork (150 to 200mm) made of hollow fired clay, hollow Lightweight Expanded Clay Aggregate (LECA), or Autoclaved Aerated Concrete (AAC) blocks. The application of insulation is required by Code 19 of the national building regulations which is mostly neglected in construction process (Riazi & Hosseyni, 2011). If applied, this layer of insulation (mostly PIR insulation boards) is mounted on the outer face of the blockwork

or less commonly is sandwiched between two layers of blockwork. PIR is a synthetic oil-based impermeable thermal insulation. If applied appropriately i.e. no joints and gaps between the boards or between boards and blockwork, it can significantly reduce heat losses through the building envelope. Creating an impermeable layer surrounding the entire surface area, it separates the indoor environment from the outdoor climate.

1.3. objectives

The overall aim of this study was to first investigate the dynamic hygrothermal performance of current wall practice of Iran's modern construction and to improve this practice taking into account environmental impacts and indoor air quality through the use of natural materials. This overall aim will be achieved through investigating the following:

- The equivalent thermal conductivity value of hollow construction blocks (in this case specific to Iranian construction techniques)
- The in-situ thermal transmittance vs. theoretically calculated thermal transmittance value of construction systems
- Thermal transmittance under fluctuating vs. steady-state boundary conditions
- Wall systems' performance in dry vs. humid boundary condition
- The effect of the characteristics of layers of the wall on moisture transport and therefore the overall thermal transmittance.

With the global awareness about the environmental impact of human activities, application of natural insulation materials has gained interest. These materials have less energy embodied in them through their manufacturing process and have more hygroscopic capacity. Therefore, their application improves wall design in terms of both the environmental impact of building and the IAQ. Expanded cork board is one of these natural insulation materials. Despite being water repellent, cork has much higher permeability than PIR insulation board, the conventional thermal insulation material used in Iran. Its steady-state thermal conductivity value is higher than PIR suggesting a higher thermal transmittance rate through the wall. However, being of a different nature to oil-based insulations with much higher specific heat capacity and vapour permeability, analysis of its dynamic performance in a wall system results in more accurate conclusion on its performance in real condition (See section 2.9.2.2).

In current practice of Iranian building construction, the internal side of blockwork facing indoor environment is rendered with a layer of gypsum plaster. This practice replaced the traditional use of earth plaster for internal finishing which was usually mixed with straw for extra reinforcement. In current practice, the external side of blockwork, either as it is or covered with thermal insulation

is rendered with a layer of cement plaster. Cement is a replacement for a traditional rendering material i.e. lime. Both cement and gypsum have higher embodied energy and less hygroscopic properties compared to lime and earth. Cement is an impermeable material that does not allow the structure underneath to breathe. If moisture penetrates to the substrate layer underneath the cement rendering, it will be trapped in the structure as cement hinders moisture transfer outside of the assembly. Gypsum, although considered as a hygroscopic material, has far less moisture ab(de)sorption capacity compared to earth.

The construction blocks used in single and multi-layer wall systems in Iran have not been tested for their dynamic hygrothermal performance. So far, the evaluation of these blocks' performance has been based on the laboratory-based measurement of their thermal conductivity value taken from the manufacturer's data sheet (declared values). In cases of hollow blocks i.e. fired clay and LECA blocks, these declared thermal conductivity values relate to the conductivity of the solid material, and do not represent the composite structure of these hollow blocks. To evaluate dynamic hygrothermal performance of these blocks in a single layer wall as well as in a multi-layer wall system, an experimental set-up combining the hot-box and in-situ methods of thermal transmittance measurements were designed. This set-up allowed not only the in-situ measurement of an equivalent thermal transmittance value for these blocks but also monitoring the heat and moisture transfer through the layers of the section of the wall. A numerical simulation was not considered appropriate for conducting the investigation due to uncertainties associated with the outcome of the computer simulation tools (see section 2.8) which in this study would have been due to the lack of data on thermo-physical and moisture-related properties of materials and the steady-state nature of these properties.

In terms of energy efficiency, improvement made by application of thermal insulation was tested in three multi-layer wall systems consisting of the three blocks named above, each insulated with 50 mm PIR board on the outside and rendered by cement externally and gypsum internally. To further improve the wall construction design taking into account EI and IAQ considerations, PIR was replaced by cork board insulation rendered with lime (as a replacement for cement) and finished internally with earth plaster (to replace gypsum plaster). Cork, lime and earth has lower embodied energy compared to PIR, cement and gypsum plaster as discussed in chapter 2, section 2.9. These proposed wall types were named low-carbon alternatives and along with the current practice wall systems were tested for their hygrothermal performance in a dynamic situation.

For many years, the wall performance was mainly evaluated through the steady-state heat transfer calculations based on thermal conductivity values measured in the laboratories. However, the actual behaviour of building fabric which is the function of heat storage capacity of materials,

fluctuating outdoor weather conditions, the presence of moisture as well as the insulative capacity of materials, required a more in-depth investigation. In response to this shortcoming, dynamic analysis methods such as admittance procedure were introduced taking into account thermal mass effect and time lag associated with heavy-weight structures. This is the approach taken by most building energy simulation tools such as IES VE that are widely used by building practitioners. However, moisture presence, its role in heat transfer through latent heat and moisture-induced changes of material properties is still missing from the equations. Recently more studies have acknowledged the importance of moisture and studied the simultaneous interactions of heat and moisture in building envelope. However, these studies have mostly used numerical models (Kočí et al., 2012; Konttoleon & Giarma, 2016). As it is discussed more in detail in chapter 2, the result of these numerical models needs to be dealt with care due to uncertainties associated with their outcome. On the other hand, examples of experimental studies on hygorthermal performance of building fabric have mostly dealt with the single-layer constructions (Moon et al., 2014; Othmen et al., 2018; Khoukhi, 2018). There is a gap in the existing body of knowledge on experimental campaigns studying heat and moisture transfer considering the interactions of the adjacent layers in a multi-layer wall system. The outcome of this study can therefore help understanding the importance of this holistic approach as opposed to analysing layers of the building fabric individually and concluding on its performance by simply summing these values up as isolated units. Moreover, the majority of the existing body of knowledge on the topic uses European and North American construction techniques which cannot be directly extended to techniques used in other parts of the world such as middle east with different climate condition and construction techniques.

The study of the Moisture Buffering Capacity (MBC) of materials and its impact on the indoor environment has been the subject of significant historical interest (Rode et al., 2008). Research has been undertaken on a wide range of materials to evaluate their ability to buffer indoor Relative Humidity (RH) on the core and insulation elements of the building envelope such as stabilised rammed earth (Alinson and Hall, 2010), extruded earth bricks (Cagnon et al., 2014), compressed earth blocks (McGregor et al.,2014), lightweight aggregate, concrete and cellular concrete (Rode et al.,2006), hygrophobic mineral wool, expanded polystyrene (Jerman and Cerny, 2012), hemp-lime (Latif et al.,2015) (Shea et al.,2012) and hemp fibre (Latif et al,2014). However, researchers such as Ramos et al., (2010), Latif et al., (2015) and Holcroft and Shea (2013) observed in their studies that the effect of final coating layers, i.e. the plaster and paint, on the overall moisture buffering capacity of the building envelope is distinct. They concluded that the buffering effect of the core decreased with the application of conventional, less porous, final coatings even though the thickness of this layer was significantly less than the core layers beneath. This shows the importance of considering

the hygroscopic properties of the final coatings when evaluating the moisture buffering capacity of the building envelope. Amongst finishing coatings, earth plaster is known for its moisture buffering capacity, making it a natural humidity regulator helping to improve Indoor Air Quality (IAQ) and comfort in buildings (Minke, 2012). This is particularly important as the drive towards more air-tight buildings highlights concerns related to occupant health (Laborel et al., 2016).

Earth has been traditionally used in Iran for plastering building envelope surfaces, usually mixed with plant-based fibrous aggregates such as straw to improve its mechanical strength. On the other hand, plant-based products contain natural polymers with hydroxyl groups that readily form hydrogen bonds with water and cause a high rate of water uptake. Existing literature suggests that the capacity of earth as a humidity regulator can be increased by the addition of plant aggregates, but a general conclusion cannot be drawn due to limited studies on this topic. Part of this study investigates whether and to what extent the addition of plant-based aggregates improves moisture buffering capacity of earth plasters using standard protocols for quantifying this property of materials. Known for its highly absorbent properties, a mineral material called Diatomaceous Earth was tested along with plant-based aggregates to further improve moisture buffering capacity of earth.

Chapter 2.

Literature review

Performing as an interface between outside and inside, external envelope of buildings has major role on their energy consumption and their occupant's health and comfort (Hegger et al., 2008). A significant amount of energy used in buildings, is spent on heating or cooling indoor space to create and maintain a comfortable environment for building occupants. The comfort condition created inside, gets disturbed by heat getting into or escaping out of the indoor confined space by transferring through the building fabric. This transfer of heat strongly depends on hygric, thermal and physical properties of materials used in building envelope.

In following sections, thermal properties of materials that are used to describe heat transfer phenomenon in building fabric, are briefly explained. Then we move to the next important factor affecting heat transfer and comfort in buildings i.e. moisture which has been subject of less interest until recently. Sources of moisture in buildings and moisture storage and transport mechanisms in hygroscopic materials were discussed. The concept of breathability was then explained and why it was introduced and matters. The role of moisture in heat transfer and heat-moisture coupled relationship was explained through mathematical equations. In the next stage, indoor relative humidity and its importance in creating a healthy environment was discussed. This follows by a discussion on the role of materials in moderating indoor RH levels through their moisture buffering capacity. Experimental protocols to evaluate and measure hygroscopic properties of materials are explained and discussed. The chapter finishes by emphasising on the role of finishing materials on humidity buffering in indoor space and focuses on moisture buffering potential of one of the most sustainable finishing materials i.e. earth plaster which has long been forgotten in modern construction and replaced by other more energy-intensive alternatives.

2.1. Heat storage and transfer in building materials

2.1.1. Basic thermo-physical properties of building materials

CIBSE (2006) lists fundamental properties of materials that control and dictate the heat storage and transfer in and through materials as density, specific heat capacity, thermal conductivity, vapour resistivity, absorptivity, emissivity, solar transmittance, solar absorptance, light transmittance. Derived parameters such as thermal transmittance (U-values), thermal admittance (Y-values), decrement factor, surface factor, are also used to explain dynamic heat transfer phenomenon in buildings. According to Givoni (1998), thermal conductivity and heat capacity, which are the values to measure thermal insulation and absorptance capacity, have the most control over the heat flow through the building envelope.

The thermal performance of a material is expressed by thermal conductivity, shown by lambda sign λ, which measures the rate of heat transfer (q=Q/t) through a cross section (A) and causing a temperature difference (ΔT) over a distance of ΔL. (Q/A) is therefore the heat flux which is causing the thermal gradient.

$$\lambda = \frac{q.d}{A.\Delta T}$$

Thermal conductivity of materials can change by temperature, age and moisture content. In porous materials, heat flow occurs through a combination of conduction, radiation, convection and latent heat exchange processes. When nonconductive modes of heat transfer occur within the material, the measured property of such materials is called apparent thermal conductivity. Materials with a low apparent thermal conductivity are called insulation materials (ASHRAE, 2009). The thermal insulation, when added to the elements of the building fabric inhibits heat transfer. Most heat loss through building insulation occurs by conduction which happens through the exchange of kinetic energy between atoms and molecules as they collide with each other. Therefore, conduction occurs only in matter. A vacuum space (which is free from atoms and molecules) is thus able to stop heat from moving through. However, vacuum is still not available as a reliable, inexpensive and practical form of insulation on a large scale. The next best approach is to minimise the amount of matter through which the heat can move. Gases have much lower density than solid, so insulation replaces as much solid material as possible with gas which is surrounding air in most insulations. If air movement by convection and pressure differences occurs, then its insulation properties are reduced. Porous insulation uses small quantities of solid material to hold the air in place. The solid material used in porous insulation can be in different forms (Wulfinghoff, 1999).

Besides thermal insulating capacity of a building envelope, its capacity to store heat, also affects the rate of heat transfer through the envelope. The capacity of a building component to store heat depends on its specific heat capacity and density (Hegger et al., 2008). Specific heat capacity C [J/kg.K] is the change in heat (energy) of unit mass of material for unit change of temperature (ASHRAE, 2009). It should be noted that, in evaluating heat storage capacity of a building envelope, density and specific heat capacity must be considered in line with thermal conductivity. As for example in case of wood, its low level of thermal conductivity limits the rate at which heat is absorbed and released in a daily cyclic variation. Thermal diffusivity and thermal effusivity are two derived material properties containing density, thermal conductivity and specific heat capacity. Thermal effusivity ($b = \sqrt{\lambda \rho c}$) indicates materials ability to exchange thermal energy with its surroundings whereas thermal diffusivity ($a = {}^{\lambda}/_{\rho c}$) represents how

fast heat diffuses through a material (Kinnane et al., 2015). A combination of these properties should be used for analysing the performance of materials. Table 2.1 compares thermophysical properties of some construction materials in relation to their thermal mass effect.

The heat storage capacity of a material which is a function of material density (ρ) conductivity (λ) and specific heat (Cp), is described as thermal mass effect. Materials with high thermal mass (i.e. heavier and denser materials) when exposed to source of heat, store more heat compared to materials with lower thermal storage capacities. They release their heat content more slowly, when the heat source is removed (Gregory et al., 2008). Therefore, in an indoor space with high levels of thermal mass, diurnal temperature swings are moderated, and cooling load peaks are reduced.

Table 2-1: Thermophysical properties of some common building materials (Clarke et al., 1990)

Building material	Specific heat capacity [J/kg. K]	Density [kg/m^3]	Thermal conductivity [W/m. K]	Diffusivity [m^2/s]	Effusivity [W.s$^{1/2}$/m^2.K]	Thermal mass effect
Timber	1600	500	0.13	1.625E-07	322.5	Low
Steel	450	7800	50	1.425E-05	13247.6	Low
Lightweight aggregate block	1000	1400	0.57	4.071E-07	893.3	Medium-high
Concrete	1000	2300	1.75	7.609E-07	2006.2	High

Thermal insulation and thermal mass are two important elements of passive design representing dynamic and steady-state thermophysical properties of materials; and materials with beneficial thermal properties are either of the two. An appropriate combination of both, results in thermal performance and energy saving benefits. In a building envelope, increasing insulation results in increases in the temperature difference between inside and outside, while increasing thermal mass increases the time taken for the outside heat to reach the interior. Therefore, for evaluating thermal performance of the building fabric, both should be taken into account simultaneously. Calculated thermal transmittance value (U-value), which is a measurement of insulative capacity of materials, on its own is not comprehensive for analysing thermal performance of the wall structure (Mohammad & Shea, 2013).

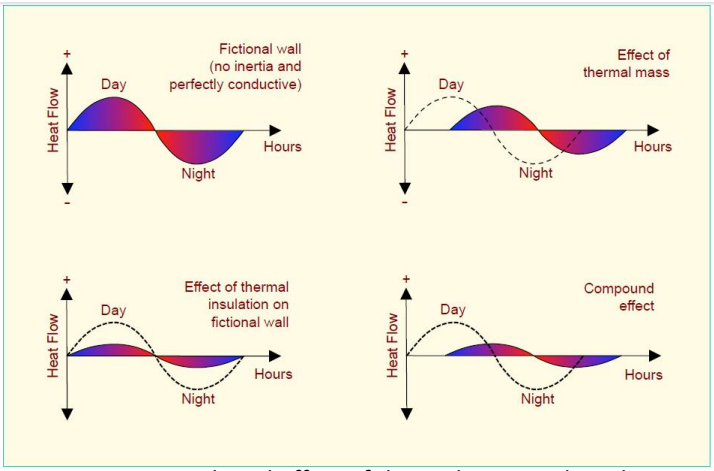

Figure 2-1: Combined effect of thermal mass and insulation

The location of thermal mass plays an important role in its effectiveness. The heat capacity of a building envelope is effective only throughout the layers in the first 100 mm of the thickness of the fabric in the case of fabrics thicker than 100 mm; or within the first half of the fabric if the thickness is less than 100 mm; or throughout the layers before an insulation layer is reached. The reason is that in a 24-hour cycle, most constructions are likely to be using only the first 50-100 mm of the thickness to provide any thermal damping effect, known as effective thickness. The effective heat capacity of an insulation layer is so small, that there is no benefit in considering further layers of construction in measuring effective heat capacity of the fabric. As an example, in the case of an internally insulated wall, the insulation separates the mass of the wall (i.e. layers underneath the insulation) from indoor air and impedes its thermal buffering potential to be effective.

Time lag is another parameter for evaluating thermal performance of opaque building components which has a direct relationship with effective heat capacity of the building. It specifies the period of time it takes for a temperature rise on the outside of the wall to pass on to the interior (Fig 2.2) (Hegger et al., 2008). The time (or phase) lag is specifically high when a material has a high effective heat capacity but at the same time a low thermal conductivity. A low thermal diffusivity indicates a high phase lag for a material, while higher diffusivities represent faster diffusion of heat through the mass of the materials (Hegger et al., 2008). In other words, the penetration depth is limited by the diffusivity of the material during one cycle (Li and Xu, 2006).

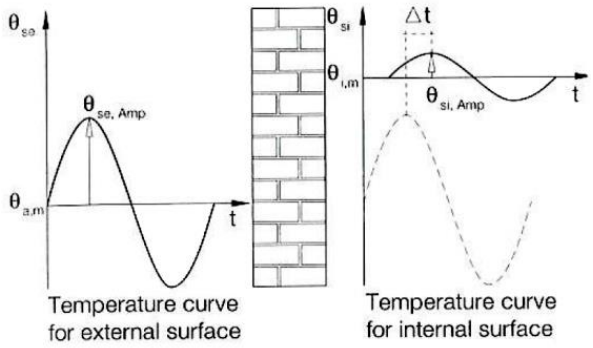

Figure 2-2: Time lag caused by materials, (Hegger et al., 2008)

2.2. Thermal transmittance measuring methods

Thermal and moisture transfer through the building envelope determines its hygrothermal performance and the energy needed to provide comfort within the boundaries of the envelop. From the materials properties characterising these transfer processes, thermal conductivity is one of the most important properties. From this property derives the thermal transmittance and

thermal resistance values (known as U-value and R-value respectively), used as design criteria in many building regulations, to express the thermal insulating capacity of a multi-layer assembly (Perez et al., 2014). Thermal transmittance is the heat flow that passes through a unit area of a complex component due to a temperature gradient equal to 1 K (unit: W/m^{2}K). This value takes into account the thickness of the material and heat transfer due to convection and radiation (Schiavoni et al., 2016) and includes thermal bridge effects and the surface heat transfer coefficient at both sides of the assembly. Thermal resistance R [m^{2}K/W] is reciprocal to thermal transmittance.

The accurate characterisation of thermal conductivity of materials, and subsequently thermal transmittance and resistance is a fundamental task for appropriate thermal design of any building. Different methods have been instructed by standards for experimental measurements or theoretical calculations of heat transfer through the section of a material or a composition of several materials. These methods have been summarised in Figure 2-3. In the following section a detailed description of these methods is given.

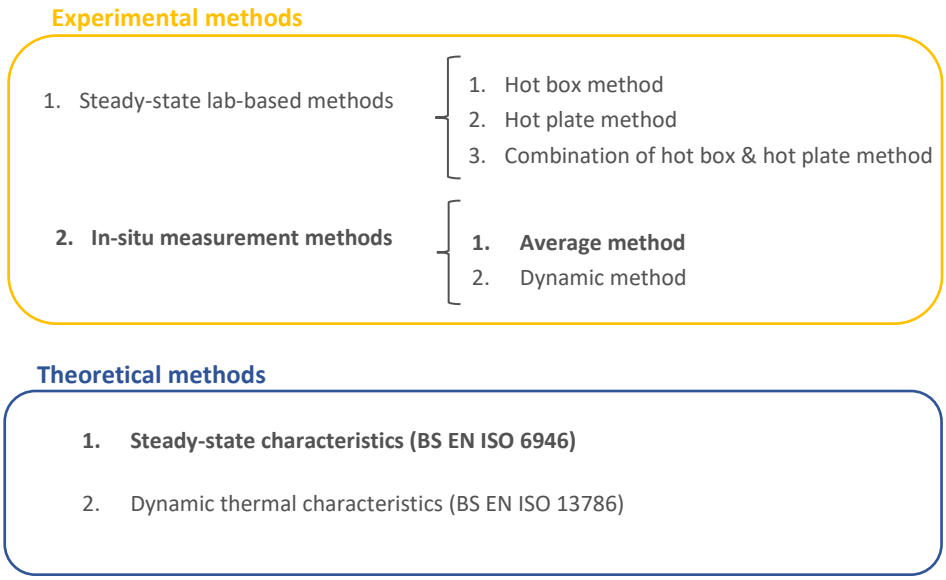

Figure 2-3: Experimental & theoretical methods to evaluate thermal performance of building components

2.2.1. Steady-state laboratory-based methods

The performance of the building envelope can be partly quantified/evaluated by its thermal transmittance. BS ISO 7345 (2018) defines this value as heat flow rate (q) in the steady state divided by area (A) and the temperature difference between the surroundings on both sides of a flat uniform system, the U-value.

$U = q/(T_1-T_2)\ A$

In principle, the U-value can be obtained by measuring the heat flow rate through an element with a heat flow meter or a calorimeter, together with the temperatures on both sides of the element under steady-state conditions (BS ISO 9869, 2014). Steady-state heat transfer properties may be measured by a number of standardised test methods (EN 12667, 2001).

1. **Hot box method** including guarded hot box (GHB) and calibrated hot box (CHB) method. Heat transfer through many thermal insulating systems is a complex combination of conduction, convection and radiation. The GHB and CHB methods measure the total amount of heat transferred from one side of the specimen to the other. BS EN ISO 8990 (1996) explains the use of CHB and GHB to impose steady-state conditions on two sides of a sample. Both hot box methods create and maintain specific boundary conditions on two sides of a specimen placed between a hot and a cold chamber. The thermal transfer properties of the specimen are calculated from measurements taken from steady-state air and surface temperatures and of the power input to the hot side of the metering box.

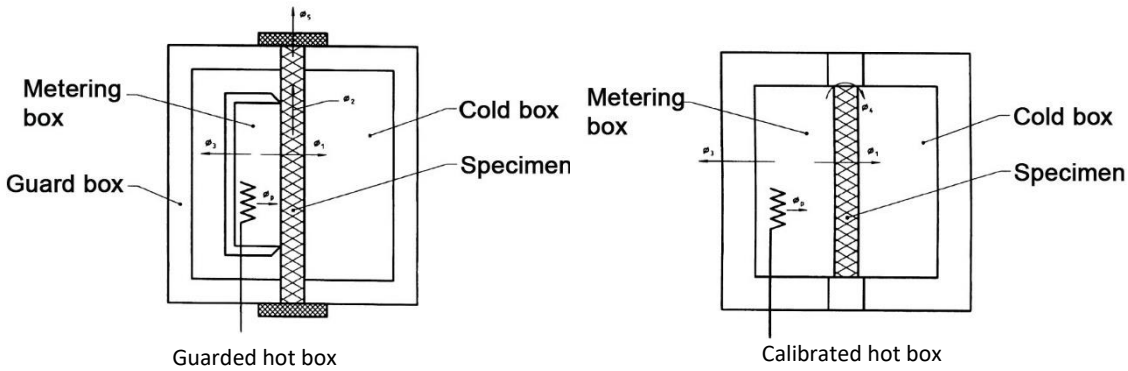

Figure 2-4: Configurations of a Guarded Hot Box (left) & a Calibrated Hot Box (right), (BS ISO 8990, 1996)

2. **Hot plate method** including guarded hot plate (GHP) and heat flow meter (HFM) methods (EN 12667, 2001). Both methods are intended to create a unidirectional constant and uniform density of heat flow rate within homogenous specimens with flat and parallel faces. Thermal resistance is then calculated by measuring the density of the heat flow rate (q) and the temperature difference (ΔT) across the specimen.

   In the guarded hot plate apparatus, the heat flow rate is calculated from the measurement of the power input to the heating unit.

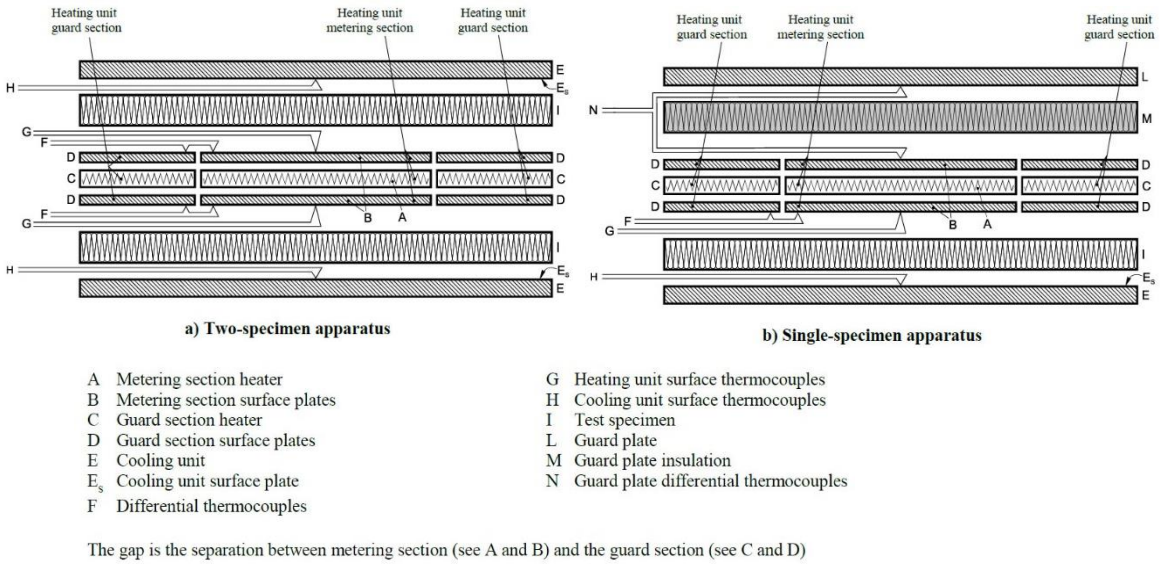

Figure 2-5: General features of two-specimen & single-specimen guarded hot plate apparatus, (EN 12667, 2001)

In HFM apparatus, the density of heat flow rate is measured through one or two heat flow sensors placed against the specimens.

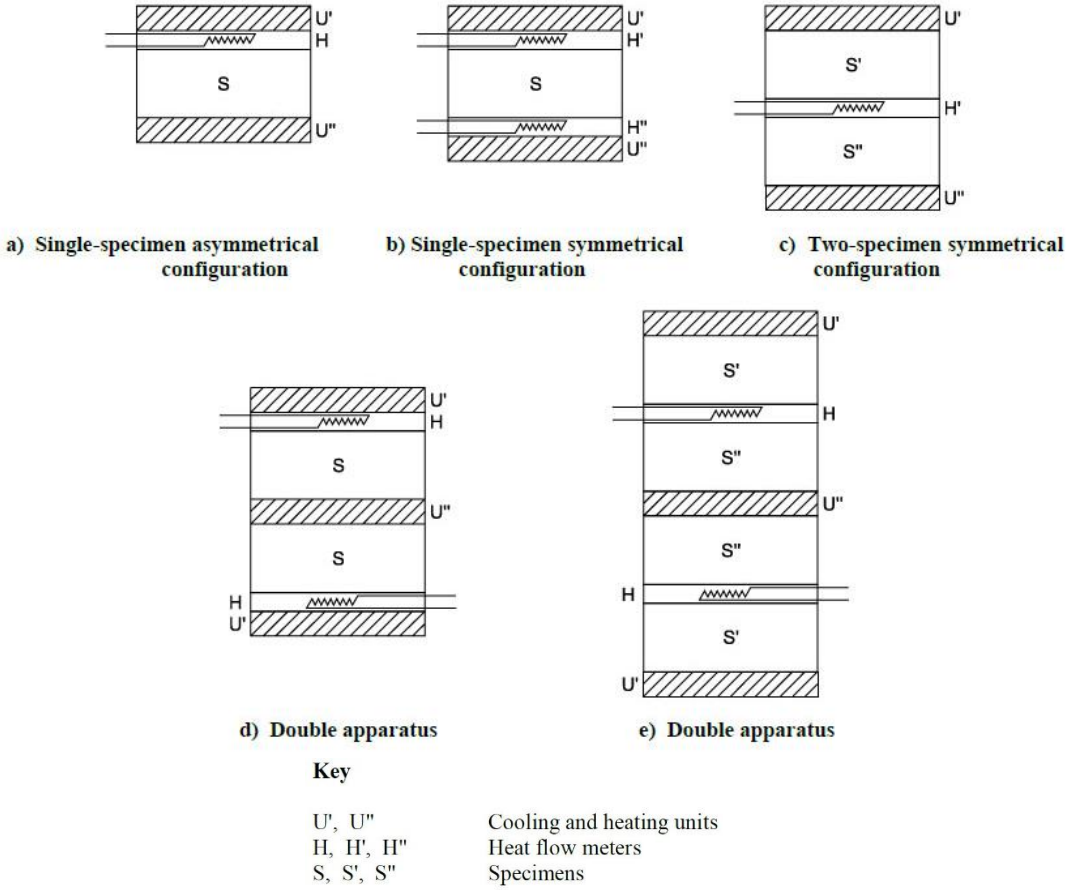

Figure 2-6: Typical layouts of heat flow meter apparatus; (EN 12667, 2001)

3. **Heat flow meter hot box:** EN 1934 (1998) uses a combination of both hot box and heat flow meter concepts to introduce another method to measure thermal transmittance properties of a construction (Figure 4-4). The Standard introduced this method as the

heat transfer through many masonry elements in practice is a complex combination of conduction, convection, radiation and mass transfer. Therefore, neither hot plate methods (requires homogeneous specimens) nor hot box methods (which cannot be used for non-steady state boundary conditions) could be relied upon for evaluating thermal transmittance properties of wall specimens.

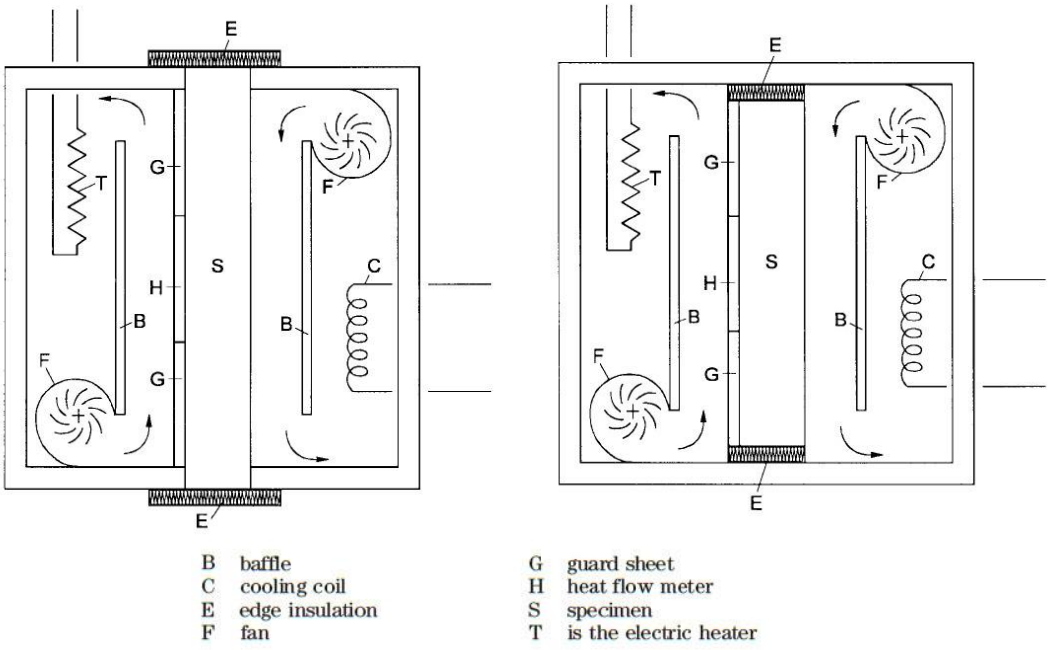

Figure 2-7: Typical layouts of heat flow meter hot box apparatus; (BS EN 1934_1998)

2.2.2. In-situ measurement methods

Steady-state conditions cannot be achieved on site or in reality. Therefore, in-situ U-value measurement methods have been proposed that rely on averaged data as an approximation for measurements under steady state conditions (Deconinck & Roels, 2016). These methods involve measurement of heat flux and temperature on both inner and outer surfaces of the building fabric component which can be analysed using two main approaches; (a) modelling of the envelope with R-C networks and use of system identification tools and (b) the use of standardised methods that introduce statistical methods (Atsonios et al., 2017). Currently, two international standards, BS ISO 9869-part 1 and ASTM C 1155, are available to analyse the heat flux and temperature data gathered on site. The ISO 9869-1 introduces the Average and the Dynamic method and ASTM C 1155 introduces the Summation and the Sum of Least Square (SLS) Method. The Average and the Summation methods are similar as they use a simple method of taking the mean values over a sufficiently long period of time. Being easy to use with rapidly generated results, these methods are most widely used. The SLS and Dynamic method, however,

require the development of complex algorithms to analyse the time series data, but are more likely to produce reliable results (Atsonios et al., 2017).

The limitations of these standardised methods are their precision, which depends on measurement conditions, and the duration of the measurement conditions. Flanders et al. (1995) studied the outcome of two ASTM methods (Summation and SLS methods) and reported that with sufficiently high indoor-outdoor temperature differences, the results from the two methods were in good agreement with each other. Deconinck and Roels (2016) and Gaspar et al. (2011) compared the two ISO methods i.e. the Average and the Dynamic method using different measuring conditions and concluded that the Average method performed similarly to the Dynamic method, provided a high temperature difference was applied across the sample. The duration of the measurement periods also plays an important role in the accuracy of the results. According to the standards this duration can range from 72 hours to more than 7 days, depending on the method, the measuring conditions and the type of the wall under test.

An example of the in-situ measurement of construction assemblies is the study conducted by Hulme and Doran (2014). The initial aim of their study was to understand how the walls of homes in the UK performed in-situ to give realistic estimates of current energy use and to quantify energy saving potential through measures such as applying wall insulation. They then compared the results of their in-situ measurements (using methods described in ISO 9869-1) with theoretical calculated thermal transmittance values (calculated according to BS EN 6946) and concluded that for solid walls, calculated values were generally higher than measured values. For insulated cavity walls, calculated values were normally lower than measured values and for uninsulated cavity walls there were approximately an equal number of cases where calculated values were above and below corresponding measured values.

The method described in BS ISO 9869-1 to measure the thermal transmittance value assumes that the mean values of heat flow rate and temperatures over a reasonably long period of time (minimum 72 hours) give an estimate of the steady-state condition. A steady-state condition of a system or process is the condition that does not change over time; broadly it is a condition that changes only negligibly over a specified time (Kosmina, 2016). The transmittance can be obtained by dividing the mean density of heat flow rate by the mean temperature difference. An estimate of the resistance is obtained by:

$$R = \frac{\sum_{j=1}^{n}(T_{sij} - T_{sej})}{\sum_{j=1}^{n} q_j}$$

And an estimate of thermal transmittance, U, by taking surface resistances into account and using air temperatures instead of surface temperatures, is obtained by:

$$U = \frac{\sum_{j=1}^{n} q_j}{\sum_{j=1}^{n} (T_{ij} - T_{ej})}$$

The test can be completed when the following conditions are met (Deconinck & Roels, 2016):

- Condition 1: the duration of the test exceeds 72 hours.
- Condition 2: the R-value obtained at the end of the test does not deviate by more than ±5 % from the value obtained 24h before;
- Condition 3: the R-value obtained by analysing the data from the first time period during INT(2 x DT/3) d does not deviate by more than ± 5 % from the values obtained from the data of the last time period of the same duration. DT is the duration of the test in days; INT is the integer part.

2.3. Thermal transmittance calculation methods

2.3.1. Steady- state thermal resistance

Where it is not possible to measure the thermal transmittance through an experimental set up, the steady state U-value of a construction assembly can be calculated using the thermal conductivity values of the materials, given by the manufacturer or found in standards or other relevant documents, the thickness of the layers and internal/external surface resistances of the assembly. BS EN ISO 6946 introduces a calculation method that applies to components and elements consisting of thermally homogeneous or combinations of homogeneous and non-homogeneous layers. This method is explained in section 4.3.2.1, where the thermal resistance of construction blocks was calculated.

2.3.2. Dynamic thermal characteristics

For a more realistic evaluation of the thermal performance of building elements, BS EN ISO 13786: 2017 (Thermal performance of building components- Dynamic thermal characteristics- Calculation methods) introduced a calculation methodology to evaluate the dynamic thermal behaviour of a building component. The methodology uses (1) thermal characteristics of building components i.e. thermal conductivity, density, specific heat capacity, (2) geometric characteristics i.e. area of the building components and thickness of each of its layers, and (3) period of temperature variations as input data for a calculation method that uses complex numbers representing a sinusoidal variation of temperature and heat flow to calculate non-steady-state thermal characteristics of that building component. The output data are heat

capacity, thermal admittance, periodic thermal transmittance, decrement factor, periodic penetration depth which are reported and used to evaluate the dynamic thermal response of a building component.

2.4. Moisture storage and transport in building materials

Moisture is an important parameter to be considered in building physics studies. On one hand, it affects materials properties such as density and thermal conductivity and consequently their thermal performance. On the other, it has a direct influence on building occupant's health and comfort as well as durability of construction materials. There are various ways moisture can get into a building component. Figure 2-8 illustrates the hygrothermal loads acting on the building envelope. These hygrothermal fluxes act simultaneously in a complex manner and need to be analysed prior to design of any building envelope component to predict its influence on hygrothermal behaviour of building assemblies (ASHRAE, 2009).

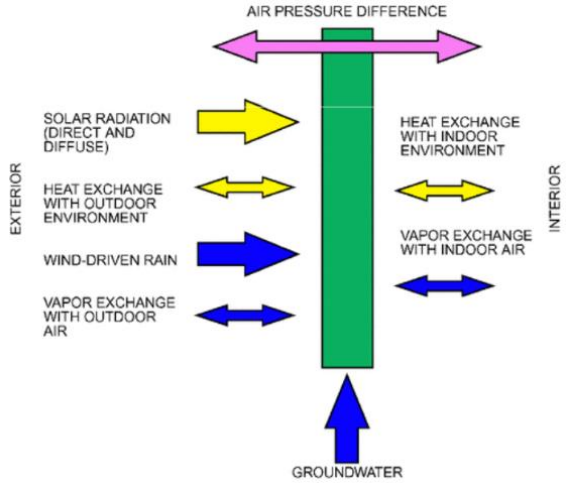

Figure 2-8: hygrothermal loads and alternating diurnal or seasonal directions on building envelope, (ASHRAE, 2009)

In following sections, basic hygric properties of materials that are needed for understanding the moisture storage and transport in and through a building component are firstly discussed; along with moisture transport mechanisms and indices to measure and quantify these hygric properties. Secondly, the importance of indoor humidity on occupant's health and comfort is briefly discussed as well as the role of humidity regulating materials in moderating indoor environment.

2.4.1. Hygroscopic materials and moisture storage

A material is called dry when it contains no water or only chemically bonded water (Kunzel, 1995). The building materials can be classified as hygroscopic and non-hygroscopic. Non-hygroscopic materials when in contact with moist air remain dry. However, if a material is hygroscopic, it absorbs moisture from the air at the inner surfaces of their pore system until it reaches an equilibrium state with the ambient conditions. Moisture absorption in building

materials, occur in three moisture regions when they are subject to increasingly intensive moisture conditions. A) sorption moisture or hygroscopic region which ranges from dry state up to an equilibrium moisture of about 95% relative humidity and includes water contents resulting from water vapour sorption up to a state of equilibrium. B) Capillary water region which follows the sorption moisture region and reaches up to free water saturation. When a capillary-active building material comes in contact with liquid water, it absorbs water until it reaches free water saturation. C) Supersaturated region which is reached only after a long time by dissolution of pores in water (Figure 2-9) (Kunzel, 1995). In this region, the RH is always 100% or higher (Kurs, 1996). in laboratory, this region occurs through suction under pressure and ranges to filling of all cavities.

This wetting process that happens in hygroscopic region is known as absorption. When the moisture source is removed, the material desorbs the moisture back to the air, this drying phenomenon is known as desorption process. The cyclical absorption and desorption process in hygroscopic materials is described as moisture buffering. Under isothermal conditions, the relationship between the volume of the accumulated water (moisture content of a material) and RH is characterised by sorption isotherm which is done through sorption measurements up to a RH of about 95%. During drying less of water is released from the material than water trapped during humidification. Therefore, there is a difference between absorption and desorption curves with desorption curve having higher values of water content for the same level of RH. This phenomenon is known as hysteresis (Kwiatkowski et al., 2009).

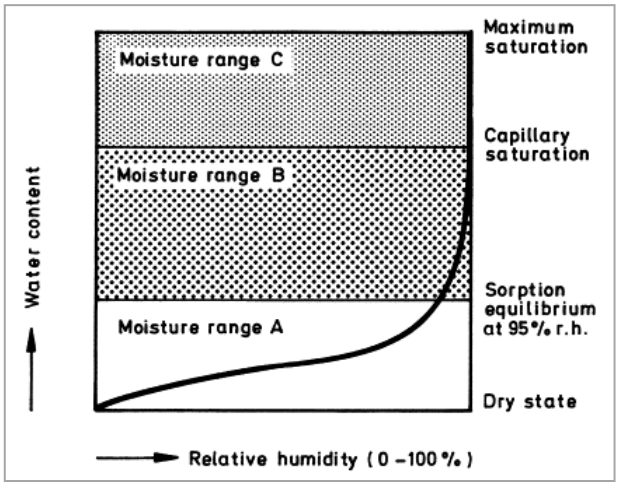

Figure 2-9: Schematic representation of the water storage function of a hygroscopic, capillary active building material (Kunzel & Kiessl, 1997)

The three regions characterise the moisture storage behaviour of hygroscopic, capillary-active building materials such as building stones, mortar and wood products. Only region C can occur in non-hygroscopic, non-capillary-active materials such as most insulation materials. This means

that under dew point conditions (at RH of 100%), moisture in liquid form can be found in these materials. On the other hand, in polymeric coatings or films, only region A occurs; since they are initially without pore spaces able to absorb water, the absorbed water must find room in polymer structure. Direct transition from region A to C is also possible as in mortar or building stones made hydrophobic that are still hygroscopic but no longer capillary-active. In practice, the actual moisture contents of building components are most of the time in hygroscopic region (region A). Data for Sorption isotherms of up to about 90% RH for many building materials can be found in literature (Krus, 1996 & Kunzel, 1995).

2.4.2. Moisture transport mechanisms

The moisture transport mechanisms relevant to calculations in building physics are water vapour diffusion and liquid transport through capillary forces. The interaction of these has been graphically shown in Figure 2-10. In this figure, the condition assumed on two sides of the enclosure is vapour pressure greater on the interior side (due to higher indoor temperature) and the relative humidity greater on the exterior side (winter condition in Germany). If the material is sufficiently dry or non-hygroscopic, then the water vapour will diffuse from inside to outside, following the direction from higher to lower vapour pressure. The water absorbed in the walls remain immobile due to high adhesive forces. When total moisture rises, the pore walls are covered with a sorbate film which is thicker on the outside because the RH outdoors is higher than indoors. The thicker the film, the more mobile the water molecules become, moving from the thicker film sections to thinner sections. This process is called surface diffusion and is superimposed on the normal vapour diffusion on the pore air. Surface diffusion (as well as capillary conduction) is therefore a part of liquid transport and its driving force is RH or the suction stress and not the vapour pressure as the thickness and the mobility of the sorbed molecular layer increases with RH. Therefore, under assumed condition surface diffusion (a type of liquid transport) and vapour diffusion go in opposite directions. Vapour diffusion takes place in the larger pores, while liquid transport – independent of vapour diffusion- takes place via the micro-pores and on the pore walls. The opposite direction of vapour and surface diffusion reduces moisture transport from inside to outside and when total humidity increases, this moisture transport is even reversed due to onset of capillary conduction. It should be noted that this capillary conduction that is initiated by surface diffusion is different from capillary transport of water as a liquid which occurs by water penetration into the material e.g. driving rain. This later form of capillary water transport happens in larger pores compared to those involved in surface and vapour diffusion. The focus of this study is on the vapour and surface diffusion and moisture movement due to water ingress into materials is ignored.

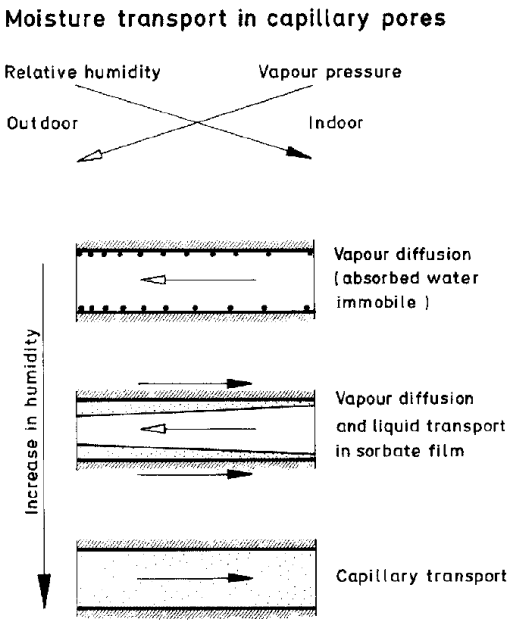

Figure 2-10: Moisture transport phenomena in the pores of a massive exterior wall in winter of a north European country, for different levels of moisture content (Kunzel, 1995)

May (2005), summarises these moisture transfer mechanisms in a property known as breathability. He states that the effect of moisture on buildings is related to three properties:

- Vapour permeability: the ability of a material to allow water vapour to pass through it.
- Hygroscopicity: the absorption/ desorption of water vapour as RH changes.
- Capillarity: which is the absorption/desorption of water as liquid.

This is what Kunzel (1995) describes as moisture transfer mechanisms through vapour diffusion, surface diffusion and capillarity and is mainly related to physical micro-porous structure of materials. A comparison of pore structure of fired clay bricks with very large capillary quality, versus calcium silicate bricks with less capillary quality but a high hygroscopic capacity, is a good example. The pores of fired clay bricks are all of a similar large size, while the calcium silicate bricks have a wide distribution of pore sizes.

2.4.3. Effect of moisture on hygrothermal characteristics of materials

Heat and moisture transfer through the building envelope depends on characteristics of its construction materials. These characteristics can change significantly by changes in temperature and moisture content of the material. The changes induced by temperature variations are not found to be significant given the limited temperature range construction materials are exposed to under normal boundary conditions. However, the dependence of these materials characteristics on moisture content is far more significant (Jerman & Cerny, 2012). The presence of water increases the effective thermal conductivity of moist materials as the air in materials'

pores gets replaced by liquid water with thermal conductivity of orders of magnitude higher than the air (Jin et al., 2016). The rate of change of thermal conductivity with moisture content is different for different materials. Inorganic lightweight insulating materials (mineral fibre) show a significant increase in thermal conductivity with only small increase in moisture content. However, for timber products, the relationship between the thermal conductivity and the moisture content is approximately linear throughout and no rapid increase is observed at low moisture contents. Masonry materials behave in a broad spectrum between the two extremes mentioned above. Figure 2-11 shows the percentage increase of thermal conductivity value for different types of materials.

Building regulations use tabulated normative conductivity values determined based on the standardized conditions of specific temperature and humidity levels. These values, therefore, do not represent the actual or design thermal conductivity that occurs in real condition. This results in discrepancy between the expected hygrothermal behaviour of buildings derived from numerical models and their actual behaviour (Perez et al., 2015).

Specific heat capacity, another material property influencing the heat and moisture transfer, gets significantly affected by variations of moisture content due to high specific heat capacity of water. Unlike thermal conductivity, an increase in heat storage parameters is, however, positive for a building envelope when high level of thermal mass is desirable (Jerman & Cerny, 2012).

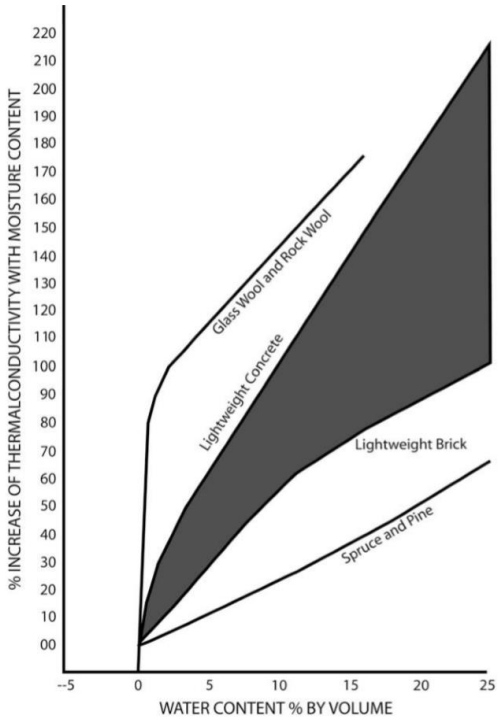

Figure 2-11: Effect of moisture on thermal conductivity of different types of materials (Clarke & Yaneske,2009)

Water vapour transmission capacity of materials also changes with changes of moisture content. When the material is dry the vapour diffusion happens through a relatively simple mechanism. As the material gets moist, the diffusion process is complemented by other forms of transport, which can result in significant increase in vapour permeability of materials. Hygroscopic and non-hygroscopic materials behave well different from each other in terms of changes in vapour permeability with moisture content. Figure 2-12 shows the differences in behaviour between a hygroscopic (plywood) and a non-hygroscopic (plasterboard) material. Plasterboard has been affected by changes in moisture content to a limited extent and a single value obtained under the highest level of humidity can adequately represent the vapour permeability. For hygroscopic materials, up until 60% RH, where vapour diffusion dominates, the behaviour is similar to non-hygroscopic materials. However, above this level the behaviour becomes non-linear showing rapid changes in permeability with small changes in humidity. The same as what was discussed for reported thermal conductivity values, most quoted data on vapour permeability is based on standardised measurements at one or two values of humidity. While this might be reasonable for non-hygroscopic materials, it does not adequately describe the behaviour of hygroscopic materials above the transition point (Clarke & Yankese, 2009).

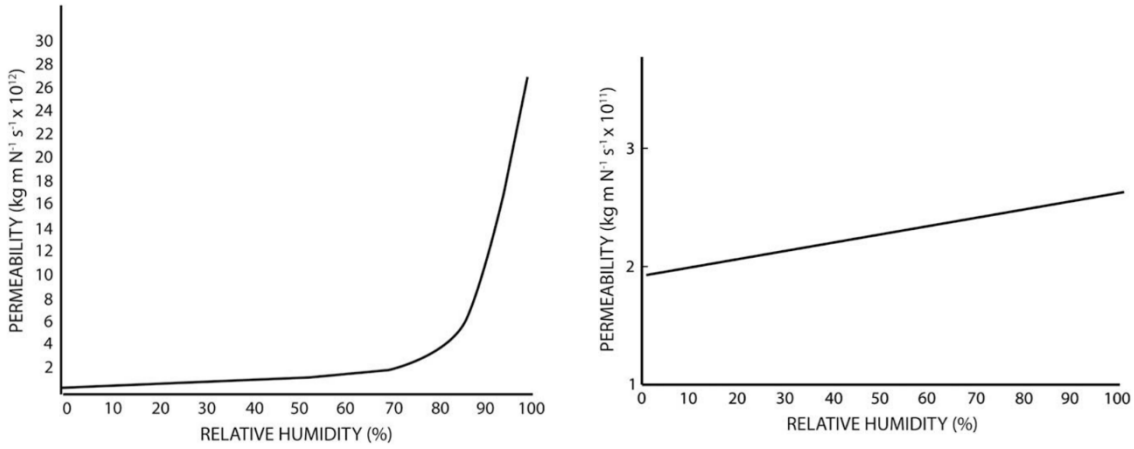

Figure 2-12: Permeability as a function of RH for plywood (left) and plasterboard (right); (Clarke & Yaneske,2009)

Therefore, an accurate assessment of the hygrothermal performance of building envelope heavily depends on the comprehensive knowledge of the characteristics of building materials in different environmental conditions (with different temperature and moisture content). This evaluation should not be limited to standardized steady-state values especially in case of hygroscopic materials.

2.5. Coupled heat and moisture relationship through mathematical equations

In this section, the equations involved to describe heat and moisture transport through the building envelope are briefly introduced to show the factors involved and affecting these phenomena (Kunzel, 1995). Heat flows through the building material due to temperature gradient or through enthalpy flows with phase change (enthalpy flows due to liquid transport play a negligible role compared to vapour diffusion flows connected with phase changes such as drying processes). The interaction of vapour diffusion and phase change is therefore taken into account in the form of a source or sink term in the heat balance equation:

$$\frac{\partial H}{\partial t} = -\nabla . q + S_h$$

H [J/m^3] total enthalpy

q [W/m^2] heat flux density

S_h [W/m^3] heat source or heat sink

The total enthalpy of a building component layer is the sum of the enthalpy of dry building material and the enthalpy of the water contained in the material:

$$H = H_s + H_w$$

Where

H_s [J/m^3] enthalpy of the dry building material

H_w [J/m^3] enthalpy of building material moisture

The heat content of a material under isobaric conditions is called the enthalpy. In the temperature range of concern in building physics, there is an approximately linear relationship between the enthalpy of a dry material and its temperature. This relationship is described by the following equation:

$$H_s = \rho_s c_s \vartheta$$

H_s [J/m^3] enthalpy of dry building material

ρ_s [kg/m^3] bulk density of the building material

c_s [J/kgK] specific heat capacity of the building material

ϑ [^{o}C] temperature

In the case of moist building materials, the enthalpy of water contained in the material should be added to the enthalpy of dry material. Enthalpy of water depends on the physical states and can be determined through the following equation:

$$H_w = [(w - w_e)c_w + w_e c_e - h_e \frac{dw_e}{d\vartheta}$$

H_w [J/m3] enthalpy of moisture in building material

c_w [J/kgK] specific heat capacity of liquid water

c_e [J/kgK] specific heat capacity of ice

h_e [J/kg] specific melting enthalpy (melting heat)

w [kg/m^3] total water content

w_e [kg/m^3] content of frozen water

the heat flux density (q) is proportional to thermal conductivity of the moist building material and the temperature gradient:

$$q = -\lambda \nabla \vartheta$$

q [W/m^2] heat flux density

λ [W/mK] thermal conductivity of the moist building material

ϑ [°C] temperature

The enthalpy flows through moisture movement and phase change can be taken into account in the form of heat source/ sink in the heat balance equation. Since only vapour diffusion with simultaneous phase transition is of practical importance (enthalpy flows as the result of liquid transport play a negligible role), the heat source/sink is explained by:

$$S_h = -h_v \nabla g_v$$

S_h [J/m^{3}s] heat source/ heat sink through condensation

h_v [J/kg] latent heat of phase change (evaporation enthalpy of pure water 2500 kJ/kg)

g_v [kg/m^{2}s] vapour diffusion flux density

The vapour diffusion flux density g_v is calculated with the moisture balance equation which in analogy to heat balance equation can be written as:

$$\frac{\partial w}{\partial t} = -\nabla.(g_w + g_v) + S_w$$

w [kg/m^3] water content of the building material layer

g_w [kg/m^{2}s] liquid transport flux density

g_v [kg/m^{2}s] vapour diffusion flux density

S_w [kg/m^{3}s] moisture source or moisture sink

The liquid transport flux density is dependent on RH gradient and is calculated through:

$$g_w = -D\varphi\nabla\varphi$$

D_φ [kg/ms] liquid conduction coefficient

φ [-] relative humidity

The vapour diffusion flux density g_v can be determined as:

$$g_v = -\delta_p\nabla p$$

δp [kg/msPa] water vapour permeability of building material

p [Pa] water vapour partial pressure

Moisture sources (S_w) e.g. leaking water pipe happen rarely in building components; therefore are not considered in these equations. Moisture sinks, also, are disregarded as they occur in chemical reactions with materials e.g. in curing process of concrete and mortar. Equations for heat balance and moisture balance are closely coupled with each other through the moisture dependence of total enthalpy, thermal conductivity and heat source/sink through condensation/evaporation, and temperature dependence of moisture flows in moisture balance equation.

2.6. Indoor humidity, comfort and moisture buffering capacity

Indoor air humidity affects indoor climate significantly. Among factors associating with indoor air quality IAQ and occupant health such as indoor temperature, humidity, ventilation rate and volatile organic compound (VOC) levels, humidity is one of the most important factors (Yoshino et al., 2009). Low indoor RH levels might result in dryness of the skin, mucous membranes, sensory irritation of the eyes and upper airways while having high RH levels may result in material deterioration and mould growth (Padfield, 1999, Kwiatkowski et al. 2011, Woloszyn et al. 2009). Moreover, in most indoor environments inhalation of air will cause a cooling of the mucous membranes in the upper respiratory tract, which contributes both to the perception of thermal environment and to the perceived air quality (Toftum et al.,1997). At high air temperatures and humidities, the respiratory cooling will decrease with the result that air may be perceived as stuffy and uncomfortable. In addition, in high RH levels rate of moisture evaporation from skin is decreased, hence reducing the evaporative cooling effect caused by sweating of the human body.

It has been shown in several studies that the upper limits for RH should not exceed 60-80% depending on the criteria (ASHRAE, 2010; ASHRAE 2009; Crump, 2002). The indoor humidity should even be kept below 60-70% RH to avoid the growth of fungi and mites and above 30% RH to reduce respiratory infections. A comfort zone in balance with the outdoor climate

conditions, which is considered both comfortable and healthy, lies between 20 and 26°C and 30 and 60% RH according to ANSI/ASHRAE standard 55-1992 with Addendum 55a-1995 and ISO 7730-1994 standard. These standards reveal a comfort zone based on a 10% dissatisfaction criterion for thermal discomfort (Hameury et al.,2004). Figure 2-13 shows a range within which health and IAQ parameter are less negatively affected.

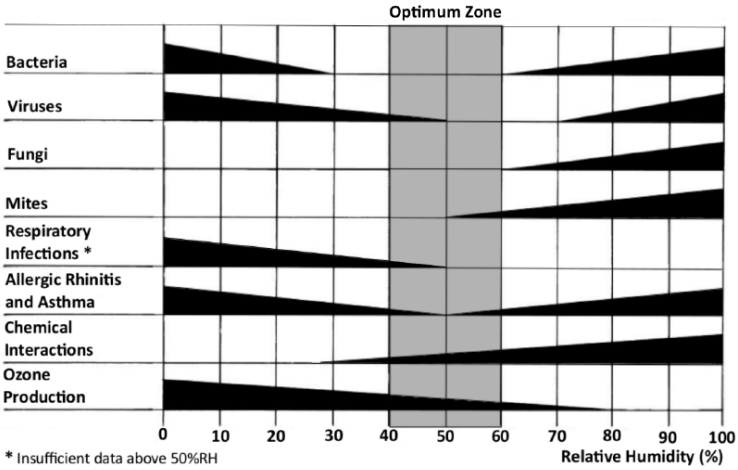

Figure 2-13: Health and IAQ parameters affected by indoor RH (Arundel et al., 1986)

By regulating indoor climate, hygroscopic materials could improve material durability, occupant health, comfort and productivity and energy performance of buildings. Since perceived IAQ is closely linked to humidity, the moisture buffering of the building fabric has potential of reducing energy use through reduction of the required ventilation rate (Simonson et al., 2004a). Moreover, indoor relative humidity affects latent heat stored in indoor air and subsequently affects cooling loads of the building. Simonson et al. (2004a) investigated the effect of hygroscopic wooden panelling on indoor humidity conditions in a bedroom in three Canadian cities using a numerical model. The comparison of hygroscopic and non-hygroscopic materials indicated the importance of hygroscopic materials specifically during the humid and cool weather. The most unpleasant conditions were nearly always improved with application of hygroscopic materials, but there were a few days in each climate that the indoor conditions were worse.

In another study, humidity, comfort and air quality in a bedroom of a wooden building located in four European countries (Finland, Belgium, Germany, and Italy) was studied by a numerical HAMT model. Comparison of the result with a non-hygroscopic case revealed that moisture transfer between indoor air and the hygroscopic structure reduced the peak indoor humidity (up to 35%) and percent dissatisfied with indoor air quality (up to 25%). Figure 2-14 illustrates the result of the numerical model on the psychrometric chart (Simonson et al., 2004b).

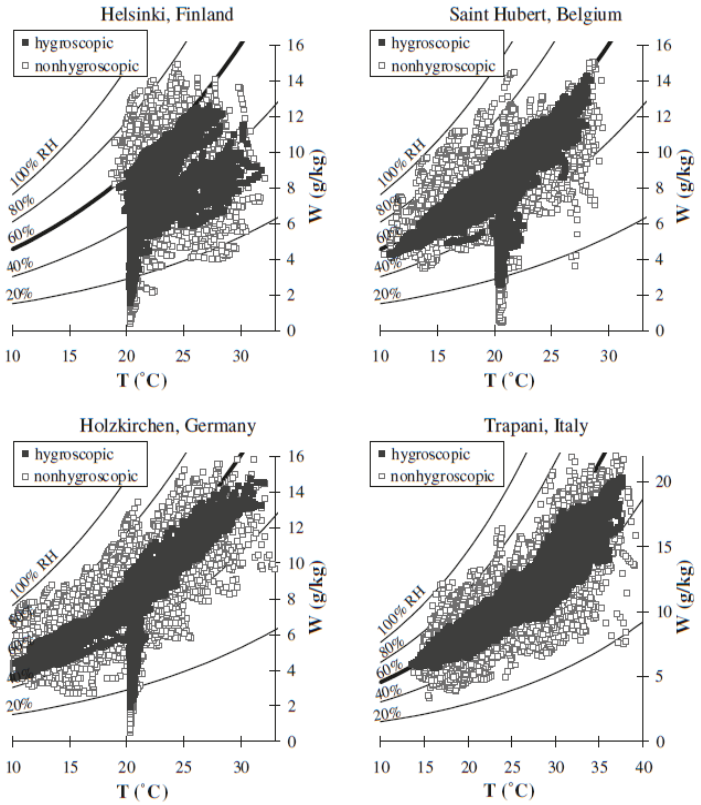

Figure 2-14: Hourly values of indoor temperature and RH during the whole year in hygroscopic and non-hygroscopic case, (Simonson et al., 2004b)

Hall and Casey (2012) studied HVAC energy consumption in a room located in Leicestershire, UK, constructed with Stabilised Rammed Earth as wall material and compared the results with non-hygroscopic and less-hygroscopic cases (foil, painted plasterboard, unpainted plasterboard) (Figure 2-15). They defined two ventilation systems, HVAC operated all day and HVAC operated according to indoor conditions. The results indicated that when used in conjunction with HVAC system, there is a significant reduction in humidification and dehumidification energy demand when compared to the conventional wall materials as shown by data in Table 2-2. When intermittent mode HVAC was simulated energy saving was less compared to the previous case. This is because extra load is imposed on HVAC unit to remove the moisture being absorbed by SRE walls when the system had been turned off.

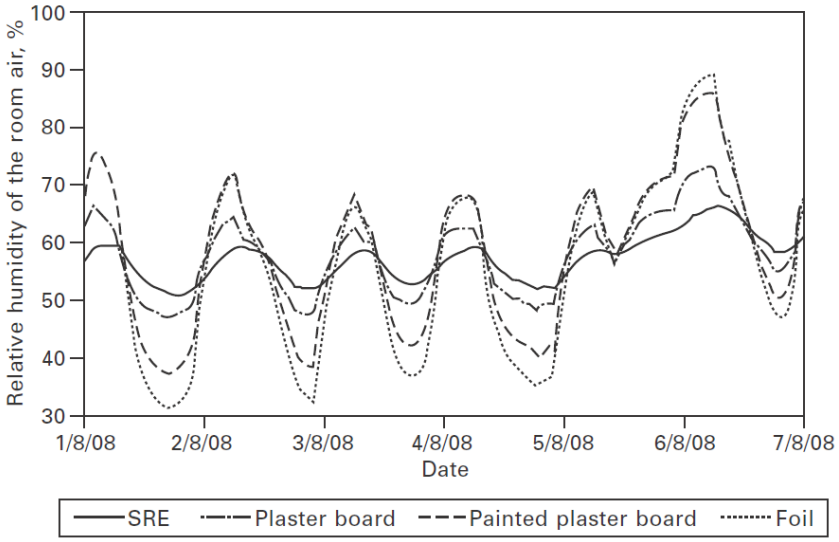

Figure 2-15: RH variation for different wall materials, in a bedroom over a typical week in summer, (Allinson and Hall, 2010)

Table 2-2: Daily HVAC energy consumption for constant mixed mode operation with SRE & conventional wall materials (Allinson and Hall, 2010)

			Plasterboard		
HVAC operated all day		SRE	Unpainted	Painted	Foil
Heating power	kW	1313.7	1313.7	1313.8	1314.1
Cooling power	kW	–135.0	–135.0	–135.0	–135.0
Latent heat humidification	kW	–1.9	–7.0	–26.2	–35.0
Latent heat dehumidification	kW	41.2	58.7	86.2	89.5
Total humidifying and dehumidifying	kW	43.1	65.7	112.4	124.5
Total energy	kW	1491.8	1514.4	1561.2	1573.5
Saving (cooling)	%	0.0	0.0	0.0	0.0
Saving (humidification)	%	94.5	79.9	25.3	0.0
Saving (dehumidification)	%	54.0	34.4	3.6	0.0
Saving (humidifying and dehumidifying)	%	65.4	47.2	9.7	0.0
Saving (heating)	%	0.0	0.0	0.0	0.0
Saving (total)	%	5.2	3.8	0.8	0.0

So far, the importance of indoor humidity level in IAQ and comfort was discussed as well as the effect of hygroscopic property of materials (and especially finishing materials) in regulating indoor humidity levels. Also, in previous sections the mechanisms of moisture storage and transfer into and through the material was described through vapour diffusion, sorption diffusion and capillary forces. These three methods of moisture storage/transport are defined with materials properties known as vapour permeability, hygroscopicity and capillarity. As stated before, capillarity that occurs due to water penetration into the material in its liquid form is not the focus of this study. Materials' behaviour when exposed to various forms of moisture is quantified through some steady-state single values (water vapour permeability, sorption isotherms, porosity) and some complex parameters consisting of a number of the single values

(moisture effusivity, MBV_{ideal}). Later on, and with the importance of humidity regulating capacity of materials being more understood, a dynamic protocol was proposed by NORDTEST project instructing a procedure to measure a quantity known as Moisture Buffer Value MBV of materials. This method is dynamic as it considers the interactions of material with its surrounding in a realistic scenario. Figure 2-16 illustrates the relationship between these material's basic hygroscopic properties, the complex parameters and dynamic protocol used to quantify this property of materials. These values, parameters and protocols are explained in next section.

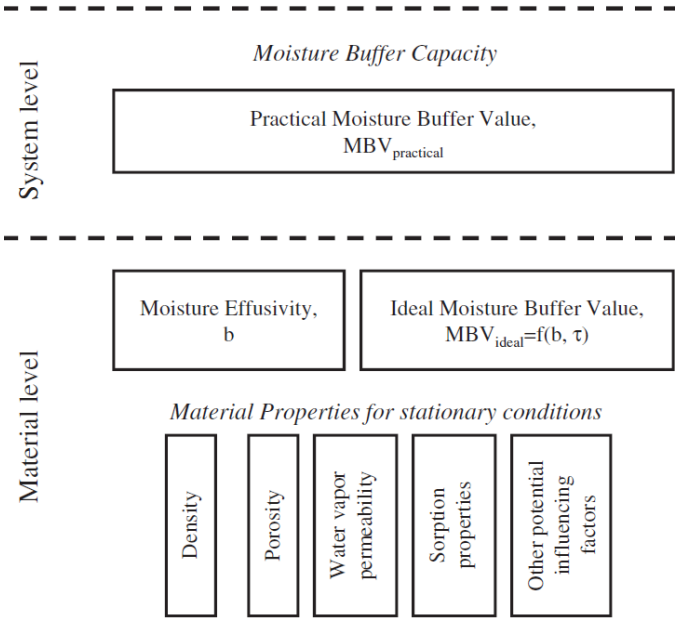

Figure 2-16: Materials' properties, parameters and protocol for quantifying moisture buffering capacity (Rode et al. 2006)

2.7. Parameters to quantify materials' moisture-related properties

2.7.1. Basic steady-state parameters

2.7.1.1. Water vapour permeability (δ_p)

Vapour permeability refers to a materials ability to allow water vapour to pass through them (Rode et al., 2003). The EN ISO 12572 instructs an experimental procedure to measure the water vapour permeability of a material at steady-state by creating a relative humidity/ vapour pressure gradient across the sample. The resulting difference in partial vapour pressure creates a vapour flux, which will reach steady-state after a period of time which is dependent on the hygroscopic properties of the material and the relative humidity range being tested. the rate of vapour transmission G (kg/s) is measured by consecutive timed weighing of the test set-up (i.e. cup + sample) until the rate of mass change stabilises. For this, samples need to be properly sealed having been placed above a container with 0% RH for the dry cup and 93% RH for the wet cup test and then placed in an environment with 50% RH and 23°C temperature. The vapour

permeability δ (kg/msPa) is measured knowing thickness d (m), exposed surface area A (m^2) and average vapour pressure difference ΔP (Pa) across the sample during the test (ISO 12572, 2001):

$$\delta = \frac{G.d}{A.\Delta P}$$

The, more convenient, water vapour diffusion resistance factor μ (-), can then be determined, which is the ratio of the water vapour permeability of still air, δ_a, to the water vapour permeability of the material, δ, and therefore is a relative quantity and has no units (ISO 12572, 2001).

$$\mu = \frac{\delta_a}{\delta}$$

2.7.1.2. Moisture storage function

The moisture storage function(ξ), or sorption isotherm, represents the relationship between the equilibrium moisture content of a material and the relative humidity of its environment at a specific temperature (Ramos et al., 2010). As described in section 2.2.1, porous material follow a hysteresis pattern in their absorption desorption loop. The differences in the sorption curves of different materials are due to micro-structural properties such as specific surface area, pore-size distribution, and total porosity (Kwiatkowski et al., 2009). Sorption experiments are carried out in accordance with standard BS EN ISO 12571 which proposes two methods for conducting test procedure i.e. the desiccator method and the climatic chamber method. The test samples are placed in a conditioned environment in steps of, first, increasing relative humidity to calculate absorption isotherm curve and, second, in steps of decreasing relative humidity to calculate desorption isotherm curve. The test samples are continuously weighed until no change in mass is observed and the equilibrium is reached. The final mass change in each RH step is recorded and plotted against the corresponding RH value in a graph known as sorption isotherm (Figure 2-17).

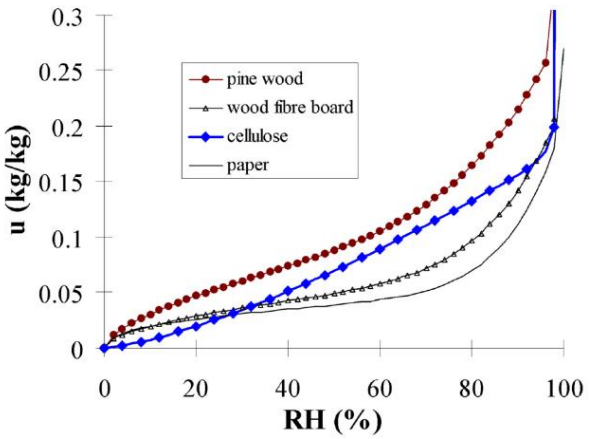

Figure 2-17: Sorption isotherms of four fibrous materials, (Simonson et al., 2004a)

Moisture capacity (ξ) is expressed by the gradient of the sorption isotherm i.e. the relationship between the equilibrium moisture content of a porous material and corresponding RH level at a specific temperature (Hall & Casey, 2012 and Rode et al.,2003). It is the term used to describe the storage capacity difference of the sample between two RH levels (McGregor et al., 2014).

2.7.2. Complex steady-state parameters

Sorption storage function on its own does not represent the hygroscopic buffering capacity of a material in a dynamic condition; it is the result of a steady-state test set-up that is done in equilibrium and therefore, does not represent the rate of moisture transport in a real condition (Peuhkuri et al., 2004). Water vapour permeability, also, due to its coupled relationship with moisture storage function does not solely represent the buffering capacity of materials as materials with a high capacity and average permeability may have a similar moisture buffer capacity as materials with an average capacity and high permeability (Janssen & Roels, 2009). Therefore, complex parameters (consisting of several standard material properties) were introduced to facilitate describing the buffering capacity of a material with one single value and comparing different building materials in design phase. The most widely used of these complex parameters are discussed in the following section.

2.7.2.1. Moisture effusivity (b_m)

Similar to thermal effusivity ($b = \sqrt{\lambda \rho c}$) which determines a materials ability to exchange thermal energy with its surrounding, the moisture effusivity constitutes one theoretical parameter to express the ability of moisture absorption/desorption by a particular material when it is subjected to a sudden change in surface humidity (Rode et al., 2006). This value is a single material property which considers an ideal case where the surface resistance of the boundary layer is ignored. Figure 10 shows moisture effusivity of six materials as a function of RH.

$$b_m = \sqrt{\frac{\delta_p . \rho_0 . \frac{\partial w}{\partial \varphi}}{P_{sat}}} = \sqrt{\frac{\delta_p . \rho_0 . \xi}{P_{sat}}}$$

Where w is moisture content (kg/kg), φ is RH (%), P_{sat} is saturation vapour pressure (Pa), ρ_0 is dry density of material (kg/m^3) and δ_p is water vapour permeability kg/(m.s.Pa).

Ideal MBV

This value informs the quantity of water absorbed or released by porous materials when a periodic variation of RH is imposed at its surface. Ideal MBV is a material characterization and is defined as a function of standard material properties (Abadie & Mendonca, 2009):

$$MBV_{ideal} \approx 0.00568\, p_{sat} b_m \sqrt{t_p}$$

2.7.3. Moisture Buffer Value; A dynamic protocol

To measure a material's moisture buffering capacity in a realistic situation, a number of small-scale laboratory tests were devised which all expose the material to a series of RH changes that comes as a square wave in diurnal cycles. The most widely used of these protocols is the one proposed by NordTest project (Rode et al., 2005) which defines cyclic RH step changes between high (75%) and low (33%) RH levels for 8 and 16 hours, respectively, to resemble the daily cycle prevalent in many rooms like bedrooms and offices. The sample is placed in an environmental chamber or a sealed container containing a salt solution and cycles of RH change are applied on the sample. The sample is weighed at the end of every step to determine the change in moisture content. The diurnal cycles continue until the amount of moisture absorbed and desorbed approaches the same value i.e. dynamic equilibrium is reached. Only one surface of the sample needs to be exposed with the rest sealed with aluminium foil or another appropriate material. Experiments should be conducted at constant temperature of 23°C (Rode et al.,2005_ Abadie & Mendonca, 2009). The Moisture Buffer Value MBV of the material is then calculated through the following equation:

$$MBV = \frac{\Delta m}{A.\Delta RH}$$

Where Δm [gr] is the average of the absorbed and desorbed mass after the system has reached a dynamic equilibrium, A [m^2] is the exposed surface area, and ΔRH is the step change in RHs. Materials could then be classified according to the classifications shown in Figure 2-18. Dynamic equilibrium is reached when Δm does not change by more than 5% over 3 cycles (Rode et al., 2005). Figure 2-19 shows MBV of a few materials measured through NordTest protocol.

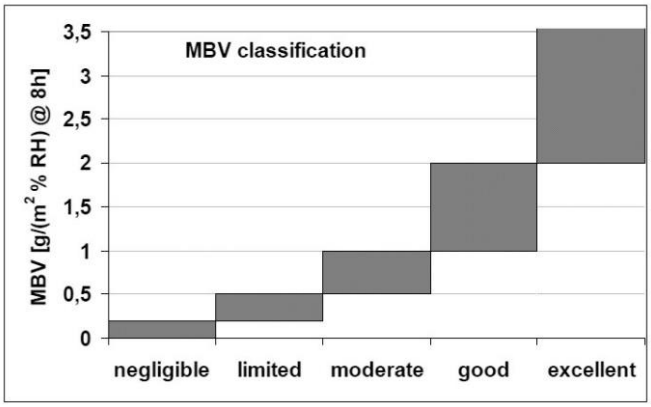

Figure 2-18: Graphic presentation of MBV classes, (Rode et al., 2006)

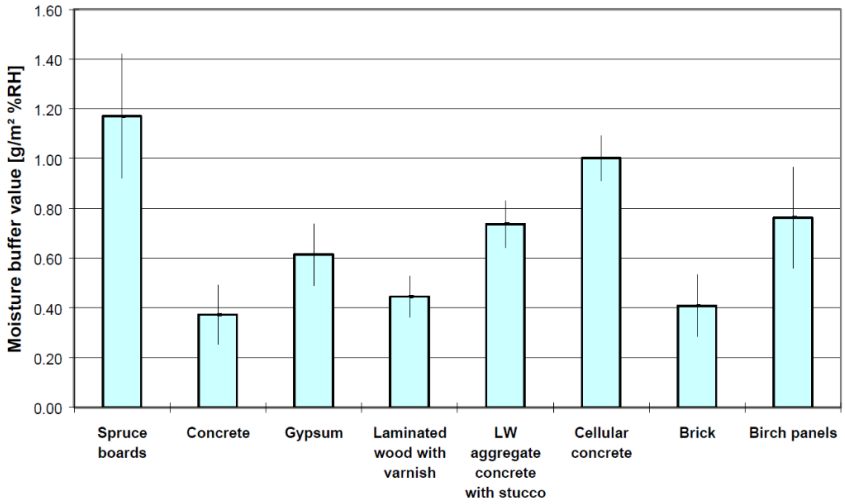

Figure 2-19: Practical Moisture Buffer Value for different materials, (Rode et al., 2005)

Japanese Industrial Standard JIS A 1470-1 (2002) and an international standard ISO 24353 instruct similar test methods to measure moisture buffering capacity which are also based on climate chamber tests and evaluation of weight changes of a specimen when subject to RH variations (Roels & Janssen, 2006). Despite having similarities in basic concept, the specification of these two methods differ from the NT protocol in the RH levels, time intervals, surface mass transfer resistance (which is defined with air velocity in the chamber) and the sample thickness (Janssen & Roels, 2009). Table 2-3 summarises the differences between these three protocols. JIS A 1470-1 was reviewed in 2008 to closely match the ISO 24353 standard. Roels and Janssen (2006) compared the NT protocol to JIS by calculating the MBV using each protocol and showed that although the internal resistance to vapour transport is larger than that of the air film for many materials, the influence of surface film resistance on moisture buffer capacity is significant and cannot be ignored.

Table 2-3: Synthesis of the different cyclic (de)sorption MBP characterization protocol (Janssen & Roels, 2009)

	RH levels high/low	Time intervals high/low (h)	Surface transfer coefficient (s/m)	Sample thickness
JIS A 1470-1	53/33 75/53 93/75	24/24	2.1×10^{-8}	As applied in practice
DIS 24353	53/33 75/53 93/75	12/12	2.1×10^{-8}	As applied in practice
Nordtest	75/33	8/16	Sufficiently high	Sufficiently thick

The indication 'sufficiently high' for the NT surface mass transfer coefficient is actually formulated as 'a surface transfer resistance that is negligibly small'.

2.8. Numerical simulation tools for modelling heat and moisture transfer

Computational simulation is one of the most powerful an analytic tools in our world today used in different areas of science and engineering. Building energy simulation tools are used to predict energy performance of a building and the level of thermal comfort provided for its occupants. Both the power and complexity of building performance modelling and simulation arise from its use of many underlying theories from diverse disciplines, mainly from physics, mathematics, material science, biophysics, human behavioural, environmental and computational sciences (Hensen & Lambers, 2011). The validity of the simulation result heavily depends on the accuracy of the input data (including building geometry, material properties, weather data, occupancy pattern and internal loads) which are partly based on assumptions or averaged data as well as all those underlying theories and thermodynamic concepts applied to make complex interrelations simplified and manageable (Maile et al., 2007). Hensen and Lamberts (2011) emphasises on the importance of the user as well as the use of the building performance simulation. In terms of its use, for example, simulation is much more effective when used to compare the relative performance of design alternatives, than when used to predict the absolute performance of a single design solution.

Much of the early work in the field of building energy simulation_ started 1960s_ was mainly focused on load calculations and energy analysis, modelling the thermal performance of the building and sizing of HVAC units (Hong et al., 2000). Over time, this domain has developed with tools integrating simulation of heat and mass transfer with and within the building fabric, airflow in and through the building, daylighting, and a wide range of building service systems (Hensen & Lamberts, 2011). IEA Annex 41 project, launched in 2004, was the first widely recognised attempt for improving simulation tools to take into account moisture in handling the whole building performance (Woloszyn and Rode, 2008). There are several studies emphasizing on the importance of hygrothermal (as opposed to only thermal) behavior of the building envelope and its role on the overall performance of a building (Koci etal., 2018; Jerman & Cerny, 2012; Antonyova et al., 2013) concluding simultaneous calculations of both thermal and heat transfer

is required for a more accurate estimation of energy efficiency, thermal comfort and mold growth risk (Moon et al., 2014).

Today there are different numerical models that evaluate moisture balance in an enclosed space or predict indoor humidity levels. They differ in the way that they deal with the moisture storage process within the material and can be categorised under two general classifications (Janssens & de Paepe, 2005). For the first group the main focus is on predicting temperature profiles and energy demands of each space, so two types of simplified approach are taken to account for water vapour exchange with surrounding materials; firstly, the effective capacitance, assumes that room and material humidity are always the same, therefore one single room moisture capacity is considered to include both parameters. Secondly the Effective Moisture Penetration Depth model, differentiates between the room humidity and a representative material humidity, so a single equivalent volume representation of the average moisture transfer and storage in the material is considered to represent the material (Janssens & de Paepe, 2005). These approaches are sufficient as long as average humidity conditions are the only concern. For exact indoor humidity fluctuations or moisture profiles in building envelope, models are needed that combine the thermal simulation with the hygrothermal component simulation (Holm et al., 2904). The second group of indoor humidity models has been produced by combining thermal building simulation with models for Heat And Moisture transfer in building components (Janssens & de Paepe, 2005). A HAM model takes moisture sources and sinks inside a room, moisture input from the envelope due to capillary action, diffusion and vapour ab- and desorption as a response to the exterior and interior climate conditions, as well as the well-known thermal parameters i.e. heat sources and sinks inside the room, heat input from the envelope, the solar energy input through walls and windows and hygrothermal sources and sinks due to natural or mechanical ventilation (Holm et al., 2004).

Despite all the improvements in building simulation domain, as discussed above, the reliability of the output depends on the accuracy of the input data and theoretical concepts. Therefore, it is important for the user to have an understanding of these theories and the extent of the sensitivity of the software to the input data. Material properties is an important part of the input data, significantly affecting the outcome of the simulation. The challenge is the accurate identification of these parameters characterising the materials' hygrothermal properties. Othmen et al. (2018) states that there is an uncertainty in parameters related to materials which originates from (a) the measurement protocol and accuracy, (b) variabilities inherent to heterogeneity especially in case of plant-based natural materials, (c) or data post-processing. Clarke and Yaneske (2009), mentioning the inherently uncertain nature of building material property, highlighted the limit it places on the accuracy of modelling real situations irrespective

of the degree of accuracy of the computational models. Material database of simulation tools contain information on materials tested under specific steady-state laboratory condition. This might not necessarily represent the condition the materials are exposed to on site. Moreover, material databases do not always have all the properties required for a thorough investigation of the construction performance which is specially the case for moisture-related properties. Reciprocally, the requirement of the computational model (usually of a simplified, steady-state nature) influences, if not dictates, the type of material properties needed and hence test protocols. One example of this is the water vapour permeability test protocol known as wet-cup and dry-cup which is based on measurements at two values of humidity. Whilst this is reasonable for non-hygroscopic materials, it does not adequately describe the behaviour of hygroscopic materials above the transition point. The transition point (usually above 60% RH) is where hygroscopic materials start to show a nonlinear behaviour against changes in RH. The best, in this case, would be to represent the vapour transmission data as a range to have at least five points on the vapour permeability versus RH curve to convey some idea of the magnitude of the changes beyond 60% RH. (Clarke & Yeneske, 2009).

There are several examples in the literature of studies conducting a comprehensive experimental campaign prior to the simulation to characterise building materials for their thermal and hygric properties (Ferroukhi et al., 2016; Kontoleon and Giarma, 2016; Moon et al., 2014). These experiments are time-consuming and labour-intensive requiring sample preparation, continuous observation of the boundary conditions and constant supervision of the experimental set-up to be able to confidently omit any unwanted interference affecting the result during the experiment. Based on what discussed, it was decided that a numerical simulation would not fit the objectives of the current study.

2.9. Embodied energy and the importance of choice of materials

The topic of environmental impacts of human activities has gained more importance in recent year after frequent occurrence of natural disasters caused by global warming and climate change and concerns raised by scientists and environmentalists about the future of the planet. The building industry is, after food production, the largest consumer of raw materials in the world (Berge, 2009). It is therefore relevant for the construction industry as one of the major consumers of energy and natural resources to focus on sustainability as a major principle to abide by. In line with this comes the importance of construction materials and their contribution to life cycle environmental impact of buildings (Pargana et al., 2014).

For many years, energy conservation research has focused on the operating energy of a building due to its large share in total life cycle energy of a building. However, with stricter building energy codes, widespread use of more effective insulation materials and efficient appliances, the energy performance of buildings has improved resulting in lower operating energy used during the lifetime of buildings. More emphasis has, therefore, been directed to the energy embodied in buildings' construction materials (Cabeza et al., 2013 (a)). Modern building materials are associated with more use of energy and natural resources in their manufacture compared to their traditional counterparts; as we have moved from earth, timber and plant-based fibres and products to concrete, metal, inorganic binders and plastic (Cabeza et al., 2013(a)). Thormark (2006), emphasised in his research the importance of the choice of materials on the total energy embodied in the building. The embodied energy refers to the energy consumed during the extraction, transportation and production of a material and depends on the manufacturing process, the availability of raw material in vicinity and the efficiency of its production (Cabeza et al., 2013 b). This importance of the choice of materials on total embodied energy and environmental impact of buildings, has resulted in increased interest in more natural and less energy intensive alternatives.

The compatibility of different layers in a wall, floor or ceiling system is another reason why the breathability of different layers and materials is important when designing the building fabric. Traditional buildings made of masonry, such as earth or limestone (permeable) could not be layered with oil-based insulation or rendered with cement, both impermeable. It is also important for renders and their substrates to be thermally, structurally and, in terms of breathability, compatible with each other (May, 2005). In moisture terms, if the substrate is as hygroscopic as the render, the moisture absorbed by the render will be dissipated into the substrate. This prevents accumulation of excess moisture in the render and consequent mould growth or build-up of moisture in internal layers of the wall causing mould growth, rot (decay) and unhealthy indoor environment, (Guelberth & Chiras, 2003).

In this study, as mentioned in chapter one, Iran's conventional wall construction materials were proposed to be replaced with more sustainable alternatives having lower embodied energy. These alternatives have higher hygroscopic capacity and therefore result in a more breathable wall construction benefiting from potential advantages of such constructions. In the following section, a discussion is made on these materials' manufacturing process, their embodied energy/ carbon, as well as their permeability and hygroscopic capacity, to introduce and explain why they have been selected.

2.9.1. Plasters

Earth, natural lime and natural gypsum are three types of plasters that have been used for many centuries in buildings envelopes, providing protection, colour and texture. In modern times, the use of lime plaster was given up in favour of Portland cement. In 1824, J. Apsin discovered the first cement and from 1835, Portland cement became the dominant binding material in construction, mostly due to standardisation of its production and its quick setting (Callebaut et al., 2001). However, due to the higher embodied energy of Portland cement compared to lime and its impermeability, (which is an undesirable characteristic if used in conjunction with other natural and breathable substrates), natural hydraulic lime has received increased interest. Cement is also a capillary active material, so it attracts water and as is impermeable, does not allow it to evaporate. It, therefore, needs to be dealt with carefully to not cause rot and damage to adjacent materials and therefore the building structure.

Earth is another natural plaster with very low embodied energy as it can be locally sourced without the need for intensive quarrying activities. It is a good absorber of moisture and VOCs which makes it a natural regulator of humidity resulting in improved air quality. More detail is given in the chapter 6 about the characteristics of earth and its ecological profile. As with lime, earth has also been replaced with a factory-prepared plaster, i.e. gypsum which is a more delicate and water soluble plaster used for interior applications. Gypsum has higher embodied energy and less moisture buffering properties than earth.

All plasters have a structural component, a binding agent, and some form of fibre (to increase strength) or additives to add specific properties (such as retarders, accelerators, water repellents etc.). The structural component, except in most gypsum plasters, is sand which provides most of the volume of the plaster as well as its structure. The binding agent bonds sand particles to one another and in most cases gives the material its name. When the binding agent is mixed with water, it becomes adhesive and causes sand grains to adhere to one another (Guelberth & Chiras, 2003). In next section cement and gypsum as conventional interior and exterior plasters are compared with earth and lime plaster as a more sustainable alternative.

2.9.1.1. Earth plaster

Soil or loam is a mixture of clay, silt and sand, and sometimes contains larger aggregates like gravel and stones. According to engineering science, particles with dimeters smaller than 0.002 mm are termed clay, those between 0.002 and 0.06 mm are called silt, and those between 0.06 and 2 mm are termed gravels and stones (Minke, 2012). In earth plasters, the clay acts as a binder for all the larger particles. Silt, sand and aggregates constitute the structural component or the filler. Clays are found all over the world and come from many different sources but are

often a product of erosion and disintegration of feldspar, a type of igneous rock, (one of the most common minerals within the Earth's crust), and some other minerals such as mica (Guelberth & Chiras, 2003). In a dry state, clay can be described chemically as Al_2O_3 x $2SiO_2$ x $2H_2O$ (Berge, 2009). Clay consists of tiny plates forming a hexagonal lamellar crystalline structure. When clay gets wet, water creeps in between the lamellary structure, surrounding the platelets with a thin film of water. This makes the clay swell and change from a solid to a plastic state (Minke, 2012). Clay is widely dispersed on Earth and is found in both topsoil and subsoil. If soil used for plastering is supplied by a factory, the associated instructions should be followed to prepare and apply the mix. If it is dug from the construction site, a few tests such as sieving, sedimentation, a smell test, the wash test, the ball dropping test, the cohesion test, and the consistency test, etc. need to be done to analyse the composition of the soil to determine if it is suitable for plastering. If not suitable, improvements need to be made (by special treatment or additives) to make the mix suitable for plastering. According to Minke (2012), earth plasters consist mainly of sand and silt with only as much clay as is necessary (usually between 5% to 12%) for developing binding forces.

2.9.1.2. Lime plaster

Lime plaster is a mixture of lime and sand. It is manufactured by calcining natural calcium carbonate, typically limestone (Lyons, 2014) which is abundant and widely distributed throughout the world (Guelberth & Chiras, 2003). The main constituent in limestone is necessarily calcium carbonate ($CaCO_3$). Limestone is quarried, crushed and then heated in a process known as calcination at approximately 800 to 1000°C. Heat drives off carbon dioxide and water, leaving calcium oxide, commonly known as quicklime:

$$CaCO_3 \xrightarrow{950^oC} CaO + CO_2$$

In order for lime to be used as renders, mortars and concrete, it needs to be slaked/ hydrated i.e. soaked in water. The slaking process starts by adding water to the lime on a slaking bench. Calcium hydroxide reacts with the water releasing a considerable amount of heat and produces calcium hydroxide. If slaked with an excess of water for a period of several weeks, a creamy texture is produced known as lime putty, the primary ingredient of lime plaster.

$$CaO + H_2O \rightarrow Ca(OH)_2 + heat$$

Lime putty is then mixed with sand to create lime plaster. When applied on walls, the calcium hydroxide in the mix begins to react chemically with carbon dioxide in the atmosphere and reverts back to calcium carbonate, a durable finish that could last for many years. The high temperatures used in the calcination process is one of the reasons for the higher embodied

energy of lime plaster compared to earth plaster. However, in the production of Portland cement a temperature between 1400 to 1500°C is needed, resulting in an even higher embodied energy of cement compared to lime (Berge, 2009 and Guelberth & Chiras, 2003).

2.9.1.3. Gypsum plaster

Gypsum is a water-soluble mineral with the scientific name of hydrous calcium sulphate. Rock gypsum is mined, crushed and ground to a fine powder. If heated at temperature of 160-200°C, most of the chemically bound water is evaporated. The resulting product is anhydrous calcium sulphate which is the material mostly used to manufacture drywall or used as an interior plaster.

$$CaSO_4.2H_2O \xrightarrow{170^oC} CaSO_4$$

hydrated gypsum *anhydrous gypsum*

The natural mineral, that gypsum plaster is manufactured from, can be white or discoloured pale pink, grey or brown due to small quantities of impurities. The mix of gypsum powder and water is light, very sticky and plastic. It adheres very well to the substrate and has a fast setting time, between 30 and 120 minutes. Gypsum plaster has a higher embodied energy compared to earthen plasters. However, compared to lime and cement render, it has a lower embodied energy due to the lower temperatures used in the calcination process (Berge, 2009 and Guelberth & Chiras, 2003).

Table 2-4: Embodied energy of a few finishing materials (Berge, 2009)

Material	Temperature required in production (°C)	Embodied energy (MJ/kg)
Lime	900-1000	4.50 – 5.0
Portland cement	1400-1500	3.6 – 4.0
Natural gypsum	200	1.2 – 1.4

Internal finishing materials directly affect the indoor air quality and comfort by regulating RH levels and absorbing/removing VOCs from indoor space. This highlights the importance of moisture buffering capacity of gypsum and earth plasters as they are used as internal plasters. Lengsfeld and Krus (2017) measured the vapour diffusion resistance value and moisture storage function of a gypsum and an earth plaster as two properties that buffering effect is strongly dependent on. The result indicates the high moisture buffering capacity of earth compared to gypsum (Table 2-5).

Table 2-5: Comparison of moisture buffering properties of gypsum and earth plaster (Lengsfeld & Krus,2017)

	Density [kg/m³]	Vapour diffusion resistance factor [-]		Moisture storage function [kg/m³]				
		Dry cup	Wet cup	50%	65%	80%	93%	97%
Gypsum	996	6.12	7.04	6.7	6.4	7.5	8.5	10.3
Earth	1867	13.96	8.57	13.5	15.8	20.4	24.0	29.4

2.9.2. Thermal insulations

The general awareness about the importance and potential of reducing buildings energy consumption by improving building fabric has been incorporated into building codes and regulations strategies which mainly recommend/ mandate the use of thermal insulative materials to cut the path of heat flow through the building fabric elements. Aditya et al. (2017) state that energy-saving potential of a well-insulated house varies between 50 to 90% compared to a conventional building. Therefore, the role of these materials in the energy performance of building envelopes and their contribution to life cycle environmental impact of buildings is significant (Pargana et al., 2014). In Europe mineral/inorganic insulation materials account for 60% of the market; oil-derived materials 30% (particularly XPS, EPS and PUR/PIR); and organic natural and others account for about 10% of the share on the market (Ardente et al., 2008). However, the market for natural insulation materials has gained more interest in recent years due to the increased awareness about the total environmental impact of human activities. Therefore, a greener alternative to common oil-based thermal insulations is introduced and discussed for its properties and their potential contribution to the reduced carbon footprint of buildings. In the following section, the properties and environmental impact of a conventional oil-based thermal insulation material (PIR) are described and compared with a more sustainable alternative, expanded cork insulation.

2.9.2.1. PIR insulation boards

Polyurethane (PU), Polyisocyanurate (PIR), Polystyrene (PS), are common forms of plastic insulations. Plastic insulation can form closed-cell foams that trap gases or air inside the bubbles; resulting in a lightweight material with very low thermal conductivity (Agarwal & Gupta, 2017).

PU and PIR are thermosetting foams produced by an exothermic chemical reaction between a polyol and a polyisocyanate. The polyol is typically part of an aqueous mixture of catalyst, surfactant (foam stabilizers), flame retardants, and blowing agents. When this mixture is combined with the isocyanate, an exothermic reaction takes places, releasing significant quantities of energy that activates the blowing agent and expands the reaction mixture into a foamed structure as it polymerizes and solidifies (Agarwal & Gupta, 2017). The difference between the two is the isocyanate ratio: 60 to 65% Ib/Ib for PIR instead of 50 to 55% Ib/Ib for PUR. The main result is a greater fire resistance (class B instead of class E of PUR) and lower thermal conductivity, between 0.018 and 0.027 W/m. K, with similar density (15 -45 kg/m^3) and specific heat (about 1.4 kJ/kg.K) (Schiavoni et al., 2016 and ASHRAE, 2013).

2.9.2.2. Expanded cork board

Cork oak forest is a sustainable resource for material production with a good potential for CO_2 sequestration (Tartaro et al., 2017). Cork is obtained from the outer bark of the cork oak tree (Quercus Suber L.). Cork oak trees are native to western Mediterranean areas of Southern Europe and North Africa. Cork oak forests cover a total area of approximately 2.1 million hectares, of which about one third is in Portugal. The production cycle of the trees starts after the first cork exploitation, which happens when the tree reaches 70 cm in perimeter (usually when tree is around 20-25 years of age). After this and during the production cycle, trees get debarked every 9-14 years depending on the region and climatic condition. This process stimulates the rapid growth of new bark. This consecutive removal of cork causes no harm to the tree, and is the basis of sustainable exploitation of cork oak forests (Knapic et al., 2016; Tartaro et al., 2017).

Cork structure and properties

Cork is a light cellular material with only 20% of solid fraction by volume (Pereira, 2011). Its structure is formed by hexagonal prismatic closed cells, stack base to base in rows (Pereira et al., 1987). The density of cork ranges from 120 to over 200 kg/m^3. It absorbs water very slowly and floats on water, partly due to the presence of hydrophobic suberin, and partly due to the closed cell structure of cork with no intercellular communication channels (Gil et al., 2000). Cork has low heat transfer properties due to its large air content and small cell size which makes it a suitable material for thermal insulation purposes. Cork is mainly composed of Suberin (45%), which is a glyceridic polyester, and is responsible for the elastic properties of cork (Knapic et al., 2016; Simoes et al., 2019). The remaining 55% is composed of lignin (27%) and polysaccharides (12%), both important to structure of cork, ash (4%), wax (6%) and tannins (6%) (Simoes et al., 2019).

Cork in construction industry

The cork used in the construction industry are cork granules which are either low value cork which is by-product from the manufacture of cork stoppers or forestry residues obtained from periodic pruning of cork trees, by removing bark from branches or other refuse raw cork such as virgin cork. What is obtained from this process is called “falca”. Falca is not pure cork and contains pieces of wood which are difficult to separate and therefore, it cannot be used in noble products such as bottle stoppers (Tartaro et al., 2017; Knapic et al., 2016). Cork granules are directed through different processes to be formed into various construction products which are mostly used for thermal and acoustic insulation and for vibration absorption (Knapic et al., 2016).

Insulation cork board also known as black expanded cork board is the end-product of one of the processing lines in a cork factory (Tartaro et al., 2017). Cork strips, when arrived in the factory, are grounded and partially cleaned by being processed through a series of crushers, mills and sieves. The resulting cork granules (5-20 mm) are then placed into autoclaves under compression and steamed at 300- 350^{o}C and 30-60 kPa. In this stage, the cork granules expand and bond together with their natural resins, without any other external adhesives. The outcome of the autoclave is a compact block which is cut in half, cooled in a water shower and placed in a storehouse where they are left to stabilise for 15 days. After this, cork blocks are cut to desired thicknesses (Tartaro et al., 2017). The number of granules inside the autoclave and their compression before steaming controls the final density. A standard density of 90 to 110 kg/m^3 and medium density of 140 to 160 kg/m^3 are mostly used for thermal insulation purposes (Simoes et al., 2019).

Hygro-thermal properties of expanded cork compared with PIR insulation boards

Simoes et al. (2019) compared the thermal and hygric properties of Cork Board Insulation (CBI) with some common oil-based thermal insulations. The dry-cup water vapour resistance value of standard and medium density of expanded cork board as well as their thermal conductivity in the dry state and at 50% RH was measured and compared with similar values of some conventional insulation materials. The result is shown in Tables 2-6 and 2-7.

Table 2-6: Water vapour transmission properties of insulation materials (Simoes et al., 2019)

	Standard CBI (90-110 kg/m^3)	Medium CBI (140-160 kg/m^3)	XPS (31 kg/m^3)	EPS (18 kg/m^3)	Mineral wool (139 kg/m^3)
μ	20.50	54.61	67.54	43.28	4.27

Table 2-7: Thermal conductivity in dry and conditioned state (Simoes et al., 2019)

	Standard CBI (90-110 kg/m^3)	Medium CBI (140-160 kg/m^3)	XPS (31 kg/m^3)	EPS (18 kg/m^3)	Mineral wool (139 kg/m^3)
$\lambda_{(23/50)}$ (W/m. K)	0.039	0.042	0.039	0.035	0.041
λ_{dry} (W/m. K)	0.037	0.041	-	-	-

Other sources have reported properties of cork and PIR or similar insulations as below:

Table 2-8: Thermophysical properties of some insulation materials (Schiovani et al., 2016)

	Density (kg/m^3)	λ (W/m K)	Specific heat capacity (kJ/kg K)	Fire classification	μ
EPS	15- 35	0.031- 0.038	1.25	E	20 - 70
XPS	32- 40	0.032- 0.037	1.45 – 1.7	E	80 - 150
Polyurethane (PU)	15- 45	0.022 – 0.040	1.3 – 1.45	E	30 - 170
Polyisocyanurate (PIR)	30- 45	0.018 – 0.028	1.4 – 1.5	B	55 - 150
Cork	110- 170	0.037 – 0.050	1.5 – 1.7	E	5 – 30

Table 2-9: Thermophysical properties of some insulation materials (EN 12424:2000)

	Density (kg/m^3)	Moisture content @23°C, 50%RH (m^3/m^3)	Moisture content @23°C, 80%RH (m^3/m^3)	Specific heat capacity (kJ/kg K)	μ	
					dry	wet
EPS	10 - 50	0	0	1.45	60	60
XPS	20 - 65	0	0	1.45	150	150
PU	28 -55	0	0	1.40	60	60
Cork	90 - 140	0.008	0.011	1.56	10	5

As seen in the tables, cork has more hygroscopic properties compared to oil-based insulations having a lower water vapour resistance value and higher moisture content when exposed to certain RH values. Clarke et al. (1990) also classifies all plastic based insulations as non-hygroscopic. In this document, cork has been classified as organic- hygroscopic. In terms of thermal properties, compared to PIR (which is the material directly interesting to us here), cork has higher heat capacity, which can be desirable while designing building fabric, but higher thermal conductivity.

Environmental impact and carbon footprint of expanded cork compared with common insulations

Evaluating the environmental footprint of CBI and its comparison to other more common insulations is more challenging and demands more in-depth and preferably some site-based study. Different results were reported in the literature depending on the methodology used and boundaries chosen for LCA studies and different approaches were taken to whether to call cork a green construction material. Gil (2011) states that the environmental impact of building materials is assessed by their embodied energy, consumption of natural resources (selecting renewable materials), impact on ecosystems, their life-time VOC emissions and their end-of-life scenario i.e. recyclability and disposal.

Knapic et al. (2016) considers cork as a renewable material with a sustainable and environmentally rich production system which plays an important part in conservation of soil, retention of water and protection of ecology of the region being a reservoir of fauna and flora biodiversity. Bribian et al. (2011) in their study compared the life cycle assessment of most commonly used building materials with some of their more sustainable counterparts; their results are summarised in Table 2-10. And shows that EPS or polyurethane are responsible for emission of, on average, 7 kg CO_2 – Eq kg^{-1}, whereas insulation materials of natural origin, such as cork, emit only 0.8 kg CO_2 – Eq kg^{-1}.

Table 2-10: LCA results for thermal insulation materials (Bribian et al., 2011)

Building product	Density (kg/m^3)	λ (W/ m. K)	Primary energy demand	GWP ($kg\ CO_2$-Eq kg^{-1})	Water demand ($1\ kg^{-1}$)
EPS foam slab	30	0.0375	105.486	7.336	192.729
Rock wool	60	0.04	26.393	1.511	32.384
Polyurethane rigid foam	30	0.032	103.782	6.788	350.982
Cork board	150	0.049	51.517	0.807	30.337
Cellulose fibre	50	0.04	10.487	1.831	20.789
Wood wool	180	0.07	20.267	0.124	2.763

Tartaro et al. (2016), calculated the carbon footprint of the CBI produced by a Portuguese company and compared it with other insulation materials. Table 2-11 shows the carbon footprint of the different stages of cork manufacturing process. As can be seen, the cork board's life cycle has a negative value for the net CO_2 emissions (-116.229 kg CO_2/m^3 CBI). This is because the total life cycle emission which is 155.957 kg CO_2/m^3 , is compensated by the CO_2 absorbed by cork (-272.186 kg CO_2/m^3) during its growth.

Table 2-11: CBI's carbon footprint (Tartaro et al., 2016)

CBI's life cycle steps	Contribution to global warming or carbon footprint ($kg\ CO_2/m^3$)
CO_2 embodied in CBI	-272.186
Pruning and cork extraction from branches	145.843
Transportation to factory	6.722
Transportation inside the factory	1.906
CBI production	1.485
Net CO_2 equivalent emissions	**-116.229**

Table 2-12 compares the CBI's carbon footprint with other common insulation materials.

Table 2-12: CBI's carbon footprint vs. other insulation materials (Tartaro et al., 2016)

Materials	Contribution to global warming or carbon footprint ($kg\ CO_2/m^3$ ICB)
Expanded polystyrene (EPS)	59.00
Extruded polystyrene (XPS)	94.40
Polyurethane (PU)	127.70
Stone wool	34.35
Light Expanded Clay Aggregate (LECA)	53.77
Insulation Cork Board (CBI)	-116.23

Authors, however, mention that if biogenic carbon embodied in the cork and stored in the CIB is discounted from calculations, carbon footprint of the CBI increases to 501.361 kg CO_2/m^3 which makes it the worst performing material.

In a more holistic approach Pargana et al. (2016) studied the environmental performance and primary energy used (renewable and non-renewable) in production of expanded cork boards along with some other conventional thermal insulation materials: expanded and extruded polystyrene and polyurethane. According to EN 15804: 2012, the impact assessment should involve seven environmental impact categories i.e. Global Warming Potential (GWP), Ozone

Depletion Potential (ODP), Acidification Potential (AP), Eutrophication Potential (EP), Photochemical Ozone Creation Potential (POCP) and Abiotic Depletion Potential (ADP). These categories are reported in Table 2-13 and shows that cork's performance in most categories is worse than PU insulation except for Global Warming Potential which is related to carbon emissions.

By directly comparing the LCA results of PIR and cork, it could be deduced that cork may have a greater negative environmental impact than PIR, if each impact category is considered with equal importance to the others. However, the figures do not show the complete picture, which may include socio-economic, as well as the established LCA factors, which could show some materials, such as cork in this case, in a different light. One point that should not be neglected in this evaluation is the role of a material to help developing a sustainable environment. For example, cork is produced from a renewable resource that helps populations reside in rural area and maintains a natural ecosystem by protecting endangered species (Tartaro et al., 2016).

Based on what has been discussed, further research needs to be done on this, sometimes controversial, subject, and a weighting system for each impact category could be developed to form part of a more comprehensive comparison between different construction materials with regard to their overall impact on the environment.

Table 2-13: comparative LCA results of cork and PU insulation materials (Pargana et al., 2016)

Insulation material	ADP [Kg Sb eq]	AP [Kg SO_2 eq]	EP [Kg PO_2 eq]	GWP [Kg CO_2 eq]	ODP [kg R-11 eq]	POCP [kg C_2H_4]
Cork	0.013	0.036	0.016	1.61	1.11E-07	2.55E-03
PU	0.035	0.013	1.56E-03	3.33	8.23E-08	1.17E-03

2.10. Iran's climate

Iran is located in the easternmost edge of the geographic cultural region of the Middle East (Foruzanmehr, 2017). Extended from 25°N to 40°N latitude with 2500 meters difference in the altitude from the lowest to the highest habitable points of the country, having two high mountain ranges elongated in the north and the west, and bordering with Caspian Sea in the north and Persian Gulf and Oman Sea in the south, it features very diverse climatic conditions in different areas of the country (Kasmaei, 1992). Almost all parts of the country experience 4 distinct seasons. Figure 2-20 shows Iran's climate based on Koppen-Geiger climate classification (Kottek et al., 2006). This map gives a quick overview on the diversity of the climate of Iran on a well-known universal classification. Koppen himself was a botanist-climatologist. He defined the climate boundaries to those of the vegetation zones. Based on this classification, terrestrial climates were divided to five major climates (A, B, C, D and E); all defined by temperature criteria

except for type B which was controlled by dryness (Arnfield, 2020). Koppen-Geiger classification having a universal scope gives a general overlook of the climate of the countries and does not closely match the characterisations of the local climates. Moreover, as it has been prepared based on vegetation criteria, it needs some interpretation and adjustments if is to be used in other subjects.

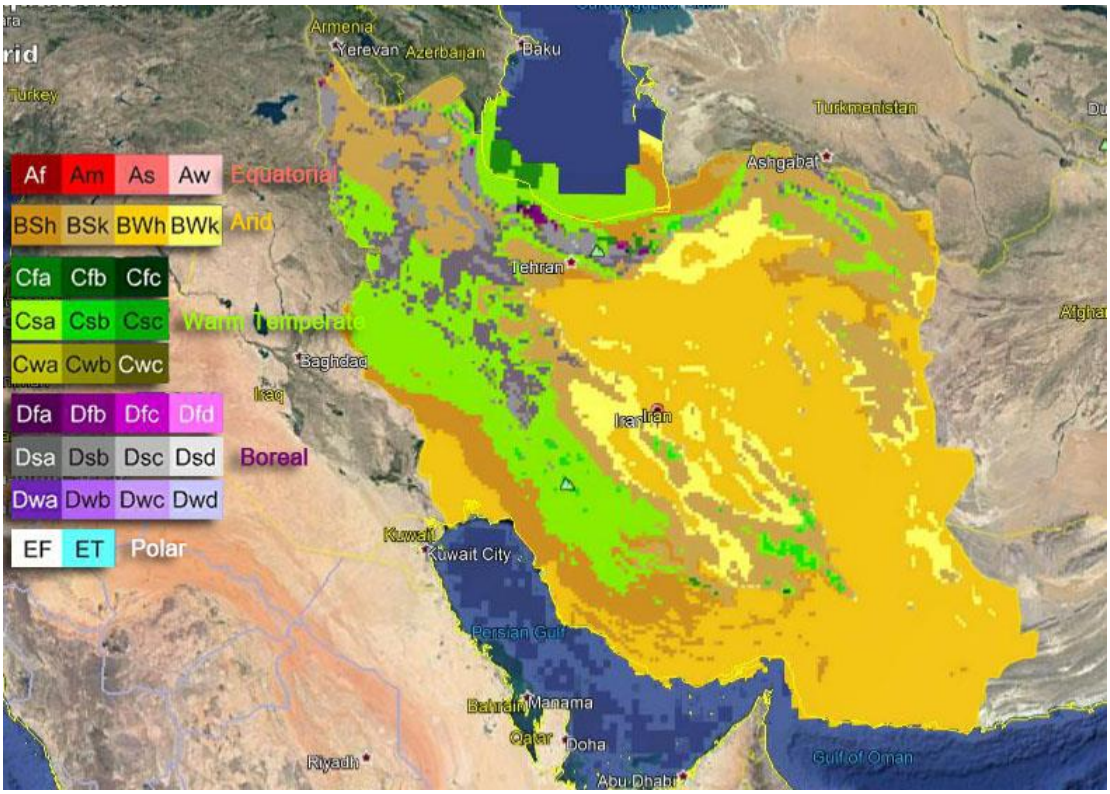

Figure 2-20: Iran climatic zones based on Koppen-Geiger climate classification for 25-year period 1986-2010, (Rubel & Kottek, 2010)

Kasmaei (1992) used Givoni building bioclimatic chart for a climate classification based on indoor thermal comfort and buildings design criteria for providing comfort which is more suitable for the purpose of this study. Kasmaei used 216 weather stations' data for durations of 7 to 15 years and defined 8 major climate classifications across the country as shown on Figure 2-21. The 8th climatic group featuring very hot and very humid weather condition, makes one of the harshest climates of the world. Cities located in this climatic region have the highest rate of energy demand in building sector (Mohammadi et al., 2018). The study conducted by Kasmaei dates back to 28 years ago. The recent changes in weather condition of the country (i.e. rising temperatures and reduced precipitation) caused by global warming (Kousari et al., 2011; Tabari & Talaee, 2011) has made it even more difficult to provide comfort for building occupants throughout the country especially during hot periods of the year. Power cuts are becoming more frequent affecting people's daily life-style. This shows the ever more importance of energy saving measures to be taken in building design. Code 19, Iran National Regulation for Energy

Conservation in Buildings, has divided the cities of the country to three groups having 1) high 2) moderate and 3) low energy requirement. All cities located in the Kasmaei's 8th climatic classification fall in high energy demand group meaning they will have to comply with stricter building regulations of maintaining lower thermal transmittance value of the building fabric.

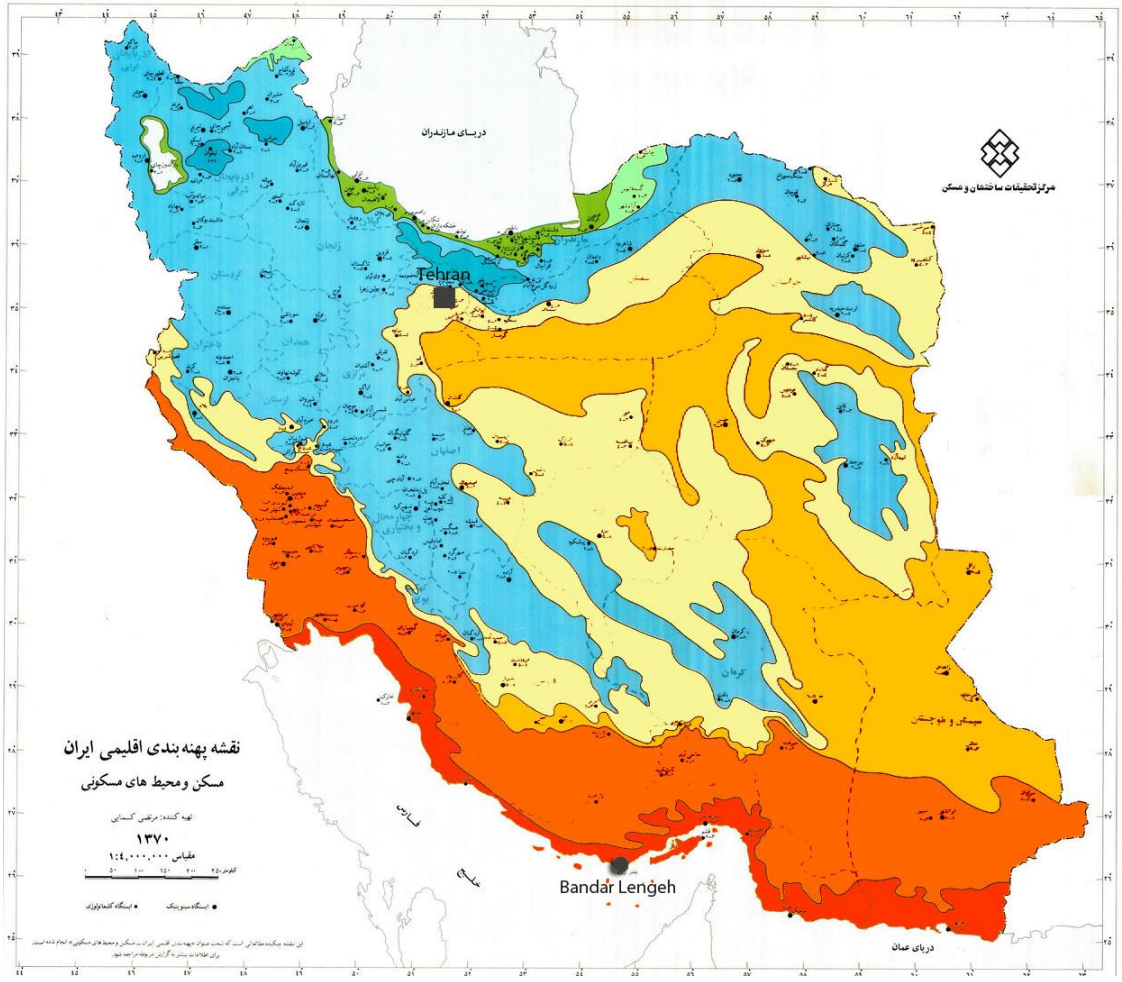

Climate classification	Climate condition in	
	Winter	Summer
1	Extremely cold	Suitable
2	Extremely cold – relatively cold	Temperate- Semi-arid
3	Very cold - Cool	Humid
4	Very cold – Relatively cold	Hot & humid
5	Cold- Relatively cold	Very hot, semi-arid, arid
6	Relatively cold - Cool	Very arid - Arid
7	Cool - Temperate	Very arid, extremely arid, extremely hot & semi-humid
8	Cool, temperate, suitable	Very hot & humid

Figure 2-21: Iran climatic classification based on buildings heating/cooling requirements, (Kasmaei, 1992)

In a more recent study, Eshraghi et al (2019) used weather data of 82 cities of Iran to calculate the heating and cooling degree days of those cities for a 15-year period (2003 – 2018). Figures

2-22 and 2-23 shows the cooling and heating degree days of the country calculated using the base temperature of 22°C and 18°C respectively. As can be concluded from these maps, the majority of the country cooling is the main conditioning requirement. There are more areas with almost zero heating requirements then those with zero cooling demands. Cooling DD map is more uniform suggesting that summer condition is more similar in different parts of the country compared to winter weather condition. This is why the country has started to face more issues regardin year.

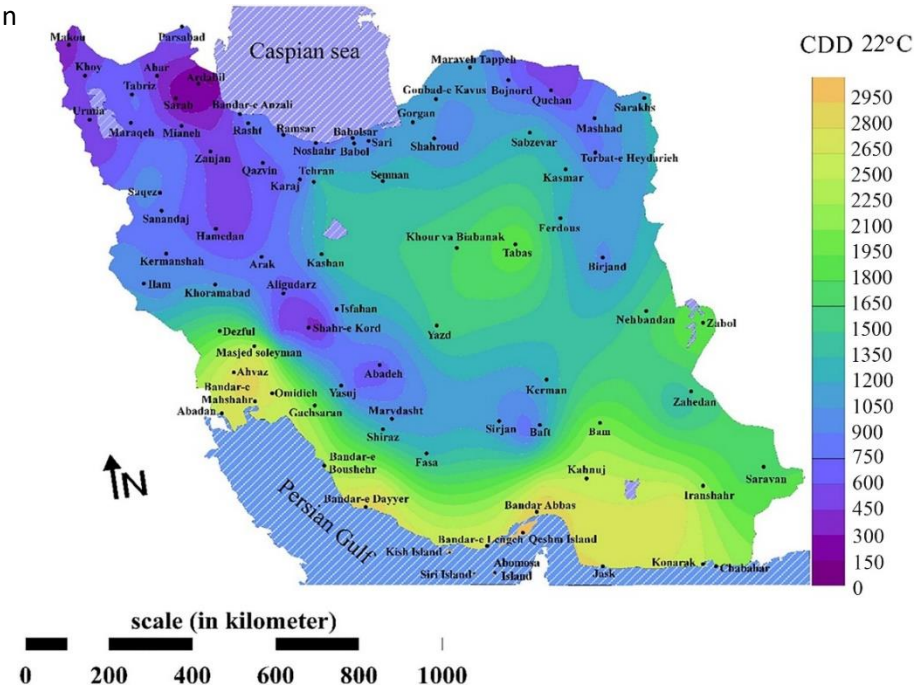

Figure 2-22: Contour lines illustrating cooling degree days variation based on 22°C base temperature, (Eshraghi et al., 2019)

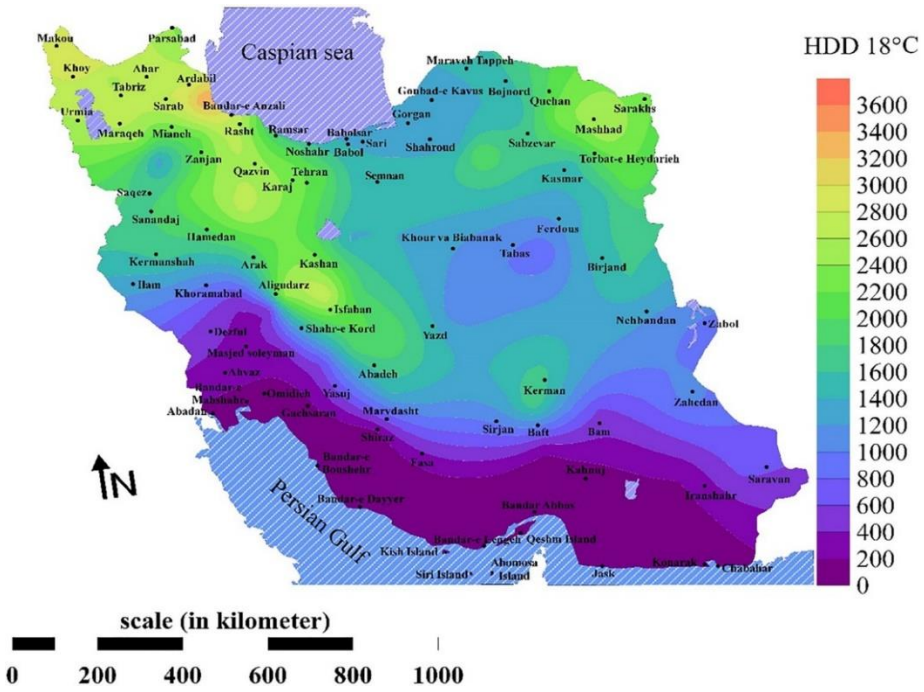

Figure 2-23: Contour lines illustrating heating degree days variation based on 18°C base temperature, (Eshraghi et al., 2019)

2.11. Summary

Building envelope as the main interface between indoor and outdoor environment, has a major role in energy consumption and comfort of building occupants. Evaluation and improvement of building envelope performance has been subject of many studies. Today, thermophysical properties of materials and derived concepts such as thermal mass, thermal insulation and their role as passive measures to moderate outdoor weather conditions is well known by building physicists. Heat transfer equations have been developed and steady-state and dynamic analysis methods have been used for many years in manual calculations and building energy software, to evaluate and improve thermal performance of the buildings' fabric. However, the importance of including moisture in heat transfer equations was not recognised until recently: materials are more thermally conductive when moistened as their pore structure is filled with water which is more conductive of heat than air. Also, condensation and evaporation which happens as moisture gets absorbed and desorbed from the material, result in latent heat of phase change to be released or captured by material, hence changing its enthalpy. Other materials properties such as specific heat capacity and vapour permeability, which have important role in influencing the hygrothermal performance of building envelope, can change remarkedly with changes in moisture content. This phenomenon is more significant for hygroscopic materials compared to non-hygroscopic materials; a point to consider especially when dealing with natural materials. The mechanism of moisture absorption and transfer into and through the materials is rather complicated and needs to be well understood for a precise evaluation of driving forces on which moderating measures can be taken. Kunzel (1995) did one of the first holistic studies on moisture transfer mechanisms, and developed coupled heat and moisture transfer equations which then resulted in development of a software called WUFI. This software is one of the most reliable simulating programs that considers moisture as well as heat to analyse the hygrothermal, and not just the thermal, performance of the building envelope. The reliability of the result of numerical modelling, however, is significantly dependent on the accuracy of input data. Materials properties are one of these game changing input factors. In another note, in multi-layer assemblies, the interactions of the adjacent layers of materials in terms of moisture transfer (when exposed to moisture) affect the overall performance of the assembly in a way that were not expected based on theoretical calculations. This emphasises on the importance of taking each layer's behaviour effect on the adjacent layer's behaviour and therefore the overall performance of the wall. This brings up the concept of the compatibility of materials when coupled in a system.

Another subject which is linked to the moisture and its interactions with materials, is materials' moisture buffering capacity which can be used to regulate humidity fluctuations in indoor space, improving air quality as well as health, comfort and productivity of occupants. It could be used as a passive measure to reduce loads on mechanical systems. Occupants heath is one of the issues raised by the scientists, believed to be partly caused by air-tight buildings built to stricter building codes using impermeable materials.

The latter subject i.e. humidity regulating capacity of materials, along with environmental concerns about the high embodied energy of modern construction materials has favoured the use of natural materials in recent years. Natural materials are known as low-carbon materials with less energy used in their manufacturing process. Their high permeability and hygroscopic capacity allow the transport of water vapour and the ab(de)sorption of moisture when exposed to fluctuations of RH. This is called a breathable material.

In line with the background summarised above, this chapter reviewed the existing knowledge on thermophysical properties of materials and how they affect heat storage/transfer and, in general, thermal performance of building fabric. Thermal transmittance value as one of the evaluation measures of envelope performance was described along with its experimental and theoretical measurement methods. The importance of moisture in evaluating envelope's performance was then highlighted, suggesting a hygrothermal analysis, as opposed to thermal analysis, would result in more accurate conclusions. The mechanism of moisture storage and transport in and through materials were discussed which is necessary for a better understanding of constructions' behaviour. The parameters and protocols used in the literature to quantify moisture buffering capacity of materials were discussed. Finally, mathematical equations were used for a more analytical explanation of the coupled heat and moisture transfer relationship. A discussion was then followed on numerical simulations describing their development process and their shortcomings. Another important factor in choice of materials is their embodied energy. Therefore, a discussion was made on the environmental profile of the conventional materials and their alternatives in the context of Iranian construction industry. In the last section of this chapter, Iran's climate was described indicating energy requirements across the country as well as the harshest climates prevalent.

Chapter 3.

Methodology

A comprehensive evaluation of the performance of wall systems requires a holistic approach considering both heat and moisture interactions through the fabric. Different methods have been used in the literature to study hygrothermal performance of the building fabric using numerical simulation tools, laboratory-based experimental set-ups, in-situ methods or a combination of these.

As discussed in chapter 2, the outcome of the numerical simulation tools cannot always be confidently relied on. Several assumptions are made in the design of numerical models. The equations used in these models often simplify the heat and moisture interactions than happen through the building envelope. The biggest challenge for using a numerical model in this research, was probably the uncertainty about the accuracy of the hygrothermal properties of materials available in software's materials database.

On the other hand, conducting in-situ measurements on site is more straight-forward in unoccupied buildings as occupants' behaviour might affect the accuracy of the result and its reproducibility. Moreover, close supervision is needed during the construction of the building to make sure about the quality of the workmanship and the construction detail delivered. This approach is also restricted to heat flux measurements through the envelope and detailed investigation of temperature and humidity profiles within the layers of the fabric system is not possible without using destructive techniques which are not desirable.

Therefore, an in-between approach was taken applying the in-situ thermal transmittance measurement technique (See section 2.2.2) to wall specimens made in the laboratory. An experimental set-up was built for this purpose based on the hot-box technique to create on site conditions using two environmental chambers. Similar methodology has been used by Hulme and Doran (2014) and Pavlík and Černý (2008). This experimental set-up was used to study the hygrothermal performance of current practice wall types in Iranian buildings as well as the proposed low-carbon alternatives. Detail of the experimental set-up is given in section 3.3. In the following sections, construction blocks are first introduced followed by a detailed description of the studied wall types. Fabrication of the wall specimens, mounting, embedding and installation of sensors on the surface of the layers and inside the construction blocks is described later as well as the boundary conditions on the sides of the specimens.

The hygroscopic property of materials can be used to regulate indoor humidity fluctuations. Earth plasters are known for their high moisture buffering capacity. In the second part of this chapter, the method used to characterise the hygroscopic capacity of earth mix plasters is described. Protocols used for quantifying this capacity and sample preparation for each of the protocols are explained in detail.

3.1. Part one:
Experimental set-up to study wall specimens' hygrothermal performance

3.1.1. Materials

Hollow fired Clay, Lightweight Expanded Clay Aggregate (LECA) and Autoclaved Aerated Concrete (AAC) blocks are the most commonly used construction blocks in Iran. In current practice, they are plastered internally with gypsum and externally with cement rendering. In some cases, a layer of oil-based insulation such as Expanded Polystyrene EPS, Extruded Polystyrene XPS or Polyisosyanurate PIR boards are used to increase the insulative properties of the building fabric. As discussed more in detail in chapter one to improve wall design in terms of environmental impact and IAQ, low-carbon alternatives i.e. cork insulation board, earth and lime plaster were proposed to replace the conventional materials i.e. PIR insulation board, gypsum plaster, and cement render. A discussion on each of the materials used, with a focus on their sustainability profile, is given in Chapter two to explain the potential benefits of using the alternative materials to reduce environmental impacts of construction industry. Detailed description of the studied wall types is given in Figure 3-2. The construction blocks consisting the core of the wall, were the same in all sets on specimens. They are each explained in the following section.

3.1.1.1. Conventional construction blocks

Hollow clay blocks

Hollow clay blocks are currently manufactured by firing the clay mud containing aluminium silicates under high pressure and temperature. In this process, firstly, the mixture of clay and water enters an extruding machine, then the air is removed from the mixture by means of a vacuum pump and is passed through a die creating the hollow structure of the blocks. During the next stage the mixture is dried in a hot air oven and finally is fired to a temperature of around 900°C in the kiln. The thermal conductivity of clay blocks varies according to the shape of web structure and the width of the blocks.

LECA blocks

To produce Lightweight Expanded Clay Aggregates, clay is made into pellets and then fired at the temperature of 1200-1500^{0}C in a rotary kiln. All clays can be expanded; however, the ideal clay is very fine with a low lime and high iron content. For this purpose, the clay needs to air for about a year; is then ground, mixed with water and made into pellets. The firing time from clay pellets into expanded clay pellets is approximately 7 minutes (Berge, 2009), when the organic compounds burn off, forcing the pellets to expand and become honeycombed inside and smooth on the outside. LECA block is produced by mixing the produced aggregates, cement,

sand and water. Use of LECA aggregate decreases the concrete density and improves thermal insulating properties of these blocks.

AAC blocks

Autoclaved Aerated Concrete (AAC) blocks are produced using no aggregate larger than sand. They are usually made of lime, fine sand, other siliceous materials, water and a small amount of aluminium powder. These materials are mixed to form a slurry which is then poured into moulds. The slurry is kept in the mould for several hours to become hydrated. During this time hydrogen gas is released within the slurry from the reaction between the aluminium particles and lime. The hydrogen gas bubbles are trapped in the slurry, creating the aerated or cellular structure of the block. When the mixture is partially set, it is cut to different block sizes and is cured at 180^0C in a pressurized steam chamber known as an autoclave to give the block its high strength. Considered to have a moderate thermal mass, AAC has a thermal conductivity of 0.11-0.2 W/mK showing good thermal insulating properties. The density of AAC blocks ranges from 460 to 750 kg/m^3.

3.1.2. Fabrication of test specimens

Samples of single-layer and multi-layer wall types were built inside a frame made of 18 mm phenolic coated plywood (Figure 3-1). The dimensions of these specimens (400 by 500 mm) were dictated by the size of the environmental chamber's opening (See Figure 3-7). To minimise the lateral heat flow from the sides of the specimens, they were covered by 50 mm PIR insulation on all sides. In total 9 samples were built; 3 single-layer and 6 multi-layer as illustrated in Figure 3-2. The single-layer wall specimens were only made of the construction blocks each i.e. fire clay, LECA and AAC blocks. In three out of the 6 multi-layer specimens, construction blocks were layered with PIR insulation board and cement render (on the external side) and gypsum plaster (on inside surface); representing conventional wall system if thermal insulation is to be used. In the remaining three multi-layer specimens, representing low-carbon alternatives, PIR boards, cement and gypsum were replaced by expanded cork boards, lime and earth plaster respectively. Figures 3-3, 3-4 and 3-5 show the final configuration of single and multi-layer wall types after fabrication. Lime, gypsum and earth plasters were factory-made product that were mixed based on the instruction given by the manufacturer. The detailed specification of these products is given in the appendices. Cement plaster was mixed with 1 to 6 ratios (one quantity of cement to 6 quantity of sand).

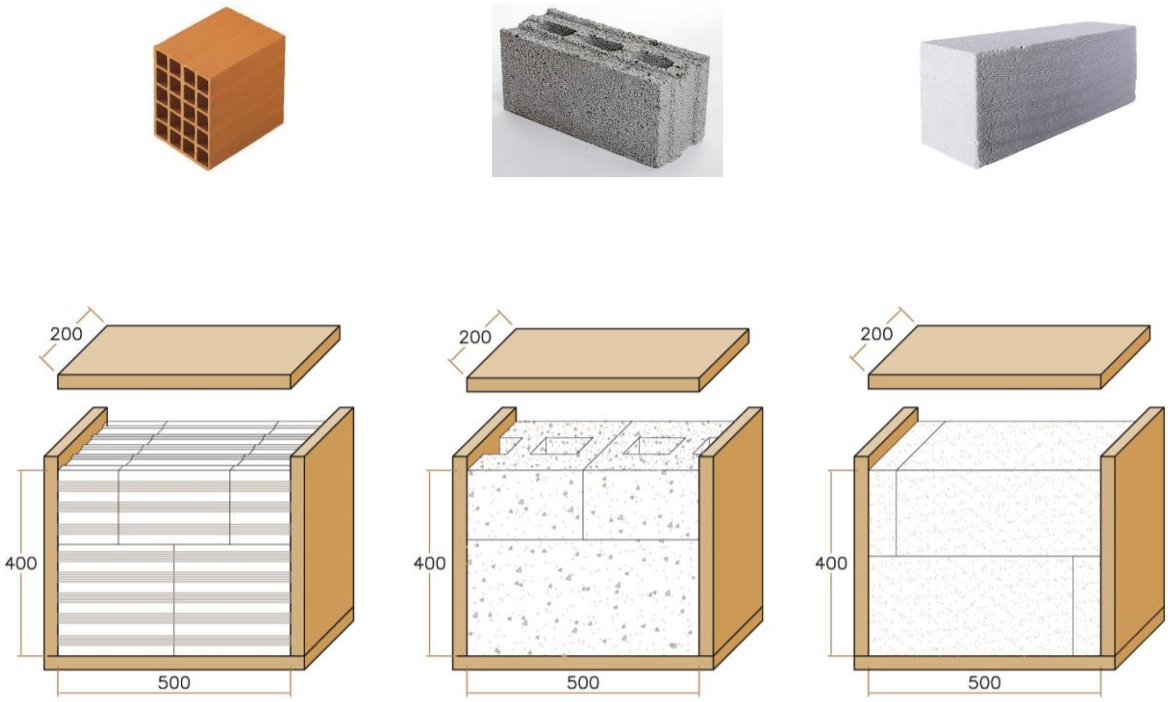

Figure 3-1: Specimens layout for fired clay (left), LECA (middle) and AAC (right) blocks

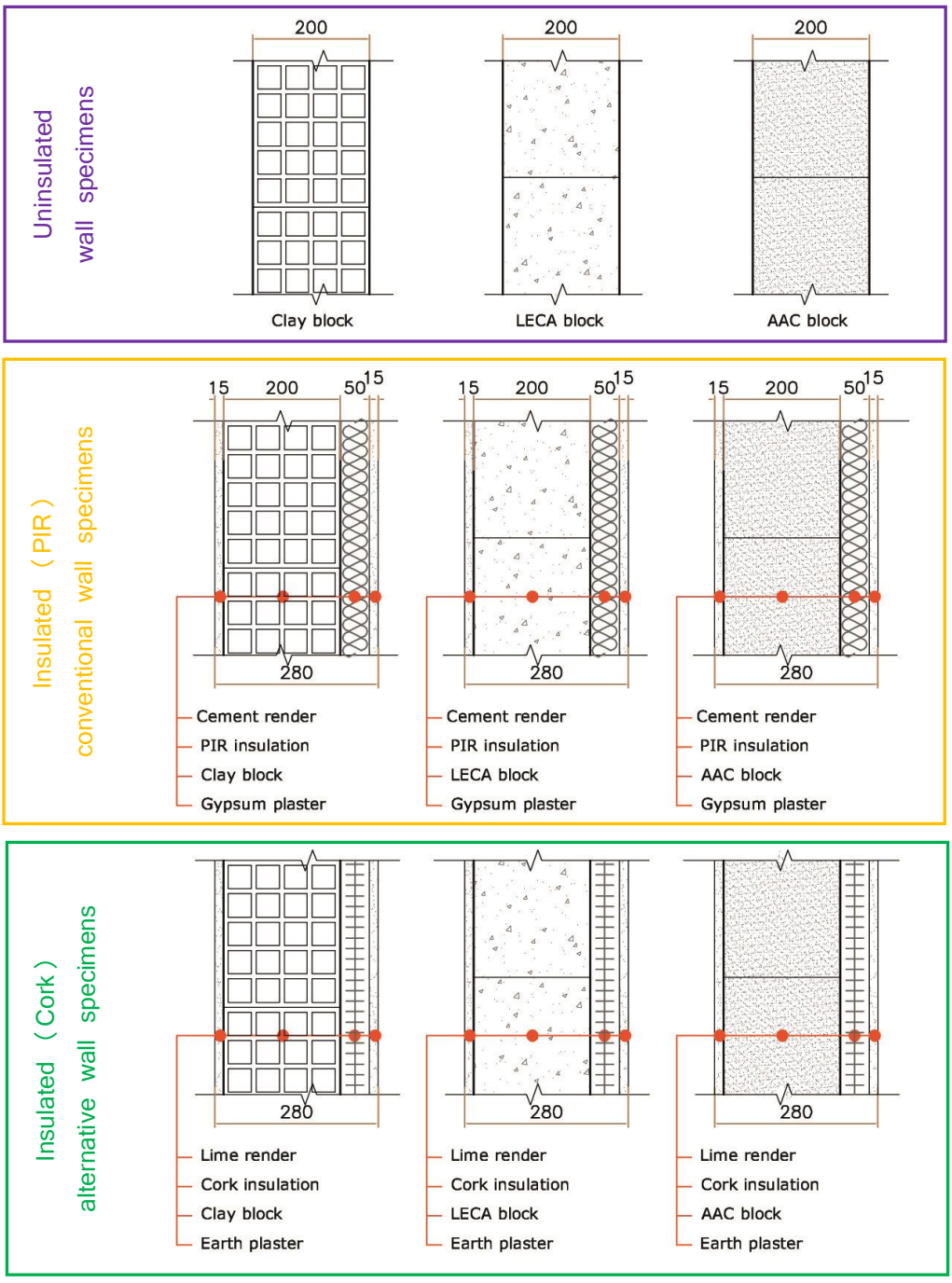

Figure 3-2: Detail of the construction layers of wall specimens

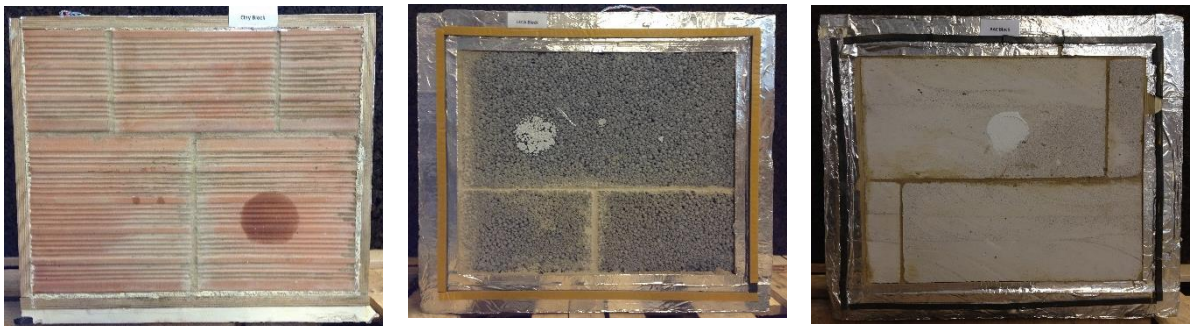

Figure 3-3: Uninsulated wall specimens; Fired clay, LECA and AAC block

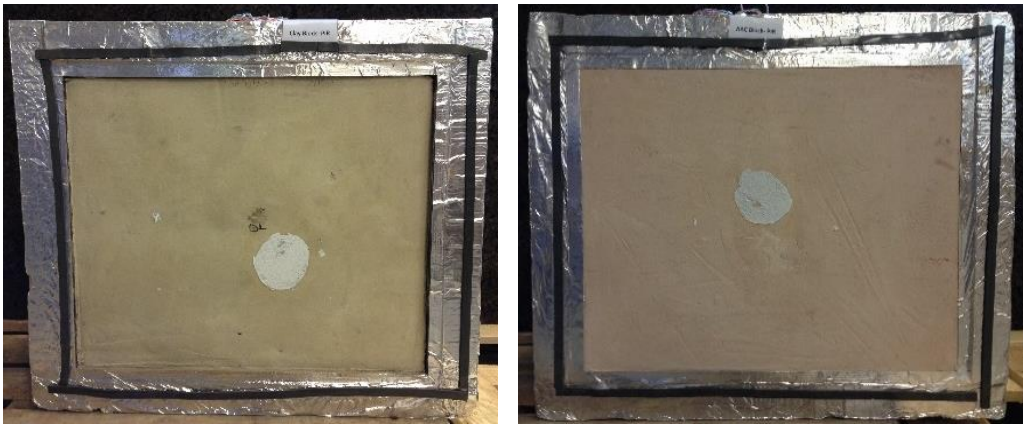

Figure 3-4: Insulated wall specimens_ PIR:
Outdoor finishing (cement render), indoor finishing (gypsum plaster)

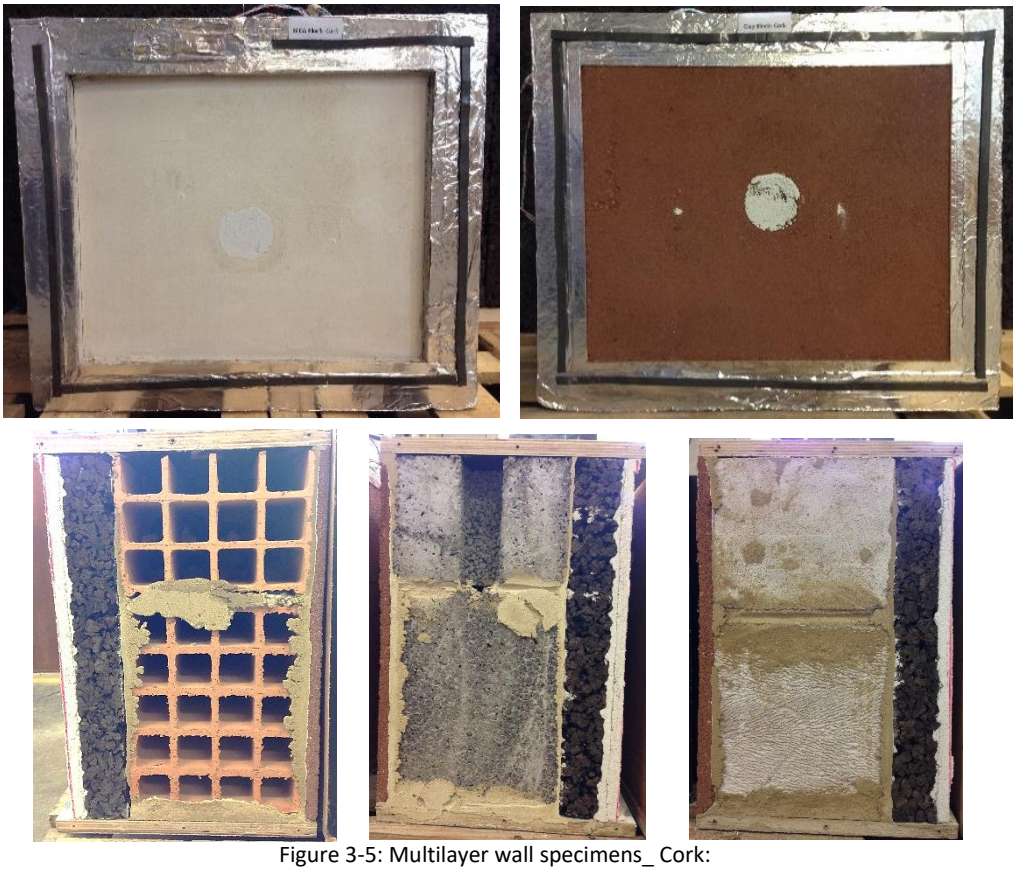

Figure 3-5: Multilayer wall specimens_ Cork:
Outdoor finishing (Lime render), indoor finishing (Earth plaster)

3.1.3. Experimental set-up and data acquisition system

The experimental method used in this study has been mainly adapted from the study conducted by Hulme and Doran (2014) with some additions to monitor heat and moisture transfer through the layers of the wall. Hulme and Doran (2014) measured in-situ thermal transmittance value of 300 dwellings in England. To validate their result, the authors installed heat flux plates on a specimen of known U-value within a guarded hot-box and compared the results from the two methods (See section 2.2.2). The result confirmed the validity of heat flux method as a field alternative to the laboratory-based hot-box method; the error in thermal conductance of the test panel determined by the HFPs was low and the mean U-value measured was approximately 5% less than that determined by the hot box, which is within the estimated calibration error of the HFPs and the hot box itself. The authors used the Average method instructed in ISO 9869-1 to analyse heat flux data and calculate the in-situ thermal transmittance value.

Similar to Hulme and Doran's validation test combining the hot-box and the in-situ heat flux plate methods, an experimental set-up was built in the laboratory of the Architecture and Civil Engineering Department of the University of Bath; using two environmental chambers as two guarded hot boxes (Figure 3-7). Wall specimens were built and placed between the two environmental chambers each one at a time with heat flux sensors, thermistors and RH sensors mounted on the surfaces of the specimens. Specimens were exposed to different boundary conditions. First, they were tested under steady state condition i.e. fixed temperature and RH on both sides. Secondly, dynamic condition was applied maintaining a constant temperature and RH on one side of the specimen (indoor condition) while having fluctuating day and night condition on the other side. For fluctuating outdoor condition, both hot- dry and hot-humid conditions were applied on multi-layer wall specimens. More detail is given in section 3.4 on the boundary conditions.

To evaluate performance of wall types, the Average method was used to calculate the in-situ thermal transmittance value having heat flux data and temperature difference on the sides of the specimens (See section 2.2.2). This thermal transmittance value is considered as an equivalent value, containing the moisture-induced modifications of heat transfer and materials properties, measured under a dynamic condition. The result of these dynamic measurements was compared with the theoretical thermal transmittance value (U-value) calculated using BS EN 6946. This standard uses declared thermal conductivity values of materials to calculate U-value of a construction (See sections 2.3.1 and 4.1.2).

To monitor the heat and moisture flow through the section of the wall assembly, additional RH sensors and thermistors were placed in the middle of the construction blocks and at the

interfaces of construction layers. By plotting heat and moisture profiles in the interfaces and inside the blocks, the interaction of adjacent layers was studied, and a discussion was made on the importance of the properties of the adjacent layers in overall performance of the wall system. Figure 3-6 shows the locations of the RH, temperature and heat flux sensors. In the following sections, the equipment used in the experimental set-up i.e. environmental chambers, thermistors, RH sensors, heat flux plates and data acquisition system are introduced. This is followed by describing the procedure of assembling multi-layer wall systems and mounting, embedding and installing the sensors. At the end of the first part of this chapter, a discussion is given on the choice of boundary conditions to which the wall specimens were exposed.

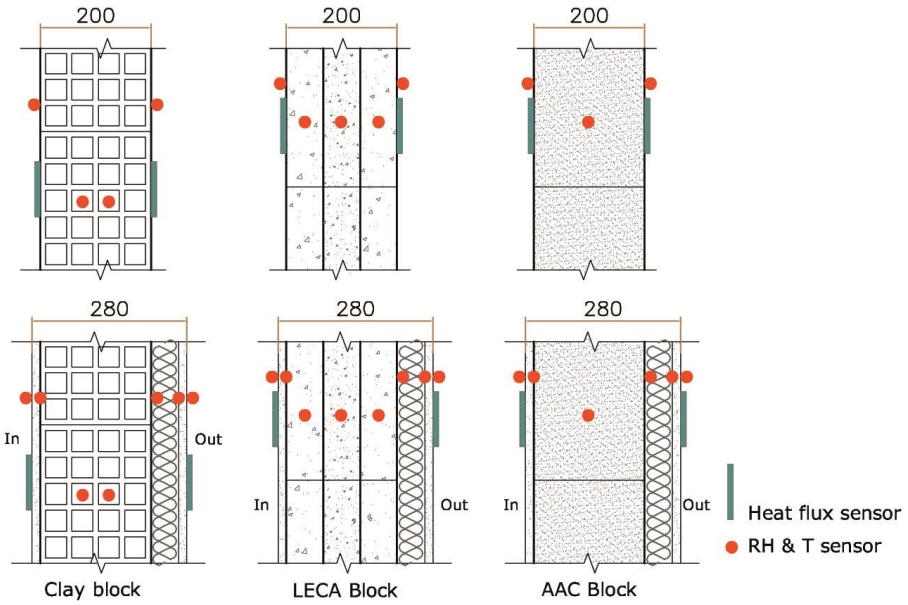

Figure 3-6: Location of temperature, RH and heat flux sensors on the specimens' surface and specimens' layers' interfaces.

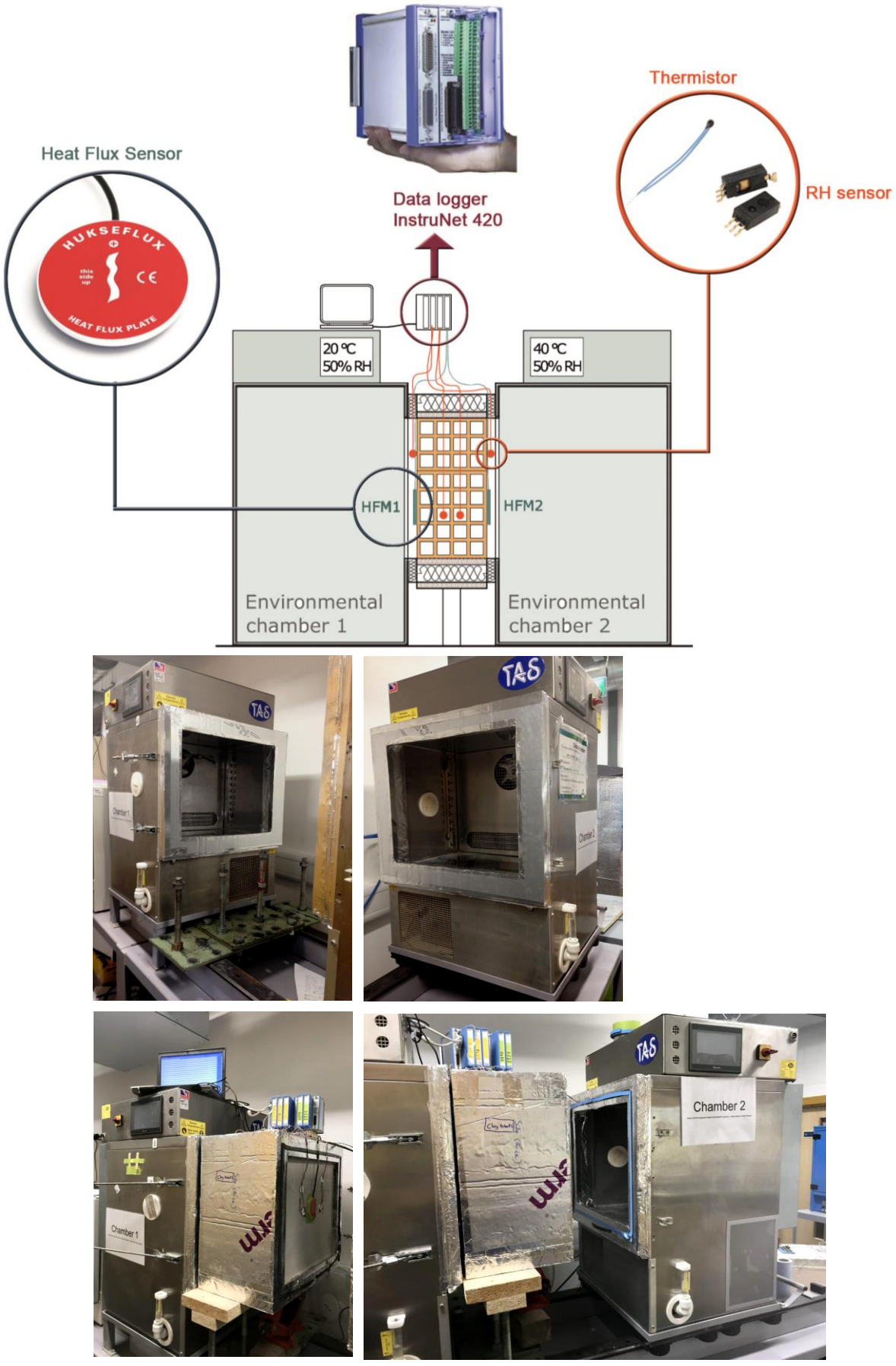

Figure 3-7: The experimental set-up showing the location of specimens, environmental chambers, sensors and data acquisition system

3.1.3.1. Environmental chambers

The environmental chambers used were ECO 135 models manufactured by Temperature Applied Sciences TAS. The chambers used in this study were customised by the manufacturer by modifying the location of the screens and installing the door clamps on both sides of the chamber. One chamber was fixed and the other can be moved on rails to seal against the faces of each specimen, creating a sealed internal environment (Figure 3-7). This allowed the environmental chambers to maintain desired boundary conditions on both sides of the specimen to resemble the external wall of a building. Each machine comprised a stainless-steel inner chamber, enclosed in a steel outer shell. Between the two, was a layer of mineral fibre and foam insulation.

3.1.3.2. Temperature sensors

Negative Temperature Coefficient (NTC) thermistors (EPCOS 3 kΩ 60 mW- B57863S0302F40) were used to measure temperature on the surface, at interfaces and inside the core of the construction block. A thermistor is a temperature- sensitive resistor composed of a semiconductor material. The electrical resistance of this material is dependent on its temperature and shows a large change in electrical resistance proportional to a small change in temperature. In NTC thermistors, their resistance decreases as temperature rises, hence the name. Thermistors are specified by their nominal resistance at 25°C. Thermistors with lower resistance (2252 Ω to 10,000 Ω) are used for lower temperature applications (-55 to 70°C). A temperature vs. resistance curve is used for each material thermistor to convert the output of the logger (resistance) t

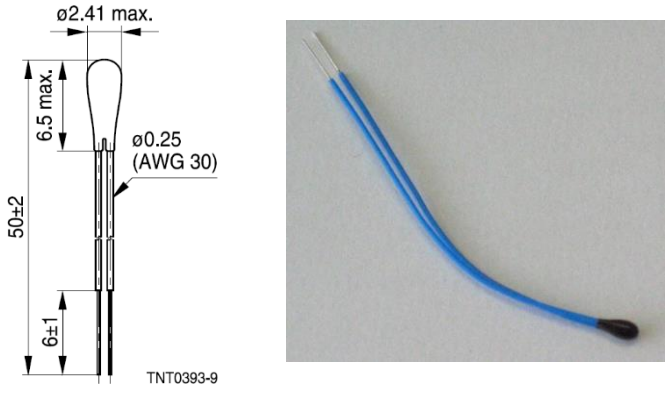

Figure 3-8: NTC thermistor; dimensions and shape

Thermistors were used as opposed to thermocouples due to their higher accuracy, sensitivity, good mechanical protection and less sensitivity to electrical noise. The thermistors used were the best compromise between accuracy, size, cost and compatibility with the data logger used. The nominal resistance of the thermistor chosen was 3000 Ω and it is coated with epoxy resin to mechanically protect the bead and wire connections from corrosion. Similarly, its wires were

PTFE-insulated for their protection. An online thermistor calculator was used (Figure 3-9) to calculate Steinhart-Hart model coefficients (A, B and C). The calculator used resistance-temperature paired values (data from manufacturer) to calculate the coefficients which were later used in the data logging software to convert the resistance values of thermistors into temperatures.

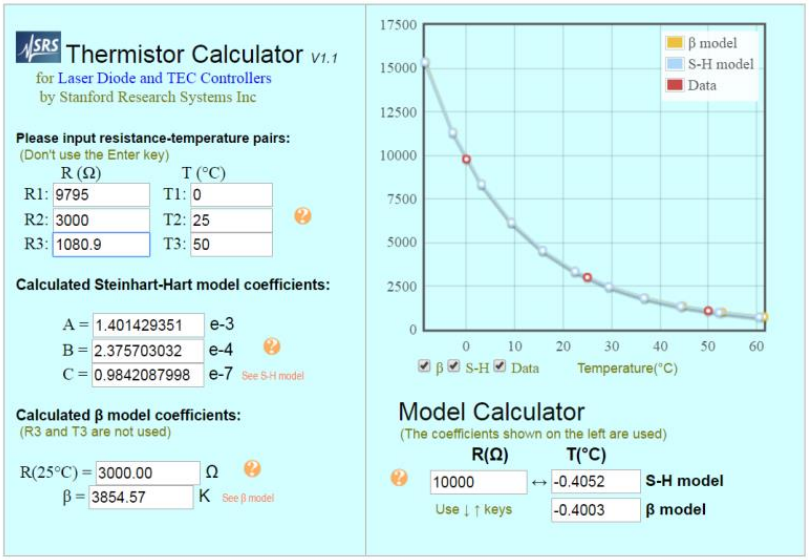

Figure 3-9: Thermistor calculator used to calculate Steinhart-Hart model coefficients

3.1.3.3. Relative humidity sensors

HIH 5031 relative humidity sensors (Figure 3-10) were used to measure RH on the surface, at interfaces of layers of wall assembly and inside the core of the construction blocks. The sensor used was a covered, moisture- resistant humidity sensor with a hydrophobic filter allowing it to be used in condensing environments. Its multilayer construction provided protection from condensation, dust, dirt, oils and common environmental chemicals. The accuracy of the sensor was ±3 %. These sensors were wired according to the instructions supplied by the manufacturer, and calibrated against a reference sensor and then mounted on, and in, the wall specimens.

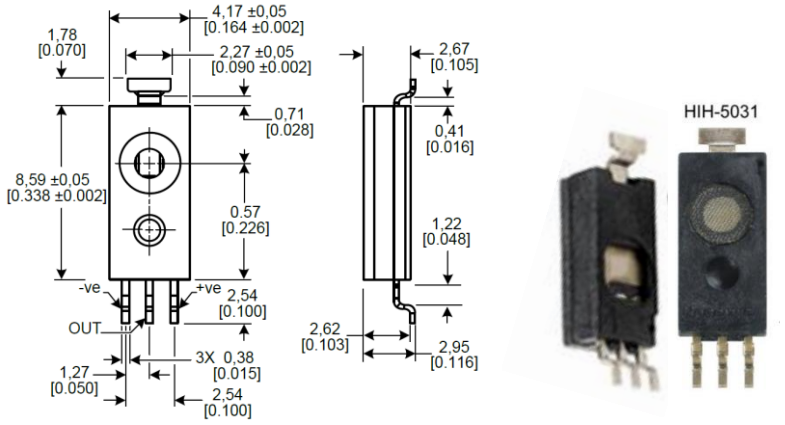

Figure 3-10: RH sensor (HIH-5031); dimensions in mm [in]

At any given temperature the air can hold a limited amount of water vapour, when it is said to be saturated. RH is the ratio of the amount of moisture in the air (or absolute humidity AH [gr/m3]) to total amount of moisture that air can hold in any temperature i.e. saturation. As RH is a temperature dependent parameter and cannot be independently analysed, for the purpose of this study, absolute humidity value was calculated using the instructions given in BS 1339-3.

3.1.3.4. Calibration of RH and temperature sensors

The outputs of the thermistors and RH sensors were checked against the temperature and RH of an environmental chamber that was itself calibrated by the manufacturer to determine their accuracy.

Thermistors: The software that converts the output of the thermistors i.e. their resistance to temperature uses Steinhart-Hart equation. The maximum and minimum temperature of the range of interest is used to calculate the mid-range temperature. These three points with their corresponding resistance values (found in temperature vs. resistance table given by the manufacturer) were then used as the input of a Steinhart-Hart calculator to calculate the Steinhart-Hart coefficients.

After wiring and soldering the thermistors, the accuracy of their readings was tested by comparing their output with actual readings from a climate chamber. The thermistors were put inside the chamber and the temperature of the chamber was varied from 10 to 40°C in 5°C intervals; each with a different RH level (10%, 50% and 70%). The results shown in Figure 3-11 shows good agreement between the thermistor's readings and readings of the climate chamber. For the RH sensors, a similar procedure was performed to check the output of the sensors against the RH reading of a calibrated environmental chamber.

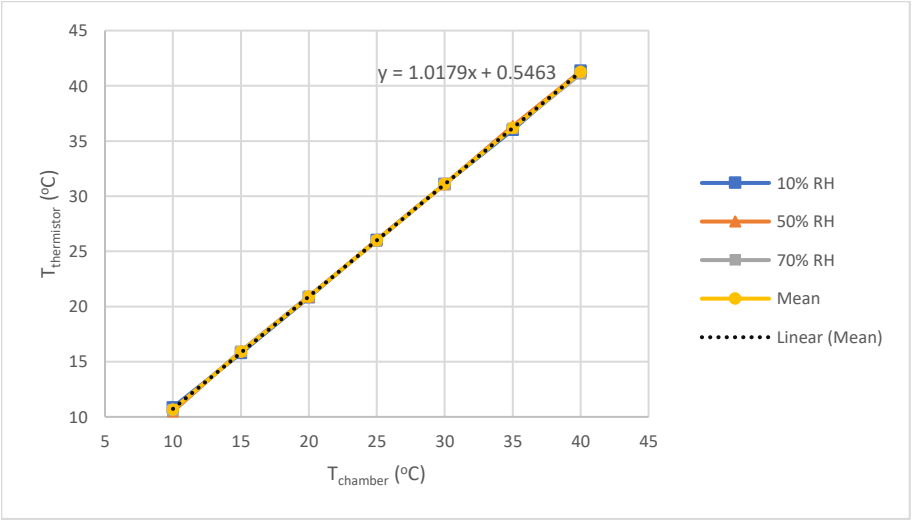

Figure 3-11: Thermistors calibration line showing $T_{thermistor}$ against the temperature readings of a calibrated chamber

3.1.3.5. Heat flux sensors

Heat flux through the wall specimen was measured using Hukseflux HFP01 heat flux sensor (Figure 3-12). A heat flux sensor measures the heat flux density, expressed in W/m^2, through the sensor itself. The sensor inside the HFP01 was a thermopile which consisted of several thermocouples electrically connected in series (to amplify the signal) encased inside a ceramic-plastic composite body. The thermopile generates a small voltage which is a linear function of temperature difference across the body of the plate. The heat flux is proportional to this temperature difference divided by the effective thermal conductivity of the heat flux body. The measured voltage is in the microvolt range (μv) and needs to be divided by sensor's sensitivity (S) to be converted to a heat flux (W/m^2). Each sensor is individually calibrated by the manufacture to determine the specific sensitivity value for that sensor. Heat flux plates were mounted on the centre of the surfaces of the wall specimen on its both sides avoiding mortar joints.

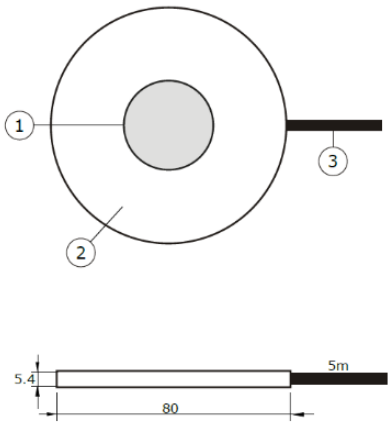

Figure 3.2.1 *HFP01 heat flux sensor dimensions in x 10^{-3} m*

(1) sensing area
(2) passive guard of ceramics-plastic composite
(3) cable (standard length 5 m, optionally longer cable in multiples of 5 m, cable lengths above 20 m in multiples of 10 m.)

Total sensor thickness including covers is 5.4 x 10^{-3} m.

Figure 3-12: Feat flux sensor; dimensions and configuration

3.1.3.6. Data logger and data acquisition software

The InstruNet data logging system connects several measuring cards (i4xx cards) installed within a card cage to a computer using a DSP controller (Figure 3-13). A communication card (i410) was used as the first card on the left of the card cage to interface to a computer. This card was connected to a computer through a DSP controller (i2x0). Because analogue sensors were being used, an i430 card was installed to covert the analogue signals into digital signals. i420 and i423 data acquisition cards were then set up in the cages and sensors were connected to these measuring cards through wiring boxes. The Instrunet World was used for monitoring and operating the data acquisition system. The output of the sensors i.e. resistance (thermistors) and voltage (RH sensors and HF sensors) was recorded by this software after being digitised. The outputs were converted to temperature, RH and heat flux values within

the software using conversion equations and coefficients. The sampling rate for all sensors was 1 per minute.

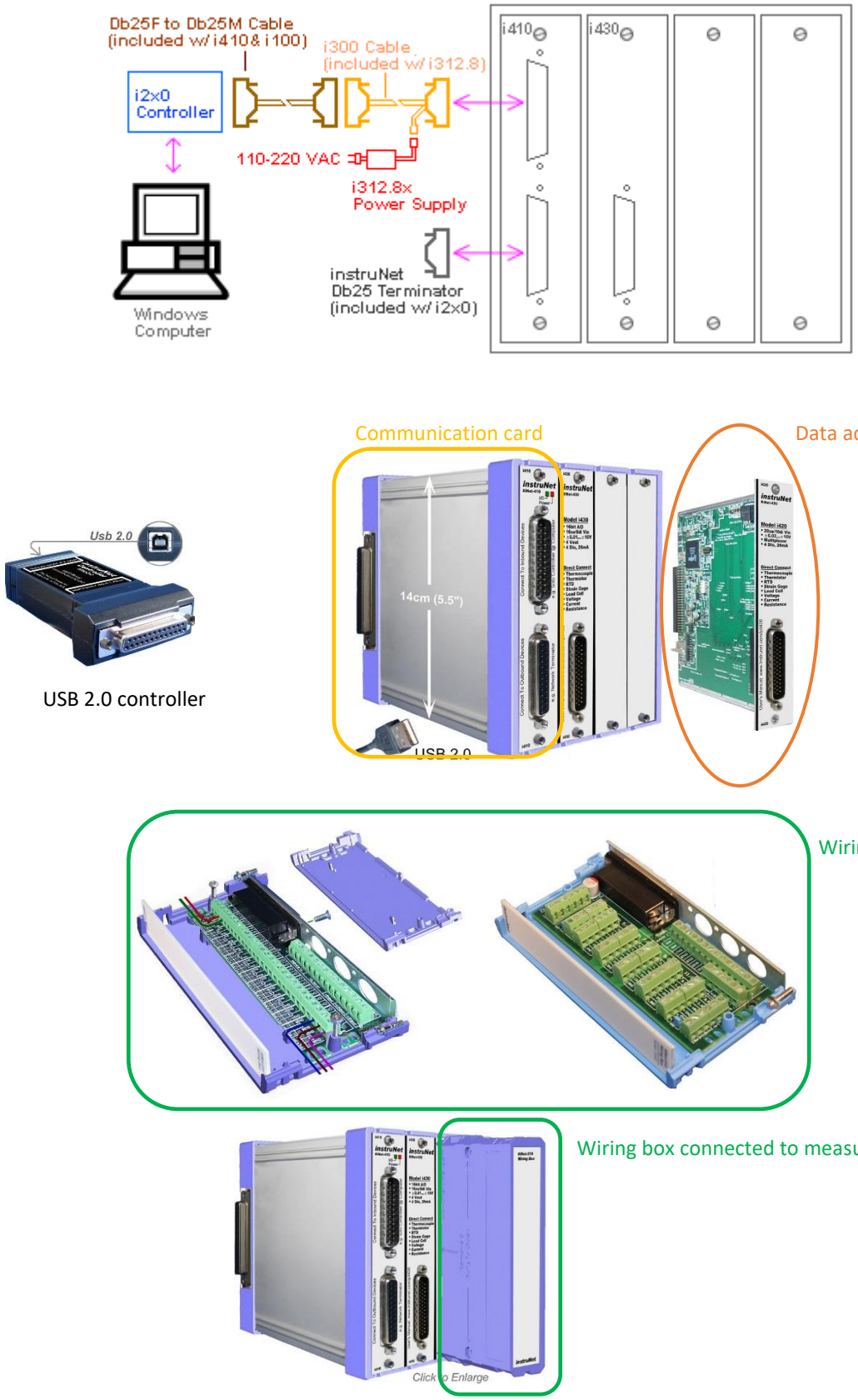

Figure 3-13: compartments of data logging system

3.1.3.7. Assembly of multi-layer wall specimens

Surface mounted sensors

Thermistors were wired and placed on both surfaces of the specimen by applying Omegatherm 201 thermal paste to create a better surface contact. RH sensors were placed next to thermistors to measure surface RH. Heat flux sensors were also mounted on the centre of the specimen surface using a layer of thermal paste applied to the surface of the sensors to create a smooth and air-gap-free contact (Figure 3-14).

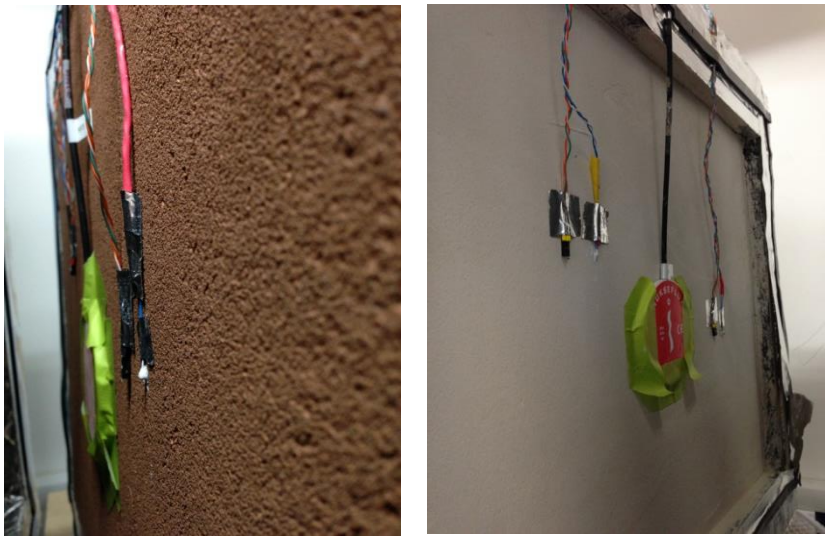

Figure 3-14: Heat flux, RH and temperature sensors mounted on the surface of the wall specimens

Sensors in the core of construction blocks

A protective shield was designed and made by a 3D printer to house the RH sensor and thermistor, protecting them from corrosion and damage (Figure 3-15). This cover shield was a perforated cylindrical capsule, inserted inside a hole drilled into the body of the blocks in the case of the AAC and LECA blocks. The drilled cavity left between the top of the capsule and the top of the block was then filled with small cylindrical pieces of block to minimise perturbations in heat path (Figure 3-16). For fired clay blocks, the capsule was simply inserted in the existing cavity in the structure of the block.

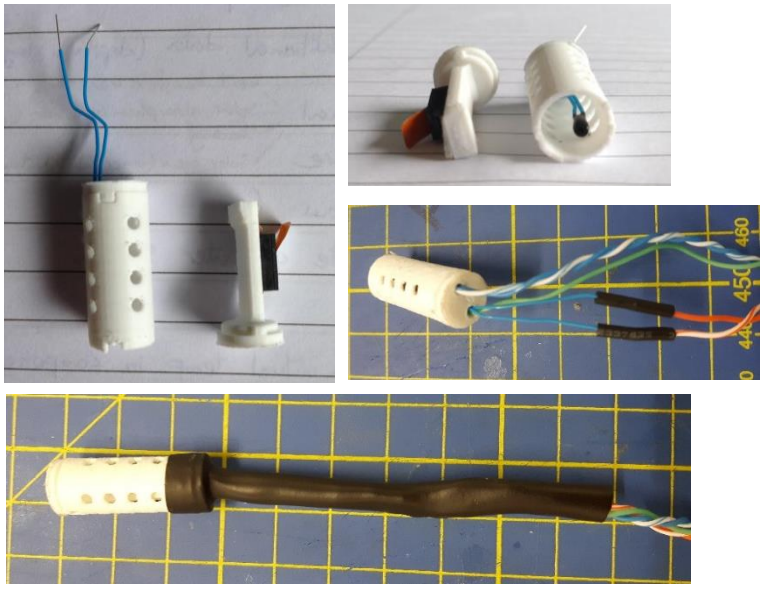

Figure 3-15: Cylindrical cover shield designed to protect RH & T sensors in the middle of the blocks

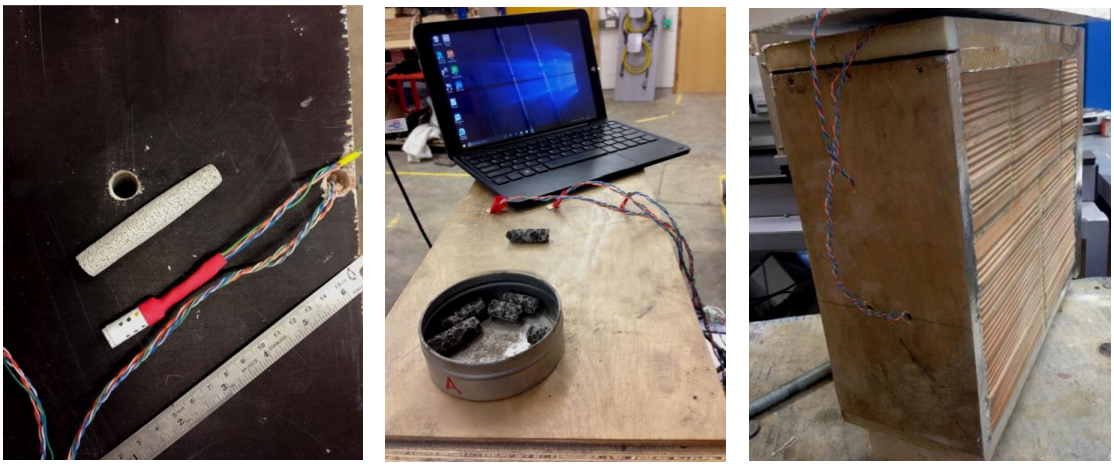

Figure 3-16: Method to embed RHT sensors showing
cylindrical cover shield inserted into the holes drilled into the blocks and filled with cylindrical cores of the same material

Sensors at specimen layers' interfaces

At interfaces where RHT sensors were covered with plasters, another cover shield was used. This shield was cubic in shape with perforations on only one of its surfaces where it was in contact with the interface (Figure 3-17). This design was intended to protect the sensors from the wet plaster and to allow more accurate temperature and RH readings of the interface itself and not the depth of the plaster.

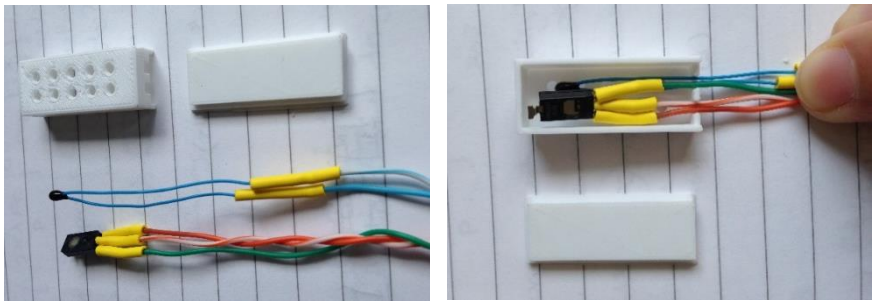

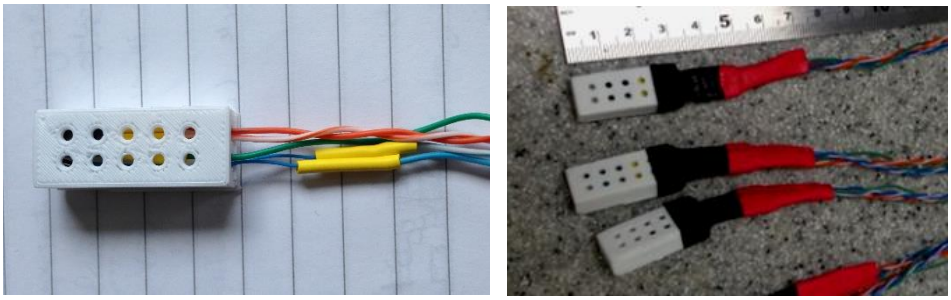

Figure 3-17: Cubic cover shield designed to imbed and protect RH & T sensors at the interfaces of the layers

Installing insulation boards

Between the insulation board and construction block, sensors were simply attached to the surface of the board using aluminium tape. Boards were then glued to the blockwork using an appropriate adhesive. cork boards were attached to the blockwork using Isovit E-Cork, a fixing and levelling lime-based mortar containing cork aggregates and a small amount of cement, specifically formulated for cork boards by SecilTek (Figure 3-18). For PIR insulation boards, small regularly spaced areas of Araldite Rapid epoxy resin were enough to hold the boards in place (Figure 3-19).

Figure 3-18: RH and T sensors mounted at the interface of the block and cork insulation board

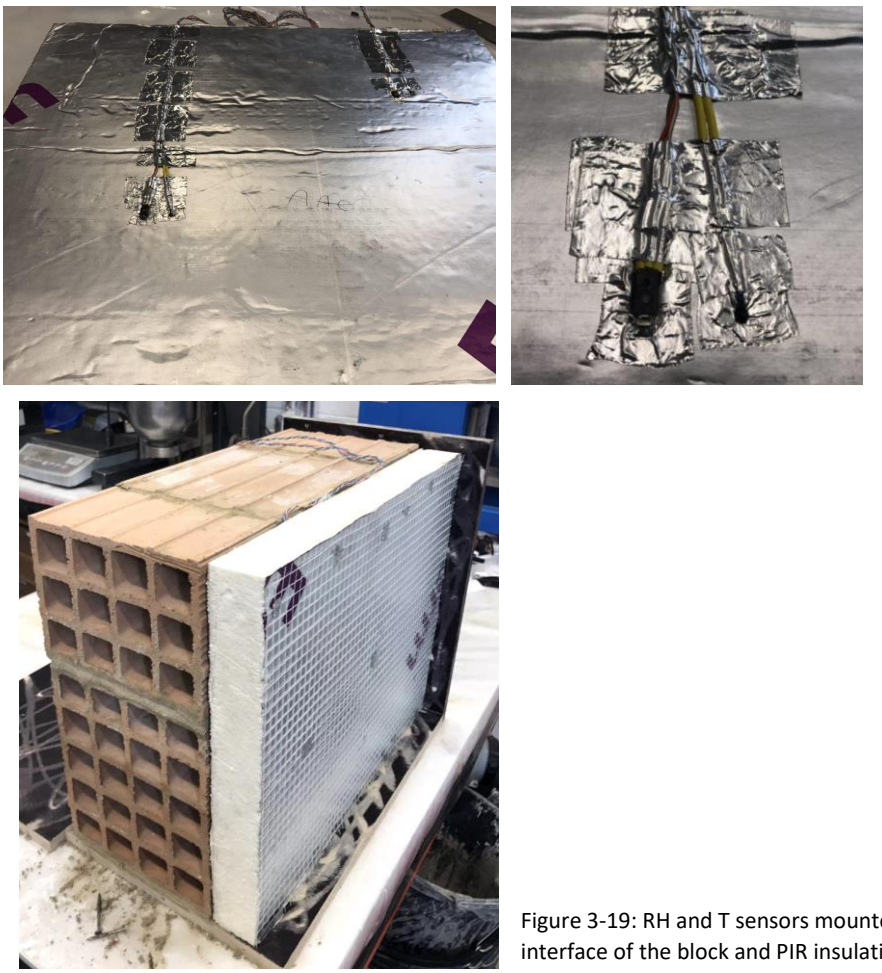

Figure 3-19: RH and T sensors mounted at the interface of the block and PIR insulation board

Applying external rendering to insulation boards

For low-carbon alternatives (insulated with cork), Isovit E-Cork was first used to attach a fiberglass reinforcement mesh to the cork insulation board. The location of the sensors was marked and temporarily protected from the wet mortar with a piece of aluminium tape which was removed when the mortar dried. Sensors were then mounted on the surface of the cork board as shown on the photos, and another layer of mortar (Reabilita Cal AC) was applied to level the surface and prepare it for the final finishing, a lime-based premixed fine top coat render, which was applied after 24 hours to allow the mortar to cure.

Similar method was used for PIR board specimens. A fiberglass reinforcement mesh was taped to the surface of PIR insulation. No binding mortar was needed to attach the fiberglass mesh to the insulation. Sensors were then mounted on the surface of the insulation board and cement render (6:1 ratio) was applied on the surface of insulation.

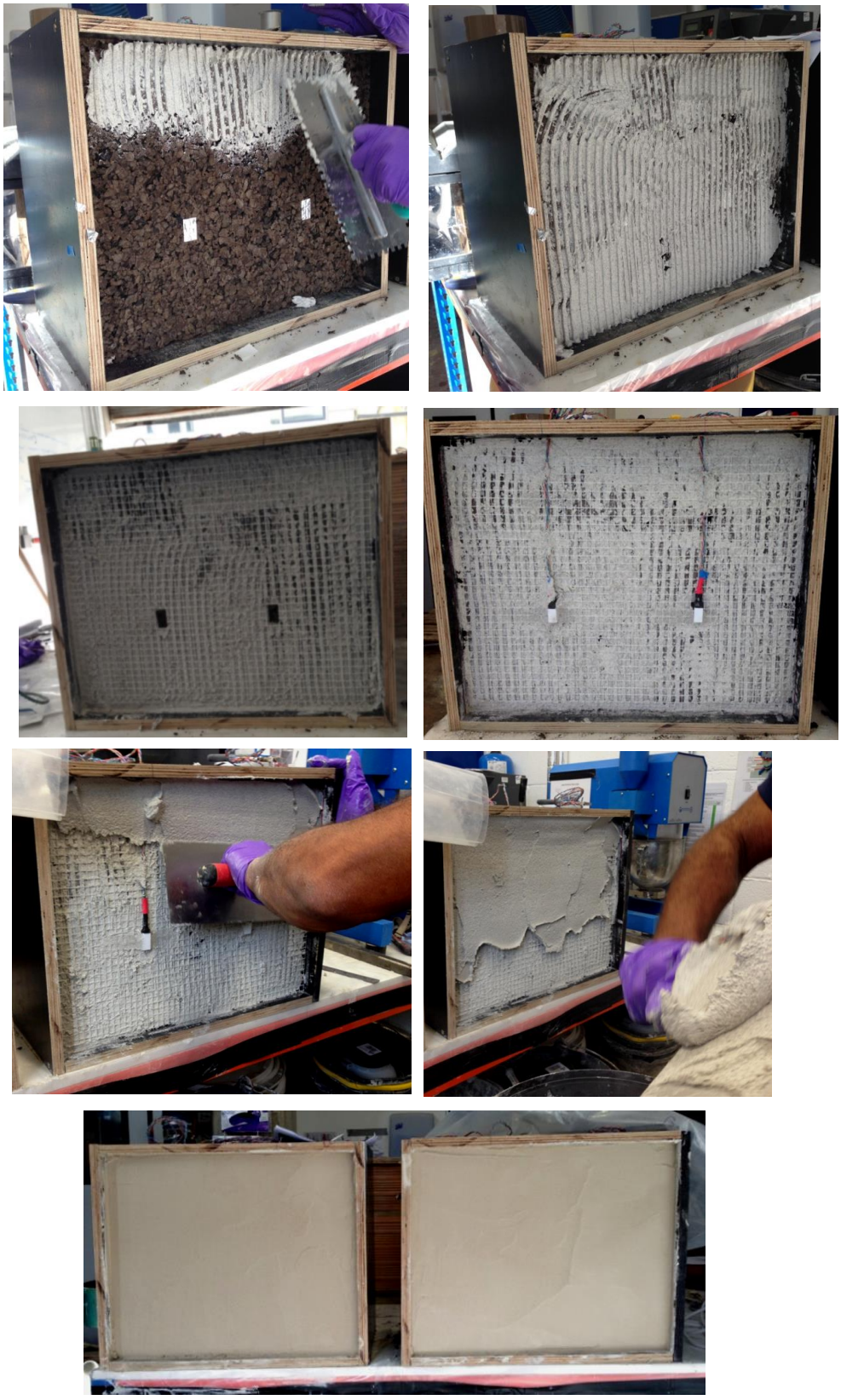

Figure 3-20: Mounting RH and T sensors mounted at the interface of cork insulation board and external rendering

Applying internal plaster to blockwork

In case of low-carbon hygroscopic wall types where earth plaster was to applied on the internal side of blockwork, a layer of Baumit DG27 primer was applied on the surface of the blockwork,

to both prepare it for clay plaster to be applied by equalising the suction of substrate and improving adhesion to the substrate. The primer does not inhibit water vapour diffusion through the substrate. After 24 hours drying time, earth plaster was applied as shown in Figure 3-21.

For conventional multi-layer wall types (insulated with PIR), gypsum plaster was directly applied on the surface of the blockwork in case of fired clay and LECA blocks. For the AAC block specimen, the surface of the block needed to be moistened before applying the gypsum plaster. After the application of gypsum plaster the specimen was covers with a plastic sheet to slow down the drying process of the wet plaster. This is to deal with the high absorptive capacity of AAC blocks that result in rapid suction of water and quick drying of wet plaster and eventually break-down of gypsum plaster.

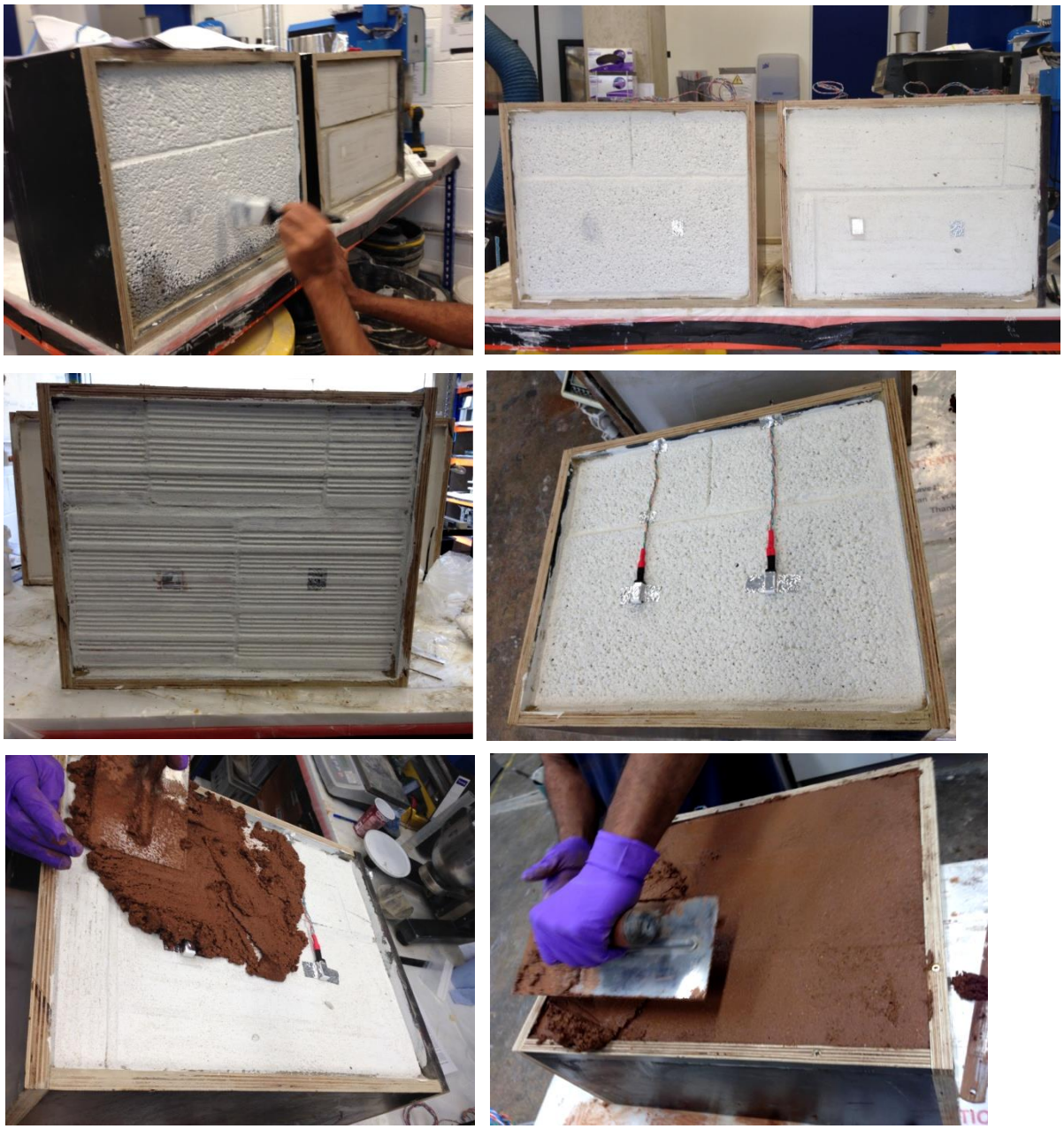

Figure 3-21: Mounting RH and T sensors mounted at the block and internal plaster

3.1.4. Boundary conditions

The wall specimens were exposed to different boundary conditions maintained by the environmental chambers. First, a steady state condition of 40°C on one side of the specimen and 20°C on the other was applied, to create a constant temperature gradient of 20°C and, therefore, a steady heat flow across the specimen. To determine the RH values, a preliminary test was carried out on the single layer fired clay block specimen, in which 3 different scenarios were defined. In the first 2 scenarios, condition (a) and condition (b), the same temperatures but different RH values were maintained inside the chambers (Figure 3-22). While having the same temperature gradient in both conditions, the RH values chosen resulted in zero vapour pressure difference in condition (a), and zero RH gradient under condition (b). As discussed in the literature review, mass transfer through the building envelope happens in the form of vapour diffusion caused by vapour pressure difference and/or in the form of sorption diffusion (or capillary conduction if pores are filled up with water) caused by RH gradient across the envelope. The defined scenarios resulted in sorption diffusion across the sample derived by the RH gradient (in the opposite direction to the heat flow) under condition (a), and vapour diffusion derived by vapour pressure gradient (in the same direction as the heat flow) under condition (b). These experiments, also, helped understanding the effects of different mechanisms of moisture transfer on heat transfer under steady-state condition. Figure 3-28 shows the heat flux data through the left specimen surface under conditions (a) and (b). These graphs show that Condition (a) resulted in slightly higher heat flux (slightly above 30 W/m^2) than condition (b) (slightly below 30 W/m^2) despite the same temperature gradient applied across the sample. However, the difference was negligible.

The result of this experiment prompted a third test, condition (c), where temperatures were kept the same at 20°C on both sides (theoretically no heat flow) and RH levels were established as 80% on one and 40% in the other chamber, imposing both vapour and surface diffusion across the specimen (Figure 3-22). Under condition (c), left heat flux sensor recorded a minor amount of heat transfer from the higher RH zone (left chamber) to the lower RH zone (right chamber), despite a zero-temperature gradient across the sample (Figure 3-26). The direction of heat flow was the same as the direction of mass flow, as shown on Figure 3-22.

Figures 3-23 & 3-24 show the temperature, RH, Vapour Pressure VP and Absolute Humidity AH profiles inside the chambers, on the surface and in the middle of the specimen. Figure 3-26 shows the heat flux across the sample under the three conditions (heat flux data from the left chamber has unfortunately not recorded during the first 2 conditions). It should be noted that the three defined steady-state scenarios were created only for experimental purposes and the

results could not be extrapolated to real conditions where wall constructions are exposed to dynamic weather conditions.

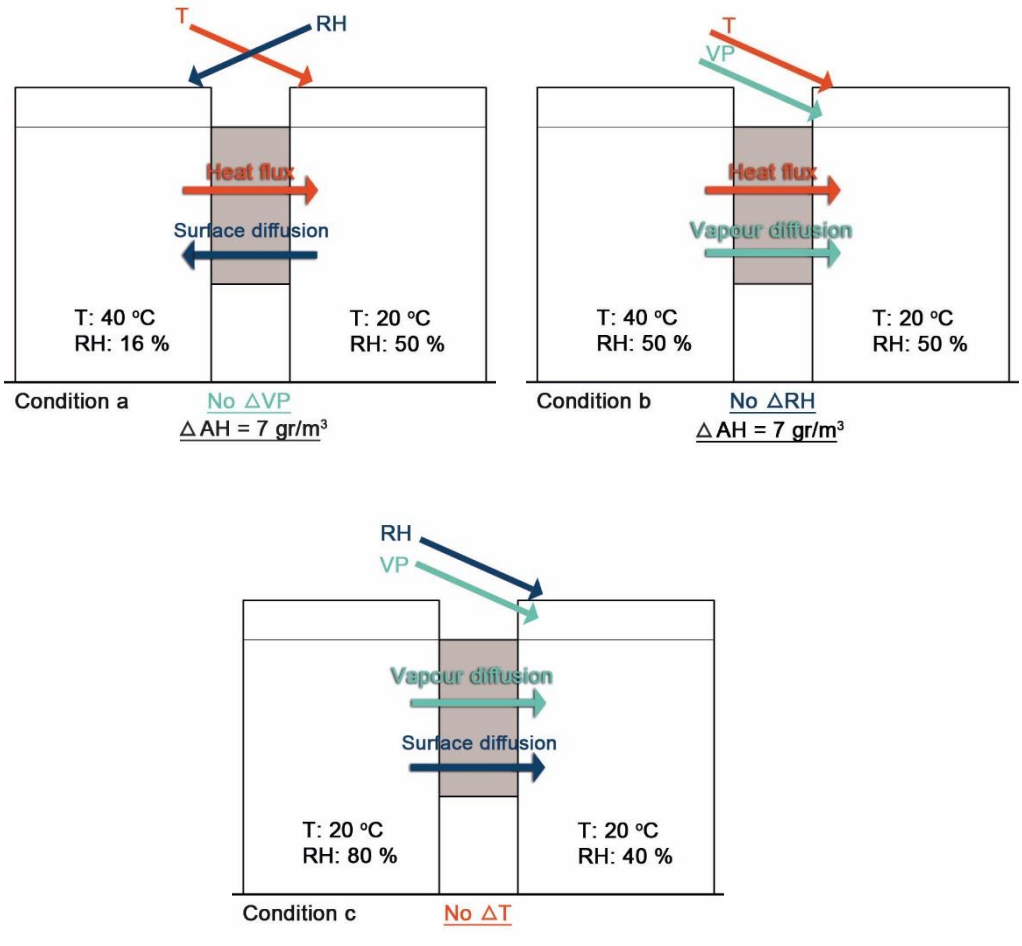

Figure 3-22: Environmental conditions inside the chambers under 3 scenarios;
RH: Relative Humidity, AH: Absolute Humidity, VP: Vapour Pressure

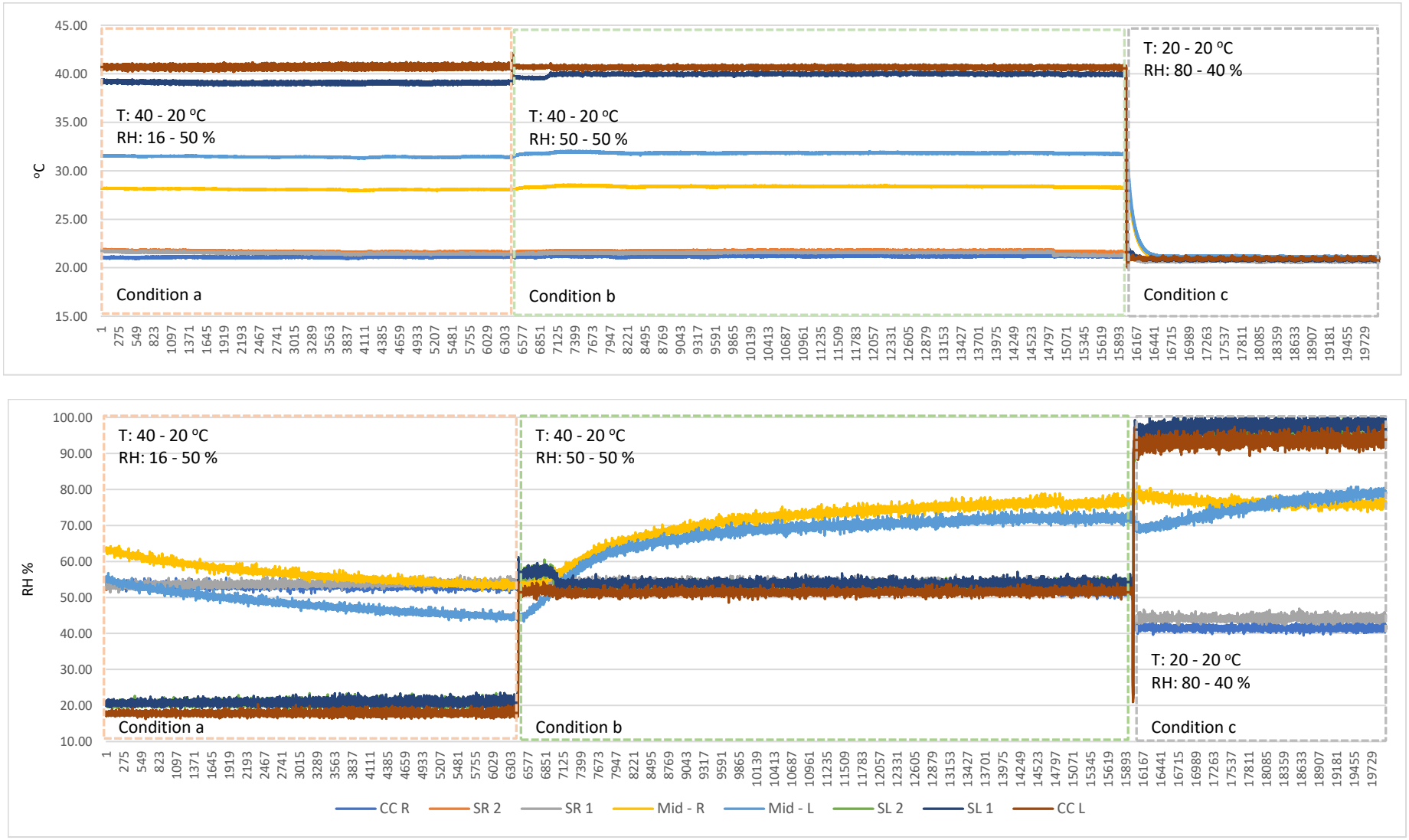

Figure 3-23: Temperature, RH profiles in conditions a, b & c across the specimen

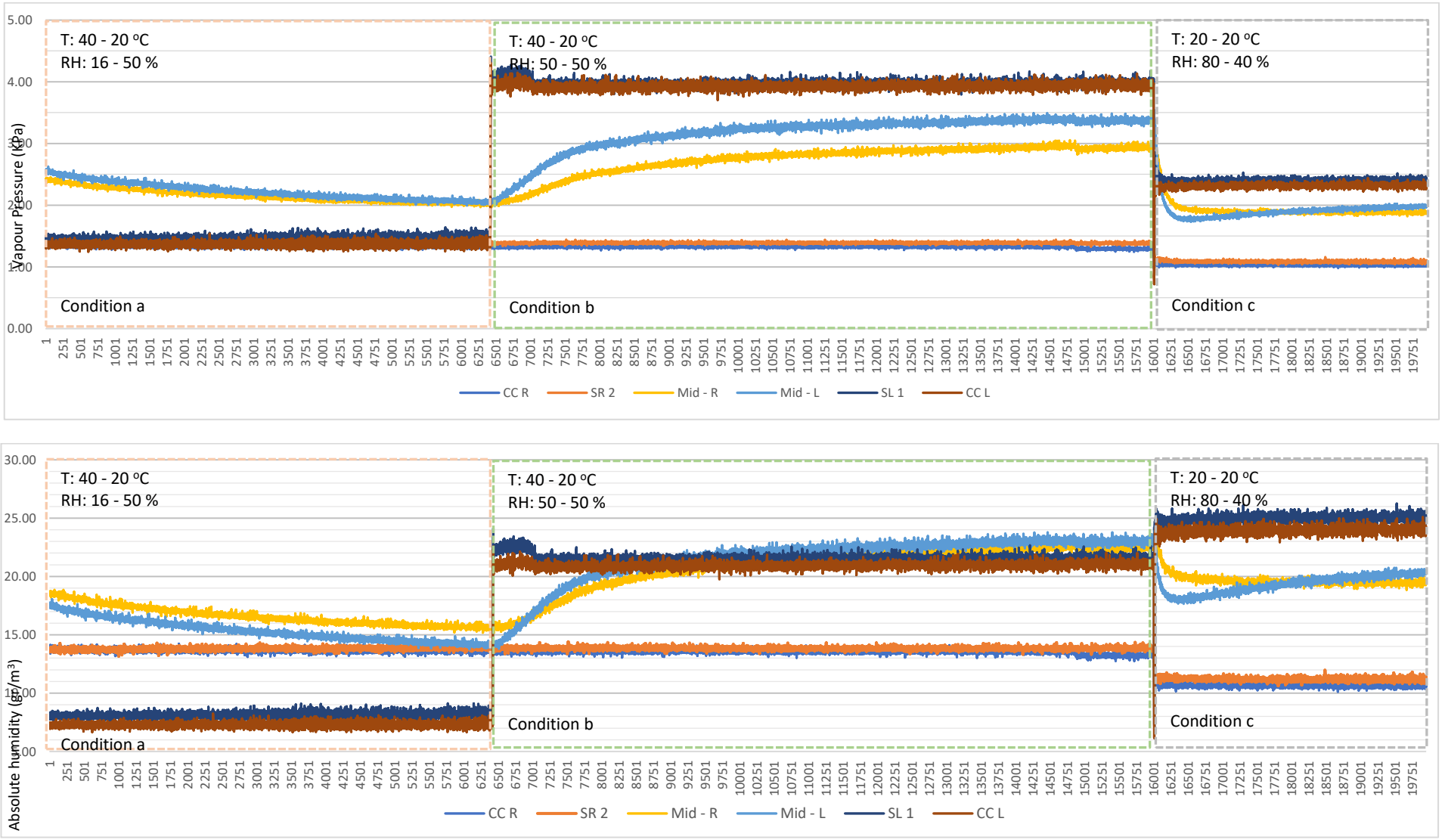

Figure 3-24: VP and AH profiles in conditions a, b & c across the specimen

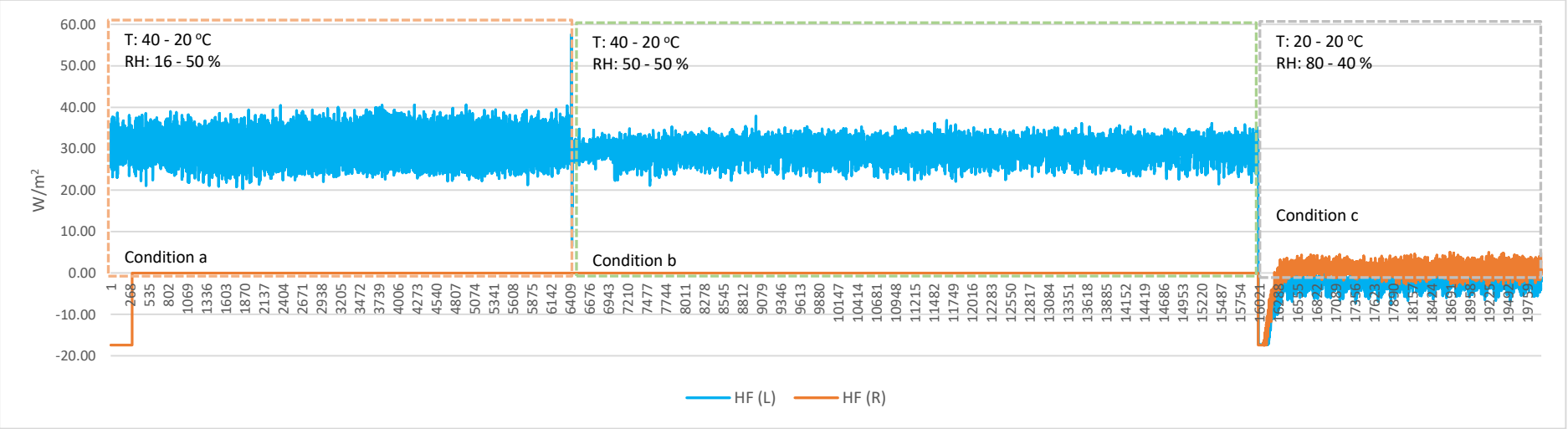

Figure 3-25: Heat flux data during conditions a, b & c from Right (R) and Left (L) climate chambers

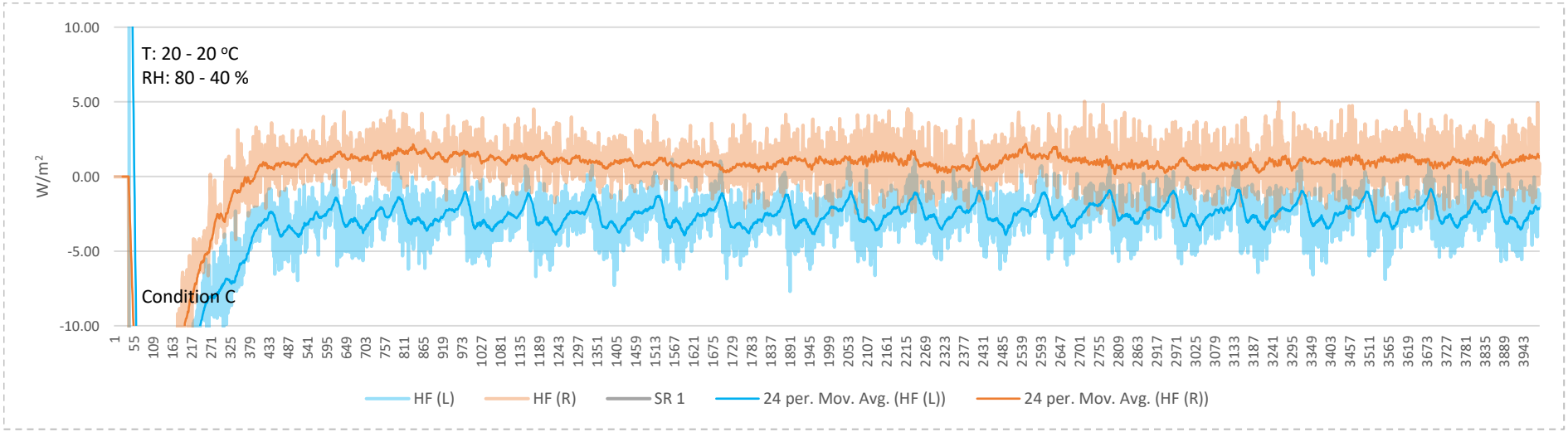

Figure 3-26: Heat flux data during condition c from Right (R) and Left (L) climate chambers

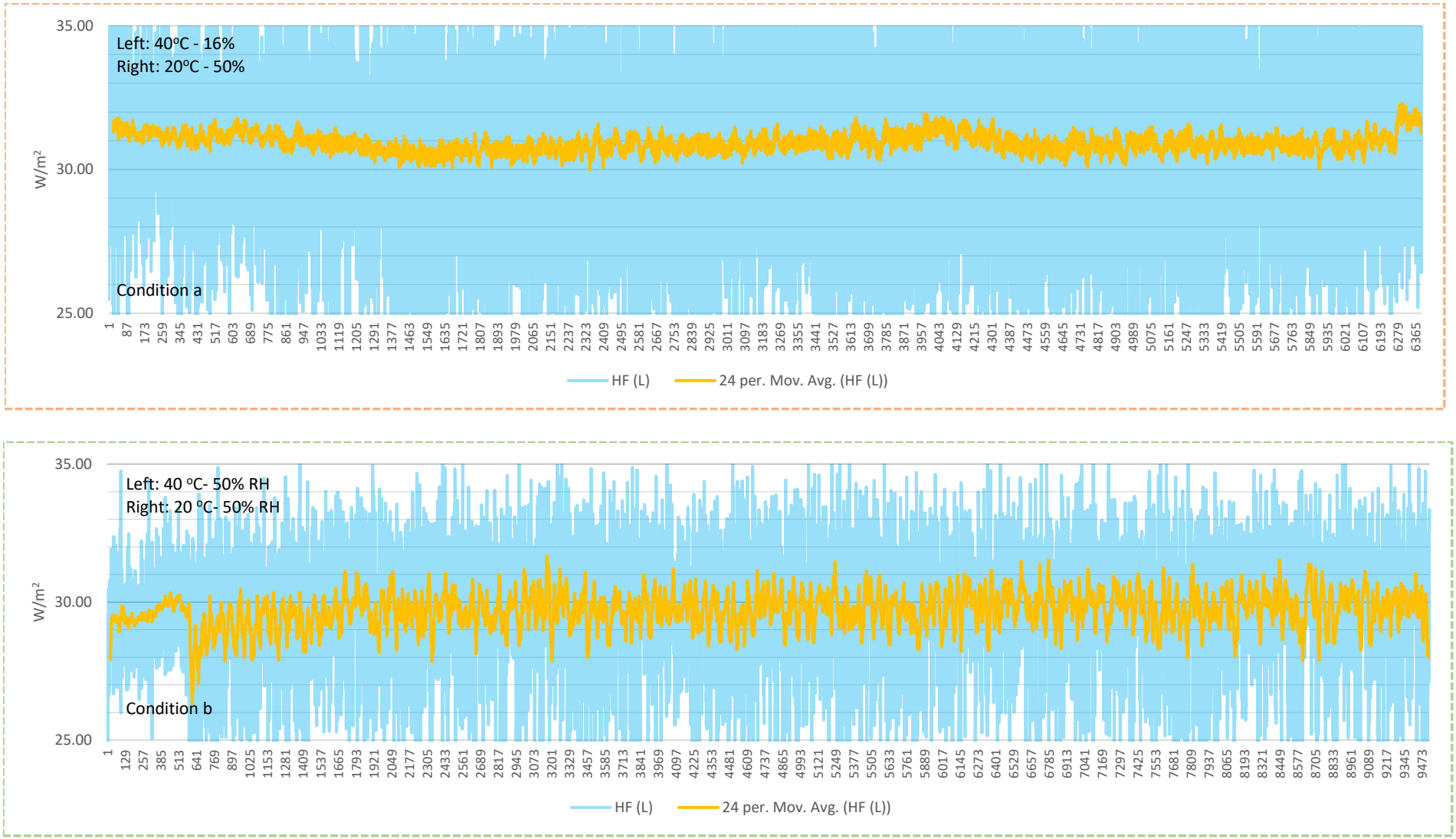

Figure 3-27: Heat flux data under condition a (top) & b (bottom) from Right (R) climate chamber

Secondly, specimens were exposed to a daily cyclic temperature and RH fluctuations representing the real outdoor weather conditions. The hot humid weather of a city in the south of Iran (Bandar Lengeh) and the hot dry weather of a city located in central north of Iran (Tehran) were selected to represent two major climatic conditions of the country. 5-year average hourly weather data files were used and analysed to extract the daily pattern of the prevalent weather conditions during hottest time of the year for Lengeh and Tehran (Figures 3-28 & 3-29). Figures 3-28 and 3-29 show the daily template of the temperature and RH square waves used in the environmental chambers. A step wave was used instead of a sine-curve due to the limitations of environmental chambers. Indoor room condition was kept at 23°C and 50% RH. It should be noted that hot summer weather condition is the most challenging weather condition in terms of providing thermal comfort for building occupants in Iran hence being the focus of this study. Most areas of the country feature long hot summers which are getting longer and hotter in recent years due to global warming effect. Whereas winters are generally mild and short.

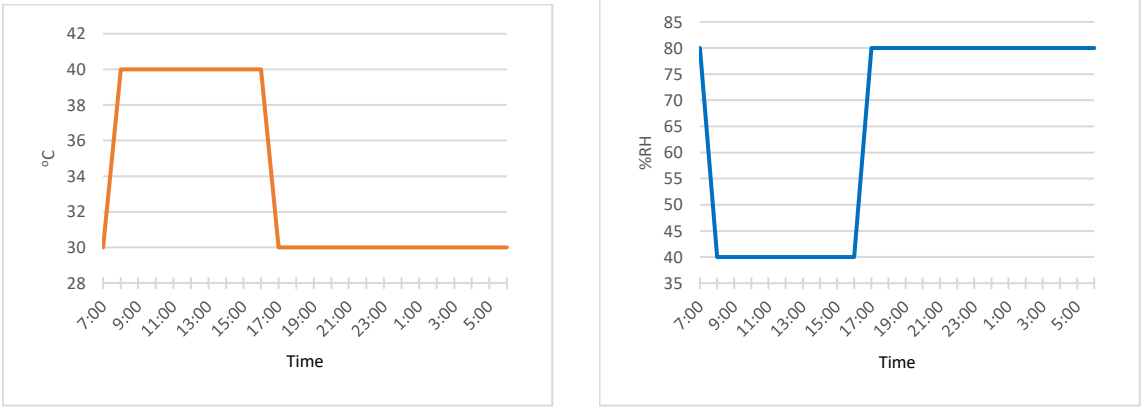

Figure 3-28: Hot humid summer condition extracted from weather data file of Bandar Lengeh

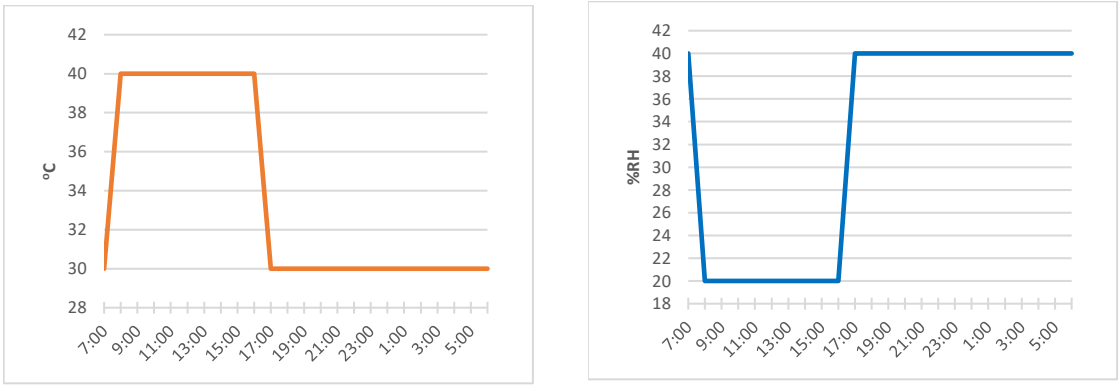

Figure 3-29: Hot dry summer condition extracted from weather data file of Tehran

3.1.5. Summary

Due to several assumptions, oversimplifications, uncertainties related to material properties in software databases, leading to uncertainties of the output of the numerical models, an experimental method was used in this study to study the hygrothermal performance of a number of wall types. This experimental set-up was built up combining hot-box and in-situ methods of measuring thermal transmittance value using two environmental chambers. These environmental chambers were designed to house a wall specimen in between allowing it to be exposed to different boundary conditions. Heat flux plates were mounted on both surfaces of the wall finish as well as RH and temperature sensors which were installed on the surfaces as well as in between the layers of the wall. Heat flux data was used to calculate an equivalent thermal transmittance value. Data from the RH and temperature sensors were used to plot the heat and moisture profiles through the section of the wall. This helped investigating the interactions of different layers and its effect on their performance. This investigation was done on 9 wall specimens made of three commonly used construction blocks in Iran. The first set of three, were made of single layer of blockwork. The second set of three, represented an insulated conventional wall system having PIR as thermal insulation, cement and gypsum plaster as external and internal finishing. The last set of three, represented an alternative wall construction proposed to improve environmental profile of the current practice wall construction. These alternative assemblies were insulated with expanded cork boards and plastered, externally, with lime plaster and internally, with earth plaster to replace PIR insulation, cement render and gypsum plaster.

A steady-state boundary condition was applied across the single-layer wall types to measure their steady-state thermal transmittance value and compare it with the result of theoretical calculations. Daily cyclic outdoor conditions were then applied on specimens to investigate their performance under a realistic hot humid and hot dry conditions. Hot dry and hot humid conditions were selected in this study as they are prevalent in most of the country and are the most challenging conditions in terms of providing thermal comfort for buildings occupants. Detail of the calculations and a discussion on results is given in chapter 4.

3.2. Part two: Experimental procedure for investigation of hygroscopic property of earth plasters

3.2.1. An introduction to earth plaster mixes

Earthen building materials are used in two forms; either as earthen walls in the form of earth blocks, rammed earth or cob wall or as clay plasters (Deliniere et al., 2014). Compared to other types of earth-based products and other conventional plasters, earth-based plasters have been characterised in very few scientific studies and despite the recent increased interest in earth-based plasters, DIN 18947 introduced by the Deutsches Institut fur Normung (DIN), is the only European standard for this type of mortar. This German standard is known to be the first that specifically focused on earth mortars (DIN, 2013). Labat et al. (2016) stated that the moisture buffer capacity of earth plasters and their effect on occupant comfort has not been thoroughly studied and is not described in the literature until recently. Plant-based aggregates such as straw and animal hair have traditionally been added to earth to improve their strength and durability. However, recently, more attention is being given to the hygroscopic properties of plant-earth mixtures and their potential impact on improving indoor climate. The main components of plant-based products are cellulose, hemicellulose and lignin which are natural polymers containing hydroxyl groups that readily form hydrogen bonds with water and cause a high rate of water uptake (Zhang et al., 2011; Khan & Mubeen, 2012; Ummah et al., 2015). Laborel et al. (2016) also concluded that, the water vapour permeability of soil is very high but the influence of plant aggregates on its moisture absorption properties had not been widely studied. They added that the capacity of earth as a humidity regulator can be increased by the addition of plant aggregates, but a general conclusion cannot be drawn due to limited studies on this topic. The main advantage of adding natural fibres to earth-based materials is to improve their thermal insulation properties. More research needs to be undertaken to devise databases of fibrous earth composites, especially regarding their hygrothermal properties (Laborel et al., 2016).

The Diatomaceous Earth (DE) is a fine mineral aggregate known for its high absorptive capacities. Diatomaceous earth or diatomite, also known as rock flour, is a light, easily crumbled, silica-rich rock that is formed mainly from fossilised skeletal remains of diatoms (Maeda and Ishida, 2011, Allaby and Park, 2013). Diatom is a microscopic, single-celled algae with an amorphous silicon skeleton that grows abundantly in both fresh and saltwater. They are a common form of marine phytoplankton and a primary food source for aquatic animals. When diatoms die, their tiny shells sink and over the centuries form thick layers that are fossilised and compressed into a soft, chalky rock that is called diatomaceous earth (Allaby and Park, 2013, Kuronic, 1998). Processed diatomite is a fine chalk-like, irregular, porous, non-caking powder with chemical

stability and inertness, high porosity (up to 70%), large surface area ranging from 5 to 200 m^2/g and high liquid absorption capacity. it is mildly abrasive and has low thermal conductivity (Loganina et al., 2014, Dolley and Moyle, 2003). Processing DE requires mild quarrying, drying and milling. The only change to DE during such processing is a reduction in moisture content and aggregate particle size (Kuronic, 1998). DE is a versatile material and its applications range from material science to biotechnology, silicon chemistry, engineering and nanotechnology (Lopez et al., 2005,). Its main uses are in filtration, absorbents, fillers and insulation (Dolley and Moyle, 2003). In the building industry, the porous structure of DE has been used by Pimraksa and Chindaprasirt (2009) and Escalera et al. (2015) to make lightweight bricks. Vu et al. (2013) sintered a mixture of DE and volcanic ash, with and without the addition of sodium perborate, to produce a humidity control material but without mentioning how and where such mixture could possibly be used.

In this study, the moisture buffering capacity of earth plasters mixed with three plant-based aggregates (wheat straw, rice husk, wood shaving) was studied and compared with buffering capacity of earth plasters mixed with DE. DE was used due to its high absorptive capacity to further improve hygroscopic properties of earth. Two types of earth plaster i.e. a base coat and a top finishing coat were used. The two plasters comprised two different particle sizes, a coarse particle size for the base plaster coat and a finer particle size for the top finishing plaster coat. The finer particle size was necessary to achieve the surface finish required by top finishing plaster coats.

Laboratory tests were performed on these earth plaster combinations to determine their vapour permeability, moisture absorption function, and the NordTest Moisture Buffer Value (MBV), using different protocols and standards to characterise their moisture buffering capacity. The DIN 18947 Standard was used to classify the MBC of these earth plaster mixes as it is the only available European Standard for earth mortars.

3.2.2. Plaster mixes and sample preparation

To prepare specimens for test protocols, two types of factory-made earth plasters were mixed with rice husk, wood shaving, wheat straw (2% of the mass of earth) and diatomaceous earth (5% of the mass of earth) (Figure 3-30). The plant-based aggregates were chosen as they are common agricultural waste products and diatomaceous earth was chosen for its aforementioned high moisture absorption properties. The percentage of the additives (i.e. 2% for plant-based additives and 5% for DE) was decided based on the workability of the plaster. The amount of water added to the mixes was based on the recommendations of the manufacturer (Clayworks Ltd, 2018). However, when needed the proportion was adjusted to

make the mixture workable for plastering. The plasters used were a Base Coat (BC) and a Topcoat (TC) and comprised of different particles sizes. The TC contained finer aggregates than the BC, as shown on Figure 3-31, and the ingredients and proportions of each mixture are outlined in Table 3-1. It should be noted that all the BC and TC mixes for the samples in each experiment were prepared from the same batch of earth so that the potential effects of variation in soil properties of the mixes were ruled out.

Figure 3-30: Materials used in plaster mixes.

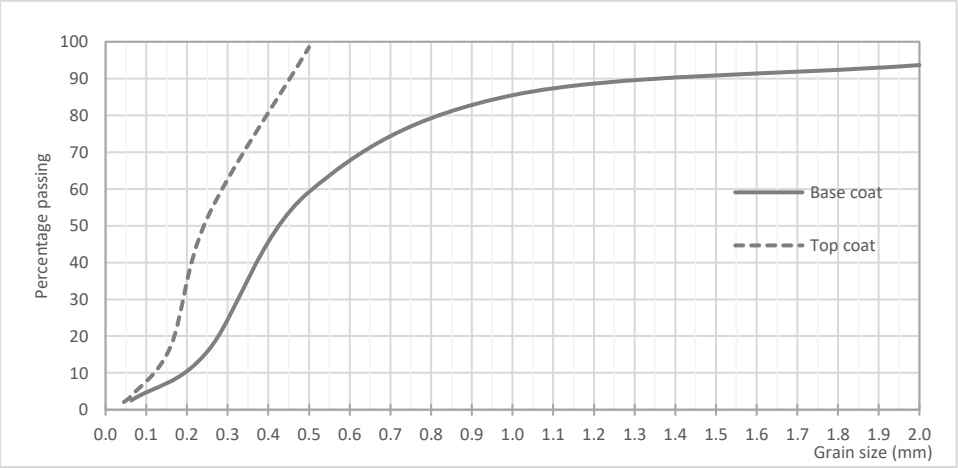

Figure 3-31: Particle size distribution of base coat and top coat earth plasters

Table 3-1: Composition of earth mix plasters

Sample	Rice husk wt%	Wood shaving wt%	Wheat straw wt%	DE wt%	Density kg/m³
BC	0	0	0	0	1950
$BC_{Rice\ husk}$	2	0	0	0	1800
$BC_{Wood\ Shaving}$	0	2	0	0	1550
$BC_{Wheat\ straw}$	0	0	2	0	1650
$BC_{Diatomaceous\ earth}$	0	0	0	5	1850
TC	0	0	0	0	1750
$TC_{Rice\ husk}$	2	0	0	0	1650
$TC_{Wood\ Shaving}$	0	2	0	0	1550
$TC_{Wheat\ straw}$	0	0	2	0	1500
$TC_{Diatomaceous\ earth}$	0	0	0	5	1750

BC: Base Coat. TC: Topcoat.

3.2.3. Protocols for quantifying hygroscopic performance of materials

3.2.3.1. Water vapour permeability (δ_p)

For the current test, silica gel beads were used as the desiccant to give 0% RH for the dry cup test and potassium nitrate KNO_3 salt solution to create 93% RH inside the cup. Cylindrical samples of 100 mm diameter and 15 mm thickness were coated in paraffin-wax on their sides (Figure 3-32) and were pre-conditioned at 23°C and 50% RH. They were then sealed above a plastic container with aluminium tape and silicon sealant and placed inside an Espec LHL-113 environmental chamber at 23°C and 50% RH (Espec corp, 1999). The accuracy of the climate chamber was given as ±0.5°C and ±3% RH by its manufacturer which was constantly monitored using an RH and temperature sensor (Tinytag Ultra 2 sensor model TGU-4500) with an accuracy of 0.45°C for temperature and ±3.0 % at 25°C for RH. This test methodology was repeated for all other experiments.

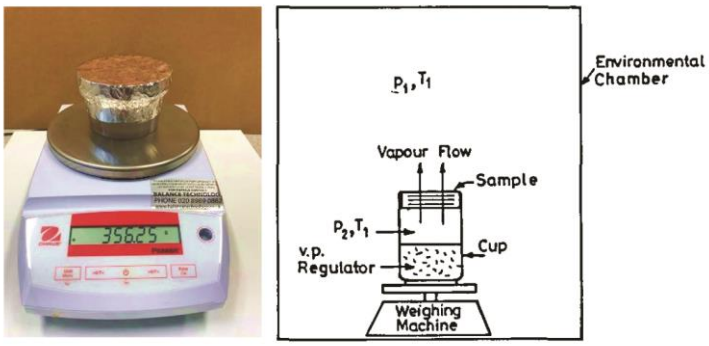

Figure 3-32: Test assembly for determining water vapour permeability

3.2.3.2. Moisture sorption capacity ($\frac{\partial w}{\partial \varphi}$)

Sorption experiments carried out in accordance with BS EN ISO 12571 propose the use of either salt solutions (Figure 3-33) or a climate chamber, to maintain a specific relative humidity in an environment where specimens are placed (at a constant temperature). The moisture content of the specimens is determined by measuring their mass change when equilibrium is reached for

every RH step within the range between 0 and 95% during absorption and desorption process, as shown in figure 3-34. The sorption isotherm curve can then be drawn by plotting the moisture content against the RH. Another instrument used to conduct the test protocol is the Dynamic Vapour Sorption (DVS) instrument. Developing sorption isotherms by use of this instrument is more rapid and less labour-intensive. This instrument measures uptake and loss of moisture in the sample by circulating a carrier gas at a specified RH over a sample suspended from the weighing mechanism that detects the absorption/desorption of water vapour by the increase/ decrease in mass of the sample. Fewer errors are likely to occur as there is no need to remove the sample from storage containers or climate chamber for periodic weighing.

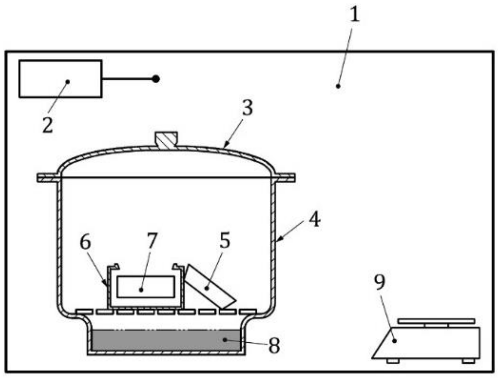

Figure 3-33: Desiccator (or salt solution) method (ISO 12571, 2013);
Key: 1. Constant temperature chamber, 2. Thermometer, 3. Lid of desiccator, 4. Desiccator,
5. Lid of weighing cup, 6. Weighing cup, 7. Test specimen, 8. Saturated salt solution, 9. Electronic balance

For measuring sorption isotherms of plasters, it was decided that the small sample specified required for use in the DVS chamber, would not be sufficiently homogenous due to the size of the aggregates and therefore was not deemed representative of the mixed plasters. Therefore, an environmental chamber was used and samples as large as 50 x 50 x 50 mm were cast (Figure 3-34) and put inside the chamber and exposed to different RH steps.

Figure 3-34: Samples for moisture sorption capacity test (50x50x50 mm) carried out in climate chamber

3.2.3.3. Moisture Buffer Value (MBV)

For practical categorisation of materials based on their moisture buffering capacity the NordTest protocol was used. This protocol was deemed the most appropriate method for evaluating the hygroscopic behaviour of a material compared to the moisture sorption capacity and permeability, as it mimicked a more realistic scenario for vapour production, as opposed to the two aforementioned methods that require the equilibrium to be achieved in their test procedure. The experiments using this protocol were conducted in a climate chamber where a specimen was subjected to cyclic step-changes in RH between high (75%) and low (33%) values for 8 and 16 hours, corresponding to a typical daily variation of RH.

To run this experiment, samples of 150 mm by 150 mm by 15 mm were cast and then sealed with aluminium tape on all surfaces except the top (Figure 3-36). They were preconditioned at 23^{o}C and 50% RH prior to the start of the experiment for 24 hours. Each sample was placed on a digital scale inside a climate chamber, programmed for 16 hours at low (35%) and 8 hours at high RH (75%). The RH step changes inside the chamber in Figure 3-35 show how the environmental chamber reached 77% and 37% (instead of 75% and 35% as desired) but still results in the same RH step change i.e. ΔRH= 40%. For each sample the experiment was run until the mass change was less than 5% between the last three cycles. The average between the absorption and desorption mass changes was calculated for each cycle. The Moisture Buffer Value was calculated based on the mean of at least 3 cycles. Another point needs mentioning is that when water vapour is transmitted from within a material to the ambient air and vice versa, the primary resistance to this flow is within the material itself. However, there is also a relatively small resistance caused by the air layer above the surface of the material known as the convective surface resistance. The Nord Test protocol requires this value to be around 5.0 x10^{7} Pa/(kg·m^{2}·s) corresponding to an ambient air velocity of 0.1 m/s (Rode et al., 2007). The air velocity inside the environmental chamber for all experiment set-ups in this study was measured both horizontally and vertically by use of a hot-wire anemometer (Testo 405) and the requirement (i.e. air velocity < 0.1) was met. The accuracy of the Testo 405 was ±0.1 m/s in the range of 0 to 2 m/s air velocity with a resolution of 0.01 m/s.

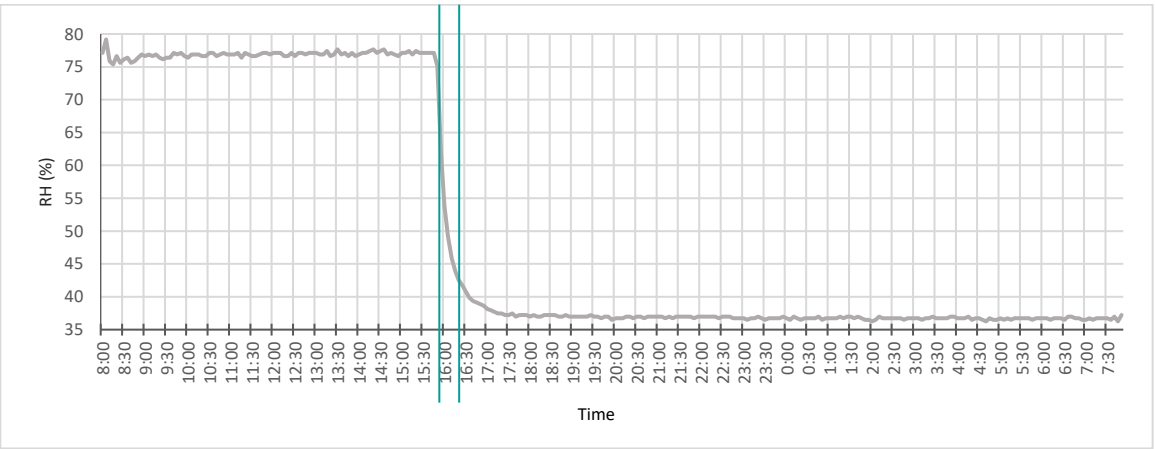

Figure 3-35: RH step inside the environmental chamber for MBV

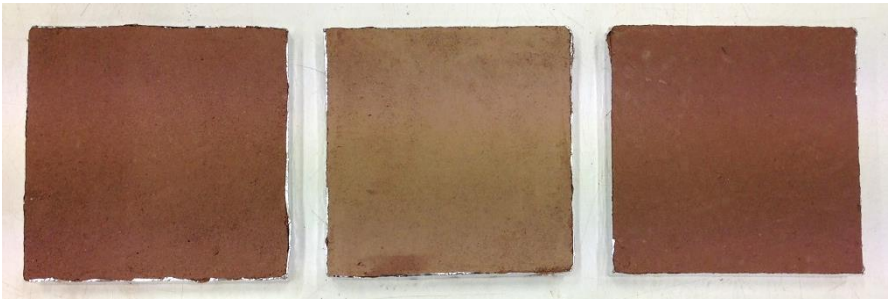

Figure 3-36: Three of the samples prepared for MBV test 150 x 150 mm

3.2.3.4. DIN 18947

The German Institute standard DIN 18947, introduces a method to measure absorption capacity of earth plasters. According to this protocol samples of 15 mm thickness and not less than 1000 cm^2, are exposed to 80% RH in a climatic chamber and the water vapour gain is measured after 0.5, 1, 3, 6 and 12 hours. Preconditioning at 50% RH and 23°C is required until constant mass is achieved which is when the result of two successive weighings in a 24-hour period is a maximum of 0.2% by mass based on the smallest measured value. Earth plasters are classified as shown in Table 3-2 based on their mass change per square meter for the afore-mentioned intervals.

Table 3-2: Materials' classification based on water absorption rate for earth plasters (DIN 18947, 2013)

	Water absorption after:				
Classes	0.5 h g/m^2	1 h g/m^2	3 h g/m^2	6 h g/m^2	12 h g/m^2
WS I	≥ 3.5	≥ 7.0	≥ 13.5	≥ 20.0	≥ 35.0
WS II	≥ 5.0	≥ 10.0	≥ 20.0	≥ 30.0	≥ 47.5
WS III	≥ 6.5	≥ 13.0	≥ 26.5	≥ 40.0	≥ 60.0

For this test, the same samples used for the MBV test were placed inside the environmental chamber and exposed to 80% RH after preconditioning. A sample of plaster board (150 by 150 mm, thickness of 18 mm) rendered with a layer of gypsum plaster was tested under the same conditions to act as a conventional plaster reference against which the earth samples could be compared. The smaller surface area was selected to allow all samples to be accommodated within the climate chamber.

3.2.4. Summary

Earth plasters were traditionally used in building construction in Iran as an internal and external finishing material. Earth plasters were usually mixed with plant-based aggregates such as straw to improve their mechanical strength and durability. According to the literature, the influence of plant aggregates on moisture buffering capacity of earth plasters has not been widely studied and a conclusion cannot be made on whether and to what extent the addition of these aggregates could improve the hygroscopic property of this material. In this study, two types of earth plasters with different particle sizes, the Base Coat (BC) and Top Coat (TC) plasters, were selected and separately mixed with three plant-based aggregates and one fine mineral aggregate i.e. Diatomaceous Earth. DE was used due to its high absorptive capacity. These four plaster mixes were assessed for their hygroscopic properties using established protocols for quantifying moisture-related properties of materials. The effect on their moisture response after adding these aggregates to earth plasters was evaluated and they were rated and classified accordingly.

Chapter 4.

Results and discussion

4.1. Part one: Hygrothermal performance of single and multi-layer wall systems

The first part of this chapter focuses on the hygrothermal performance of wall types specimens followed by the characterisation tests on earth plaster mixes. In the following sections thermophysical properties of the materials involved in the construction of wall types are given for an understanding of the materials performance individually and in conjunction with other materials. The thermal performance of the building envelope is partly quantified by thermal transmittance value. Various methods (both theoretical and experimental) have so far been standardised to calculate this value (See section 2.2). In the following section, the result of the theoretical calculations of thermal transmittance value of the wall specimens (instructed in BS EN 6946) is described including the combined method for calculating the U-value of composite structures (in this case hollow blocks i.e. fired clay and LECA). The result is compared with the result of in-situ thermal transmittance values measured using the experimental set-up in the laboratory. The in-situ U-value calculations is based on the Average method (instructed in BS ISO 9869-1). Having temperature and moisture profiles through the layers of the wall, allowed a more detailed analysis of the hygrothermal performance of the wall assembly under hot-humid and hot-dry weather conditions. Also, by plotting the temperature and moisture profiles of the layers of the wall specimen, a discussion was made on the influence of the adjacent layers' properties on moisture transport and the overall performance of the wall.

4.1.1. Thermophysical properties of materials

The thermophysical properties of the materials involved in the construction of the specimens (thermal conductivity [λ], heat capacity [C_p] and water vapour resistance value [μ]) were taken from standard EN 1745 and in the case of AAC block from the manufacturers datasheet as shown in Table 4-1. For PIR insulation and expanded cork board, thermal conductivity was measured in heat flow meter. Values of density were measured in the laboratory. This data was used for calculating theoretical U-value of the assembly using the combined method described in BS EN 6946. For μ-value, for some materials it was specified whether the data is the result of the wet-cup or dry-cup method. For others there was no specification; therefore, only one value is given for cork, gypsum, earth, cement and lime plaster.

Table 4-1: Thermophysical properties of wall construction materials

	ρ [kg/m^3]	λ [W/m. K]	C_p [J/kg. K]	a= λ/ρ. C_p [m^2/s]	$b = \sqrt{\lambda \rho C}$ [W.s$^{1/2}$/m^2.K]	μ dry/wet
Clay (Fired)	1522	0.38	850	2.94 E-07	701	16/10
LECA	725	0.20	850	3.25 E-07	351	6/4
AAC	630	0.16	850	2.99 E-07	292	10/6
PIR insulation	38	0.022	1450	3.99 E-06	34.8	60/60
Cork	150	0.041	1880	1.45 E-07	107.5	10
Gypsum plaster	1000	0.40	850	4.71 E-07	583	7.5
Earth plaster	1514	0.90	1000	5.94 E-07	1167	11
Cement plaster	1800	0.97	850	6.34 E-07	1218	19
Lime plaster	1600	0.7	850	5.15 E-07	975	7

Derived material properties i.e. thermal diffusivity and thermal effusivity represent a collective behaviour combining three basic properties i.e. λ, C and ρ (See section 2.1.1). Higher thermal diffusivity (a) represents faster diffusion of heat through the mass of the material; whereas a low thermal diffusivity indicates a high time lag for heat to pass through the material (Givoni, 1998 & Hegger et al., 2008). In this respect, Table 4-1 shows the different behaviour of cork and PIR insulation as cork has much lower diffusivity value compared to PIR. The same goes to their effusivity value; cork with much higher effusivity transfers the heat much faster to its surrounding environment whether it is air or the adjacent material in a wall system. The thermal mass effect of the construction blocks is quite similar to one another due to their close diffusivity values with fired clay showing slightly higher effect than AAC than LECA block. Their effusivity values, however, are different from one another with fired clay block having much faster capacity for transferring heat to the adjacent environment. It should be noted that the values given in Table 4-1 relate to the materials in their solid state; hence not representing the hollow shape of the fired clay and LECA blocks. In the next section the thermal resistance of these two hollow blocks is calculated using the combined method described in BS EN ISO 6946. It is not possible to directly report a thermal conductivity value for these hollow blocks as heat gets transferred through a combination of conduction, convection and radiation. Having the thickness of the blocks, an equivalent thermal conductivity value could be reported by dividing the thickness by thermal resistance. Thermal transmittance value of the single-layer wall specimens is then calculated considering the effect of mortar joints conductivity in total wall's resistance value.

4.1.2. Theoretical thermal transmittance calculations (combined method)

Theoretically, thermal performance of the envelope can be evaluated by calculating the steady-state thermal resistance value dividing the thickness of materials by their thermal conductivity values given by manufacturer, found in standards or measured through laboratory methods. The

instructions for these calculations are given in BS EN ISO 6946. As an analogy to resistances in series in an electric circuit, the thermal resistance of a building component consisting of thermally homogeneous layers perpendicular to heat flow direction can be calculated through the following formula (BS EN 6946, 2007):

$$R_T = R_1 + R_2 + \cdots + R_n \qquad (1)$$

Where

R_1, R_2, …, R_n are the design thermal resistances of each layer

For building components consisting of thermally homogeneous and thermally inhomogeneous layers, BS EN 6946 introduces a simplified method. This method considers an upper and a lower limit of resistance and the total resistance is the mean of the two:

$$R_T = \frac{R'_T + R''_T}{2} \qquad (2)$$

R'_T is the upper limit of the total thermal resistance,

R''_T is the lower limit of the total thermal resistance.

To conduct the calculation, the component needs to be broken down to sections (m = a, b, c, ...) and layers (j = 1, 2, 3, …), in such way that each part *mj* is thermally homogeneous.

The section *m* is perpendicular to the surfaces of the component with a fractional area f_m.

The layer *j* is parallel to the surfaces of the component and has a thickness of d_j.

The part *mj* has a thermal conductivity λ_{mj}, thickness d_j, fractional area f_m and thermal resistance R_{mj}.

The upper limit of total thermal resistance, R'_T, is determined by assuming one-dimensional heat flow through sections of the component (a,b, c, ...) similar to calculation of electric resistances in parallel in a circuit. Sections are either thermally homogeneous i.e. consisting of one single material in which case the resistance of the section is calculated through $R_q = d/\lambda$ equation or they are thermally inhomogeneous i.e. consisting of more than one material with different conductivity values in which case the total resistance of the section R_{Tq} is calculated through equation 1.

$$\frac{1}{R'_T} = \frac{f_a}{R_{Ta}} + \frac{f_b}{R_{Tb}} + \cdots + \frac{f_q}{R_{Tq}} \qquad (3)$$

$R_{Ta}, R_{Tb}, \ldots, R_{Tq}$ are total thermal resistance of each section;

$f_a, f_b, \ldots, f_q$ are the fractional area of each section.

For calculation of the lower limit of the thermal resistance, R''_T, the component is divided to layers parallel to the surface of the component. Then the thermal resistance of each of these layers is calculated. If the layer is thermally homogeneous i.e. single material, the resistance is calculated by dividing the thickness of the layer by its conductivity. If the layer is thermally inhomogeneous i.e. consists of different materials with different conductivity values, an equivalent thermal resistance shall be calculated through the following formula (BS EN 6946, 2007):

$$\frac{1}{R_j} = \frac{f_a}{R_{aj}} + \frac{f_b}{R_{bj}} + \ \ldots + \frac{f_q}{R_{qj}} \qquad (4)$$

The thermal resistance of small airspaces (where the width of an airspace is less than 10 times the thickness of the void) is calculated through method explained in Annex B of ISO 6946. In there, the thermal resistance of the airspace, R_g, is given by

$$R_g = \frac{1}{h_a + h_r}$$

Where

$$h_r = \frac{h_{r0}}{\frac{1}{\varepsilon_1} + \frac{1}{\varepsilon_2} - 2 + \frac{2}{(1 + \sqrt{1 + d^2/b^2} - d/b)}}$$

h_a is the conduction/convection coefficient (1.25 W/m^2.K for horizontal heat flow)

h_r is the radiative coefficient

h_{r0} is the radiative coefficient for a black-body surface.

$\varepsilon_1, \varepsilon_2$ are the hemispherical emissivities of the surfaces on the warm and cold faces of the airspace.

Table 4-2: resistance of air spaces

Clay block		
d	0.0395	m
b	0.25	m
R_g	**0.180**	m^{2}K/W
LECA block		
d	0.05	m
b	0.105	m
R_g	**0.199**	m^{2}K/W

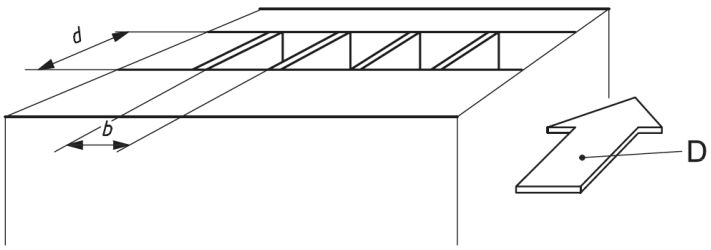

The methods explained above were used to calculate the thermal resistance value of the fired clay and the LECA as they had a composite structure with air spaces in between the solid material. Detail of the calculations are shown in the following tables (Tables 4-3 to 4-6). For each block, the lower and upper limit of thermal resistance value was calculated in separate tables

and the total resistance value is calculated as the mean of the two limits (summarised in Table 4-7).

Table 4-3: Lower limit of thermal resistance/ combined method/ BS EN 6946

	Clay Block	d (m)	λ (W/mK)	R (m²K/W)	
Layer 1	Clay	0.0085	0.38	0.022	Series
Layer 2	Air/ Clay	0.0395		0.157	
Layer 3	Clay	0.0085	0.38	0.022	
Layer 4	Air/ Clay	0.0395		0.157	
Layer 5	Clay	0.0085	0.38	0.022	
Layer 6	Air/ Clay	0.0395		0.157	
Layer 7	Clay	0.0085	0.38	0.022	
Layer 8	Air/ Clay	0.0395		0.157	
Layer 9	Clay	0.0085	0.38	0.022	
	R Total			**0.740**	
	Air/ Clay layer				
		Fraction		**R (m²K/W)**	Parallel
	Air	0.8		**0.180**	
	Clay fins	0.2		0.104	
	$R_{Air/Clay}$ (Layers 2, 4, 6, 8)			**0.157**	

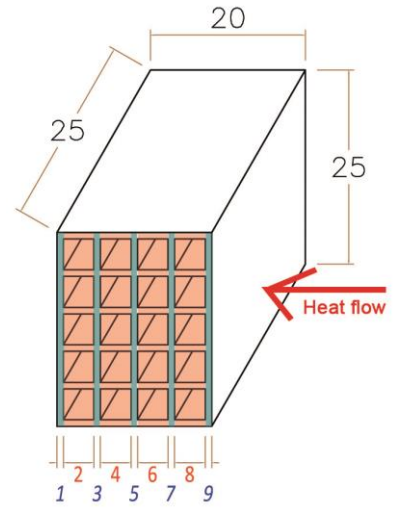

Dimensions in cm

Table 4-4: Upper limit of thermal resistance/ combined method/ BS EN 6946

	Clay Block	d (m)	Fraction	λ (W/mK)	R=d/λ (m²K/W)	
Section a	Clay	0.2	0.034	0.38	0.526	Parallel
Section b	Air/ Clay	0.2	0.016		**0.832**	
Section c	Clay	0.2	0.034	0.38	0.526	
Section d	Air/ Clay	0.2	0.016		**0.832**	
Section e	Clay	0.2	0.034	0.38	0.526	
Section f	Air/ Clay	0.2	0.016		**0.832**	
Section g	Clay	0.2	0.034	0.38	0.526	
Section h	Air/ Clay	0.2	0.016		**0.832**	
Section i	Clay	0.2	0.034	0.38	0.526	
Section j	Air/ Clay	0.2	0.016		**0.832**	
Section k	Clay	0.2	0.034	0.38	0.526	
	R Total				**0.744**	
	Air/ Clay section					
		d (m)	**Fraction**	**λ**	**R (m²K/W)**	Series
	Air (4 layers)	0.0395			**0.180**	
	Clay (5 layers)	0.0085		0.38	0.104	
	$R_{Air/Clay}$ (Sections b, d, f, h, j)				**0.832**	

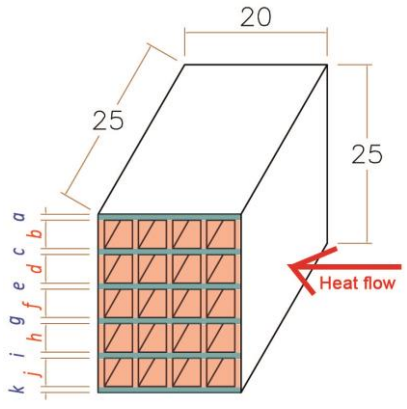

Dimensions in cm

Table 4-5: Lower limit of thermal resistance/ combined method/ BS EN 6946

	LECA Block	d (m)	λ (W/mK)	R (m²K/W)	
Layer 1	LECA	0.075	0.20	0.375	Series
Layer 2	Air/ LECA	0.05		0.214	
Layer 3	LECA	0.075	0.20	0.375	
	R Total			**0.964**	
	Air/ LECA layer				
		Fraction		**R (m²K/W)**	Parallel
	Air	0.65		0.199	
	LECA fins	0.35		0.25	
	$R_{Air/LECA}$ (Layer 2)			0.214	

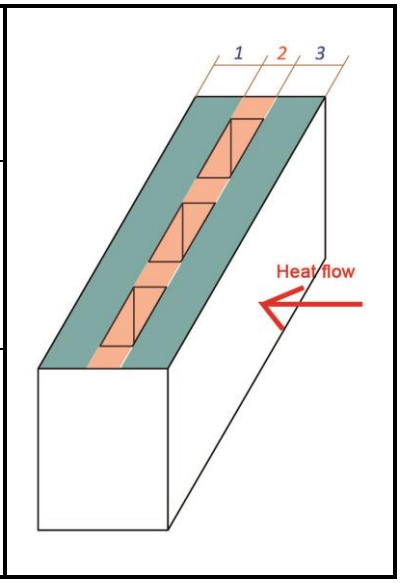

Table 4-6: Upper limit of thermal resistance/ combined method/ BS EN 6946

	LECA Block	d (m)	Fraction	λ (W/mK)	R=d/λ (m²K/W)	
Section a	LECA	0.2	0.082	0.20	1.00	Parallel
Section b	Air/ LECA	0.2	0.216		0.949	
Section c	LECA	0.2	0.082	0.20	1.00	
Section d	Air/ LECA	0.2	0.216		0.949	
Section e	LECA	0.2	0.082	0.20	1.00	
Section f	Air/ LECA	0.2	0.216		0.949	
Section g	LECA	0.2	0.082	0.20	1.00	
	R Total				**0.966**	
	Air/ Clay section					
		d (m)	**Fraction**	**λ**	**R (m2K/W)**	Series
	LECA	0.075		0.20	0.375	
	Air	0.05			0.199	
	LECA	0.075		0.20	0.375	
	$R_{Air/Clay}$ (Sections b, d, f)				0.949	

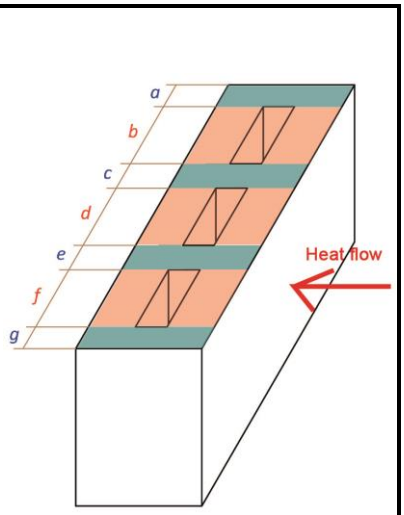

Therefore, the total resistance (R_T), the mean of the upper and lower limit of thermal transmittance, was calculated as 0.742 and 0.965 m²K/W for the Clay and the LECA blocks respectively. Calculating the thermal resistance of the AAC block did not require a combined calculation method as it was a solid block. The R-values for all 3 blocks are summarised in Table 4-7.

Table 4-7: Construction blocks; dimensions [cm] and thermal transmittance values

	Clay block	LECA Block	AAC Block
Configuration	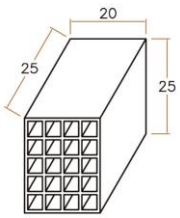	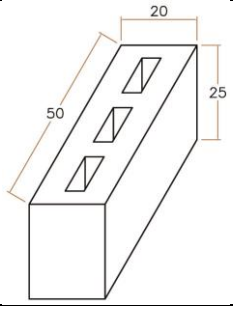	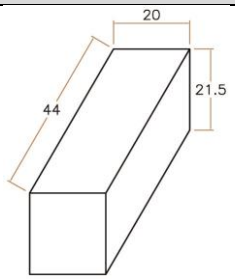
R (m^2K/W)	0.742	0.965	1.25
U (W/m^2K)	1.35	1.04	0.8

In order to measure the thermal conductivity of the small wall specimens, the effect of mortar joints on total thermal conductivity needs to be considered. The following equation, based on the proportions of the area of mortar and blocks, was used to calculate the total thermal conductivity:

$$\lambda_{unit} = \frac{a_{block}}{a_{unit}} . \lambda_{block} + \frac{a_{mor}}{a_{unit}} . \lambda_{mor}$$

Using the above equation, the R-value of the specimens made of clay, LECA and AAC blocks were calculated as shown in Table 4-8:

Table 4-8: Wall specimens; Configuration and thermal resistance values

	Clay block	LECA Block	AAC Block
Configuration	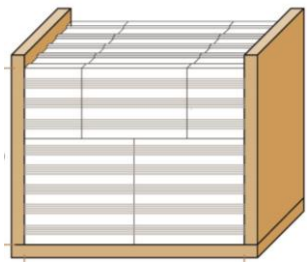	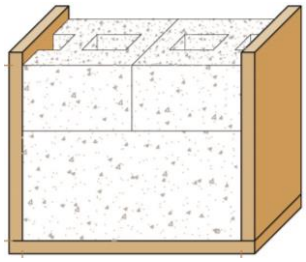	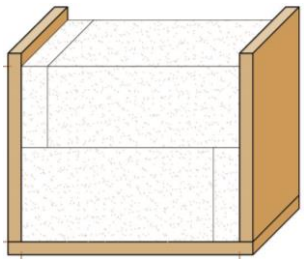
R (m^2K/W)	0.51	0.86	0.99

4.1.3. In-situ thermal transmittance measurements

It has been stated in different studies that the thermal performance of materials in real dynamic conditions differ from that calculations suggest and that the result of the in-situ measurements do not necessarily agree with the results of theoretical calculations which are mostly based on the values measured under steady-state conditions. Therefore, in this study, a realistic environmental condition was created in the laboratory (See chapter 3) to study the thermal performance of selected wall systems using in-situ measurement techniques. The outcome of the experimental set-up described in Chapter 3, results in a time series database of heat flux and

temperature differences. This collected database was then analysed by the Average method instructed in BS ISO 9869-1 to calculate the in-situ thermal transmittance values of the wall specimens.

4.1.3.1. Single layer and multi-layer (PIR insulated) wall types

Single layer wall specimens were first exposed to steady-state conditions of 40°C- 50% RH and 20°C-50% RH and their in-situ transmittance value was measured using the Average method explained in the previous section. Wall specimens were then exposed to daily cyclic weather condition for a comparison of the specimens under steady-state and dynamic conditions. Figure 4-1 shows the development of U-values calculated based on the Average method for the three wall specimens. The results show that AAC had the best performance (lowest U-value) followed by LECA and fired clay specimens. This result agrees with that suggested by theoretical calculations; however, different values were reported in cases of LECA and AAC block specimens (Table 4-9).

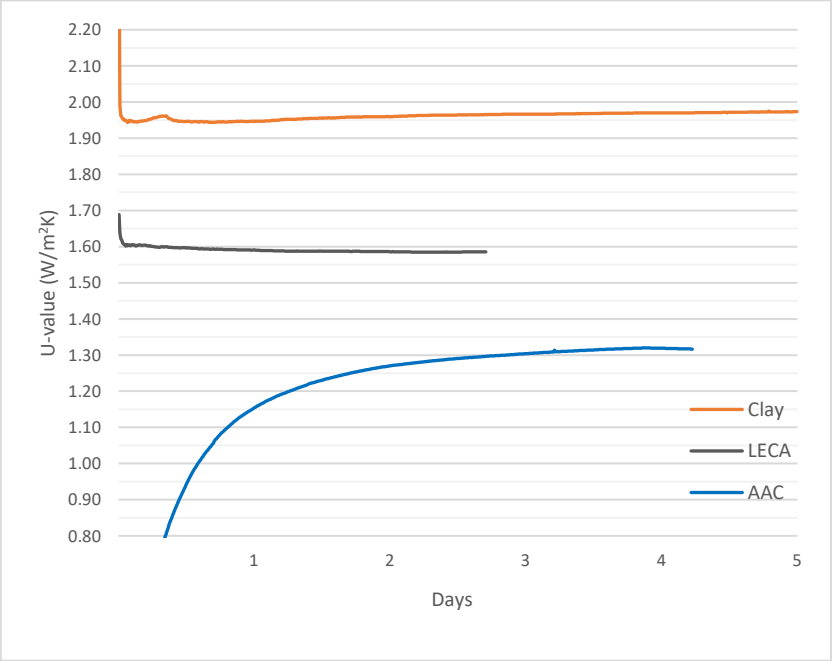

Figure 4-1: In-situ thermal transmittance under steady-state condition for single-layer specimens

Table 4-9: Calculated and measured U-value [W/m²K] of specimens under steady-state condition

	Calculated	Measured (steady-state)
Clay block	1.96	1.97
LECA block	1.16	1.60
AAC block	1.01	1.32

In the next step, realistic conditions were created on the sides of the specimens simulating daily cyclic fluctuations of temperature and RH in a hot- humid climate. The daily weather cycles were adapted from hourly weather data of a city in south of Iran featuring hot humid climate. The

development of the in-situ thermal transmittance value these three wall specimens is shown in Figure 4-2 which, the same as theoretical calculations and results of steady-state condition, indicates better performance of AAC followed by LECA and fired clay wall specimens. However, the actual numbers differ with U-values measured under dynamic condition being lower than the steady-state ones suggesting the better performance of blocks under dynamic conditions. This can be explained by the fact that under fluctuating conditions, the heat capacity of materials becomes activated i.e. materials start absorbing and releasing heat as surrounding temperatures fluctuate above and below the materials temperature.

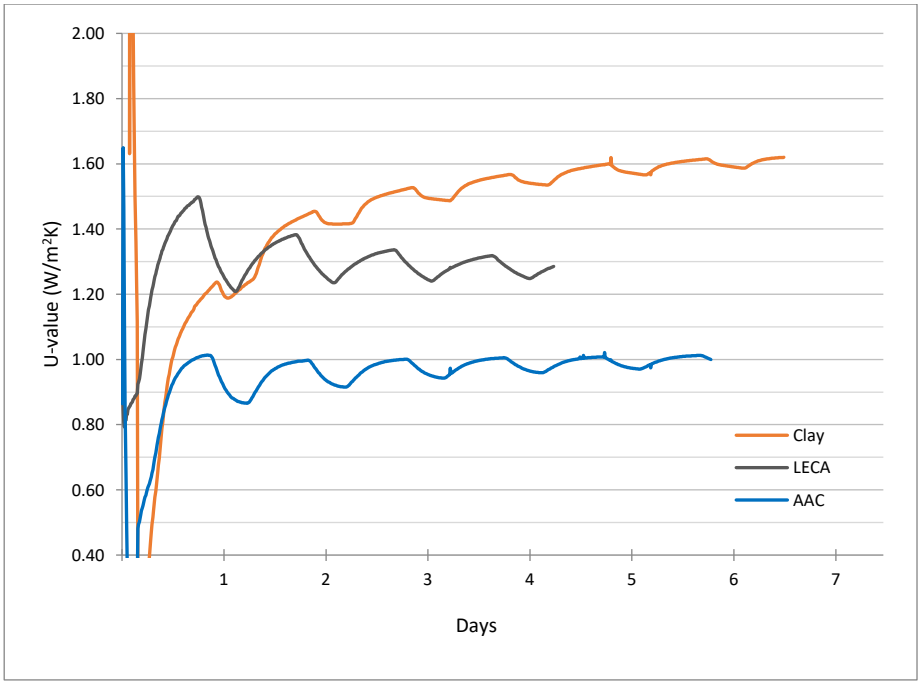

Figure 4-2: In-situ thermal transmittance measurements under dynamic conditions for single-layer specimens

Table 4-10: Calculated and measured U-value [W/m²K] of single-layer specimens

	Calculated	Measured Steady-state	Measured Dynamic-state
Clay block	1.96	1.97	1.60
LECA block	1.16	1.60	1.30
AAC block	1.01	1.32	1.00

The temperature variation through the wall construction in summer conditions in a hot and humid climate are shown in Figure 4-3 as an example of the thermal performance of three specimen blocks. The yellow line on graphs indicate temperature variations in the middle of the block. As shown in Figures 4-10, temperature rises to its maximum more rapidly in the clay block (low time lag). However, LECA and AAC showed a more gradual increase during periods of high outdoor temperature and then a gradual decrease during cooler outdoor temperatures.

Figure 4-3: Temperature swing in the middle of a) Fired clay b) LECA and 3) AAC specimens in a daily temperature cycle of a hot-humid summer day.

The second set of wall specimens, insulated with PIR and plastered with gypsum and cement plaster, internally and externally, were tested in this part of the study (Figure 4-4). This construction technique is applied in Iran, if external walls are insulated. Multi-layer specimens were then exposed to the same conditions as the single-layer walls for the duration of at least 4 consecutive days to allow enough time for stabilising the specimens. This target, however, was not always fulfilled due to unexpected failure of the environmental chambers or other technical issues such as out-of-hour power cuts.

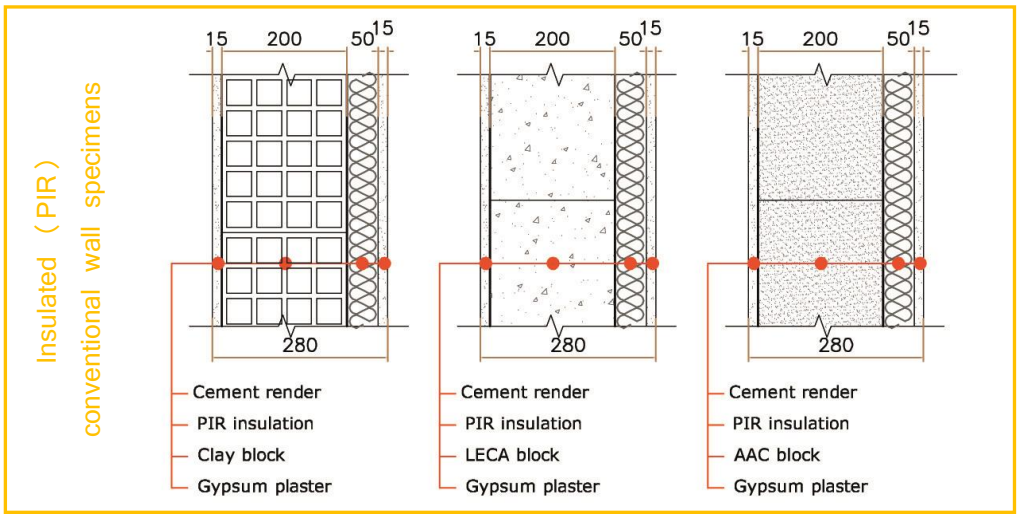

Figure 4-4: Detail of the construction layers of wall specimens insulated with PIR, dimensions in mm

Nevertheless, the results of thermal transmittance measurements (Figure 4-5 & 4-6) indicated distinct differences in heat transfer through the specimens before and after the application of the PIR insulation board. The thermal properties of the PIR insulation had a leading role in dictating the overall performance of the walls and the U-value of all specimens, despite being made of different construction blocks, is converging towards one single value i.e. 0.45 W/m^{2}K as shown on Figure 4-5. Under dynamic conditions (Figure 4-6), again, insulation layer has a leading role in thermal performance of the specimens and the thermal transmittance values of specimens are very close to each other compared to uninsulated specimens when their corresponding U-values were well different from one another. This observation can be explained by looking at the diffusivity and effusivity values of materials in Table 4-1. PIR insulation has a very high diffusivity and a low effusivity value and is considered as a poor thermal mass. As discussed in Chapter 2, the first 50-100 mm of the thickness of the building envelope plays the most important role in any thermal damping effect. The application of a layer of PIR insulation with no thermal mass effect, as in the case of the tested specimens, separates the mass of the wall from the fluctuating boundary condition; impeding the wall's thermal buffering potential. It should be noted that in a real building due to solar gain and other internal gains (hence

fluctuating indoor condition), thermal mass is more effective when directly exposed to the indoor environment especially in residential buildings. Accordingly, the thermal insulation is best to be located on the outer side of the wall to allow the mass of the wall to have its maximum thermal buffering effect.

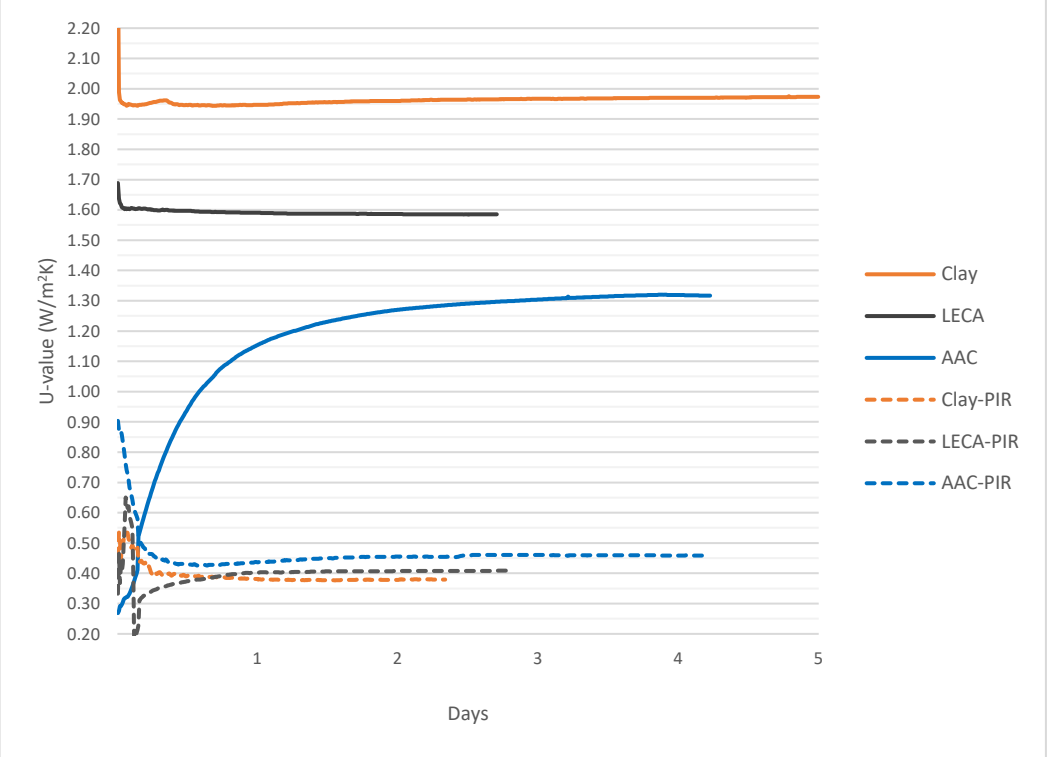

Figure 4-5: Transmittance values of single-layer and multi-layer wall specimens under steady-state condition

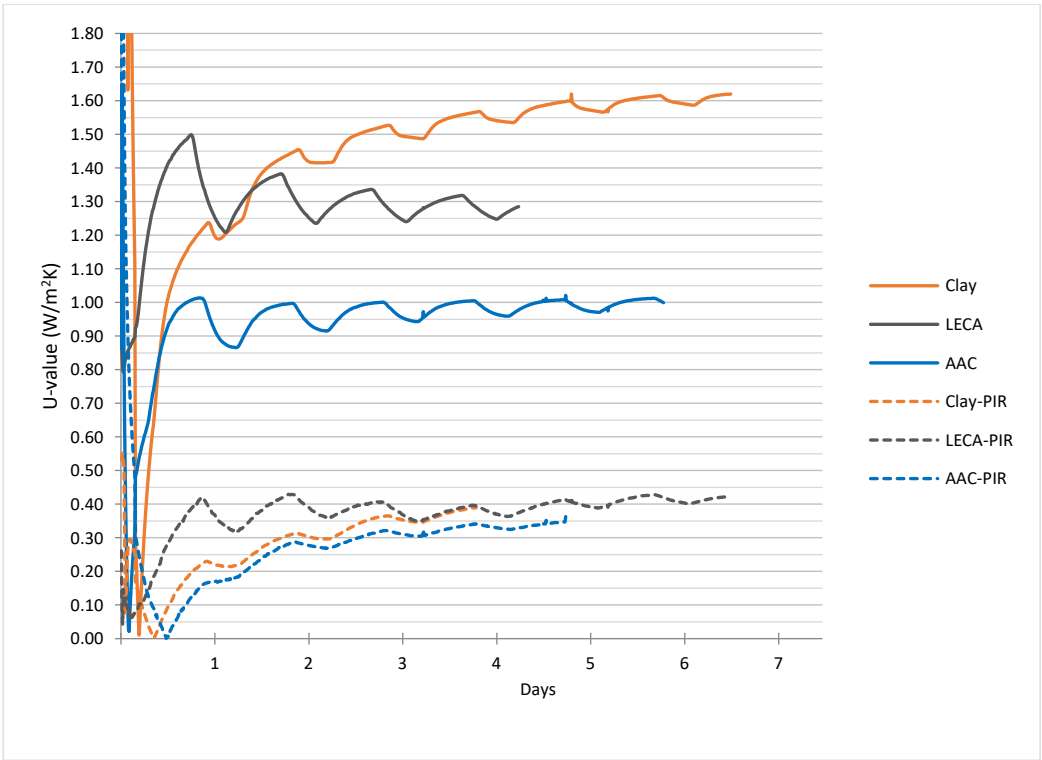

Figure 4-6: Transmittance values of single-layer and multi-layer wall specimens under dynamic condition

Table 4-11: Thermal transmittance value of insulated walls; Calculated & measured

	d [m]	λ [W/m K]	R* [m²K/W]	$U_{calculated}$ [W/m²K]	$U_{measured}$ Steady-state [W/m²K]	$U_{measured}$ dynamic HD [W/m²K]	$U_{measured}$ dynamic HH [W/m²K]
Clay Block_ Synthetic							
Cement plaster	0.025	0.97	0.03				
PIR insulation board	0.05	0.022	2.27				
Fried clay block	0.2		0.51				
Gypsum plaster	0.025	0.4	0.06				
Total			**2.87**	**0.35**	**0.44**	**0.38**	**0.52**
LECA Block_ Synthetic							
Cement plaster	0.025	0.97	0.03				
PIR insulation board	0.05	0.022	2.27				
LECA block	0.2		0.86				
Gypsum plaster	0.025	0.4	0.06				
Total			**3.22**	**0.31**	**0.48**	**0.39**	**0.27**
AAC Block_ Synthetic							
Cement plaster	0.025	0.97	0.03				
PIR insulation board	0.05	0.022	2.27				
AAC block	0.2		0.99				
Gypsum plaster	0.025	0.4	0.06				
Total			**3.35**	**0.30**	**0.46**	**0.33**	**0.36**

*Calculated based on λ-values from BS EN 12524 & Clarke et al.,1990.

4.1.3.2. Multi-layer wall systems: PIR and Cork-insulated wall types

This section compares a set of current practice wall constructions in Iran having PIR insulation, with a set of low-carbon alternatives having expanded insulation cork board as thermal insulation. Wall specimens insulated with cork were plastered with earth internally and lime externally to compose a less energy-intensive, healthier and more hygroscopic alternative. The composition of the layers of the wall is illustrated in Figure 4-7.

Similar to previous experiments, a steady-state condition was first created on the sides having 40°C 50%RH in one chamber and 20°C 50%RH in the other. These steady-state conditions were selected to compare the performance of the walls under steady-state and dynamic conditions. In the next step, realistic conditions were created on the sides of the specimens simulating daily cyclic fluctuations of temperature and RH in a hot- humid and a hot-dry climate (See section 3.4.)). The aim was to study the performance of the wall constructions when exposed to high humidity levels. For theoretical calculations, method described in BS EN 6946 and for in-situ measurement of thermal transmittance, the Average Method described in BS ISO 9869-1 was used. The results of both are given in Tables 4-12, 4-13 and 4-14.

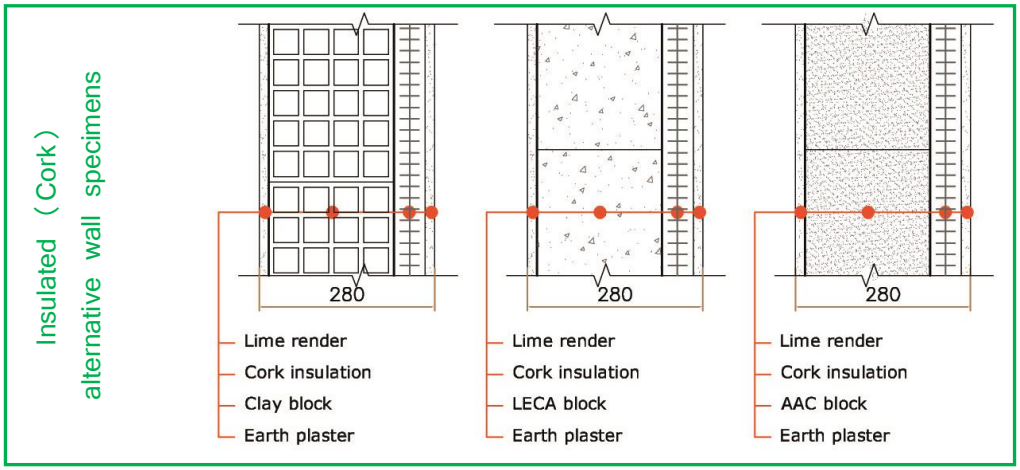

Figure 4-7: Detail of the construction layers of wall specimens insulated with cork, dimensions in mm

Hygrothermal performance under steady- state condition

Figure 4-14 illustrates the development of U-values over time, based on the Average method technique, for all 6 multi-layer specimens under steady-state conditions i.e. 40°C 50% RH on one side and 20°C 50% RH on the other. Specimens insulated with PIR, showed similar performance with their U-values converging towards one single number i.e. 0.45 W/m^{2}K. In wall specimens insulated with cork, fired clay and AAC specimens had similar performance (Figure 4-8 & Table 4-13) and resulted in higher U-values (0.70 and 0.68 W/m^{2}K) than the LECA wall sample (0.52 W/m^{2}K) unlike what calculations suggested. All six samples resulted in higher U-values than calculations suggested (Tables 4-12 & 4-13). In specimens insulated with PIR, the insulation had

the leading role in defining the performance of the whole construction. However, without having detailed information about the hygroscopic properties of the blocks, plasters and insulation such as porosity, sorption isotherms and liquid transport coefficients, it is difficult to confidently explain why in cork insulated samples, AAC and fired clay performed similarly and different from LECA specimen. The role of thermal mass (heat capacity) in steady-state heat transfer is ruled out. Therefore, the reason could be the difference in moisture content of the layers and moisture distribution of the interfaces between the layers. Also, as fired clay and AAC blocks are more capillary active (smaller pore size) compared to LECA, and as the cork is a vapour permeable material, it might be that clay and AAC blocks absorb the water vapour that passes through the cork layer in a higher rate than LECA. This results in higher moisture content in the blocks and hence higher thermal conductivity and lower thermal performance. The higher permeability of LECA block also helps it to dry out more quickly towards especially the internal surface of the wall. It should be kept in mind that in all these scenarios, the environments on both sides of the wall were being constantly conditioned.

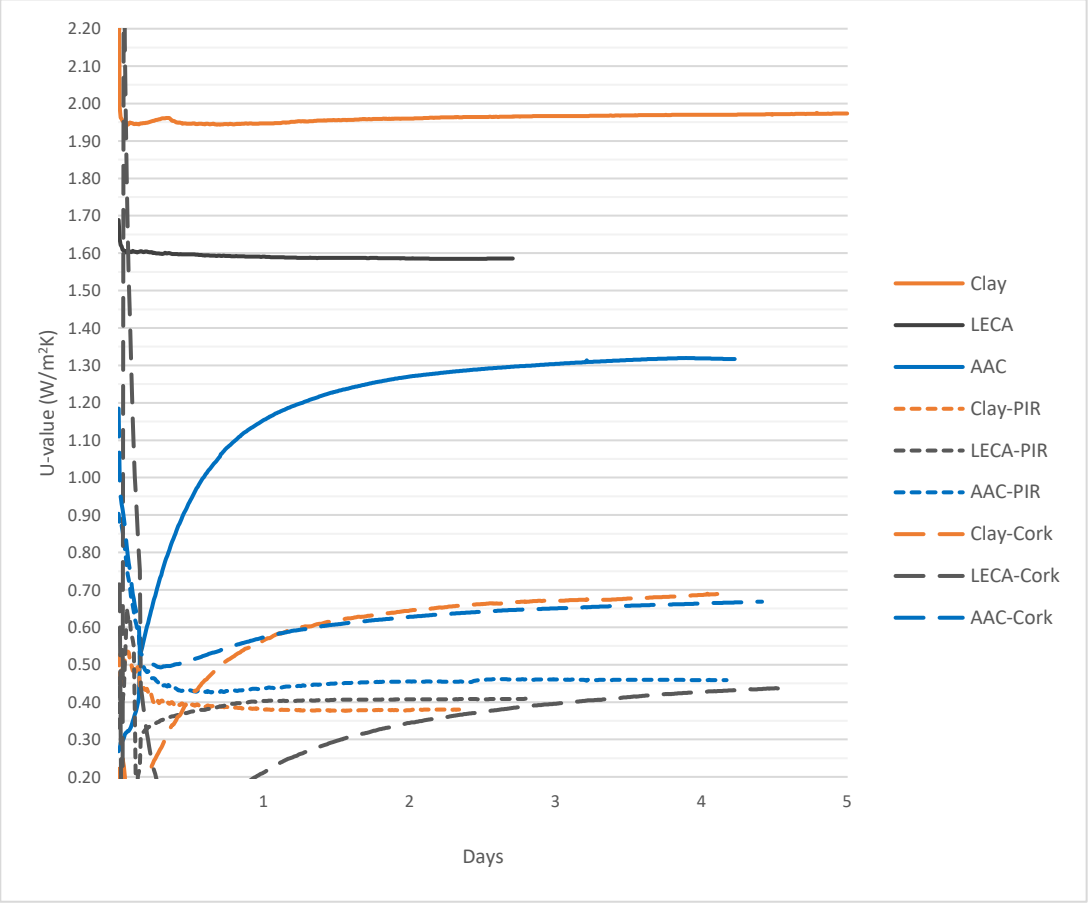

Figure 4-8: Thermal resistance of insulated walls under steady-state condition

Table 4-12: Steady-state thermal transmittance of PIR-insulated walls; Calculated & measured

	d [m]	λ [W/mK]	R [m^2K/W]	$U_{calculated}$ [W/m^2K]	$U_{measured}$ [W/m^2K]
Clay Block_ Synthetic					
Cement plaster	0.025	0.97	0.03		
PIR insulation board	0.05	0.022	2.27		
Fried clay block	0.2		0.51		
Gypsum plaster	0.025	0.4	0.06		
Total			**2.87**	**0.35**	**0.44**
LECA Block_ Synthetic					
Cement plaster	0.025	0.97	0.03		
PIR insulation board	0.05	0.022	2.27		
LECA block	0.2		0.86		
Gypsum plaster	0.025	0.4	0.06		
Total			**3.22**	**0.31**	**0.48**
AAC Block_ Synthetic					
Cement plaster	0.025	0.97	0.03		
PIR insulation board	0.05	0.022	2.27		
AAC block	0.2		0.99		
Gypsum plaster	0.025	0.4	0.06		
Total			**3.35**	**0.30**	**0.46**

Table 4-13: Steady-state thermal transmittance of cork-insulated walls; Calculated & measured

	d [m]	λ [W/mK]	R [m^2K/W]	$U_{calculated}$ [W/m^2K]	$U_{measured}$ [W/m^2K]
Clay Block_ Natural					
Lime plaster	0.025	0.8	0.03		
Cork insulation board	0.05	0.041	1.22		
Fried clay block	0.2		0.51		
Earth plaster	0.025	0.97	0.03		
Total			**1.79**	**0.55**	**0.70**
LECA Block_ Natural					
Lime plaster	0.025	0.8	0.03		
Cork insulation board	0.05	0.041	1.22		
LECA block	0.2		0.86		
Gypsum plaster	0.025	0.97	0.03		
Total			**2.14**	**0.46**	**0.52**
AAC Block_ Natural					
Lime plaster	0.025	0.8	0.03		
Cork insulation board	0.05	0.041	1.22		
AAC block	0.2		0.99		
Gypsum plaster	0.025	0.97	0.03		
Total			**2.27**	**0.44**	**0.68**

The Breakdown of the resistance of the layers of the wall assembly gives a more in-detail understanding of the performance of the layers and materials. For this purpose, wall assembly was divided to two sections, (1) insulation+ external rendering (2) block + internal plaster. Having heat flux data through the wall and temperature on the sides of the wall and at the interface of block and insulation, the thermal transmittance values of each of the 2 sections was calculated. U-values were converted to R-values in this part of analysis, due to direct (non-reciprocal) relation of the resistance of isothermal layers allowing a direct summation of layers' R-values. Graphs on Figure 4-9 show the resistance of layers of specimens as R_{block}, R_{ins} and R_{total}. These values have been summarised in Table 4-14. The highest resistance value has been reported for LECA-PIR (2.44 m2K/W) followed by LECA-Cork specimen (2.17 m2K/W). Table 4-15 summarises the theoretically calculated values for the specimens. Unlike what these calculated values suggest, specimens consisting of AAC block, did not result in the highest resistance in experimental measurements. Comparison of these tables shows that AAC samples, particularly AAC-Cork, has performed far from the expectations.

Table 4-14: Breakdown of R-values of layers of wall_ Measured under steady-state condition

Specimen	R_{block}	R_{ins}	R_{total}
	[m^2K/W]		
Clay-PIR	0.62	1.54	2.16
LECA-PIR	0.98	1.46	**2.44**
AAC-PIR	0.81	1.38	2.18
Clay-Cork	0.53	0.91	1.45
LECA-Cork	0.93	1.23	**2.17**
AAC-Cork	0.57	0.92	1.50

R_{block}: consists of R_{block} + $R_{plaster}$ (Plaster is earth for cork insulated specimens; gypsum for PIR insulated specimens)

R_{ins}: consists of R_{ins} + R_{render} (Render is lime for cork insulated specimens; cement for PIR insulated specimens)

Table 4-15: Breakdown of R-values of layers of wall _ Calculated

Specimen	R_{block}	R_{ins}	R_{total}
	[m^2K/W]		
Clay-PIR	0.57	2.30	2.87
LECA-PIR	0.92	2.30	3.22
AAC-PIR	1.05	2.30	**3.35**
Clay-Cork	0.54	1.25	1.79
LECA-Cork	0.89	1.25	2.14
AAC-Cork	1.02	1.25	**2.27**

R_{block}: consists of R_{block} + $R_{plaster}$ (Plaster is earth for cork insulated specimens; gypsum for PIR insulated specimens)

R_{ins}: consists of R_{ins} + R_{render} (Render is lime for cork insulated specimens; cement for PIR insulated specimens)

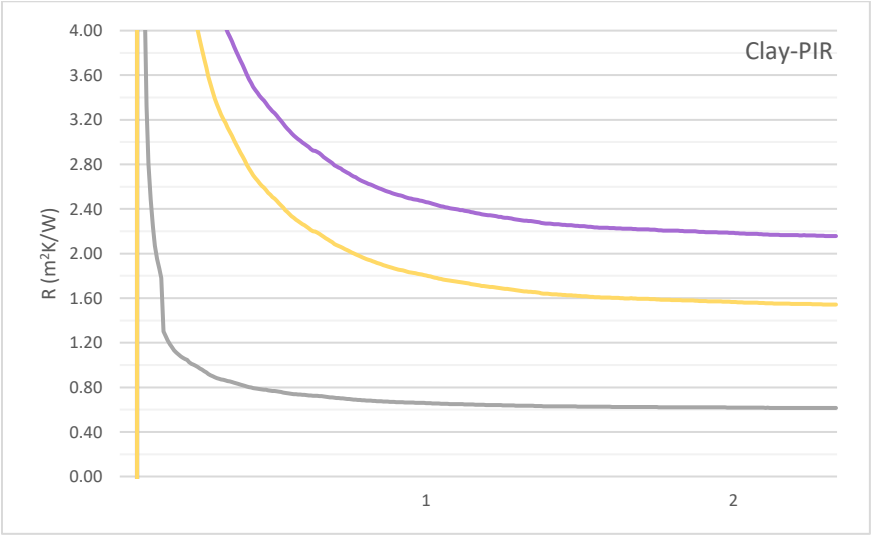
Clay-PIR
R (m²K/W)
4.00
3.60
3.20
2.80
2.40
2.00
1.60
1.20
0.80
0.40
0.00
1
2

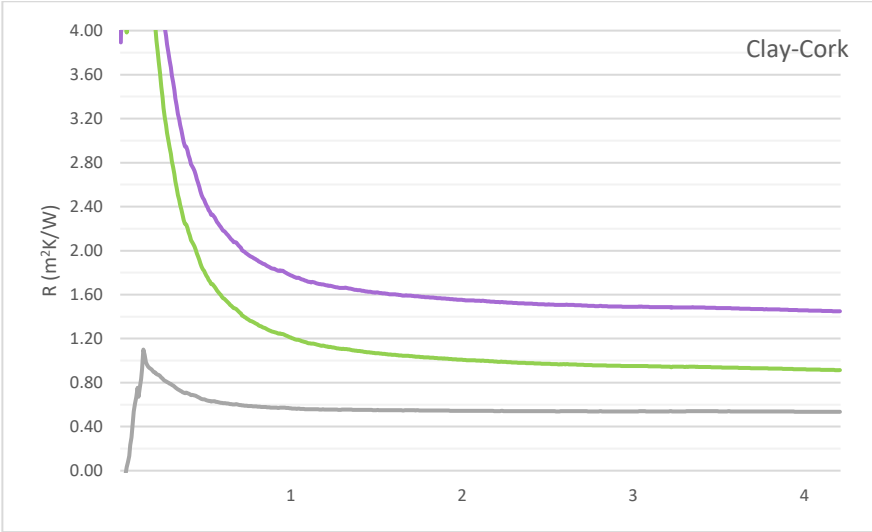
Clay-Cork
R (m²K/W)
4.00
3.60
3.20
2.80
2.40
2.00
1.60
1.20
0.80
0.40
0.00
1
2
3
4

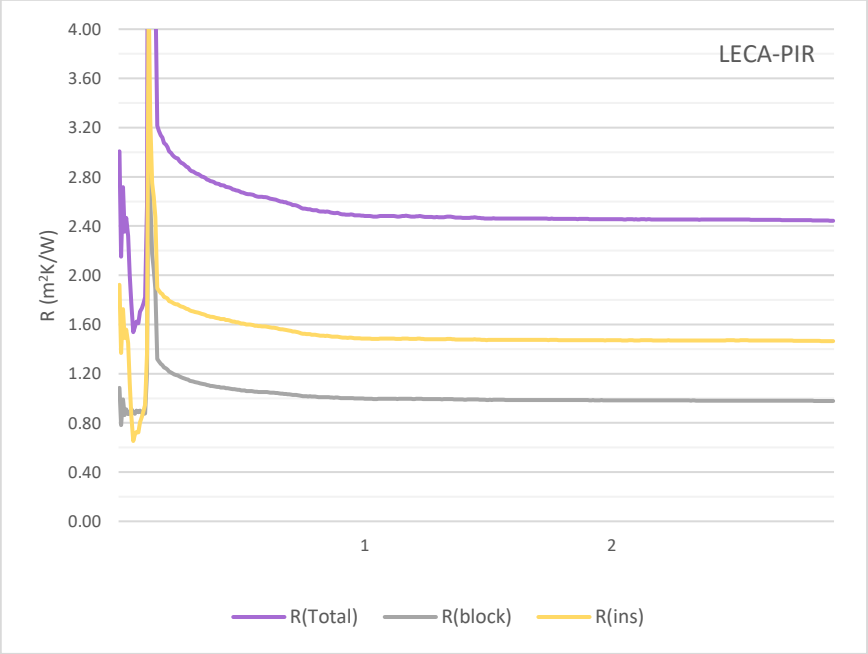
LECA-PIR
R (m²K/W)
4.00
3.60
3.20
2.80
2.40
2.00
1.60
1.20
0.80
0.40
0.00
1
2
R(Total)
R(block)
R(ins)

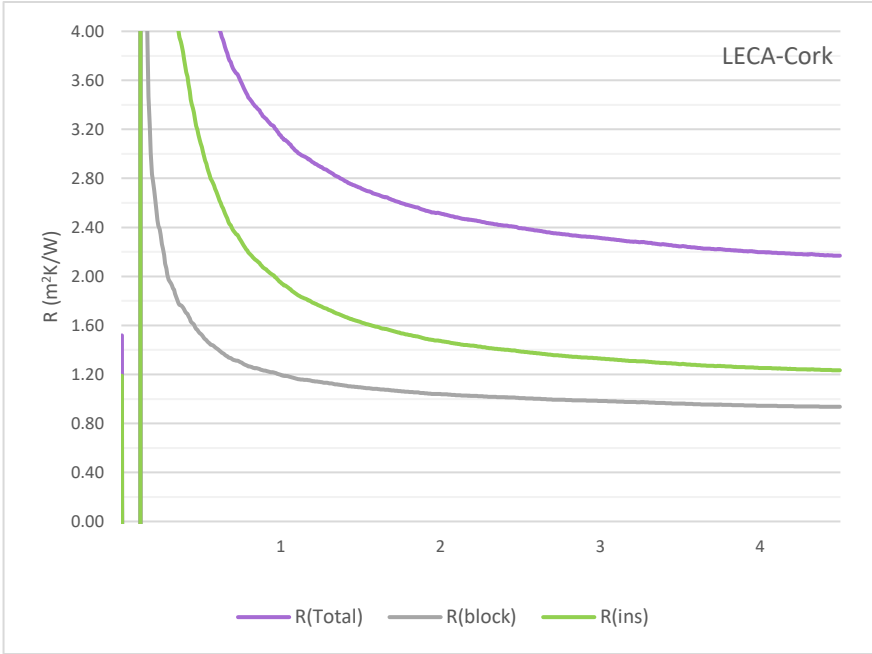
LECA-Cork
R (m²K/W)
4.00
3.60
3.20
2.80
2.40
2.00
1.60
1.20
0.80
0.40
0.00
1
2
3
4
R(Total)
R(block)
R(ins)

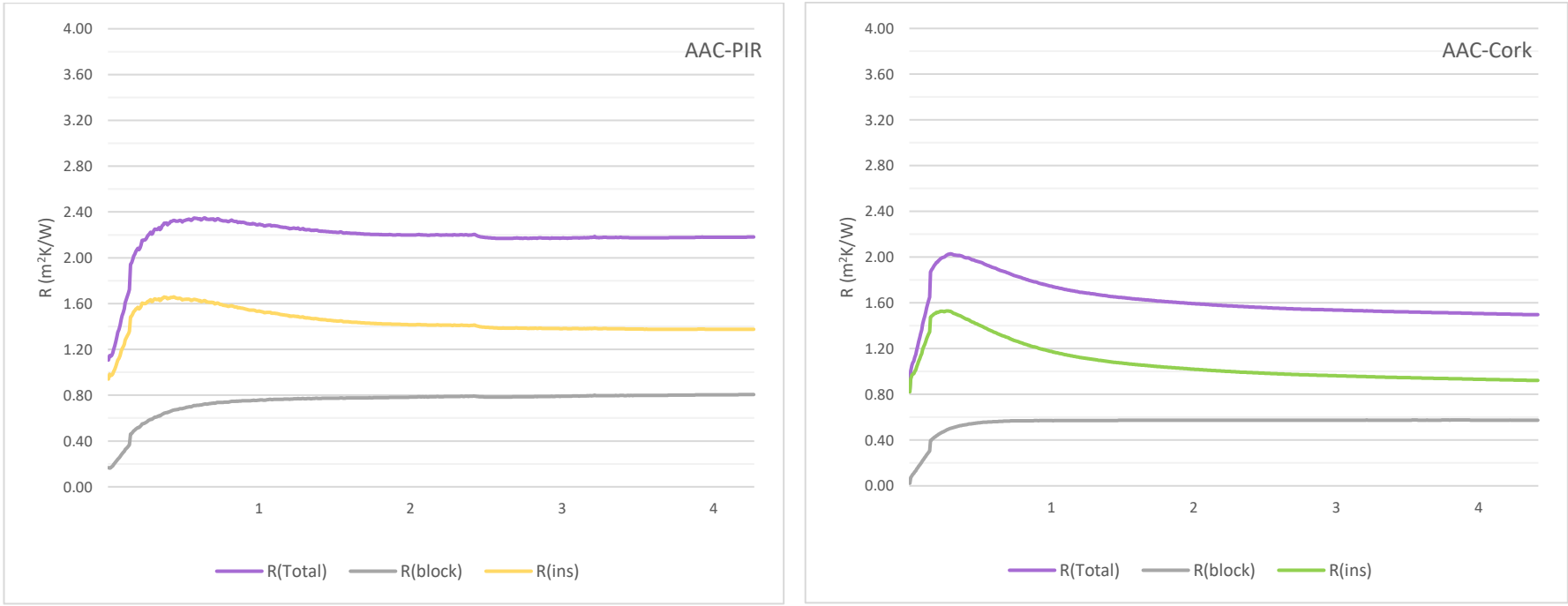

Figure 4-9: Breakdown of in-situ R-value of the layers of wall specimens under steady-state condition
Top: Fired clay specimens; Middle: LECA specimens; Bottom: AAC specimens

R_{ins}: Resistance of insulation layer+ external plaster
R_{block}: resistance of block layer + internal plaster
R_{total}: $R_{ins} + R_{block}$

Hygrothermal performance under dynamic boundary condition

Figures 4-10 and 4-11 show the development of in-situ U-value calculations over time for all samples under daily cyclic conditions in hot humid and hot dry conditions. Figure 4-10 shows that in dry condition, the U-value of all three wall specimens (insulated with PIR) are close to one another. However, when exposed to hot humid condition, the specimens performed differently with LECA exhibiting the lowest U-value (best performance) and fired clay the highest. It seems that, as with the steady-state condition, in the absence of moisture, the thermal transmittance value of the wall assemblies is dominated by the PIR insulation (Figure 4-10). For more conclusive results, the experiments could have been run for a longer period of time to ensure equilibrium was reached in cases of CP/HD, CA/HD, and LP/HH. The result of LECA-PIR specimen under HH condition was not consistent with the rest and was omitted from the analysis.

Based on theoretical calculations for determining the U-value, specimens made of AAC should have exhibited the lowest U-value and hence the best performance (0.30 W/m^{2}K when insulated with PIR). This was confirmed by the experimental measurements under both HD and HH conditions (Table 4-16). LECA, however, performed worse than expected by calculations in HD condition with a higher U-value than fired clay. The distinct drop in performance of Fired clay in the HH condition compared to HD condition is also an interesting fact which should be considered while designing wall assemblies in humid climates.

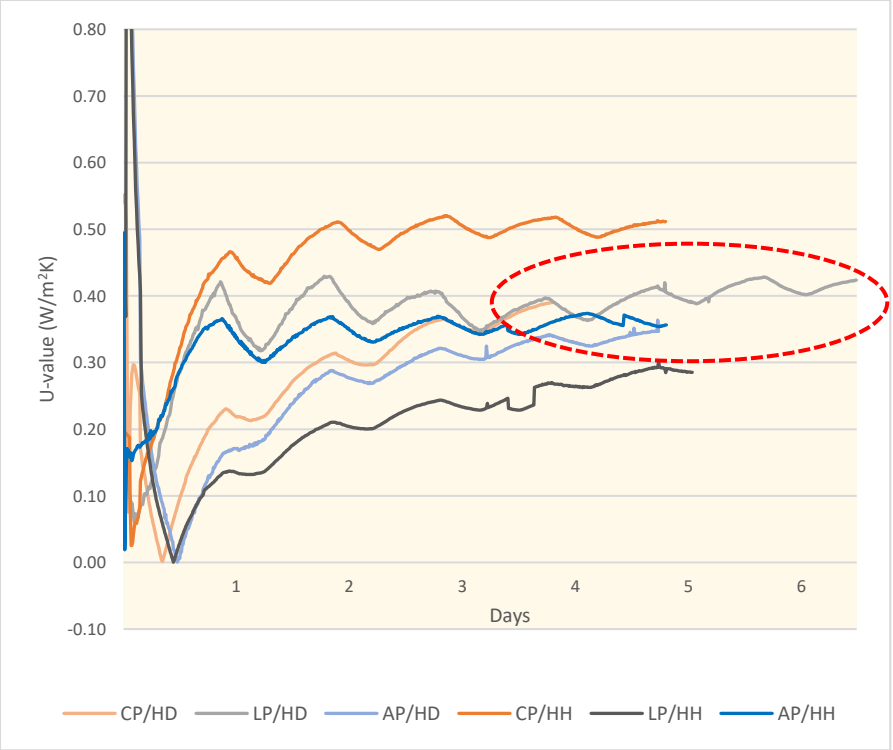

Figure 4-10: Development of in-situ thermal transmittance value for three wall specimens in Hot-Dry HD (HD) & Hot-Humid (HH) conditions
CP: Clay-PIR; LP: LECA-PIR; AP: AAC-PIR.

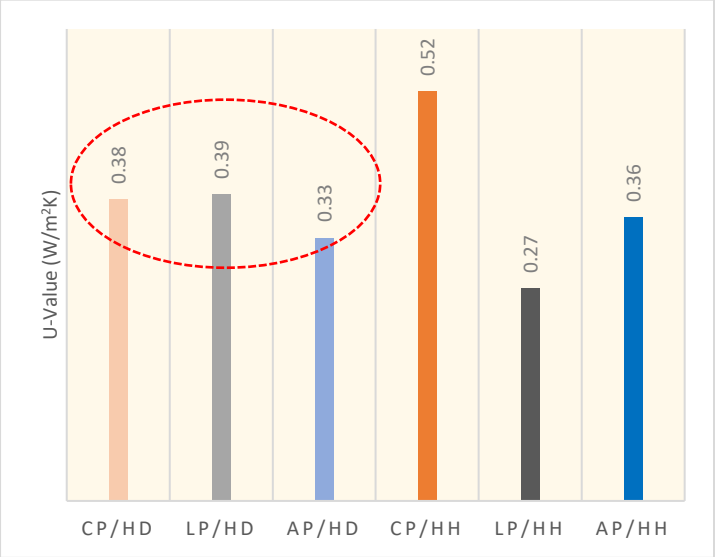

Figure 4-11: In-situ thermal transmittance value for three wall specimens in Hot-Dry (HD) and Hot-Humid (HH) conditions.
CP: Clay-PIR; LP: LECA-PIR; AP: AAC-PIR.

Table 4-16: U-value of PIR-insulated specimens & % in(de)crease from calculated value

	U-value [W/m². K]		
	Calculated	Measured (HD)	Measured (HH)
Clay-PIR	0.35	0.38 (-8%)	0.52 (-48%)
LECA- PIR	0.31	0.39 (-25%)	0.30
AAC-PIR	0.30	0.33 (-10%)	0.36 (-20%)

Three alternative wall specimens insulated with cork performed differently from the first three specimens. Figure 4-12 shows the development of in-situ U-value calculations for these samples over time. Similar to PIR samples, except for fired clay block, the rest of the specimens exhibited lower thermal transmittance value (better performance) in dry condition than in humid. However, unlike PIR samples, the performance of specimens was not similar to each other under dry condition and the thermal transmittance values were well apart from one another. Under both humid and dry conditions, the LECA sample performed better than the rest resulting in the lowest U-value. The AAC-cork unexpectedly resulted in higher U-value than fired clay and LECA in humid condition. However, the fired clay-cork, despite a lower U-value at the beginning of measurement period, exhibited a steady increase in U-value which was still increasing at the end, when experiment was stopped.

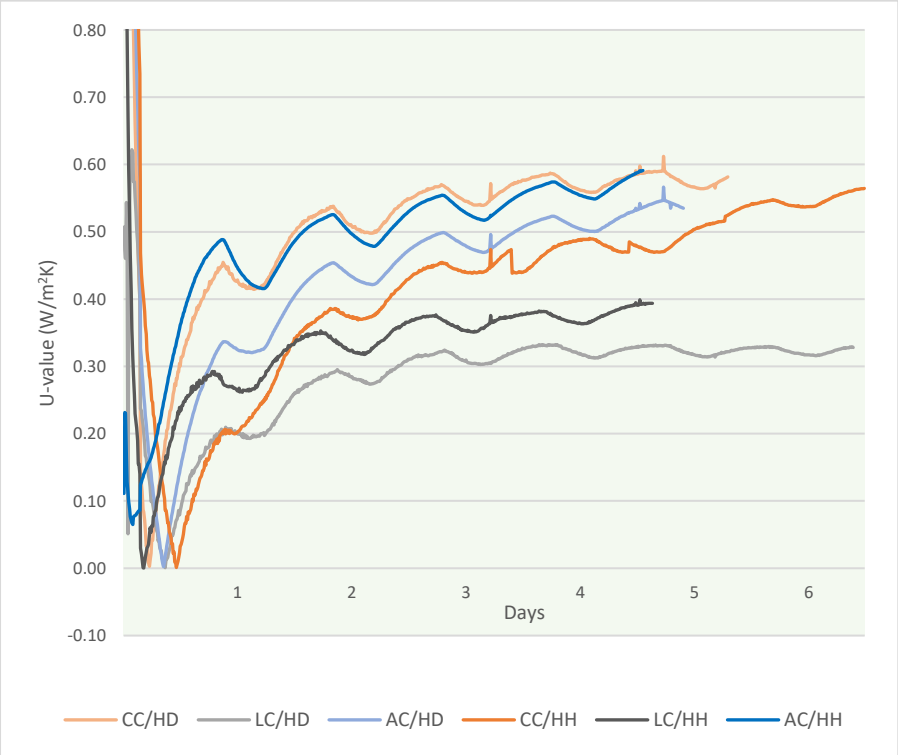

Figure 4-12: Development of in-situ thermal transmittance value for three wall specimens in Hot-Dry HD (HD) & Hot-Humid (HH) conditions.
CC: Clay-Cork; LC: LECA-Cork; AC: AAC-Cork.

Figure 4-13 and Table 4-15 show the U-values calculated and measured for three hygroscopic wall specimens under HD and HH conditions. As can be seen, the LECA specimen resulted in the most unexpected behaviour compared to the other samples with lower U-values under both conditions when compared to their calculated values. The rest of the wall assemblies (i.e. AAC and fired clay blocks) resulted in higher U-values than that suggested by theoretical calculations, with AAC showing the most discrepancy (22 and 34% under HD and HH condition).

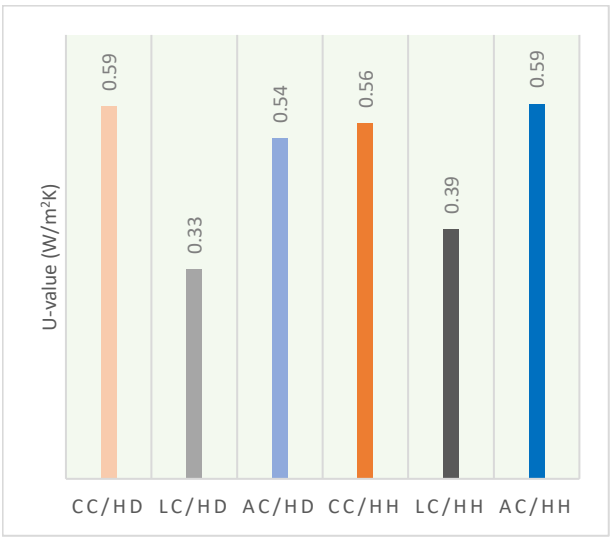

Figure 4-13: In-situ thermal transmittance value for three wall specimens in Hot-Dry (HD) and Hot-Humid (HH) conditions
CC: Clay-Cork; LC: LECA-Cork; AC: AAC-Cork.

Table 4-17: U-value of Cork-insulated specimens & % in(de)crease from calculated value

	U-value [W/m^2. K]		
	Calculated	Measured (HD)	Measured (HH)
Clay- Cork	0.55	0.59 (-7%)	0.56 (-1.8)
LECA- Cork	0.46	0.33 (+28%)	0.39 (+15%)
AAC- Cork	0.44	0.54 (-22%)	0.59 (-34%)

For a better understanding of what happens through the section of the wall specimens and the proportion of insulation and block in heat transfer, the resistance of the layers was calculated separately. Having the heat flux value on the internal side of the wall and temperatures on both sides (inside and out) as well as at the interface between the block and the insulation, the resistance of the insulation layer and block layer were calculated separately. (The calculated R-value includes the resistance of layers of internal and external plastering which is negligible in overall R-value due to their thickness.) For this part of analysis, resistance value was used instead of transmittance value due to the direct (non-reciprocal) relation of the resistance of isothermal layers as opposed to U-value.

Graphs on Figure 4-14 show the resistance of layers of the specimens as R_{block}, R_{ins} and R_{total}. The result of LECA-PIR specimen under HH condition, did not seem to be consistent with the rest of the results and therefore was assumed faulty. Almost in all samples, the resistance of the layers under HD condition was higher than HH condition. The only exception to this was the fired clay- cork specimen which, at first, seems to not to follow this pattern; however, there was a gradual decrease in the resistance of the layers (especially cork) in time which ultimately resulted in lower resistance under HH than in HD condition. The fired clay blocks performed equally well under both HD and HH conditions and when coupled with PIR or expanded cork as thermal insulation, resulted in R-values of 0.6 m^{2}K/W in all experiments. AAC blocks, on the other hand, resulted in nearly 40% lower R-value when coupled with cork (0.62 m^{2}K/W) than when coupled with PIR (1 m^{2}K/W). Therefore, different weather conditions did not affect the performance of these blocks as much as the layers adjacent to it did (Table 4-18 & Figure 4-14). LECA blocks had the most deviation in different scenarios and performed the least close to the theoretical expectations.

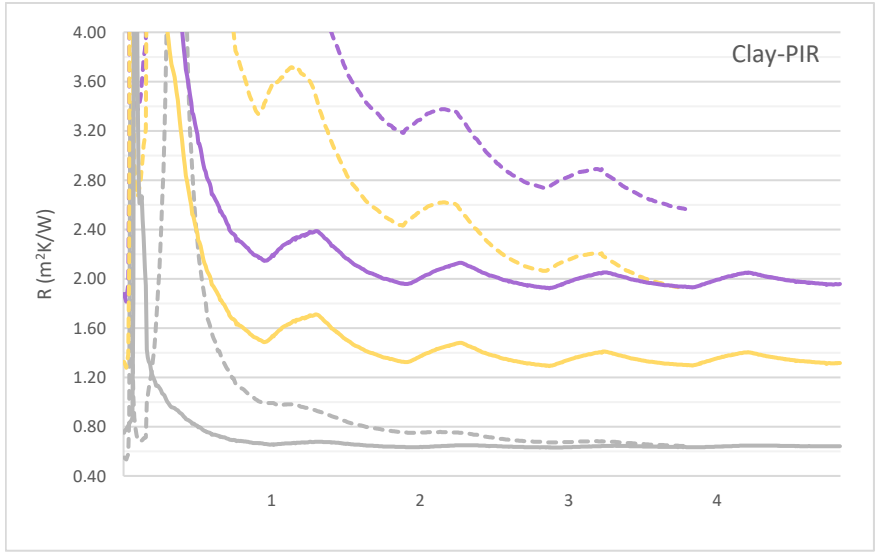
Clay-PIR
R (m²K/W)
4.00
3.60
3.20
2.80
2.40
2.00
1.60
1.20
0.80
0.40
1
2
3
4

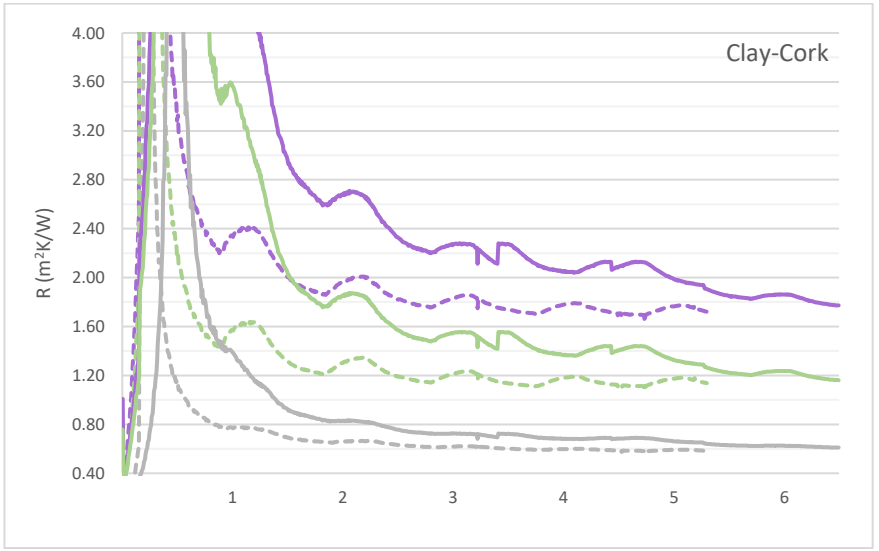
Clay-Cork
R (m²K/W)
4.00
3.60
3.20
2.80
2.40
2.00
1.60
1.20
0.80
0.40
1
2
3
4
5
6

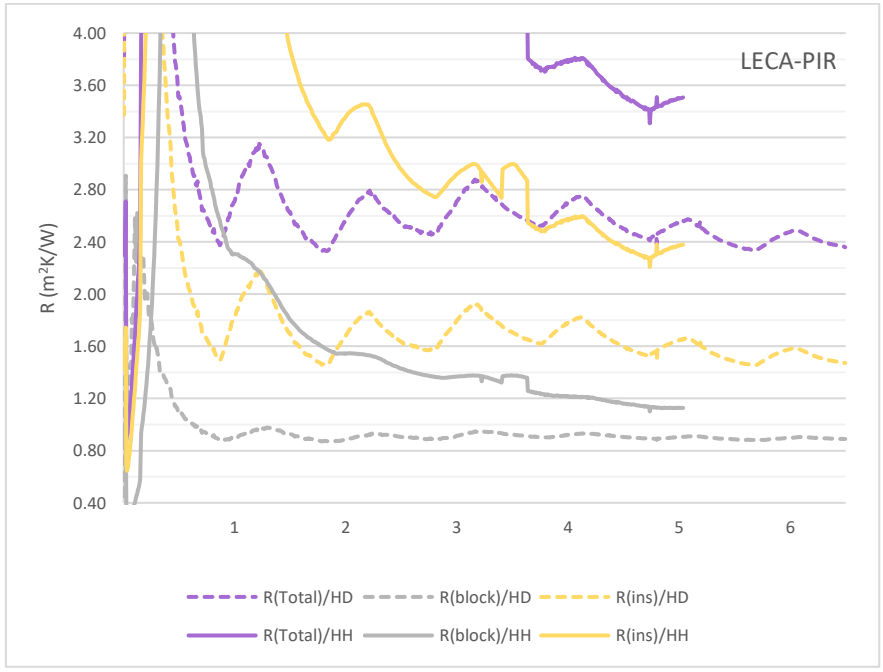
LECA-PIR
R (m²K/W)
4.00
3.60
3.20
2.80
2.40
2.00
1.60
1.20
0.80
0.40
1
2
3
4
5
6
R(Total)/HD
R(block)/HD
R(ins)/HD
R(Total)/HH
R(block)/HH
R(ins)/HH

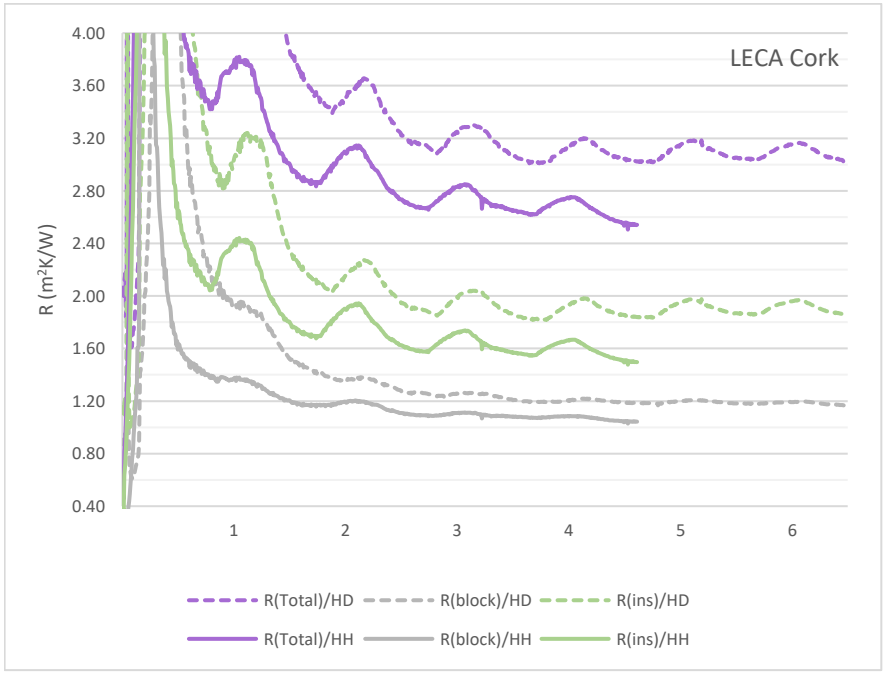
LECA Cork
R (m²K/W)
4.00
3.60
3.20
2.80
2.40
2.00
1.60
1.20
0.80
0.40
1
2
3
4
5
6
R(Total)/HD
R(block)/HD
R(ins)/HD
R(Total)/HH
R(block)/HH
R(ins)/HH

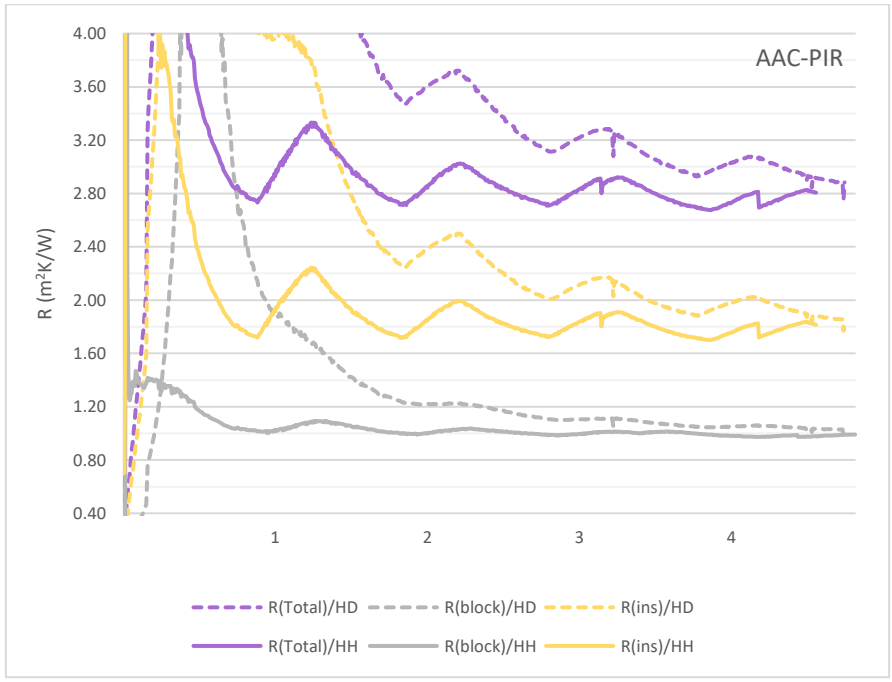

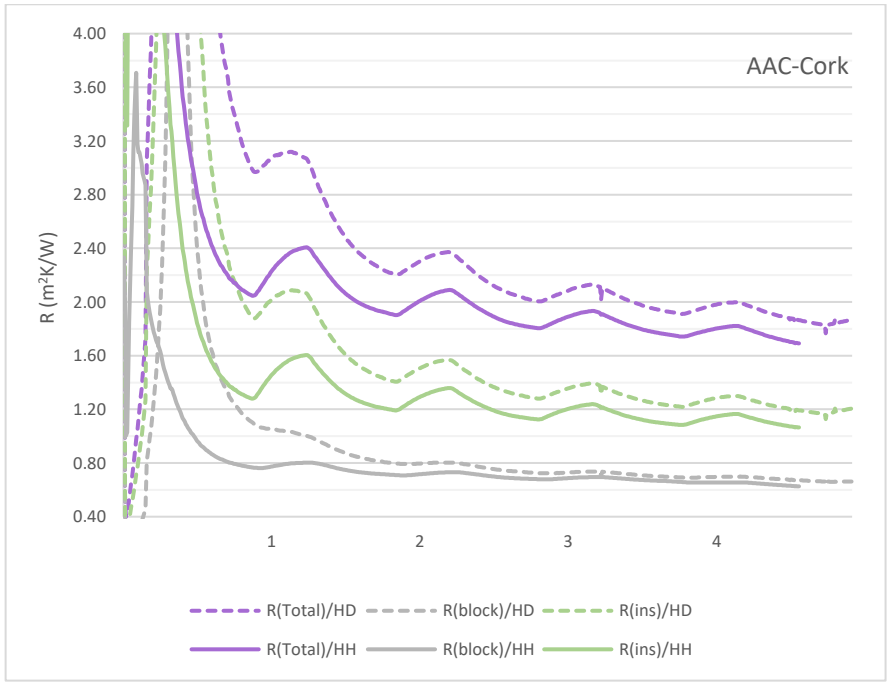

Figure 4-14: Breakdown of in-situ R-value of the layers of wall specimens under Hot-Dry (HD) and Hot-Humid (HH) condition
Top: Fired clay specimens; Middle: LECA specimens; Bottom: AAC specimens

R_{ins}: Resistance of insulation layer+ external plaster
R_{block}: resistance of block layer + internal plaster
R_{total}: R_{ins} + R_{block}

Table 4-18: Breakdown of R-value of the layers of wall

	d [m]	λ [W/mK]	R [m²K/W]	$R_{calculated}$ [m²K/W]	R_{HD} [m²K/W]	R_{HH} [m²K/W]		d [m]	λ [W/mK]	R [m²K/W]	$R_{calculated}$ [m²K/W]	R_{HD} [m²K/W]	R_{HH} [m²K/W]
Clay Block_ PIR					**Measured**		**Clay Block_ Cork**					**Measured**	
Cement plaster	0.025	0.97	0.03	2.30	R_{ins} 1.80	R_{ins} 1.30	Lime plaster	0.025	0.8	0.03	1.25	R_{ins} 1.20	R_{ins} 1.15
PIR insulation board	0.05	0.022	2.27				Cork insulation board	0.05	0.041	1.22			
Fried clay block	0.2		0.51	0.57	R_{block} 0.60	R_{block} 0.60	Fried clay block	0.2		0.51	0.54	R_{block} 0.60	R_{block} 0.60
Gypsum plaster	0.025	0.4	0.06				Earth plaster	0.025	0.97	0.03			
Total				**2.87**	**2.40**	**1.90**	**Total**				**1.79**	**1.80**	**1.75**
LECA Block_ PIR							**LECA Block_ Cork**						
Cement plaster	0.025	0.97	0.03	2.30	R_{ins} 1.50		Lime plaster	0.025	0.8	0.03	1.25	R_{ins} 1.90	R_{ins} 1.50
PIR insulation board	0.05	0.022	2.27				Cork insulation board	0.05	0.041	1.22			
LECA block	0.2		0.86	0.92	R_{block} 0.90		LECA block	0.2		0.86	0.89	R_{block} 1.20	R_{block} 1.00
Gypsum plaster	0.025	0.4	0.06				Earth plaster	0.025	0.97	0.03			
Total				**3.22**	**2.40**		**Total**				**2.14**	**3.10**	**2.50**
AAC Block_ PIR							**AAC Block_ Cork**						
Cement plaster	0.025	0.97	0.03	2.30	R_{ins} 1.80	R_{ins} 1.70	Lime plaster	0.025	0.8	0.03	1.25	R_{ins} 1.20	R_{ins} 1.10
PIR insulation board	0.05	0.022	2.27				Cork insulation board	0.05	0.041	1.22			
AAC block	0.2		0.99	1.05	R_{block} 1.00	R_{block} 1.00	AAC block	0.2		0.99	1.02	R_{block} 0.65	R_{block} 0.60
Gypsum plaster	0.025	0.4	0.06				Earth plaster	0.025	0.97	0.03			
Total				**3.35**	**2.80**	**2.70**	**Total**				**2.27**	**1.85**	**1.70**

More data is needed on properties of materials e.g. their porosity, moisture storage function and vapour permeability to be able to explain why wall assemblies performed as they did. Figure 4-15 plots the temperature and moisture profile (absolute humidity in gr/m^3) of LECA-Cork and AAC-cork specimens beside one another. Despite having similar temperature profiles, the moisture content in the layers of construction differs from AAC sample to LECA; hence their different thermal performance.

Another interesting observation is the comparison of temperature and moisture profiles between the AAC-PIR specimen and the AAC-cork. As seen in Figure 4-16, the temperature profile of the two samples is slightly different with the PIR sample performing better in terms of buffering the temperature swings within the block and at its interface with the insulation (purple & cyan lines). However, in terms of moisture content within the layers of the wall assembly, specimens showed different behaviour as for example the highest absolute humidity value in the cork sample was observed to be in the middle of the block whereas in the PIR sample at the interface between the block and the insulation.

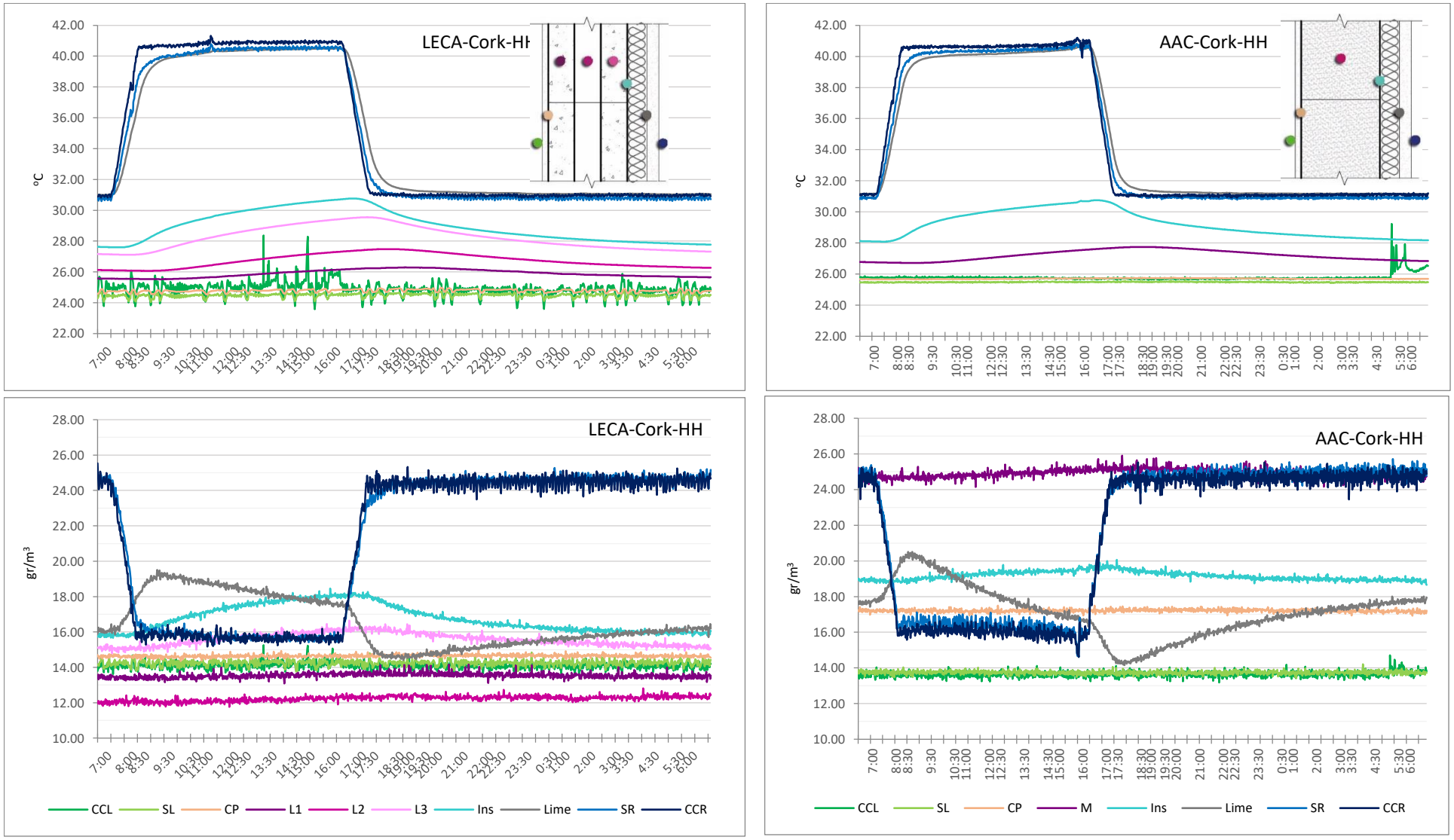

Figure 4-15: Temperature and moisture profile in LECA-Cork (Left) and AAC-Cork (Right) specimens under HH condition

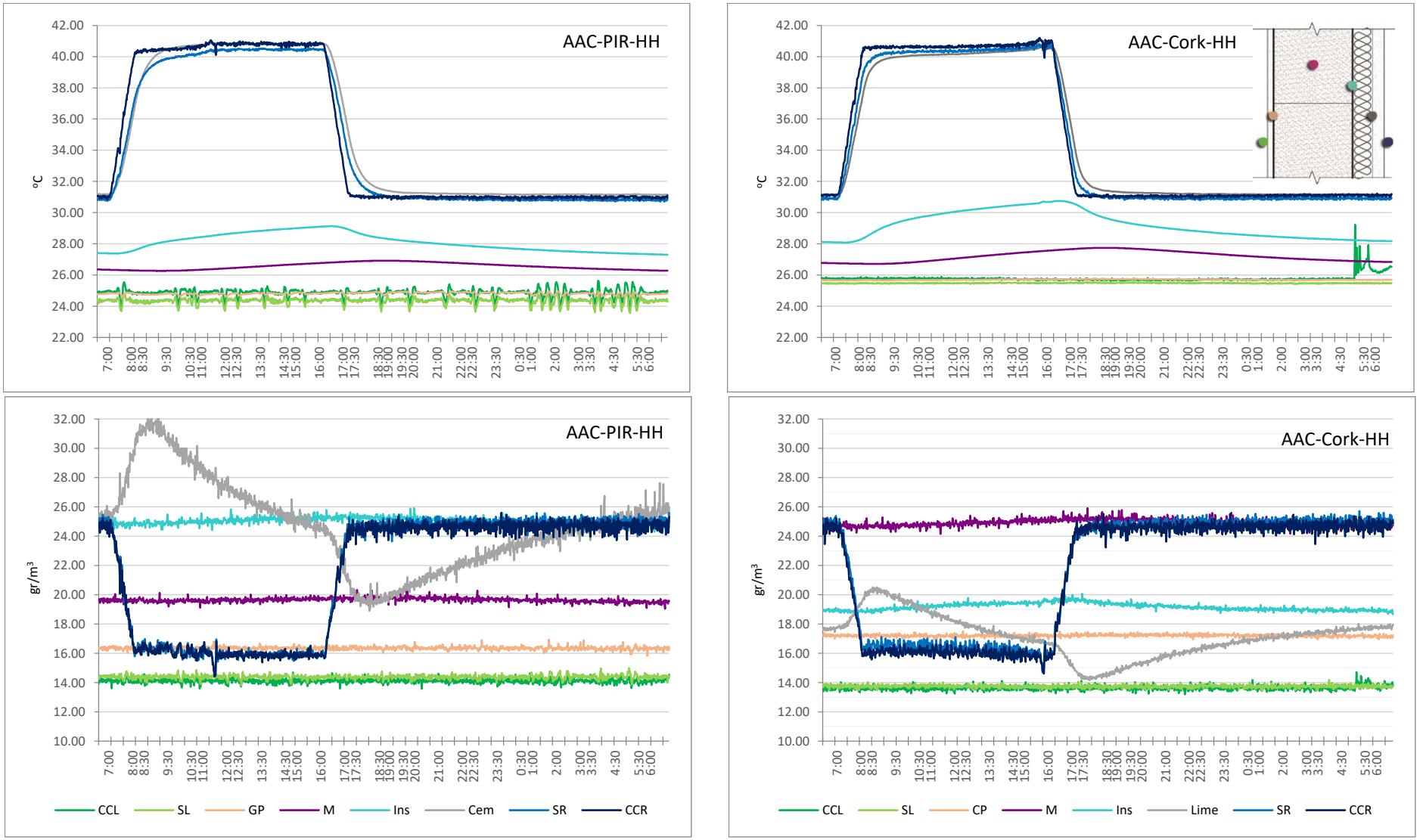

Figure 4-16: Temperature and moisture profile in AAC-PIR (Left) and AAC-Cork (Right) specimens under HH condition

4.1.4. Summary and conclusion

Single-layer wall specimens, conventional insulated and alternative low-carbon wall types were tested in an experimental set-up for their hygrothermal performance. Heat flux data and temperature difference data were used to measure in-situ thermal transmittance value of these wall types. The performance of the single layer wall types was studied under steady-state and cyclic boundary conditions and were compared against that of the specimens insulated with PIR.

- The result for single-layer (uninsulated) specimens, indicated higher thermal resistance values under dynamic hot-humid condition compared to the steady-state condition. The better performance of wall specimens under a dynamic condition, can be related to the thermal inertia of the mass of the blocks that gets charged and discharged during daily thermal cycles and inhibits a constant high-rate heat flow across the sample compared to the steady-state condition. This was supported by a comparison between the results as the higher the thermal mass of a block, the higher the difference between steady-state and dynamic results_ 20% for Fired clay, 27% LECA and 33% for AAC block.
- The comparison of in-situ U-value measurements under steady-state condition shows 78%, 70% and 65% improvement for clay, LECA and AAC walls after being insulated with PIR as shown in Table 4-19.

Table 4-19: Reduction in wall types' U-value after applying PIR insulation (steady state condition)

	Uninsulated [W/m^{2}K]	Insulated with PIR [W/m^{2}K]
Clay block	1.97	0.44
LECA block	1.60	0.48
AAC block	1.32	0.46

- The uninsulated specimens showed a distinctive difference in their performance under steady-state and dynamic conditions with U-values being lower under dynamic condition than steady-state condition. However, in insulated specimens, no distinct difference in resulting U-values were observed when exposed to fluctuating or steady-state condition. This was because the layer of insulation neutralises the heat capacity of the blocks and thermal mass effect has less opportunity to play any role in heat transfer equations. Therefore, the performance of specimens under both conditions was closer to one another and was mainly dictated by the thermal conductivity of the insulation.

In the next stage, multi-layer wall specimens made of low-carbon materials i.e. cork, earth plaster and lime render were compared against the conventional PIR-insulated wall types. The in-situ

thermal transmittance measurements under steady-state can be extrapolated to the performance under hot dry condition only in terms of pattern of performance i.e. how similar blocks perform compared to one another. The actual values under steady state are different from dynamic conditions.

Multi-layer wall types were then exposed to cyclic hot-humid and hot-dry conditions:

- Almost all 6 specimens performed better (i.e. lower thermal transmittance value) under dry condition than under humid condition.
- Some constructions were affected more considerably in the presence of moisture e.g. Clay-PIR; some negligibly e.g. AAC-PIR.
- Unlike that suggested by theoretical calculations, LECA when coupled with cork, performed unexpectedly better than fired clay and AAC specimens exhibiting a lower U-value.
- When insulated with cork, amongst the 3 blocks considered, AAC performed far from theoretical expectations.
- The breakdown of the resistance of layers of wall assemblies shows that it is not just the environmental condition, but sometimes the characteristics of the adjacent layers that affect the performance of the blocks and hence the whole assembly.

In summary, when insulated with cork and breathable plasters, specimens performed less according to the theoretical expectations. Therefore, theoretical calculations especially in the case of breathable construction, is not an appropriate way of evaluating performance of wall constructions. Under HD condition, LECA-Cork performed the best resulting in U-value of 0.33 W/m^2K and under HH condition, AAC-PIR performed the best with U-value of 0.36 W/m^2K which is not far off from what achieved by LECA-Cork (0.39 W/m^2K). This shows that with appropriate combination of materials for wall assembly, a less energy-intensive alternative can perform as well as, or even better than their conventional counterparts.

Experiments need to be run for a longer period for a more definite interpretation of the result which unfortunately was not feasible due to the limitations of the laboratory. A thermal imaging camera would also be useful in monitoring the specimens during the test to look for any thermal bridges and for better positioning of the sensors.

4.2. Part two: Hygroscopic properties of earth plasters

Different standards and protocols were used, as discussed in chapter 3, to quantify the moisture buffering capacity of earth plaster mixes. In the following sections the result of the vapor permeability, moisture storage function, MBV and DIN 18947 Standards are reported and discussed. In each section, a comparison is made with the existing data in the literature.

4.2.1. Water vapour permeability (δ_p)

The results of the water vapour resistance value (also known as the μ-value) for the wet cup method ranged between 8.5 and 12 and for the dry cup tests were between 15.5 and 25 (Figure 4-17). Amongst plain plasters, the base coat had higher vapour resistance compared to the top coat. For the base coat mixes, the addition of plant-based aggregates, with the exception of wheat straw, increased the vapour permeability by between 5% and 12%. This result was the reverse for top coat mixes where the addition of fibrous aggregates resulted in a decrease in the permeability of plasters by up to 28%.

These results are close to what has been reported in the literature when Faria et al. (2015) measured the water vapour resistance of a ready-mixed earth plaster in a climate chamber with 40% RH, 23°C and reported the value of 8 μ ± 0.3 for the wet cup method. Palumbo et al. (2016) measured the wet cup vapour permeability of clay plasters containing 0%, 1% and 2% of barley straw, barley wool and corn pith and reported a μ-value of 6.5 for plain clay plaster. According to their results this value increased to 8 and 7.5 respectively, when 1% of barley straw and barley wool was added and decreased to just below 6 with the addition of 1% corn pith. Liuzzi et al. (2013) measured the vapour permeability of a clay mixture internal wall coating made with different mixes of quarry fine, kaolinite and bentonite and reported μ-values between 8 and 11 for the wet cup method. The numbers reported in the literature are very close to the result of the experiment conducted in this study. The results from the literature also suggest that the addition of plant-based aggregates does not always result in higher permeability; a fact that was also observed in this study.

4.2.2. Moisture sorption capacity ($\xi = \frac{\partial w}{\partial \varphi}$)

For this study, firstly the sorption isotherm of plain materials, i.e. before being used in plaster mixes, was measured using a DVS instrument for a general characterisation of the sorption capacity of these materials in their initial state. The sorption properties of plant aggregates and diatomaceous earth was much higher than earth plasters all throughout the RH range with wheat straw having the highest mass gain. From the sorption isotherm data shown in Figure 4-18, one might conclude that the earth-straw mix would result in the highest moisture absorption followed by wood shaving-

earth and rice husk-earth mixes. However, absorption behaviour of plant aggregates is different from this initial expectation when mixed with earth as shown in sorption isotherm curves of earth mixes (Figure 4-19).

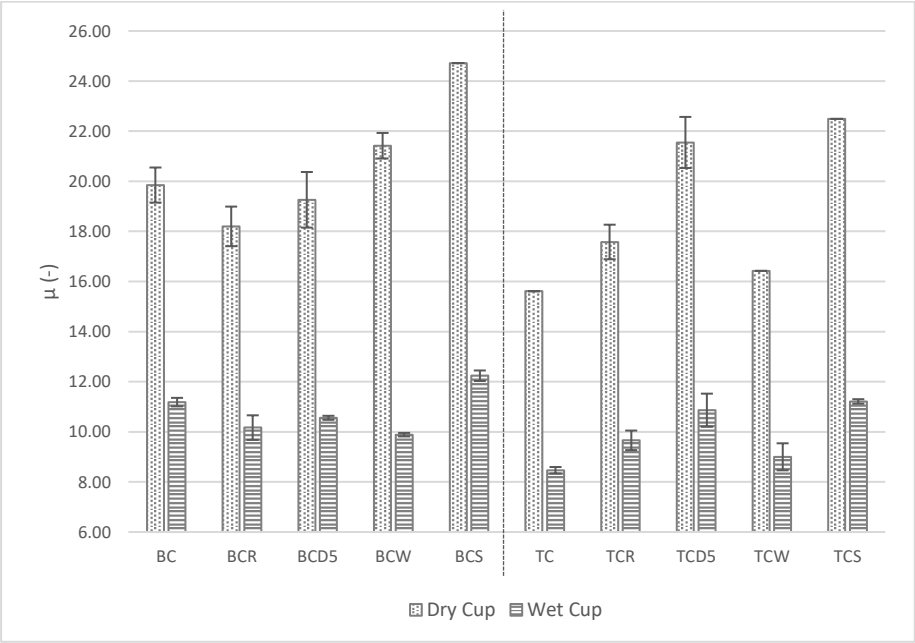

Figure 4-17: Water vapour resistance value of plaster mixes
R: Rice husk, D: Diatomaceous earth, W: Wood shaving, S: wheat Straw

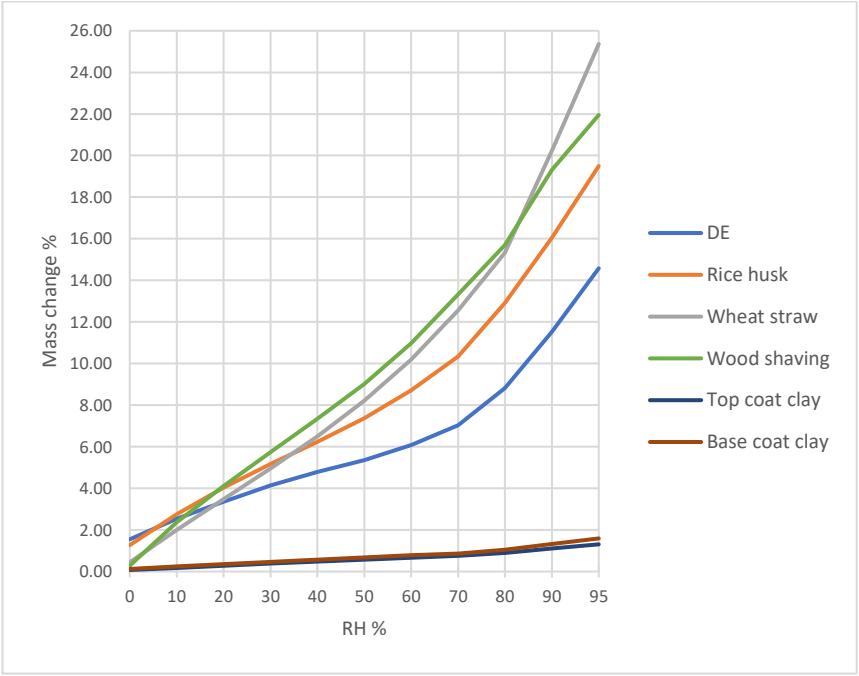

Figure 4-18: Sorption isotherms of materials in their initial state before being mixed in plaster mixes

The results in Figure 4-19 show that in plain form, the base coat plaster sorption capacity was 20% higher than that of the top coat plaster. The addition of plant-based aggregates increased the moisture absorption capacity of plasters by 7%, 23%, 29% and 31% in the BCR, BCS, BCD and BCW mixes compared to the BC mix (at the 95% RH step). The increase was more distinct for the top coat mixes than the BC mixes as the addition of DE to the top coat plaster resulted in 46% more moisture absorption at 95% RH. For both BC & TC plasters, the wood shaving and diatomaceous earth exhibited the greatest increase in moisture storage properties as shown in Figure 4-19. Ashour et al. (2010) studied the Equilibrium Moisture Content (EMC) of earth plasters mixed with wheat straw, barley straw and wood shaving in different proportions and concluded that the addition of natural fibres increased the absorption rate from 1.7% for plain earth plaster up to 6.5% when mixed with barley straw. It is not clear whether the increase was in terms of the gradient of the total absorption isotherm or for any single absorption point. Oudhof et al. (2015) and Liuzzi et al. (2013) also measured water vapour sorption isotherms of clay mixtures. However, in Oudhof et al. the density of samples was far less than the ones in this study (between 320 to 530 kg/m^3 compared to 1500 to 1900 kg/m^3 in this study) and in Liuzzi et al. results were reported as volumetric moisture content in kg/m^3 and is not directly comparable to the results of this study.

Another observation was the difference in sorption isotherms from the DVS and climate chamber methods for the TC and the TCD (Figure 4-20). As these two mixes were reasonably homogenous even for a small sample, the DVS method as well as the climate chamber method was used to measure and plot the sorption isotherms. This allowed a comparison between the results of these two methods which, in theory, were expected to be the same. However, as seen in Figure 4-20, the mass increase was higher for every RH step using the DVS instrument compared to equivalent RH steps inside the climate chamber. The reason behind this observation was not completely clear but it is thought to be due to the more effective drying process inside the DVS chamber, the geometry of the samples i.e., surface to volume ratio, and the surface resistance.

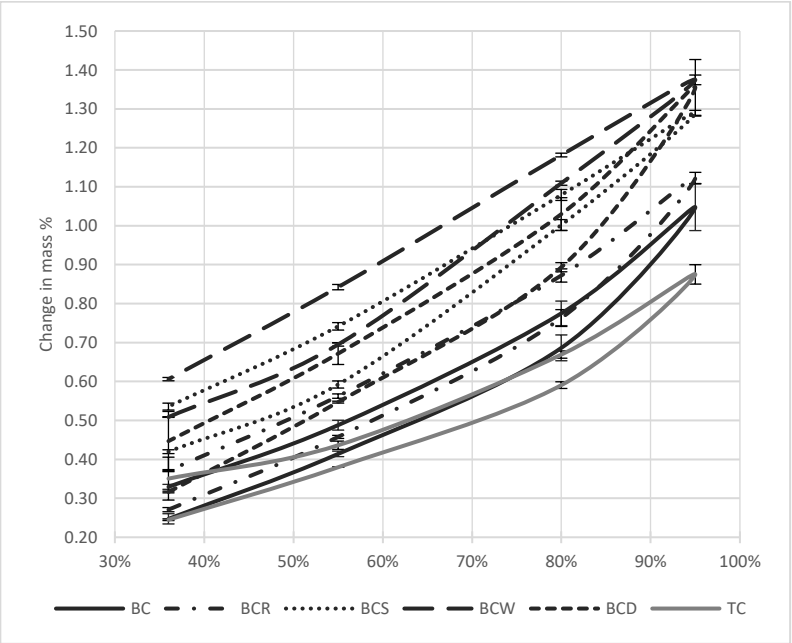

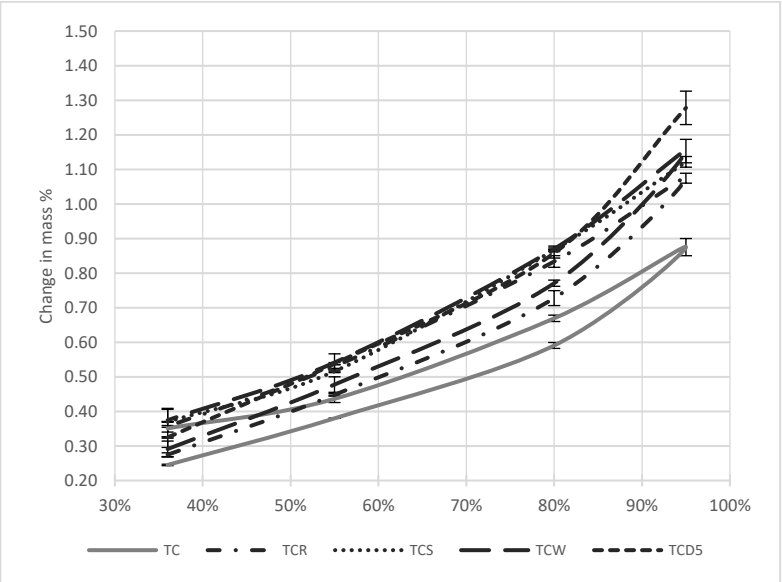

Figure 4-19: Absorption-desorption isotherms of base coat (top) and top coat (bottom) earth plaster mixes
R: Rice husk, S: wheat Straw, W: Wood shaving, D: Diatomaceous earth

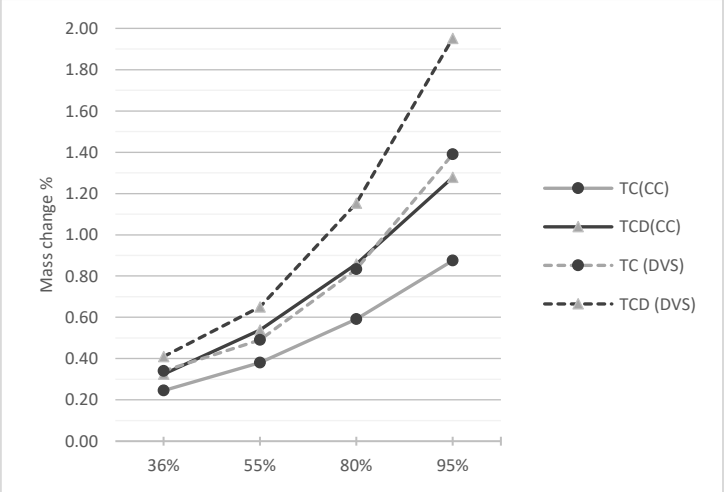

Figure 4-20: Sorption isotherms of TC and TCD; DVS vs. climate chamber method

4.2.3. Moisture Buffer Value (MBV)

The result of the NT MBV experiment shows that, the TC mixes, in general, exhibited a higher moisture buffering capacity compared to the BC mixes. In the case of both BC and TC plasters, the addition of all aggregates apart from wheat straw increased the MBV. All plaster mixes had a MBV of between 1 and 2 falling in the "Good" classification of the NT MBV classification. As explained in section 2.2.3, the MBV introduced in NordTest project, is calculated after 8 hours of exposure to high RH level i.e. 75% (MBV_{8h}). Here we also calculated the (MBV_{1h}) and (MBV_{3h}) by dividing the mass change of the samples after 1 and 3 hours of exposure by the surface area and RH step (Figure 4-27). This allows the comparison of the rate of mass gain of different mixes and does not introduce any new experimental protocol.

Figure 4-21 shows that the difference in moisture buffering ability of different mixes was more pronounced after 8 hours of exposure to high RH. According to these values, the TC mixes, in general, exhibited a higher moisture buffering capacity compared to the BC mixes. In the case of both BC and TC plasters, the addition of all aggregates apart from wheat straw increased the MBV. All plaster mixes had a MBV of between 1 and 2 falling in the "Good" classification of the NT MBV classification. Another observation was that the difference in the MBVs of different plasters was more pronounced after 8 hours of exposure implying that a material's moisture buffer capacity would be greater when exposed to moisture for longer.

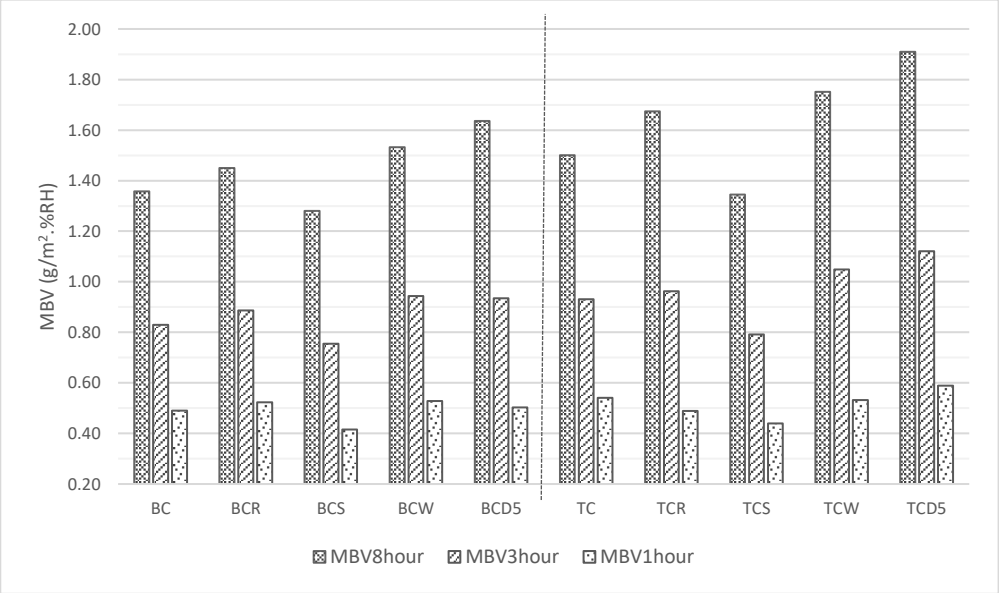

Figure 4-21: Moisture Buffer Value of plasters
R: Rice husk, S: wheat Straw, W: Wood shaving, D: Diatomaceous earth

When Oudhof et al. (2015) used the NT protocol to measure the MBV of a straw-clay mixture (density unknown), they reported that the minimum MBV measured during the last 9 cycles was 2.86 g/m^2.%RH. Palumbo et al. (2016) did the same for clay samples mixed with barley straw and corn pith in 1 and 2 % mass of clay. Their results indicated that the addition of plant fibres had little impact on the moisture buffering capacity of mixtures but increased the moisture penetration depth resulting in faster reaction to changes in RH. Samples with plant fibres reached EMC faster; therefore, they performed less efficiently over extended periods of time.

Similar to the measured MBV, the ideal MBV indicates the quantity of water absorbed or released by porous materials when a periodic variation of RH is imposed at its surface and is calculated through the following equation based on material properties measured through steady-state protocols i.e. water vapour permeability and the moisture storage function (Abadie & Mendonca, 2009):

$$MBV_{ideal} \approx 0.00568\, p_{sat} b_m \sqrt{t_p} \qquad (2)$$

Where b_m is moisture effusivity (equation 1) and t_p is period of time in seconds.

The result was plotted against the results of the practical MBV for both the BC and TC plasters (Figure 4-22). The results of the calculated and measured MBV were within a range reasonably close to one another, especially for the TC mixes; however, the calculated MBVs were generally higher than the measured values. Changes for the BC, BCR, BCW, BCS and BCD were 27, 32, 29, 37 and

22% respectively and for the TC, TCR, TCW, TCS and TCD were 12, 4, 3, 20 and 0.05% respectively. This difference in the results could be due to the mass increase (∂W) used in the ideal MBV calculation being the outcome of the moisture storage function, a steady-state test procedure that allows plenty of time for the material to reach the equilibrium state. The same applies to water vapour permeability value (δ_p) which is derived from a steady-state test procedure. The moisture penetration depth might also play a role as thicker samples were used for measuring sorption isotherms compared to samples prepared for the NT MBV protocol, so a deeper thickness was available for moisture absorption.

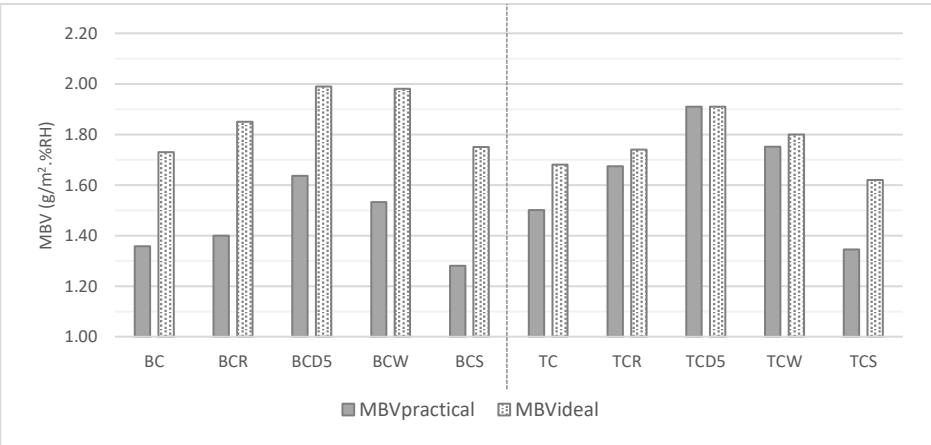

Figure 4-22: MBV_{ideal} and $MBV_{practical}$ of earth plaster mixes
R: Rice husk, D: Diatomaceous earth, W: Wood shaving, S: wheat Straw

4.2.4. DIN 18947 Standard

Based on the results shown in Table 4-20, all earth plasters were categorised in the WS III classification of the DIN standard defining the highest moisture buffering capacity, whereas gypsum plaster only just meets the requirements of the first classification, WS I. According to this test, the addition of diatomaceous earth increased the water vapour absorption of the BC and TC earth plasters by 21% and 19% respectively.

Table 4-20: Mass absorption of earth mixes in g/m² in time intervals

	0.5 h	1 h	3 h	6 h	12 h
BC15	11.07	15.09	30.18	43.76	60.87
BC30	10.34	14.28	28.07	41.37	60.08
BCR	11.57	15.43	30.38	43.89	60.77
BCD5	12.24	17.35	34.69	51.02	73.47
TC15	11.57	17.36	31.35	45.33	58.83
TCR	10.76	17.12	31.79	47.44	63.57
TCW	14.27	19.02	34.72	48.99	64.21
TCD5	11.90	18.85	35.71	52.07	69.93
PB+G*	6.75	8.68	15.43	20.74	24.11

*Plaster board+ Gypsum

Lima and Faria (2016) also used this standard to measure the dynamic absorption and desorption of an earth plastering system mixed once with oat straw and another time with typha fibre wool. The results showed that all samples including the reference sample (made of plain clay), presented a very high absorption and desorption capacity. Maddison et al. (2009) tested clay-sand plaster mixed with fibre wool from Typha and chips of Typha and reed under the same protocol. They concluded that the addition of fibrous aggregates accelerated and increased the amount of moisture absorbed, however, absorption decreased when more than 1 wt% of Typha wool was added to clay plaster as there would be insufficient clay for air moisture absorption.

4.2.5. Summary of the results

The results of the NT MBV test showed that the addition of diatomaceous earth contributed to the greatest improvement in moisture buffering capacity, with all plaster mixes found to be classified as WS III, the "good" MBV class, representing the highest MBC class.

To identify the impact of adding different aggregates on the moisture buffering capacity of earth mixes, the values of all their MBC indices are compared in Figure 4-23. The significance was plotted on the vertical axis and the value of the exponent is given below Figure 4-23. If the $MBV_{practical}$ is to be considered as the most representative value for the MBC in real life, it can be concluded that wheat straw mixes (BCS, TCS) behaved differently from the rest as their MBVs decreased as opposed to the increased MBVs of other mixes. This occurred despite the increase in the moisture storage function of these two mixes. This indicated that the permeability had a more pronounced effect on the MBV than the moisture sorption capacity (ξ) as even though the moisture sorption capacity of these two mixes had increased, their MBV had dropped as well as their permeability. This implied that over a relatively short period of time (i.e. 8 hours in the MBV test as opposed to the time taken to achieve complete equilibrium moisture content in moisture sorption capacity test) a high vapour permeability allowed water vapour to be absorbed by the material more easily and quickly and therefore improved the moisture buffering capacity more rapidly resulting in higher MBVs. Apart from straw mixes, for base coat mixes, all indices for top coat mixes, except permeability, increased after the addition of aggregates. The improvement is more distinct for TC mixes than the BCs especially after the addition of diatomaceous earth and wood shavings.

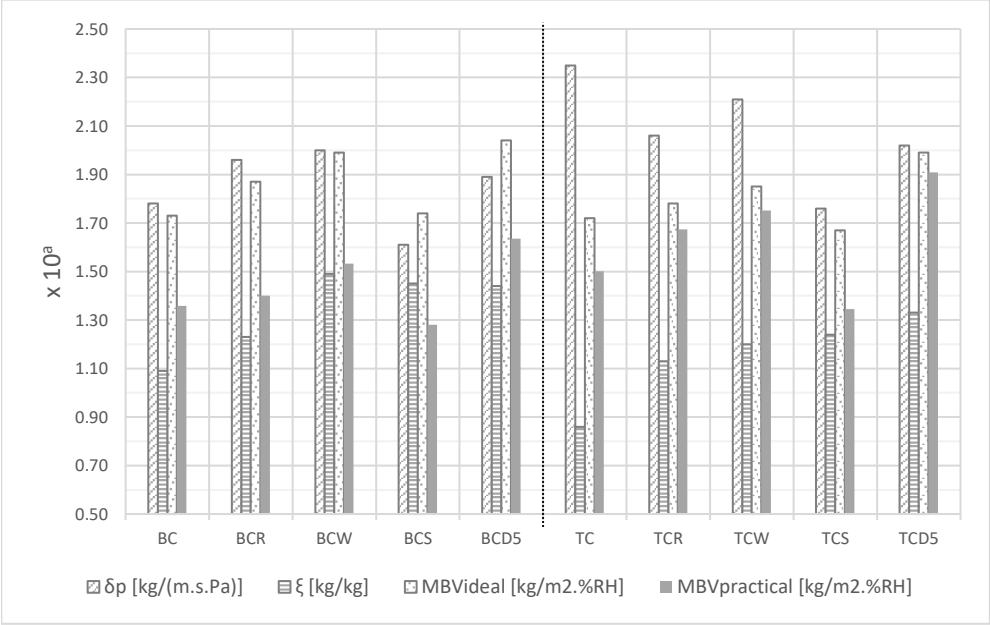

Figure 4-23: Summary of all MBC indices for plaster mixes
a = δ: 10^{-11}, ξ: 10^{-2}, MBV: 10^{-3}
R: Rice husk, W: Wood shaving, S: wheat Straw, D: Diatomaceous earth

4.2.6. Conclusions

In this study, two types of earth plasters with different particle sizes, the Base Coat (BC) and Top Coat (TC) plasters, were selected and separately mixed with three plant-based aggregates and one fine mineral aggregate i.e. diatomaceous earth. These four plaster mixes were assessed for their hygroscopic properties using established protocols for quantifying moisture-related properties of materials. The effect on their moisture response after adding these aggregates to earth plasters was evaluated and they were rated and classified accordingly.

The results showed that in the case of the BC plaster (with coarser particles), the addition of aggregates reduced the water vapour resistance; however, in case of TC plasters (with finer particles) the water vapour resistance value increased. The BC and TC plasters both showed an improvement in their moisture sorption capacity (as in sorption isotherms) when mixed with other aggregates. For the TC plaster, the increase was more distinct at higher RH levels (more than 60%) whereas for the BC plaster it was noticeable even at lower RH levels. The NT MBV test classified all the aforementioned earth plaster mixes as “good” moisture buffering materials. The addition of aggregates to earth plasters improved the MBC in almost all mixes apart from those mixed with wheat straw. Diatomaceous earth and wood shavings resulted in the highest increase in MBC when

mixed with both the BC, (with increases of 20% and 13%, respectively) and the TC plaster (with increases of 27% and 17%, respectively). Based on the DIN 18947 protocol, all mixes were classified in the highest grade of the moisture absorption capacity for earthen plasters, namely WS III in this standard compared to gypsum plaster that only just meets the lowest classification WS I.

This is the first time that diatomaceous earth has been mixed with earth plaster to successfully improve its moisture buffering performance. However, the workability of all plaster mixes in full-scale practice needs to be examined as the samples tested in this study were sized to satisfy the requirements of the standards or test protocol. Also, a more holistic cradle-to-grave approach should be adopted to assess the benefits and disadvantages of adding DE compared to other plant-based aggregates. This requires further research to evaluate the benefits gained through the higher moisture buffering capacity of DE-earth mixes against potential environmental impacts.

Chapter 5.

Conclusion & future work

5.1. Summary and conclusion

The first part of this study consisted of the investigation of hygrothermal performance of wall types commonly used in residential buildings of Iran with some alterations to improve their ecological profile. The high energy consumption rate in the country, the harsh nature of the climate prevalent in a vast area of the country alongside shortcomings of the current wall practice in terms of heat transmittance, highlight the necessity and the potential for improving wall design and reducing heat transfer. On the other hand, there is a gap in research about the experimental study of heat and moisture transfer particularly through multi-layer buildings' envelope. Research on simultaneous heat and moisture transfer has been mostly carried out with numerical models which are not free from the inherent uncertainty in their outcome. On the other hand, experimental studies on the matter have been limited to single layer constructions. In a multi-layer fabric system, the construction layers interact with each other. The characteristics of each layer affects the heat and moisture transport. At the same time, materials properties change with changes in environment temperature and moisture levels. This results in a dynamic condition that cannot be explained with steady-state theoretical calculations and requires investigation under a real situation. In investigating the common wall types of Iran, the research sought to investigate:

- The equivalent thermal conductivity value of hollow construction blocks (in this case specific to Iranian construction techniques)
- The in-situ thermal transmittance vs. theoretically calculated thermal transmittance value of construction systems
- Thermal transmittance under fluctuating vs. steady-state boundary conditions
- Wall systems' performance in dry vs. humid boundary condition
- The effect of the characteristics of layers of the wall on moisture transport and therefore the overall thermal transmittance.

The conventional construction blocks were studied in single layer and multi-layer assemblies. Single layer wall specimens were tested to experimentally measure the thermal transmittance and hence the equivalent thermal conductivity values of the construction blocks. This was particularly important for hollow blocks i.e. fired clay and LECA blocks as the conductivity values reported in products' data sheets were related to the solid material, not helpful in determining the conductivity of the composite structure of these hollow blocks. The U-value of these composite construction blocks were first calculated theoretically using the combined method (BS EN 6946), resulting in calculation of the wall specimens' U-value taking into account mortar

joints. The experiments on single-layer specimens confirmed the theoretical calculations in terms of the order of the performance i.e. AAC being the best performing followed by LECA and fired clay under both steady-state and fluctuating hot humid conditions. However, the actual values measured were different. All three samples performed better i.e. lower thermal transmittance under dynamic than the steady-state condition indicating the role of the dynamic properties of materials next to their insulative capacity on heat transfer.

A set of the multi-layer wall assemblies represent a conventional wall system consisting of impermeable layers e.g. PIR insulation and cement render which was compared against a set of low-carbon wall assemblies made of hygroscopic and permeable materials such as expanded cork board insulation and lime plaster. PIR insulation board has lower thermal conductivity (0.02 W/m.K) than cork (0.04 W/m.K). The same applies to AAC compared to LECA and fired clay blocks. Therefore, and judging by thermal conductivity values, the combination of PIR + AAC, in theory, should result in the lowest thermal transmittance under all boundary conditions. However, an experimental evaluation of wall systems considering interacting behaviour of adjacent layers led to interesting results confirming different performance of wall systems from what calculations suggest. LECA- Cork wall system under hot dry condition resulted in highest resistance to heat transfer (R= 3.10 m^2K/W). Theoretically, it was expected that all wall types insulated with PIR result in higher resistance to heat transfer.

Break down of the heat flux through the sections of the wall gives interesting result on the performance of the (insulation+ plaster) layer in different wall types. In impermeable wall types insulated with PIR, (PIR+ Cement) performs significantly different from the calculated R-value (2.30 m^2K/W) in all three samples resulting in 1.80, 1.50 and 1.80 m^2K/W, for Clay, LECA and AAC respectively. On the other hand, in hygroscopic wall types insulated with cork (Cork+ Lime) layer resulted in R-values closer to or above what calculations (1.25 m^2K/W) suggest i.e. 1.20, 1.90 and 1.20 m^2K/W in assemblies made of Clay, LECA and AAC respectively. This might be explained by the accumulation of moisture between cement render and PIR board

In terms of performance in presence of moisture, all wall types resulted in higher thermal transmittance under humid conditions with some getting affected more significantly than others (Table 4-18). Plotting of temperature and humidity profiles within the layers of the assembly shows that specimens despite having very similar temperature profiles, might have different humidity profiles hence their different overall performance.

For internal finishing, the alternative wall system proposed the use of earth plaster instead of the conventional finishing plaster i.e. gypsum. Earth is known for its high moisture absorptivity. Amongst the layers of the wall, the internal final finishing has the highest contribution to regulating indoor humidity fluctuations. These two facts make earth plaster a good candidate for being used as a passive measure to control indoor RH levels. Earth plasters were traditionally used in Iran for rendering building envelope surfaces both internally and externally. Different additives including plant-based aggregates were mixed with earth to improve the workability, durability and mechanical strength of these plasters. However, the effect of these additives on hygroscopic capacity of earth plasters has not been extensively studied. In this study, wheat straw, rice husk and wood shaving were mixed with two types of earth plasters with fine (TC) and coarse (BC) aggregates. Diatomaceous earth, a highly absorptive fine mineral aggregate, was also added separately to both earth plasters (TC and BC) to increase the moisture buffering capacity of earth plasters. Vapor permeability, moisture storage function and MBV are the most widely used protocols characterising moisture-related properties of materials. In terms of vapour permeability, earth plasters performed differently when mixed with the additives. For BC mixes vapour permeability increased after the addition of additives except for straw mix (BCS); while for TC mixes the reverse was observed. For moisture storage function, the addition of aggregates increased the absorption capacity for all mixes. Ideal MBV is a derived value combining vapour permeability and moisture storage function together in one parameter. Ideal MBV values confirm increase in moisture buffering capacity of earth mixtures after addition of plant-based and DE aggregates except for wheat straw. This result was confirmed by the Nordtest MBV protocol except that lower values were measured compared to ideal MBV values. This is because of the static nature of permeability and sorption isotherm tests that give enough time for equilibrium to be reached and therefore plenty of time for moisture absorption. From all the additives, DE and wood shaving resulted in the highest increase in MBC when mixed with both BC (20% and 13% increase) and TC plasters (27% and 17% increase). Based on the DIN 18947 protocol, all mixes were classified in the highest grade of the moisture absorption capacity for earthen plasters, namely WS III in this standard compared to gypsum plaster that only just meets the lowest classification WS I.

If we consider the MBV protocol and DIN 18947 as dynamic methods of evaluating moisture buffering capacity which more realistically represent a real-life scenario, it can be concluded that the addition of all aggregates improved this property of earth mixes with DE showing the highest improvement in hygroscopicity when mixed with earth.

5.2. Limitations

The size of the specimens was the first limitation imposed by the size of the environmental chambers available in the laboratory. The data from a larger scale wall specimen could be relied on with more confidence. Alternatively, smaller heat flux sensors could be more appropriate to the size of the specimens. This could not be done due to budgetary constraints. Also, the duration of time allowed for each specimen under different boundary condition especially in case of dynamic conditions could result in more reliable data. As for some of the experiments, the data indicates specimens had not yet been stabilized. Ideally, specimens should have stayed under the same condition for a few months to investigate the effect of moisture on their durability and any potential rot and damage, especially in case of cork boards. This was not feasible due to time constraint of a PhD project and unavailability of environmental chambers for longer periods of time. The robustness of experimental work could be confirmed with the help of a thermal imaging camera, which could be used for monitoring the specimens during the test to look for any thermal bridges and to help determine the optimal positioning of the sensors.

For the second part of study i.e. earth plasters, the workability of all plaster mixes in full-scale practice needs to be examined as the samples tested in this study were sized to satisfy the requirements of the standards or test protocol. Also, a more holistic cradle-to-grave approach should be adopted to assess the advantages and disadvantages of adding DE compared to other plant-based aggregates. This requires further research to evaluate the benefits gained through the higher moisture buffering capacity of DE-earth mixes against potential environmental impacts.

5.3. Future work

Further studies could investigate the hygroscopic properties of all materials used in wall constructions in detail; properties such as porosity, vapour permeability, sorption isotherms, liquid transport coefficient for suction and redistribution. These parameters could then make it possible for a computer simulation to be run for the same wall constructions under similar conditions. The simulation could be calibrated against the real data achieved through the experimental data in this study. It would be then easier to have a long-term test period (yearly data) and it would also be easier to modify various parameters to achieve the best design under different conditions.

For measuring moisture buffer capacity of earth plasters, a more realistic moisture production regime, simulating occupancy patterns within a building, could be produced in a room or a scaled

test chamber with its walls plastered with the proposed mixture. The fluctuation of indoor RH could be monitored and a more realistic conclusion on the plasters' suitability and applicability could be made.

References

- Abadie M.O., Mendonca K.C., 2009. Moisture performance of building materials: From material characterisation to building simulation using the Moisture Buffer Value concept. Building and environment, 44, pp. 388-401.
- Aditya, L., Mahlia, T.M.I., Rismanchi, B., Ng, H.M., Hasan, M.H., Metselaar, H.S.C., Muraza, O. and Aditiya, H.B., 2017. A review on insulation materials for energy conservation in buildings. *Renewable and Sustainable Energy Reviews*, *73*, pp.1352-1365.
- Agarwal, S. and Gupta, R.K., 2017. Plastics in buildings and construction. In *Applied Plastics Engineering Handbook* (pp. 635-649). William Andrew Publishing.
- Allaby, M. and Park, C. eds., 2013. *A dictionary of environment and conservation*. OUP Oxford.
- Allinson, D. and Hall, M., 2010. Hygrothermal analysis of a stabilised rammed earth test building in the UK. *Energy and Buildings*, *42*(6), pp.845-852.
- Allouhi, A., El Fouih, Y., Kousksou, T., Jamil, A., Zeraouli, Y. and Mourad, Y., 2015. Energy consumption and efficiency in buildings: current status and future trends. *Journal of Cleaner production*, *109*, pp.118-130.
- American Society of Heating, Refrigerating and Air-Conditioning Engineers, Inc, 2013. *2013 ASHRAE Handbook: Fundamentals*. American Society of heating, refrigerating and air-conditioning engineers.
- Antonyová, A., Korjenic, A., Antony, P., Korjenic, S., Pavlušová, E., Pavluš, M. and Bednar, T., 2013. Hygrothermal properties of building envelopes: reliability of the effectiveness of energy saving. *Energy and buildings*, *57*, pp.187-192.
- Ardente, F., Beccali, M., Cellura, M. and Mistretta, M., 2008. Building energy performance: a LCA case study of kenaf-fibres insulation board. *Energy and Buildings*, *40*(1), pp.1-10.
- Arnfield A.J., 2020. Koppen climate classification. *Encyclopædia Britannica, inc.* Available online: https://www.britannica.com/science/Koppen-climate-classification
- Arundel, A.V., Sterling, E.M., Biggin, J.H. and Sterling, T.D., 1986. Indirect health effects of relative humidity in indoor environments. *Environmental Health Perspectives*, *65*, p.351.
- Asdrubali, F., D'Alessandro, F. and Schiavoni, S., 2015. A review of unconventional sustainable building insulation materials. *Sustainable Materials and Technologies*, *4*, pp.1-17.
- Asdrubali, F., Baldassarri, C. and Fthenakis, V., 2013. Life cycle analysis in the construction sector: Guiding the optimization of conventional Italian buildings. *Energy and Buildings*, *64*, pp.73-89.
- Ashour, T., Georg, H. and Wu, W., 2011. An experimental investigation on equilibrium moisture content of earth plaster with natural reinforcement fibres for straw bale buildings. *Applied thermal engineering*, *31*(2-3), pp.293-303.
- Ashour, T., Wieland, H., Georg, H., Bockisch, F.J. and Wu, W., 2010. The influence of natural reinforcement fibres on insulation values of earth plaster for straw bale buildings. *Materials & Design*, *31*(10), pp.4676-4685.
- ASHRAE, 2010. Standard 55-2010, Thermal environmental conditions for human occupancy. *American Society of Heating, Refrigerating and Air Conditioning Engineers*.

- ASHRAE, 2009, ASHRAE Handbook- Fundamentals (SI edition), American Society of Heating, Refrigerating and Air-conditioning Engineers, Atlanta, Ga., USA.
- Atsonios, I.A., Mandilaras, I.D., Kontogeorgos, D.A. and Founti, M.A., 2017. A comparative assessment of the standardized methods for the in–situ measurement of the thermal resistance of building walls. *Energy and Buildings*, *154*, pp.198-206.
- Berge, B., 2009. *The ecology of building materials*. Routledge.
- Binici, H., Aksogan, O. and Shah, T., 2005. Investigation of fibre reinforced mud brick as a building material. *Construction and Building Materials*, *19*(4), pp.313-318.
- Bollini, G., 2012. The first Italian experience of industrialized earthen products for the building trade. In *Rammed Earth Conservation* (pp. 469-474). CRC Press.
- Bribián, I.Z., Capilla, A.V. and Usón, A.A., 2011. Life cycle assessment of building materials: Comparative analysis of energy and environmental impacts and evaluation of the eco-efficiency improvement potential. *Building and environment*, *46*(5), pp.1133-1140.
- BS EN 1339-3: 2004. *Humidity_ Part 3: Guide to the measurement of humidity*. BSI
- BS EN 1745: 2012. *Masonry and masonry products_ Methods for determining thermal properties.* BSI.
- BS EN 1934: 1998. *Thermal performance of buildings_ Determination of thermal resistance by hot ox method using heat flow meter_ Masonry*. BSI.
- BS EN ISO 6946: 2007. *Building components and building elements_ Thermal resistance and thermal transmittance_ Calculation method.* BSI.
- BS EN ISO 7345: 2018. *Thermal performance of buildings and building components-Physical quantities and definitions*. BSI.
- BS EN ISO 8990: 1996. *Thermal insulation_ Determination of steady-state thermal transmission properties_ Calibrated and guarded hot box.* BSI.
- BS ISO 9869-1: 2014. *Thermal insulation_ Building elements_ In-situ measurement of thermal resistance and thermal transmittance; Part 1: Heat flow meter method.* BSI.
- BS EN ISO 12571, 2013. *Hygrothermal performance of building materials and products - Determination of hygroscopic sorption properties*. British Standards Institute, London.
- BS EN ISO 12572, 2001. *Hygrothermal performance of building materials and products - Determination of water vapour transmission properties*. British Standards Institute, London.
- BS EN 12667: 2001. *Thermal performance of building materials and products_ Determination of thermal resistance by means of guarded hot plate and heat flow meter methods_ products of high and medium thermal resistance* BSI.
- BS EN ISO 13786: 2017. *Thermal performance of building components_ Dynamic thermal characteristics_ Calculation methods.* BSI.
- BS EN ISO 15026, 2007. Hygrothermal performance of building components and building elements- Assessment of moisture transfer by numerical simulation. British Standards Institute, London.
- Bui, Q.B., Hans, S., Morel, J.C. and Do, A.P., 2011. First exploratory study on dynamic characteristics of rammed earth buildings. *Engineering Structures*, *33*(12), pp.3690-3695.

- Cao, X., Dai, X. and Liu, J., 2016. Building energy-consumption status worldwide and the state-of-the-art technologies for zero-energy buildings during the past decade. *Energy and buildings*, *128*, pp.198-213.
- Cabeza, L.F. (a), Barreneche, C., Miró, L., Martínez, M., Fernández, A.I. and Urge-Vorsatz, D., 2013. Affordable construction towards sustainable buildings: review on embodied energy in building materials. *Current Opinion in Environmental Sustainability*, *5*(2), pp.229-236.
- Cabeza, L.F (b)., Barreneche, C., Miró, L., Morera, J.M., Bartolí, E. and Fernández, A.I., 2013. Low carbon and low embodied energy materials in buildings: A review. *Renewable and Sustainable Energy Reviews*, *23*, pp.536-542.
- Cagnon, H., Aubert, J.E., Coutand, M. and Magniont, C., 2014. Hygrothermal properties of earth bricks. *Energy and Buildings*, *80*, pp.208-217.
- Callebaut, K., Elsen, J., Van Balen, K. and Viaene, W., 2001. Nineteenth century hydraulic restoration mortars in the Saint Michael's Church (Leuven, Belgium): Natural hydraulic lime or cement?. *Cement and Concrete Research*, *31*(3), pp.397-403.
- CIBSE, 2000. *Application manual AM13: Mixed mode ventilation.* CIBSE: London.
- Clarke, J.A. and Yaneske, P.P., 2009. A rational approach to the harmonisation of the thermal properties of building materials. *Building and Environment*, *44*(10), pp.2046-2055.
- Clarke, J.A., Yaneske, P.P. and Pinney, A.A., 1990. The harmonisation of thermal properties of building materials. *BRE, UK*.
- Clayworks Ltd, 2018. Accessed Oct 2018, https://clay-works.com/specifications/application-2/
- Curtis, G.E. and Hooglund, E., 2008. *Iran: A Country Study: A Country Study*. Government Printing Office.
- Crump, D., 2002. *A protocol for the assessment of indoor air quality in homes and office buildings* (Vol. 450). Building Research Establishment.
- Deconinck, A.H. and Roels, S., 2016. Comparison of characterisation methods determining the thermal resistance of building components from onsite measurements. *Energy and Buildings*, *130*, pp.309-320.
- DIN (Deutsches Institut für Normung), 2013. Earth plasters – Terms and definitions, requirements, test methods (In German), NABau: Berlin.
- Dolley, T.P. and Moyle, P.R., 2003. *History and overview of the US diatomite mining industry, with emphasis on the Western United States*. US Department of the Interior, US Geological Survey.
- Enerdata, 2020. Global energy statistical Yearbook 2019. Available from: https://yearbook.enerdata.net/total-energy/world-consumption-statistics.html
- Escalera, E., Garcia, G., Terán, R., Tegman, R., Antti, M.L. and Odén, M., 2015. The production of porous brick material from diatomaceous earth and Brazil nut shell ash. *Construction and Building Materials*, *98*, pp.257-264.
- Eshraghi, H., Ansari, M., Moshari, S. and Gholami, J., 2019. Climatic zoning and per capita demand forecast of Iran using degree-day method. *Advances in Building Energy Research*, pp.1-26.
- Faria, P., Santos, T. and Aubert, J.E., 2015. Experimental characterization of an earth eco-efficient plastering mortar. *Journal of materials in civil engineering*, *28*(1), p.04015085.

- Ferroukhi, M.Y., Abahri, K., Belarbi, R., Limam, K. and Nouviaire, A., 2016. Experimental validation of coupled heat, air and moisture transfer modeling in multilayer building components. *Heat and mass transfer*, *52*(10), pp.2257-2269.
- Foruzanmehr, A., 2017. *Thermal Comfort in Hot Dry Climates: Traditional Dwellings in Iran*. Routledge.
- Gasparella, A., Pernigotto, G., Baratieri, M. and Baggio, P., 2011. Thermal dynamic transfer properties of the opaque envelope: Analytical and numerical tools for the assessment of the response to summer outdoor conditions. *Energy and Buildings*, *43*(9), pp.2509-2517.
- Gil, A.M., Lopes, M.H., Neto, C.P. and Callaghan, P.T., 2000. An NMR microscopy study of water absorption in cork. *Journal of materials science*, *35*(8), pp.1891-1900.
- Givoni, B., 1998. *Climate considerations in building and urban design*. The USA: Van Nostrand Reinhold.
- Gregory, K., Moghtaderi, B., Sugo, H., Page, A., 2008. Effect of thermal mass on the thermal performance of various Australian residential constructions systems. *Energy and buildings,* 40, pp. 459-465.
- Guelberth, C. and Chiras, D., 2003. *The natural plaster book: Earth, lime, and gypsum plasters for natural homes*. New society publishers.
- Hall, M.R. and Casey, S., 2012. Hygrothermal behaviour and occupant comfort in modern earth buildings. In *Modern earth buildings* (pp. 17-40).
- Hall M.R., Allinson D., 2009. Analysis of the hygrothermal functional properties of stabilised rammed earth materials. Building & environment, Vol. 44, pp. 1935-1942.
- Hameury, S. and Lundström, T., 2004. Contribution of indoor exposed massive wood to a good indoor climate: in situ measurement campaign. *Energy and buildings*, *36*(3), pp.281-292.
- Hegger, M., Fuchs, M., Stark, Th., Zeumer, M., 2008. *Energy manual; sustainable architecture.* Berlin: Birkhauser.
- Hensen, J.L. and Lamberts, R., 2011. Introduction to building performance simulation. *Building performance simulation for design and operation*, pp.365-401.
- Holcroft, N., Shea, A., 2013. Heat of Sorption and Moisture Buffering Properties of Building Insulation Materials. Proc. Int. Civ. Infrastruct. Eng. Conf., Malaysia.
- Holcroft, N. and Shea, A., 2013. Moisture buffering and latent heat effects in natural fibre insulation materials. *Portugal SB13-Contribution of Sustainable Building to meet the EU*, pp.20-20.
- Holm, A., Radon, J., Künzel, H. and Sedlbauer, K., 2004. Description of the IBP holistic hygrothermal model. *IEA ANNEX*, *41*.
- Hulme, J. and Doran, S., 2014. In-situ measurements of wall U-values in English housing. *Prepared for: Alex Boss, DECC. BRE Output*, (290-102).
- IEA and UNEP (United Nation Environment Programme), 2019. *Global status report for buildings and construction: Towards a zero-emissions, efficient and resilient buildings and construction sector*. Available from: https://wedocs.unep.org/bitstream/handle/20.500.11822/30950/2019GSR.pdf?sequence=1&isAllowed=y

- Janssen, H. and Roels, S., 2009. Qualitative and quantitative assessment of interior moisture buffering by enclosures. *Energy and Buildings*, *41*(4), pp.382-394.

- Janssens A., Woloszyn M., Rode C., Kalagasidis A.S., De Paepe M., 2008. From EMPD to CFD- Overview of different approaches for heat air and moisture modeling in IEA Annex 41. IEA ECBCS Annex 41 closing seminar.

- Janssens A., De Paepe M., 2005. Effect of moisture inertia models on the predicted indoor humidity in a room. 26th AIVC conference, Brussels, 21- 23 Sep.

- Jerman, M. and Černý, R., 2012. Effect of moisture content on heat and moisture transport and storage properties of thermal insulation materials. *Energy and Buildings*, *53*, pp.39-46.

- Jin, H.Q., Yao, X.L., Fan, L.W., Xu, X. and Yu, Z.T., 2016. Experimental determination and fractal modeling of the effective thermal conductivity of autoclaved aerated concrete: Effects of moisture content. *International journal of heat and mass transfer*, *92*, pp.589-602.

- Kasmaei, M., 1992. Building and Housing Research Center affiliated to the ministry of housing and Urban Development. *Building and Housing Research Center: Tehran, Iran*.

- Khan, T.S. and Mubeen, U., 2012. Wheat straw: A pragmatic overview. *Current Research Journal of Biological Sciences*, *4*(6), pp.673-675.

- Khoukhi, M., 2018. The combined effect of heat and moisture transfer dependent thermal conductivity of polystyrene insulation material: Impact on building energy performance. *Energy and Buildings*, *169*, pp.228-235.

- Kinnane, O., McGranaghan, G., Walker, R., Pavia, S., Byrne, G. and Robinson, A., 2015, September. Experimental investigation of thermal inertia properties in hemp-lime concrete walls. In *Proceedings of the 10th conference on advanced building skins* (pp. 942-949). Bern: Author.

- Knapic, S., Oliveira, V., Machado, J.S. and Pereira, H., 2016. Cork as a building material: a review. *European Journal of Wood and Wood Products*, *74*(6), pp.775-791.

- Kočí, V., Maděra, J. and Černý, R., 2012. Exterior thermal insulation systems for AAC building envelopes: Computational analysis aimed at increasing service life. *Energy and Buildings*, *47*, pp.84-90.

- Kontoleon, K.J. and Giarma, C., 2016. Dynamic thermal response of building material layers in aspect of their moisture content. *Applied Energy*, *170*, pp.76-91.

- Kosmina, 2016. In-situ measurement of U-value. BRE.

- Kottek, M., Grieser, J., Beck, C., Rudolf, B. and Rubel, F., 2006. World map of the Köppen-Geiger climate classification updated. *Meteorologische Zeitschrift*, *15*(3), pp.259-263.

- Kousari, M.R., Ekhtesasi, M.R., Tazeh, M., Naeini, M.A.S. and Zarch, M.A.A., 2011. An investigation of the Iranian climatic changes by considering the precipitation, temperature, and relative humidity parameters. *Theoretical and Applied Climatology*, *103*(3-4), pp.321-335.

- Krus, M., 1996. *Moisture transport and storage coefficients of porous mineral building materials: Theoretical principles and new test methods* (p. 106). Stuttgart: Fraunhofer IRB Verlag.

- Kunzel H.M., Kiessl K., 1997, Calculation of heat and moisture transfer in exposed building components. Int. J. Heat Mass Transfer, Vol. 40, NO.1, pp. 159-167.

- Kunzel, H.M., 1995. Simultaneous heat and moisture transport in building components. *Fraunhofer Institute of building physics, Allemagne*.

- Kuronic, Z., 1998. Diatomaceous earths, a group of natural insecticides. Review. *J. Stored prod. Res*, *34*(2-3), pp.87-97.

- Kwiatkowski, J., Woloszyn, M. and Roux, J.J., 2011. Influence of sorption isotherm hysteresis effect on indoor climate and energy demand for heating. *Applied Thermal Engineering*, *31*(6-7), pp.1050-1057.

- Labat, M., Magniont, C., Oudhof, N. and Aubert, J.E., 2016. From the experimental characterization of the hygrothermal properties of straw-clay mixtures to the numerical assessment of their buffering potential. *Building and Environment*, *97*, pp.69-81.

- Laborel-Préneron, A., Aubert, J.E., Magniont, C., Tribout, C. and Bertron, A., 2016. Plant aggregates and fibers in earth construction materials: A review. *Construction and Building Materials*, *111*, pp.719-734.

- Latif, E., Lawrence, M., Shea, A. and Walker, P., 2015. Moisture buffer potential of experimental wall assemblies incorporating formulated hemp-lime. *Building and Environment*, *93*, pp.199-209.

- Latif, E., Tucker, S., Ciupala, M.A., Wijeyesekera, D.C. and Newport, D., 2014. Hygric properties of hemp bio-insulations with differing compositions. *Construction and Building Materials*, *66*, pp.702-711.

- Laughton, M.A. and Say, M.G. eds., 2013. *Electrical engineer's reference book*. Elsevier.

- Lengsfeld K., Krus M., 2017. Impact to the indoor climate depending on the moisture buffering of building materials. Proceedings of *Healthy Buildings conference,* 2-5 July 2017, Lublin (Poland).

- Li Y., Fazio P., Rao J., 2012. *An investigation of moisture buffering performance of wood panelling at room level and its buffering effect on a test room*. Building and Environment, Vol. 47, PP. 205-216.

- Li, Y. and Xu, P., 2006. Thermal mass design in buildings–heavy or light? *International Journal of Ventilation*, *5*(1), pp.143-150.

- Lima, J. and Faria, P., 2016. Eco-efficient earthen plasters: the influence of the addition of natural fibers. In *Natural Fibres: Advances in Science and Technology Towards Industrial Applications* (pp. 315-327). Springer, Dordrecht.

- Liuzzi S., Hall M.R., Stefanizzi P., Casey S.P., 2013. *Hygrothermal behaviour and relative humidity buffering of unfired and hydrated lime-stabilised clay composites in a Mediteranean climate*. Building and environment, Vol. 61, pp.82-92.

- Loganina, V.I., Simonov, E.E., Jezierski, W. and Małaszkiewicz, D., 2014. Application of activated diatomite for dry lime mixes. *Construction and Building Materials*, *65*, pp.29-37.

- Lopez, P.J., Descles, J., Allen, A.E. and Bowler, C., 2005. Prospects in diatom research. *Current opinion in Biotechnology*, *16*(2), pp.180-186.

- Lyons, A., 2014. *Materials for architects and builders*. Routledge.

- Maddison, M., Mauring, T., Kirsimäe, K. and Mander, Ü., 2009. The humidity buffer capacity of clay–sand plaster filled with phytomass from treatment wetlands. *Building and Environment*, *44*(9), pp.1864-1868.

- Maeda, H. and Ishida, E.H., 2011. Hydrothermal preparation of diatomaceous earth combined with calcium silicate hydrate gels. *Journal of hazardous materials*, *185*(2-3), pp.858-861.

- Maile, T., Fischer, M. and Bazjanac, V., 2007. Building energy performance simulation tools-a life-cycle and interoperable perspective. *Center for Integrated Facility Engineering (CIFE) Working Paper*, *107*, pp.1-49.

- May, N., 2005. Breathability: The key to building performance. *Oakley: Natural Building Technologies. Available at: http://responsible-retrofit.org/reference/breathability-the-key-to-building-performance/33 (Accessed: 08 July 2019)*.

- McGregor F., Heath A., Shea A., Lawrence M., 2014. The moisture buffering capacity of unfired clay masonry. Building and environment, 82, pp.599-607.

- McGregor, F., Heath, A., Fodde, E. and Shea, A., 2014. Conditions affecting the moisture buffering measurement performed on compressed earth blocks. *Building and Environment*, *75*, pp.11-18.

- Minke, G., 2012. *Building with earth: design and technology of a sustainable architecture*. Walter de Gruyter.

- Mohammad, S. and Shea, A., 2013. Performance evaluation of modern building thermal envelope designs in the semi-arid continental climate of Tehran. *Buildings*, *3*(4), pp.674-688.

- Mohammadi, A., Saghafi, M.R., Tahbaz, M. and Nasrollahi, F., 2018. The study of climate-responsive solutions in traditional dwellings of Bushehr City in Southern Iran. *Journal of Building Engineering*, *16*, pp.169-183.

- Moon, H.J., Ryu, S.H. and Kim, J.T., 2014. The effect of moisture transportation on energy efficiency and IAQ in residential buildings. *Energy and Buildings*, *75*, pp.439-446.

- Nejat, P., Jomehzadeh, F., Taheri, M.M., Gohari, M. and Majid, M.Z.A., 2015. A global review of energy consumption, CO2 emissions and policy in the residential sector (with an overview of the top ten CO2 emitting countries). *Renewable and sustainable energy reviews*, *43*, pp.843-862.

- Othmen, I., Poullain, P. and Leklou, N., 2018. Sensitivity analysis of the transient heat and moisture transfer in a single layer wall. *European Journal of Environmental and Civil Engineering*, pp.1-19.

- Oudhof, N., Labat, M., Magniont, C. and Nicot, P., 2015, June. Measurement of the hygrothermal properties of straw-clay mixtures. In *Clermont-Ferrand, International Conference on Bio-Based Building Materials*.

- Padfield T., 1999. The role of absorbent building materials in moderating changes of relative humidity. Ph.D. thesis, Department of Structural Engineering and Materials, Technical University of Denmark.

- Palumbo, M., McGregor, F., Heath, A. and Walker, P., 2016. The influence of two crop by-products on the hygrothermal properties of earth plasters. *Building and Environment*, *105*, pp.245-252.

- Pargana, N., Pinheiro, M.D., Silvestre, J.D. and de Brito, J., 2014. Comparative environmental life cycle assessment of thermal insulation materials of buildings. *Energy and Buildings*, *82*, pp.466-481.

- Pavlík, Z. and Černý, R., 2008. Experimental assessment of hygrothermal performance of an interior thermal insulation system using a laboratory technique simulating on-site conditions. *Energy and Buildings*, *40*(5), pp.673-678.

- Pereira, H. ed., 2011. *Cork: biology, production and uses*. Elsevier.
- Pereira, H., Rosa, M.E. and Fortes, M.A., 1987. The cellular structure of cork from Quercus suber L. *IAWA Journal*, *8*(3), pp.213-218.
- Pérez-Bella, J.M., Dominguez-Hernandez, J., Cano-Suñén, E., del Coz-Diaz, J.J. and Rabanal, F.P.Á., 2015. A correction factor to approximate the design thermal conductivity of building materials. Application to Spanish façades. *Energy and Buildings*, *88*, pp.153-164.
- Peuhkuri R., Rode C., Hansen K.K., 2004. Moisture buffer capacity of different insulation materials. ORNL Institute.
- Ramos N.M.M., de Freitas V.P., 2006. Evaluation strategy of finishing materials contribution to the hygroscopic inertia of a room, Research in Building Physics and Building Engineering, Concordia University, Montreal, Canada, pp. 543-548.
- Ramos, N.M.M., Delgado, J.M.P.Q. and de Freitas, V.P., 2010. Influence of finishing coatings on hygroscopic moisture buffering in building elements. *Construction and Building Materials*, *24*(12), pp.2590-2597.
- Reilly, A. and Kinnane, O., 2017. The impact of thermal mass on building energy consumption. *Applied Energy*, *198*, pp.108-121.
- Riazi, M. and Hosseyni, S.M., 2011. Overview of current energy policy and standards in the building sector in Iran. *Sustainable Development and Planning V*, *150*, pp.189-200.
- Rode C., Woloszyn M., 2007. Whole building hygrothermal modelling in IEA Annex 41. ASHRAE Tansaction.
- Rode C., Hansen K., Padfield T., Time B., Ojanen T., Arfvidsson J., 2003. NORDTEST workshop on moisture buffer capacity- summer report, Department of civil engineering; Technical university of Denmark.
- Rode C., 2005. Moisture buffering of building materials. Department of Civil Engineering, Technical University of Denmark, Report R-126.
- Rode C., Peuhkuri R., Time B., Svennberg K., Ojanen T., 2006. Moisture buffer value of building materials. *ASTM symposium on Heat-Air-Moisture transport: Measurements on building materials: Toronto*.
- Rode, C., Peuhkuri, R., Time, B., Svennberg, K. and Ojanen, T., 2007. Moisture buffer value of building materials. *Journal of ASTM International*, *4*(5), pp.1-12.
- Roels, S. and Janssen, H., 2006. A comparison of the NordTest and Japanese test methods for the moisture buffering performance of building materials. *Journal of Building Physics*, *30*(2), pp.137-161.
- Rubel, F. and Kottek, M., 2010. Observed and projected climate shifts 1901–2100 depicted by world maps of the Köppen-Geiger climate classification. *Meteorologische Zeitschrift*, *19*(2), pp.135-141.
- Ruuska, A.P. and Häkkinen, T.M., 2015. The significance of various factors for GHG emissions of buildings. *International Journal of Sustainable Engineering*, *8*(4-5), pp.317-330.
- Shea, A., Lawrence, M. and Walker, P., 2012. Hygrothermal performance of an experimental hemp–lime building. *Construction and building materials*, *36*, pp.270-275.
- Schiavoni, S., Bianchi, F. and Asdrubali, F., 2016. Insulation materials for the building sector: A review and comparative analysis. *Renewable and Sustainable Energy Reviews*, *62*, pp.988-1011.

- Simões, N., Fino, R. and Tadeu, A., 2019. Uncoated medium density expanded cork boards for building façades and roofs: Mechanical, hygrothermal and durability characterization. *Construction and Building Materials*, *200*, pp.447-464.

- Simonson C.J., Olutimaayin S., Salonvaara M., Ojanen T., O'Connor J., 2004 (a). Potential for hygroscopic building materials to improve indoor comfort and air quality in the Canadian climate. ASHRAE Transaction

- Simonson C.J., Salonvaara M., Ojanen T., 2004 (b). Heat and mass transfer between indoor air and a permeable and hygroscopic building envelope: Part II- verification and numerical studies. Thermal envelope and building science. Vol. 28, pp. 161-185.

- Stulz, R. and Mukerji, K., 1983. *Appropriate building materials* (No. 12). Skat.

- Szokolay, S.V., 2014. *Introduction to architectural science: the basis of sustainable design*. Routledge.

- Tabari, H. and Talaee, P.H., 2011. Analysis of trends in temperature data in arid and semi-arid regions of Iran. *Global and Planetary Change*, *79*(1-2), pp.1-10.

- Tártaro, A.S., Mata, T.M., Martins, A.A. and da Silva, J.C.E., 2017. Carbon footprint of the insulation cork board. *Journal of cleaner production*, *143*, pp.925-932.

- Taylor, P. and Luther, M.B., 2004. Evaluating rammed earth walls: a case study. *Solar Energy*, *76*(1-3), pp.79-84.

- Thormark, C., 2006. The effect of material choice on the total energy need and recycling potential of a building. *Building and environment*, *41*(8), pp.1019-1026.

- Toftum J., Jorgensen A.S., Fanger P.O., 1997, Upper limits of air humidity for preventing warm respiratory discomfort. Energy and Buildings, Vol. 28, PP.15-23.

- Ummah, H., Suriamihardja, D.A., Selintung, M. and Wahab, A.W., 2015. Analysis of chemical composition of rice husk used as absorber plates sea water into clean water. *ARPN J. Eng. Appl. Sci*, *10*(14), pp.6046-6050.

- Vieira J., Senff L., Goncalves H., Silva L., Ferreira V.M., Labrincha J.A., 2014. Functionalization of mortars for controlling the indoor ambient of buildings. Energy and buildings, 70, pp. 224-236.

- Vu, D.H., Wang, K.S., Bac, B.H. and Nam, B.X., 2013. Humidity control materials prepared from diatomite and volcanic ash. *Construction and building materials*, *38*, pp.1066-1072.

- Woloszyn M., Kalamees T., Abadie M.O., Steeman M., Kalagasidis A.S., 2009. The effect of combining a RH sensitive ventilation system with the moisture buffering capacity of materials on indoor climate and energy efficiency of buildings. Building and Environment, Vol. 44, PP. 515-524.

- Woloszyn, M. and Rode, C., 2008, March. Tools for performance simulation of heat, air and moisture conditions of whole buildings. In *Building Simulation* (Vol. 1, No. 1, pp. 5-24). Springer-Verlag.

- Wulfinghoff, D.R., 1999. *Energy efficiency manual* (Vol. 3936). Maryland: Energy Institute Press.

- Yoshino H., Mitamura T., Hasegawa K., 2009. Moisture buffering and effect of ventilation rate and volume rate of hygrothermal materials in a single room under steady state exterior conditions. Building and Environment, Vol. 44, PP. 1418- 1425.

- Zhang, Y., Hosseinaei, O., Wang, S. and Zhou, Z., 2011. Influence of hemicellulose extraction on water uptake behavior of wood strands. *Wood and Fiber Science*, *43*(3), pp.244-250.

Appendix

Temperature and absolute humidity profiles in wall specimens

Location of the sensors

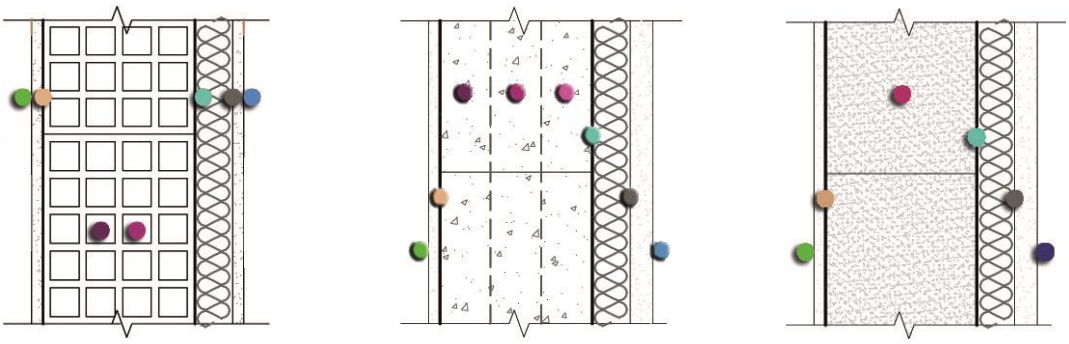

(a) (b) (c)

(a) Hollow clay block + insulation wall specimens

(b) LECA block + insulation wall specimens

(c) AAC block + insulation wall specimens

Legend guide

CCL: Climate Chamber Left (Indoor condition)

SL: Surface Left (on the internal surface of the wall)

GP: Gypsum Plaster (at the interface of gypsum plaster and block)

CP: Clay Plaster (at the interface of clay plaster and block)

M: Middle (Middle of the block)

Ins: Insulation (at the interface of insulation and block)

Lime: Lime render (at the interface of insulation and lime render)

Cem: Cement render (at the interface of insulation and cement render)

SR: Surface Right (on the external surface of the wall)

CCR: Climate Chamber Right (Outdoor condition)

Clay PIR wall specimen (Hot dry condition)

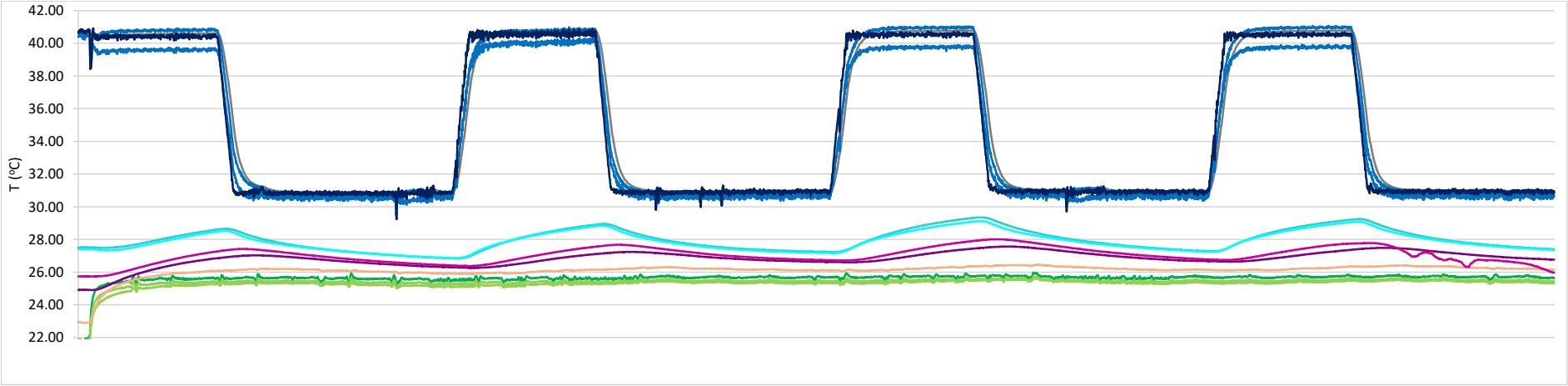

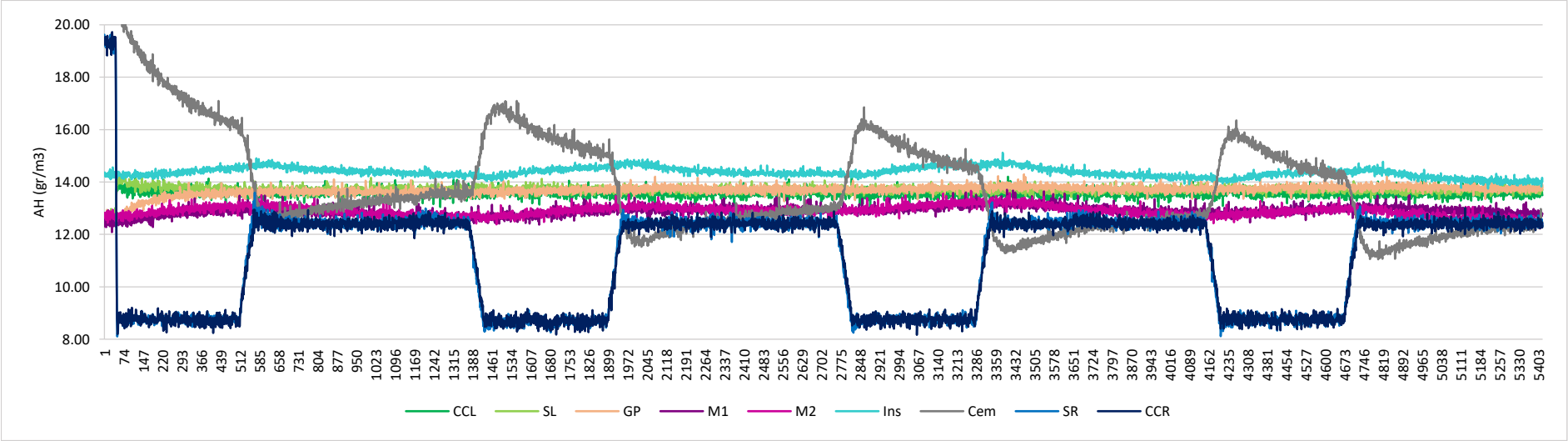

Clay PIR wall specimen (Hot humid condition)

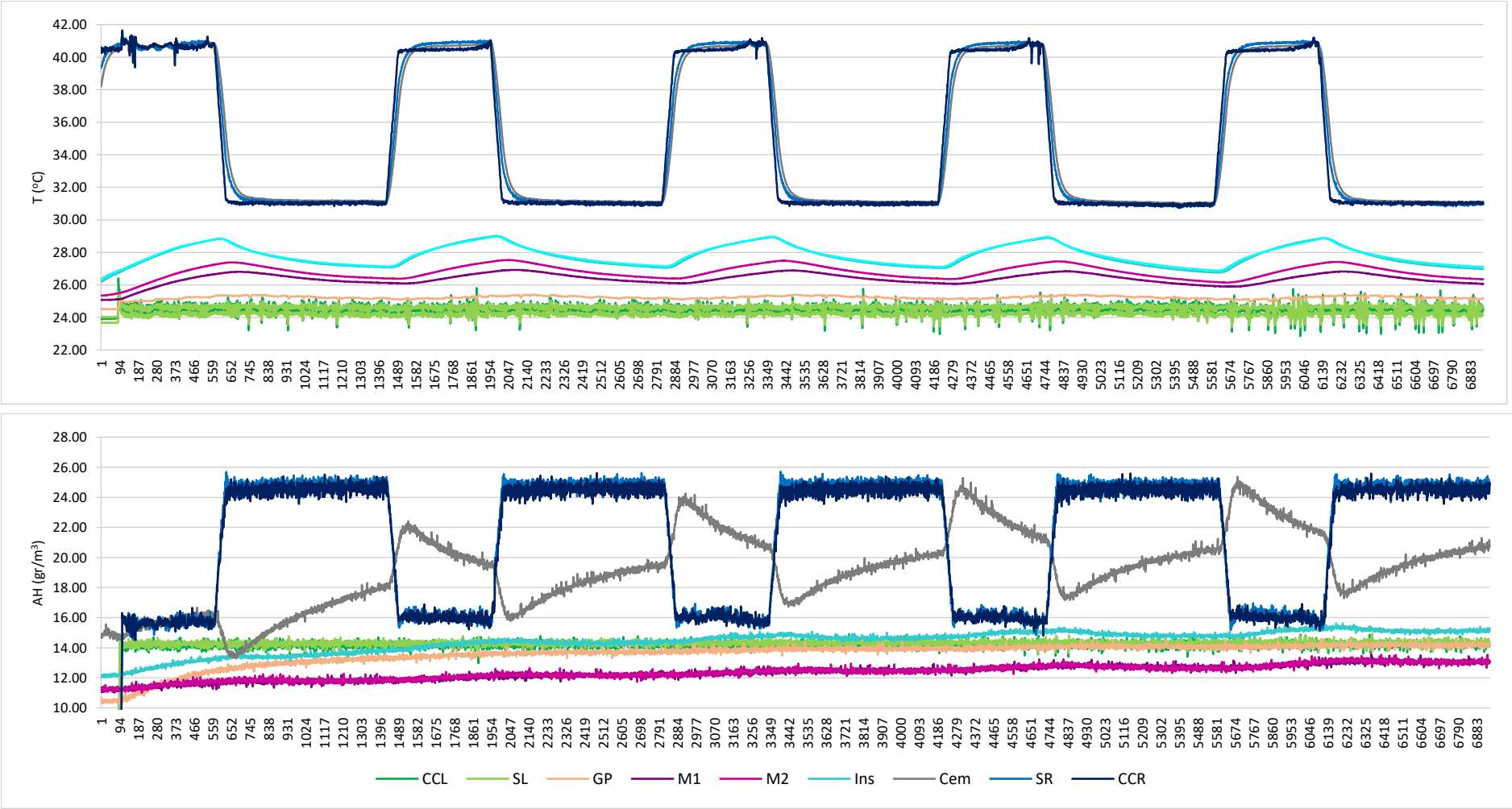

LECA PIR wall specimen (Hot dry condition)

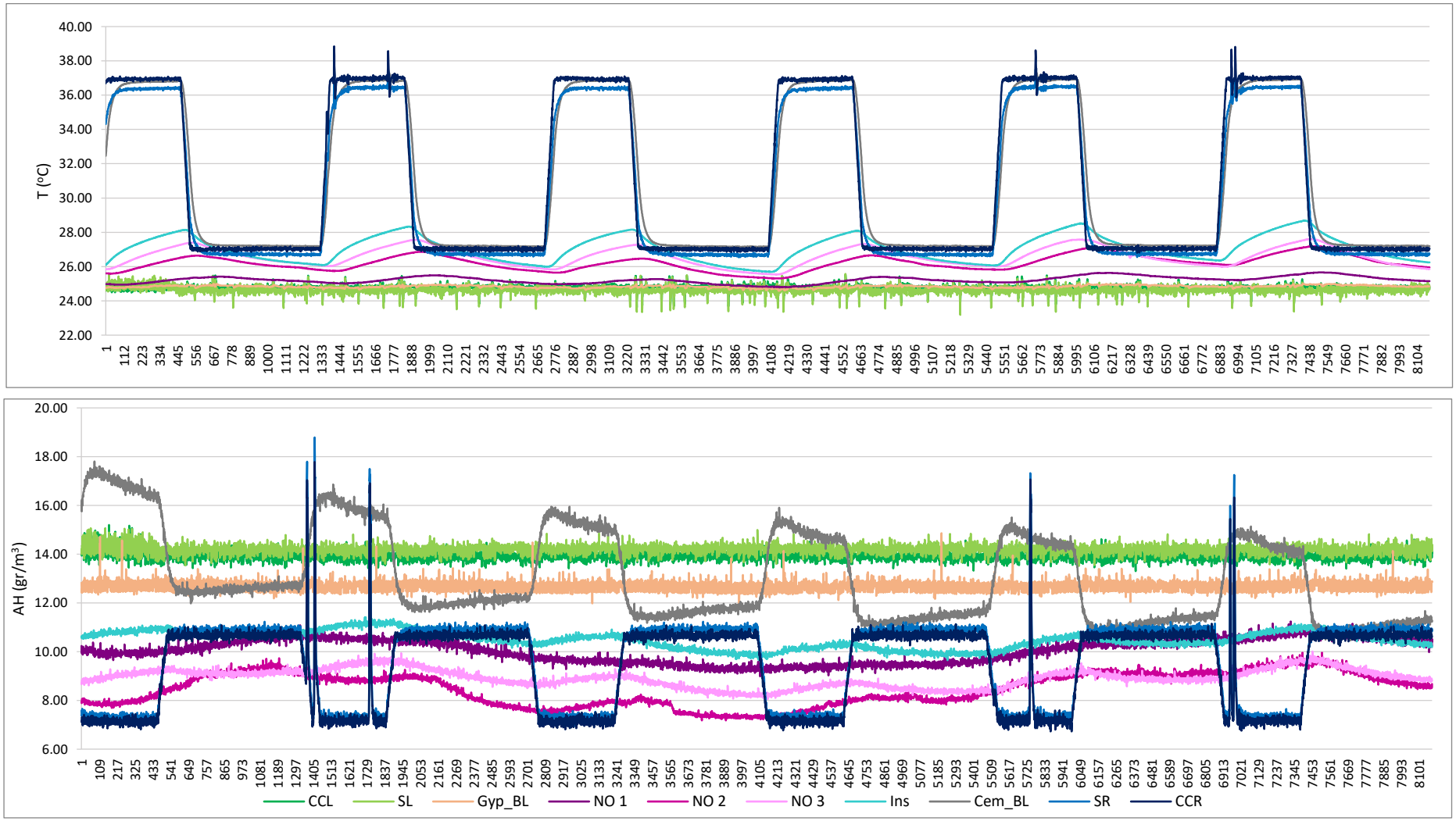

AAC PIR wall specimen (Hot dry condition)

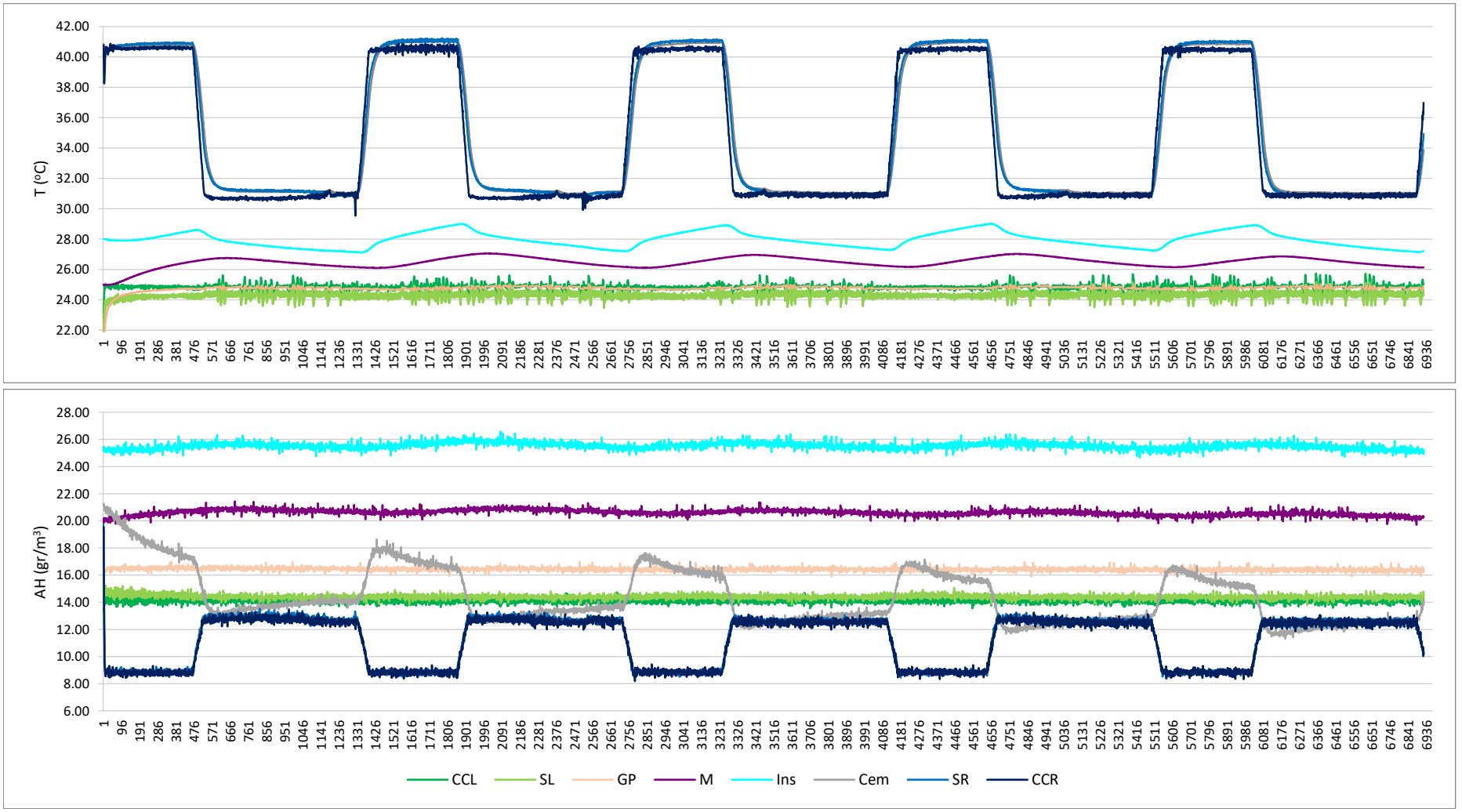

AAC PIR wall specimen (Hot humid condition)

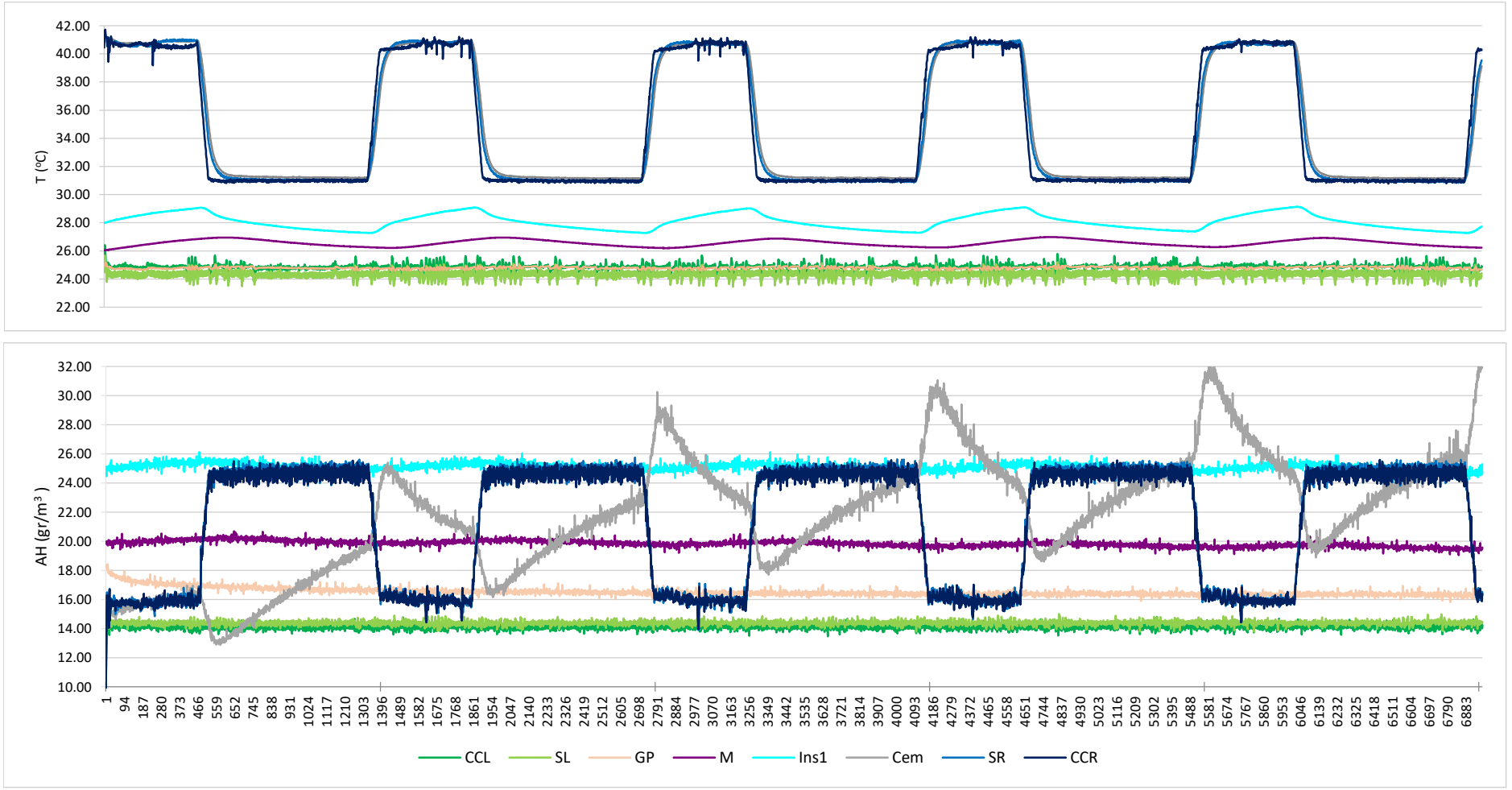

Clay Cork wall specimen (Hot dry condition)

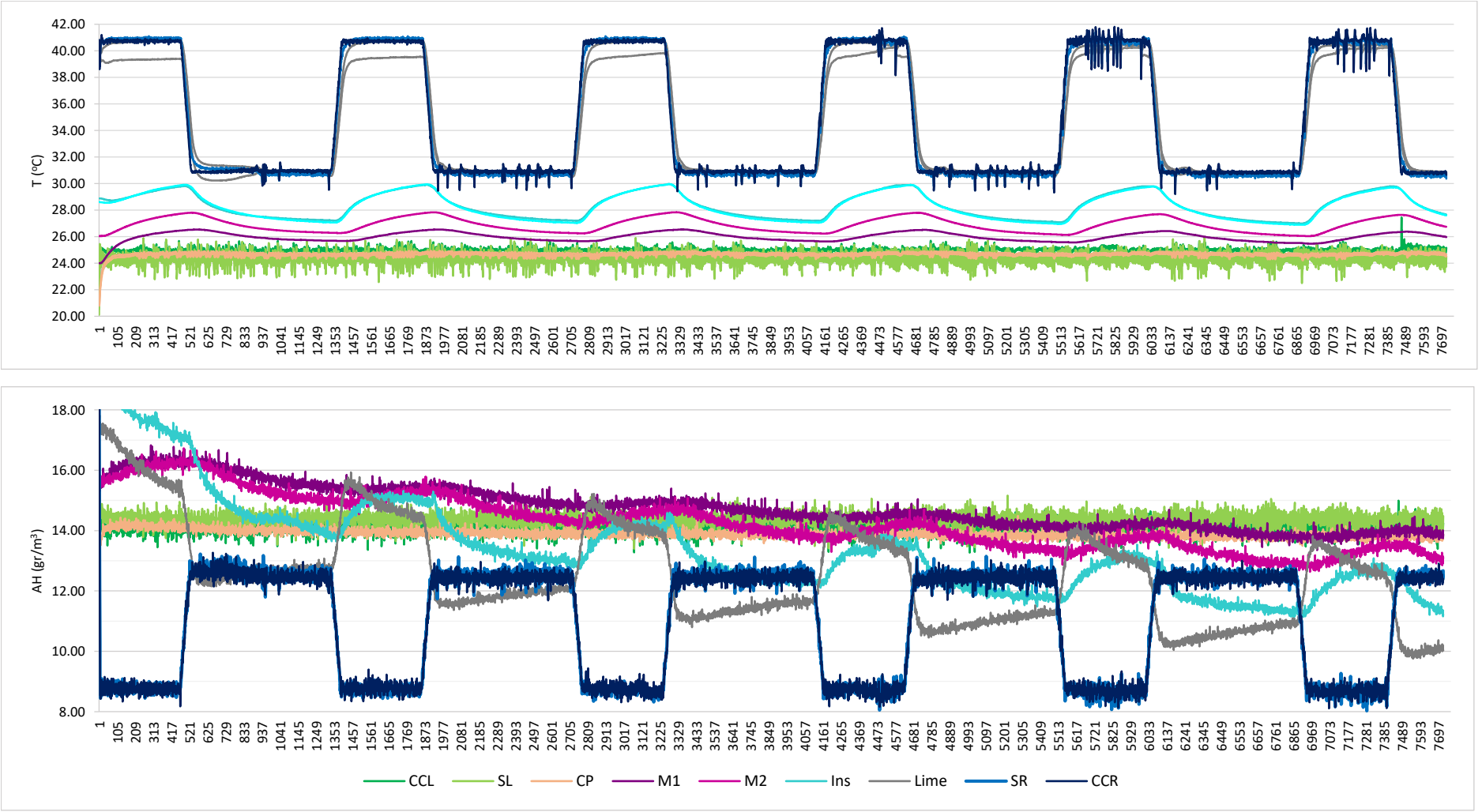

Clay Cork wall specimen (Hot humid condition)

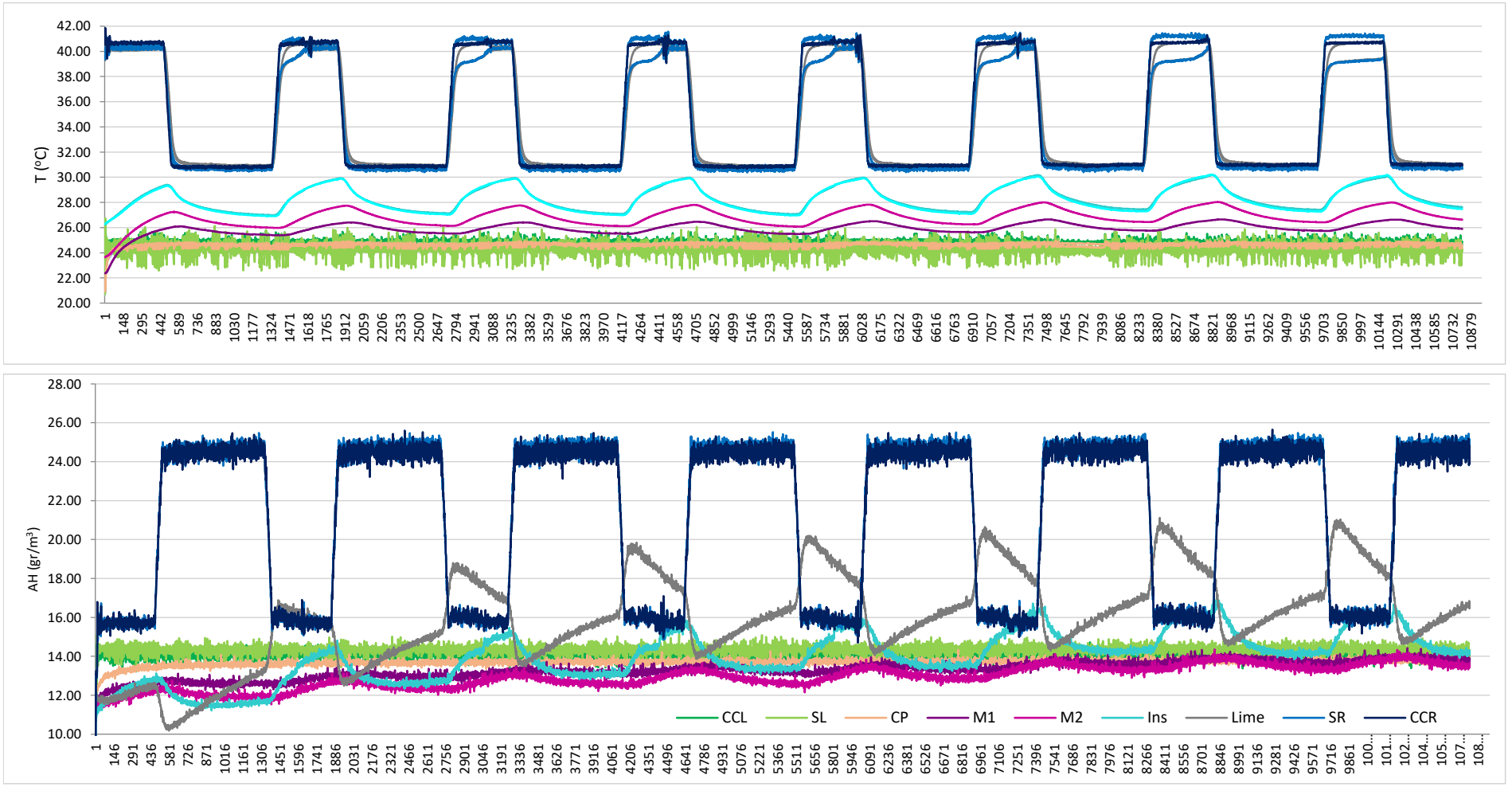

LECA- Cork wall specimen (Hot dry condition)

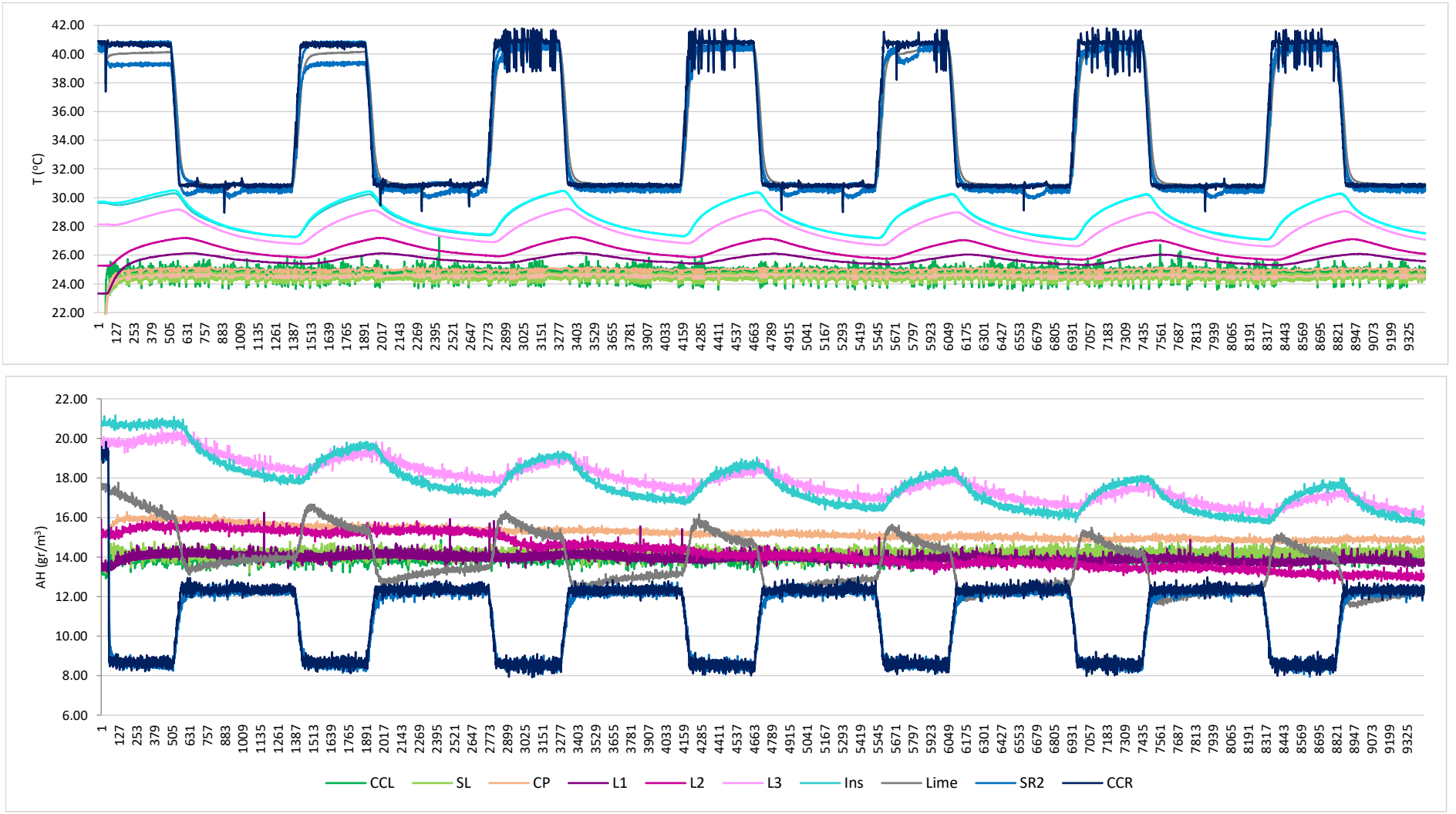

LECA cork wall specimen (Hot humid condition)

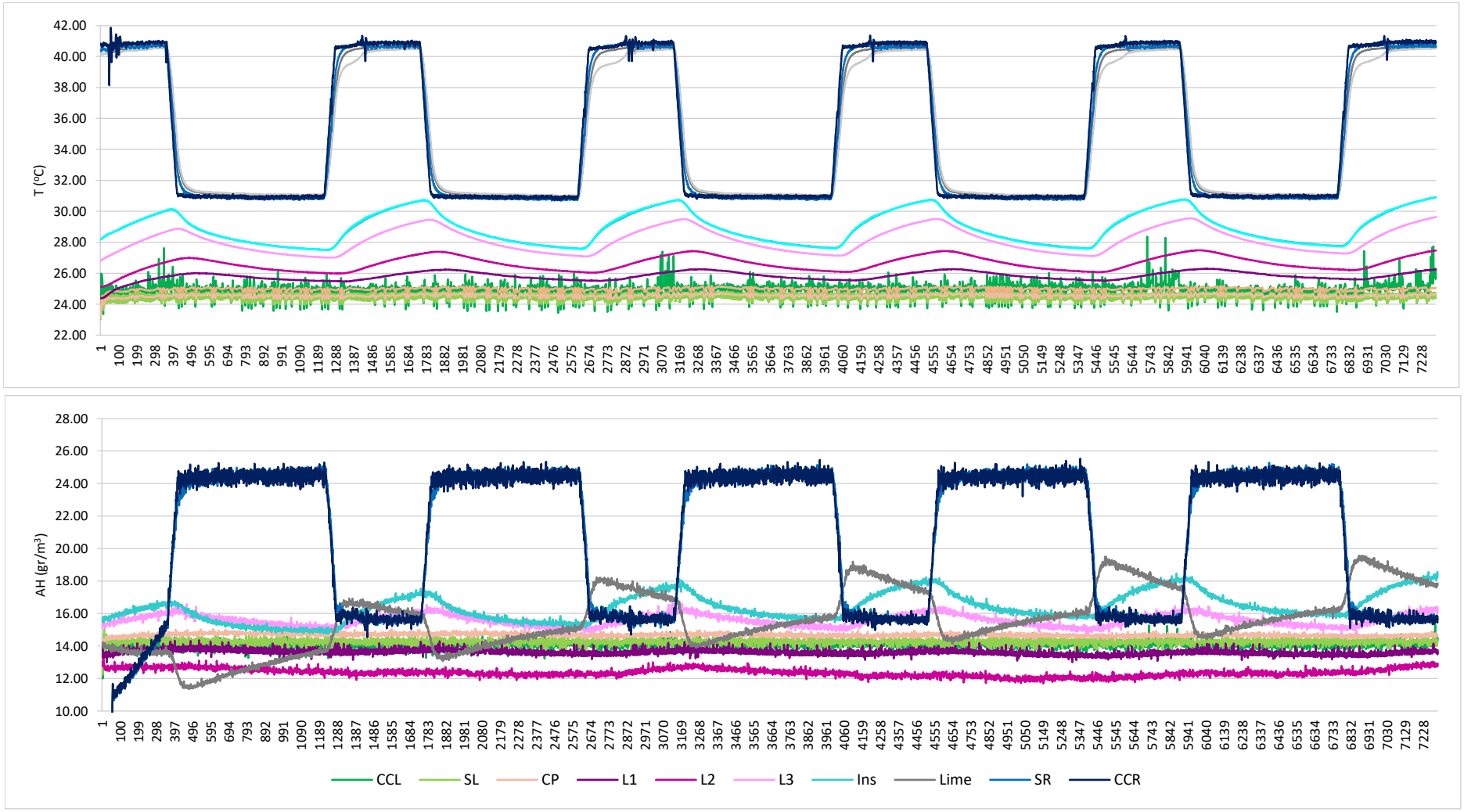

AAC Cork wall specimen (Hot dry condition)

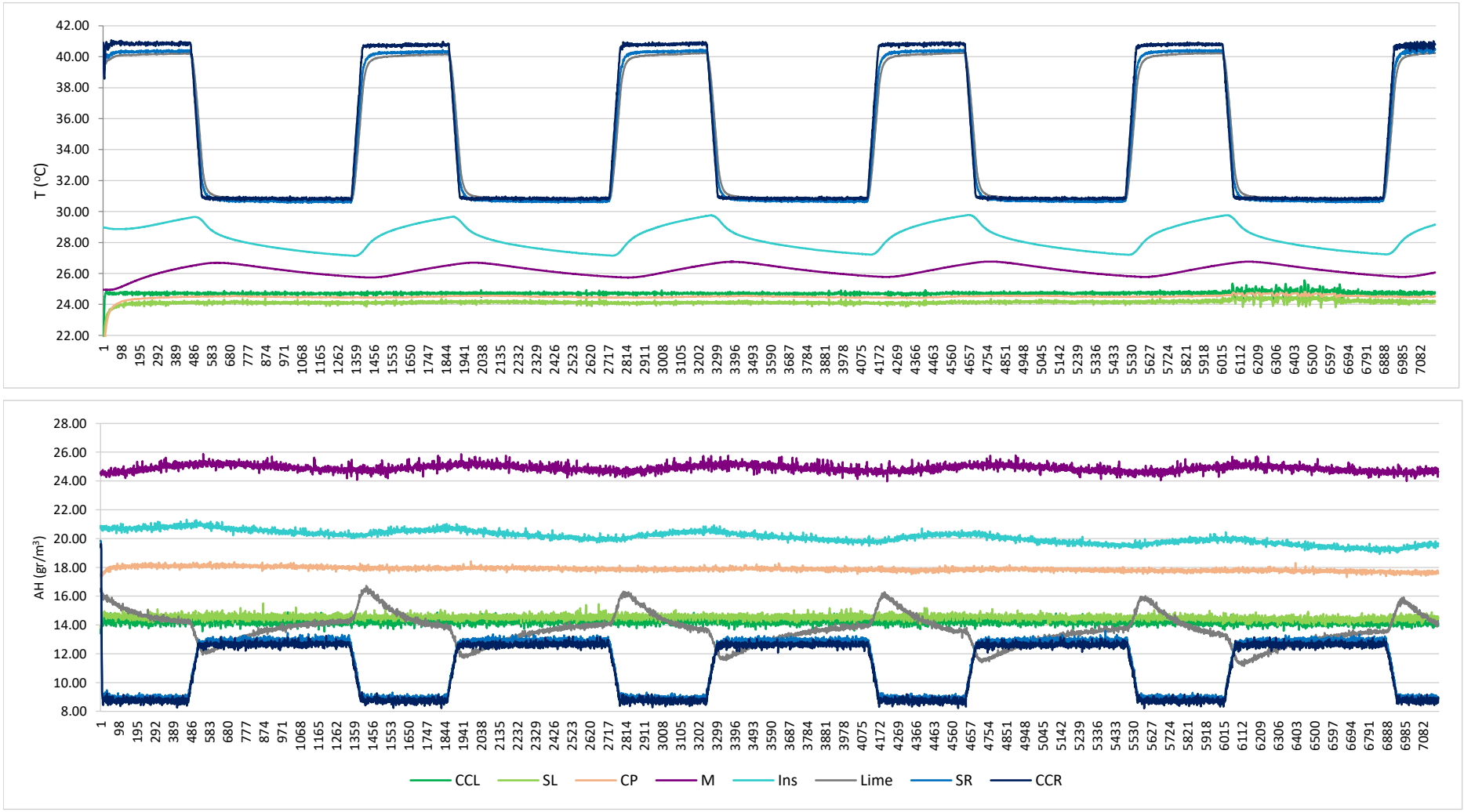

AAC Cork wall specimen (Hot humid condition)